PHD THESIS

Institute of Physcial Chemistry
Polish Academy of Sciences
Kasprzaka 44/52
01-224 Warsaw, Poland

PhD Thesis

Synthesis of new 2,2'-bisbithienylmethane and fullerene derivatives, and their application as functional monomers for preparation of recognition polymer films of chemosensors for selective determination of biologically significant compounds

A-21-7, A-21-9, K-9-152

Marta Sosnowska

Supervisors:

Wlodzimierz Kutner, D. Sc.
Institute of Physical Chemistry
Polish Academy of Sciences
Warsaw, Poland

Francis D'Souza, D. Sc.
University of North Texas
Denton, Texas
United States of America

Warsaw, November 2014

INNOVATIVE ECONOMY
NATIONAL COHESION STRATEGY

FNP
Foundation for Polish Science

EUROPEAN UNION
EUROPEAN REGIONAL
DEVELOPMENT FUND

Nikt z nas nie żyje dla siebie i nikt nie umiera dla siebie: jeżeli bowiem żyjemy, żyjemy dla Pana; jeżeli zaś umieramy, umieramy dla Pana. I w życiu więc i w śmierci należymy do Pana.

Rz 14, 7-8

For none of us lives for ourselves alone, and none of us dies for ourselves alone. If we live, we live for the Lord; and if we die, we die for the Lord. So, whether we live or die, we belong to the Lord.

Ro 14, 7-8

waniem pochodnych tiofenu, sposób jej otrzymywania, jak również jej zastosowanie do selektywnego wykrywania i oznaczania inozyny" ("Thiophene derivatives, way of their preparation, recognizing conducting polymer layer prepared via molecular imprinting by using thiophene derivatives, method of preparation as well as its application towards selective inosine detection and quantification").

5. Wojnarowicz, A., Sharma, P. S., **Sosnowska, M.**, D'Souza, F., Kutner, W., Polish Pat. Appl., No. P. P.409325, 29 August 2014, „Nowy przewodzący bisbitiofenowy polimer molekularnie wdrukowany za pomocą karnozyny i sposób jego przygotowania oraz zastosowanie do selektywnego wykrywania i oznaczania karnozyny" ("New conducting polymer molecularly imprinted with carnosine, its method of preparation, and application for selective determination of carnosine").

6. Bartołd, K., Pietrzyk-Le, A., Huynh, T-P., Iskierko, Z., Noworyta, K., **Sosnowska, M.**, Lisowski, W., Kutner, W., Sannicolò, F., Mussini, P. R., Polish Pat. Appl., No. P. 409328, 29 August 2014, „Nowa sonda DNA zawierająca pochodne tiofenu i sposób jej wytwarzania, warstwa przewodzącego polimeru wdrukowywanego molekularnie z zastosowaniem tych pochodnych i sposób jej wytwarzenia oraz zastosowanie tej sondy do selektywnego wykrywania i oznaczania oligonukleotydu TATAAA" ("New DNA probe containing thiophene derivatives and its method of preparation, a film of the conducting polymer molecularly imprinted with the use of these derivatives and the method of its preparation as well as application of this probe for selective detection and determination of the TATAAA oligonucleotide").

Acknowledgements

First, I would like to greatly acknowledge my supervisors, Prof. Włodzimierz Kutner and Prof. Francis D'Souza for attracting me to the so much rewarding field of molecular imprinting, for help and guidance. I am particularly grateful to Prof. Francis D'Souza for his help and encouragement when doing research in his lab.

Then, I am grateful to all my colleagues of the Group of Molecular Films of IPC PAS, especially to Dr. Piyush Sindhu Sharma, Dr. Tan-Phat Huynh, and M. Sc. Marcin Dąbrowski, for enlightening discussions on research and life. Members of the Prof. D'Souza group, i.e., B.Sc. Chandra B. KC, B.Sc. Venugopal Bandi, and B.Sc. Gary Lim, are gratefully acknowledged for all their help and support.

Moreover, I owe gratitude to:

- Dr. Piotr Pięta for AFM imaging

- Dr. Vladimir N. Nesterov for X-ray crystal structure determination and advices on how to grow crystals

- Dr. Tan-Phat Huynh and M.Sc. Agnieszka Wojnarowicz for quantum-chemical calculations

- B.Sc. Chandra Bikram KC and B.Sc. Venugopal Bandi for teaching me how to perform synthesis

- Mr. H. J. J. Szaniawski for artwork.

Last but not least, I would like to thank all my family and friends that helped me to get through this period of my life. Ewa, Celina, and Ania - without your support my thesis would not be finished and I would not be where I am now.

Publications

1. **Marta Sosnowska**, Piotr Pieta, Piyush S. Sharma, Raghu Chitta, Chandra B. KC, Venugopal Bandi, Francis D'Souza, and Wlodzimierz Kutner, *Anal. Chem.*, **2013**, *85*, 7454–7461, "Piezomicrogravimetric and Impedimetric Oligonucleotide Biosensors Using Conducting Polymers of Biotinylated Bis(2,2'-bithien-5-yl)methane as Recognition Units".

2. Tan-Phat Huynh, **Marta Sosnowska**, Janusz W. Sobczak, Chandra B. KC, Vladimir N. Nesterov, Francis D'Souza, and Wlodzimierz Kutner, *Anal. Chem.*, **2013**, *85*, 8361-8368, "Simultaneous chronoamperometry and piezoelectric microgravimetry determination of nitroaromatic explosives using molecularly imprinted thiophene polymers".

3. Tan-Phat Huynh, Chandra B. KC, **Marta Sosnowska**, Janusz W. Sobczak, Vladimir N. Nesterov, Francis D'Souza, and Wlodzimierz Kutner, *Biosens. Bioelec.*, **2015**, *64*, 657-663, "Nicotine molecularly imprinted polymer: synergy of coordination and hydrogen bonds".

4. Tan-Phat Huynh, Agnieszka Wojnarowicz, **Marta Sosnowska**, Simcha Srebnik, Tiziana Benincori, Francesco Sannicolo, Francis D'Souza, and Wlodzimierz Kutner, **2014**, submitted, "Cytosine derived molecularly imprinted polymer for 6-thioguanine".

Patent applications

1. **Sosnowska, M.**, Pięta, P., Sharma, P. S., KC, C. B., Bandi, V., D'Souza, F., Kutner, W., Polish Pat. Appl. No. P.403766, 6 May 2013, „Nowy bis(2,2'-bitienylo)-(4-hydroksyfenylo)metanowy ester biotyny, sposób jego wytwarzania, oraz zawierająca ten ester warstwa rozpoznającego polimeru i jej zastosowanie do wykrywania i/lub oznaczania oligonukleotydów" ("A new bis(2,2'-bithien-5-yl)-(4-hydroxyphenyl)methane biotin ester, method of its preparation as well as the containing this ester recognition polymer film and its application for detection and/or determination of oligonucleotides").

2. Huynh, T-P., **Sosnowska, M.**, Sobczak, J. W., KC C. B., Nesterov, V. N., D'Souza, F., Kutner, W., Polish Pat. Appl. No. P.404175, 3 June 2013; UK Pat. Appl. No. GB1409820.6, 03 June 2014, „Nowa pochodna bis(2,2'-bitienylo)metanu i sposób jej wytwarzania, warstwa molekularnie wdrukowanego polimeru, sposób jej wytwarzania i jej zastosowanie do selektywnego wykrywania i oznaczania związków nitroaromatycznych" ("New bis(2,2'-bithienyl)methane derivative and the method of its preparation, a film of the molecularly imprinted polymer, method of its preparation, and its application for selective detection and determination of nitroaromatic compounds").

3. Huynh, T-P., KC. C. B., **Sosnowska, M.**, Sobczak, J. W., Nesterov, V. N., D'Souza, F., Kutner, W., Polish Pat. Appl. No. P.407167, 13 February 2014, „Pochodne bis(2,2'-bitienylo)metanu i sposoby ich wytwarzania, warstwa rozpoznającego polimeru utworzona metodą wdrukowania molekularnego i sposób jej otrzymywania, jak również jej zastosowanie do selektywnego oznaczania i uwalniania nikotyny" ("Derivatives of bis(2,2'-bithienyl)methane and methods of their preparation, a recognizing polymer film prepared by molecular imprinting and the method of its preparation as well as its application for selective determination and release of nicotine").

4. Iskierko, Z., **Sosnowska, M.**, Sharma, P. S., D'Souza, F., Benincori, T., Noworyta, K., Polish Pat. Appl., No. P.408507, 11 June 2014, „Pochodne tiofenu i sposób ich otrzymywania, warstwa rozpoznającego polimeru przewodzącego wytworzonego metodą wdrukowywania molekularnego z zastoso-

Presentations at international conferences

As a presenting author

Oral presentations

Sosnowska, M., Pieta, P., Sharma, P. S., Chitta, R., KC, C. B., Bandi, V., D'Souza, F., and Kutner, W., 6th International Workshop on Surface Modification for Chemical and Biochemical Sensing, Institute of Physical Chemistry of the Polish Academy of Sciences, 8-12 November 2013, Lochow, Poland, "Piezomicrogravimetric and impedimetric oligonucleotide biosensors using conducting polymers of biotinylated bis(2,2'-bithien-5-yl)methane as recognition units".

Posters

1. **Sosnowska M.**, Huynh T-P., Pietrzyk-Le A., Chitta R., D'Souza F., and Kutner W., 5th International Workshop on Surface Modification for Chemical and Biochemical Sensing, Polish Foundation for Supramolecular Chemistry, 4-8 November 2011, Lochow, Poland, "Molecularly imprinted polymer (MIP) chemosensors for surface plasmon resonance (SPR) and differential pulse voltammetry (DPV) determination of melamine".

2. **Sosnowska, M.**, Sharma, P. S., KC, C. B., D'Souza, F., and Kutner, W., The 68th Southwest Regional Meeting of the ACS, SWRM 2012, The American Chemical Society, 4-7 November 2012, Baton Rouge, LA, USA, "Design and synthesis of new electroactive biotin derivatized bis(2,2'-bithienyl)methane conducting polymer for devising a DNA sensor".

3. **Sosnowska, M.**, D'Souza, F., and Kutner, W., Biosensors 2014: 24th Anniversary World Congress on Biosensors, 27-30 May 2014, Melbourne, Australia, "Molecularly imprinted polymers for myoglobin sensing".

As a co-author

Oral presentations

1. **Kutner, W.**, Sosnowska, M., Pieta, P., Sharma, P. S., Chitta, R., KC, B. K. Bandi, V., and D'Souza, F., International Conference ElecNano 5. The nanoscale and electroanalysis: surface nanostructuration, nanobiological systems, coupled methods, microsystems, 15-17 May 2013, Bordeaux, France, "Surface nanostructured films of a conducting polymer of biotinylated bis(2,2'-bithien-5-yl)methane as recognition units of piezomicrogravimetric and impedimetric oligonucleotide biosensors".

2. **Kutner, W.**, Huynh, T-P., Sosnowska, M., KC., C. B., Nesterov, V., Sobczak, J. W., and D'Souza, F., the 64th Annual Meeting of the International Society of Electrochemistry (ISE), 8-13 September 2013, Santiago de Queretaro (Mexico), "A general protocol of designing and fabricating thin films of conducting molecularly imprinted polymers for application to selective sensing".

3. **Huynh, T-P.**, Sosnowska, M., KC, C. B., Nesterov, V., Sobczak, J. W., D'Souza, F., and Kutner, W., 6th International Workshop on Surface Modification for Chemical and Biochemical Sensing, Institute of Physical Chemistry of the Polish Academy of Sciences, 8-12 November 2013, Lochow, Poland, "Selective determination of explosive nitroaromatic compounds by simultaneous chronoamperometry and piezoelectric microgravimetry using conducting molecularly imprinted polymers (MIPs)".

4. Huynh, T-P., KC, C. B., Sosnowska, M., Sobczak, J. W., Nesterov, V. N., D'Souza, F., and **Kutner, W.**, Regional Biophysics Conference, RBC'2014, Slovak Biophysical Society, Comenius University, Slovak Academy of Sciences, 15-20 May 2014, Smolenice Castle, Slovakia, "Recent advances in electrochemical molecular imprinting for biomimetic sensing".

5. Huynh, T-P., Sosnowska, M., Sobczak, J.W., KC, C. B., Nesterov, V. N., D'Souza, F. and **Kutner, W.**, 15th International Conference on Electroanalysis, ESEAC 2014, Division of Analytical Chemistry of the Swedish Chemical Society, 11-15 June 2014, Malmö, Sweden, "Selective simultaneous chronoamperometric and piezomicrogravimetric determination of some toxins at electrodes coated with conducting molecularly imprinted polymer films".

6. **Kutner, W.**, Huynh, T-P., Sosnowska, M., KC, C. B., Nesterov, V., Sobczak, J. W., and D'Souza, F., 65th Annual Meeting of the International Society of Electrochemistry (ISE), 31 August-5 September, 2014, Lausanne, Switzerland, "Selective chemosensing with molecularly imprinted polymers of thiophenes".

Posters

1. **Huynh, T-P.**, Sosnowska, M., D'Souza, F., and Kutner, W., The 68th Southwest Regional Meeting of the ACS, the American Chemical Society, 4-7 November 2012, Baton Rouge, LA USA, "Watson-Crick mimicked molecularly imprinted polymer for capacitive impedimetric determination of 5-fluorouracil".

2. **Iskierko, Z.**, Sosnowska, M., Sharma, P. S., D'Souza, F., and Noworyta, K., 6th International Workshop on Surface Modification for Chemical and Biochemical Sensing, Institute of Physical Chemistry of the Polish Academy of Sciences, 8-12 November 2013, Lochow, Poland, "Development of inosine–imprinted polymer as a recognition unit in chemosensors for early detection of renal disfunctions".

3. **Iskierko, Z.**, Sosnowska, M., Sharma, P. S., D'Souza, F., and Noworyta, K., 15th International Conference on Electroanalysis, ESEAC 2014, Division of Analytical Chemistry of the Swedish Chemical Society, 11-15 June 2014, Malmö, Sweden, "Early Detection of Renal Disfunctions: Development of Inosine-Imprinted Polymer as a Recognition Unit in the Extended-Gate Field-Effect Transistor Sensors".

4. **Pietrzyk-Le, A.**, Bartold, K., Huynh, T-P., Iskierko, Z., Sosnowska, M., Ciesielczuk, A., KC, C. B., D'Souza, F., Kutner, W., Sannicolò, F. and Mussini, P. R., 65th Annual Meeting of the International Society of Electrochemistry (ISE), 31 August-5 September, 2014, Lausanne, Switzerland, "Determination of the TATAAA oligonucleotide via hybridization of the electrosynthesized molecularly imprinted polymer (MIP) bearing complementary adenine and thymine nucleobases".
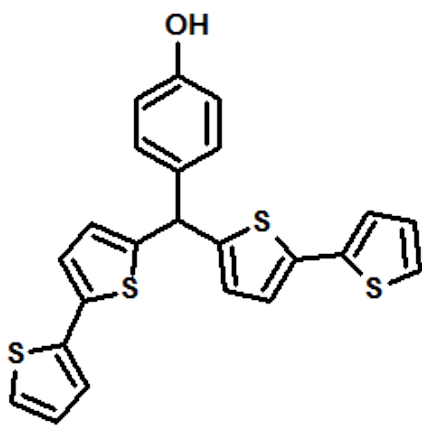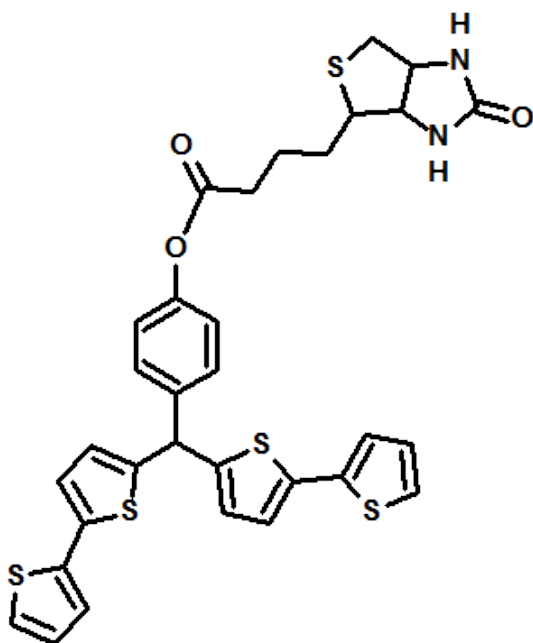
List of abbreviations

Abbreviation	Meaning
6-TG	6-thioguanine
AFM	atomic force microscopy
B-NHS	biotin N-hydroxysuccinimide ester
CA	chronoamperometry
CP	conducting polymer
CRP	redox conducting polymer
CV	cyclic voltammetry
DFT	density functional theory
DMF	dimethylformamide
DMSO	dimethyl sulfoxide
ECP	electronically conducting polymer
EDCI	(1-ethyl-3-(3-dimethylaminopropyl)carbodiimide)
EIS	electrochemical impedance spectroscopy
EQCM	electrochemical quartz crystal microbalance
FIA	flow injection analysis
FM	functional monomer
GCE	glassy carbon electrode
gp41	glycopotein 41
HIV	human immunodeficiency virus
HIV-1	human immunodeficiency virus type 1
ICP	ionically conducting polymer
LOD	limit of detection
MeOH	methanol
MIP	molecularly imprinted polymer
MS	mass spectrometry
NIP	non-imprinted polymer
PM	piezoelectric microgravimetry
SPR	surface plasmon resonance
ssDNA	single stranded DNA
ssRNA	single stranded RNA
THF	tetrahydrofuran
QCR	quartz crystal resonator

List of symbols

Symbol	Meaning
A	area, cm^2
c	concentration, M
C_{dl}	double-layer capacitance, F m^{-2}
CPE	constant phase element
D	diffusion coefficient, cm^2 s^{-1}
E	potential, V
E_{pa}	anodic peak potential, V
E_{pc}	cathodic peak potential, V
E_0	potential amplitude, V
f_0	fundamental frequency of a resonator, here 10 MHz
f	resonant frequency, Hz
G	Gibbs free energy, J mol^{-1}
I	current, A
I_0	current amplitude, A
K_s	complex stability constant, M^{-1}
k^2_{QCR}	the elctrochemical coupling factor of a quartz crystal resonator, 7.74×10^{-3}A^2 s m^{-2}
L	inductance
m	mass, g
n	number of electrons exchanged in the electrochemical process
R	resistance, Ω
R_{ct}	charge transfer resistance, Ω
R_d	dynamic resistance, Ω
R_s	solution resistance, Ω
t	time, s
T	frequency independent proportionality factor
W	Warburg impedance
v	potential scan rate, mV s^{-1}
Z	impedance, Ω
Z_{CPE}	impedance of a constant phase element, Ω
Z_{im}	imaginary part of impedance, Ω

Symbol	Meaning
Z_{real}	real part of impedance, Ω
α_{a}	charge transfer coefficient of an anodic process
α_{c}	charge transfer coefficient of a cathodic process
δ	chemical shift, ppm
θ	angle of incidence
μ_{q}	shear modulus of quartz, 2.947×10^{11} g s^{-2} cm^{-1}
μ_{L}	shear modulus of film deposired on quartz, g s^{-2} cm^{-1}
ρ_{q}	quartz density, 2.648 g cm^{-3}
ρ_{L}	density of film deposited on quartz, g cm^{-3}
ω	angular frequency
ϕ	exponential factor
φ	angular shift of current

List of functional monomers

No.	Name	Structural formula
1	4-Bis(2,2'-bithiophen-5-yl) methylphenol	
2	4-Bis(2,2'-bithien-5-yl) methylphenol biotin ester	

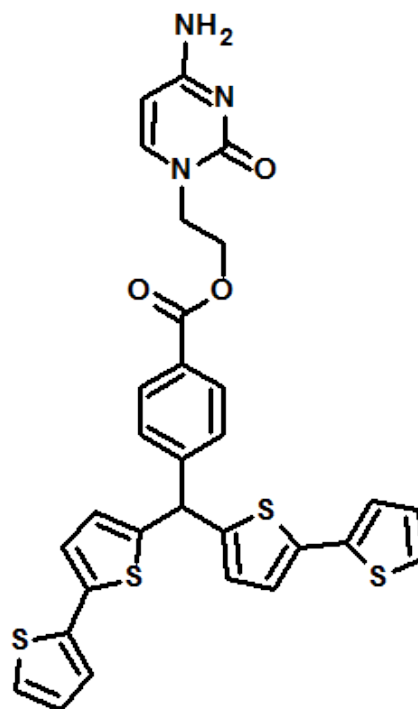| No.	Name	Structural formula
3	4-Bis(2,2'-bithien-5-yl)methylphenol glycol ether	
4	4-Bis(2,2'-bithien-5-yl)methylphenol-2-*O*-(4-tert-butylcalix[6]arene) ethoxyl ether	
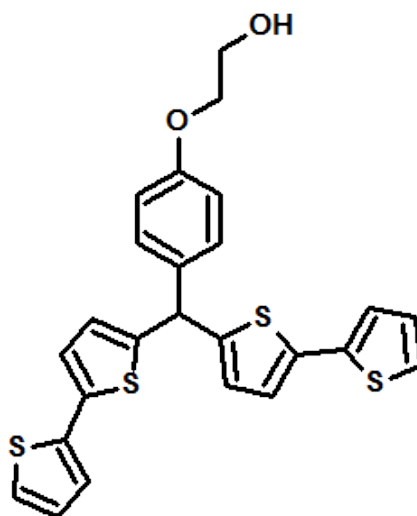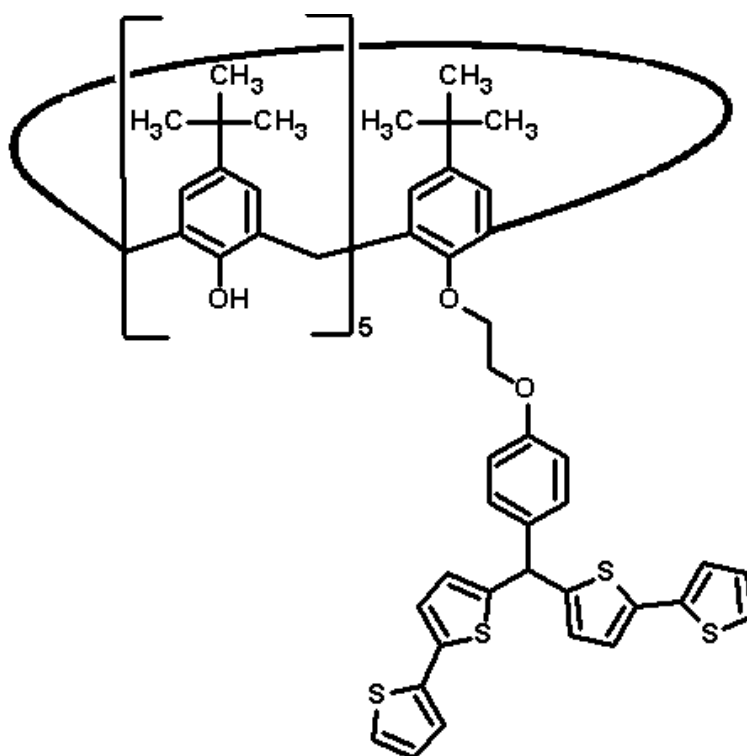
No.	Name	Structural formula
5	4-Bis(2,2'-bithien-5-yl) methylphenol 2-bromoethyl ether	
6	4-Bis(2,2'-bithien-5-yl) methylphenol 2-(1-*N*-succinimidoxy)ethyl ether	
7	4-Bis(2,2'-bithien-5-yl) methylalanine	

No.	Name	Structural formula
8	4-Bis(2,2'-bithien-5-yl)methyl-nitrobenzene	
9	4-Bis(2,2'-bithien-5-yl) methylbenzoic acid glycol ester	
10	4-Bis(2,2'-bithien-5-yl) methylbenzoic acid	

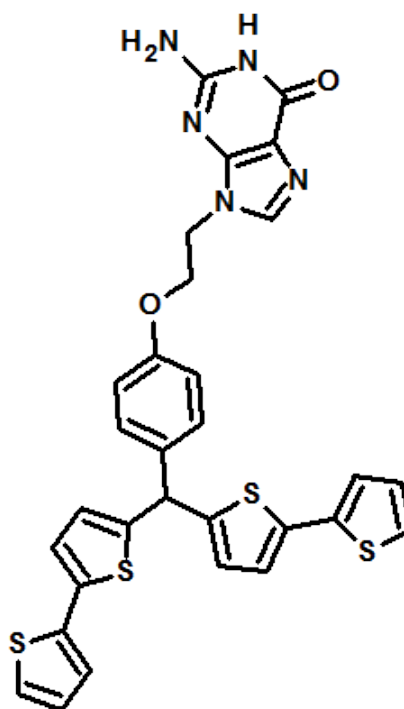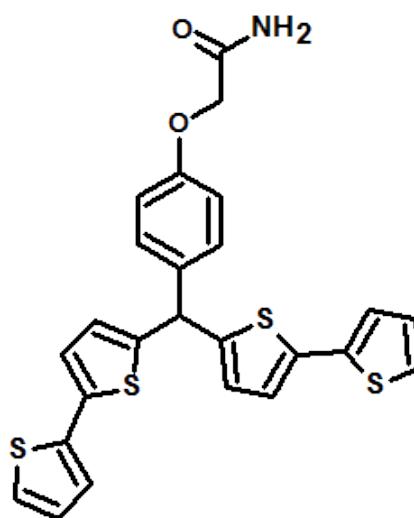| No.	Name	Structural formula
11	2-(Cytosin-1-yl)ethyl 4-bis(2,2'-bithien-5-yl)methylbenzolate	
12	4-Bis(2,2'-bithienyl)-(4-hydroxy-phenyl)methane thymine-1-acetate	
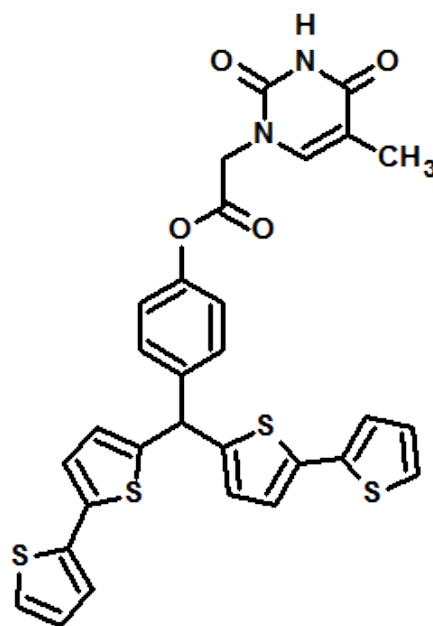
No.	Name	Structural formula
13	4-Bis(2,2'-bithien-5-yl) methylphenol 2-(guanin-9-yl)ethyl ether	
14	4-Bis(2,2'-bithien-5-yl) methylphenol 2-hydroxyacetamide ether	

No.	Name	Structural formula
15	4-Bis(2,2'-bithien-5-yl)methyl-*o*-catechol pentaethyleneglycol diether	
16	4-Bis(2,2'-bithiophen-5-yl) methyltoluene	
17	4-(1-Methylfulleropyrrolidin-2-yl)phenol-3,4-[18-crown-6] benzyl ether	
18	2-(Acetylamino)ethyl 3-formylbenzoate	

Abstract

The present Ph.D. thesis focuses on the designing and synthesizing of new functional monomers (FMs) and their use for the preparation of chemical sensors for biologically significant substances. One of the synthesised monomers was used for the preparation of a chemical sensor capable of selective determination of oligonucleotide of the nucleobase sequence characteristic for the HIV virus. For that, the FM bearing the biotin moiety was potentiodynamically electropolymerized on the surface of an electrode. On top of the resulting films, neutravidin was irreversibly immobilized by the complexation of the biotin moieties of the polymer. Finally, the recognizing biotinylated oligonucleotide was immobilized on top of the thus prepared structure by complexing the surface-immobilized neutravidin. This layer-by-layer assembly served for the determination of the target oligonucleotide. Electrochemical impedance spectroscopy (EIS) and piezoelectric microgravimetry (PM) were used for signal transduction. Analytical parameters of EIS and PM chemosensors, including the limit of detection, linear dynamic concentration range, and selectivity, were 50 nM and 0.5 pM, from 50 to 600 nM and from 0.5 pM to 30 μM, respectively. The developed method of surface modification with neutravidin was utilized for the preparation of molecularly imprinted polymer (MIP) chemosensor for the determination of myoglobin. Prepared EIS chemosensor was characterized by linear dynamic concentration range of 10 to 500 ng/mL.

Moreover, eighteen functional monomers were designed and synthesised. Sixteen of them were derivatives of (2,2'-bisbithienyl)methane and two others were [C60]fullerene derivatives. The presence of the thiophene or fullerene moiety assured polymer film formation via oxidative or reductive electropolymerization, respectively. Each FM contained a recognizing moiety in order to interact with various template molecules. Those interactions included ionic interactions, hydrogen bondings, π-π interactions, van der Waals interactions, and weak dispersion interactions.

After FM preparation, their binding capabilities were assessed via quantum-chemical calculations. For that, structures of pre-polymerization complexes of FMs with selected templates were optimized using the DFT method. Then, the energy gain of complex formation was calculated. Apparently, the synthesised FMs formed stable complexes with certain classes of templates and, therefore, could be used for the preparation of MIP films. These films then served as recognition units of the chemical sensors fabricated.

Some of the synthesized FMs were used for the preparation of chemosensors for important analytes such as 6-thiogunanine (chemotherapeutic drug), nicotine (toxin), and nitroaromatic compounds (explosives). Moreover, the MIP chemosensor for melamine, previously studied and described by the Group of Molecular Films of IPC PAS, was prepared in order to evaluate its capability to determine melamine in real samples of pet feed as well as to assess the feasibility of a new transduction platform, namely, surface plasmon resonance spectroscopy, in MIP chemosensing.

Streszczenie

Przedstawiona rozprawa doktorska opisuje przygotowanie nowych monomerów funkcyjnych (FMs) i ich zastosowanie jako elementy rozpoznające w czujnikach chemicznych i biochemicznych do oznaczania substancji o istotnym znaczeniu biologicznym. Jeden z przygotowanych FMów zastosowano do przygotowania warstwy rozpoznającej biosensora do oznaczania oligonukleotydu o sekwencji zasad nukleinowych charakterystycznej dla wirusa HIV. W tym celu na powierzchni elektrody osadzono za pomocą elektropolimeryzacji potencjodynamicznej monomer zawierający w swojej strukturze biotynę. Następnie tak przygotowaną warstwę polimeru zmodyfikowano neutrawidyną, a w kolejnym etapie biotynowanym oligonukleotydem rozpoznającym. Następnie warstwę tę zastosowano jako element rozpoznający biosensorów z piezomikrograwimetrycznym (PM) i impidymetrycznym (EIS) przetwarzaniem sygnału chemicznego rozpoznawania na użyteczny sygnał analityczny. Wyznaczono parametry analityczne wykonanych biosensorów, w tym wykrywalność (50 nM i 0.5 pM) i liniowy zakres stężeniowy (od 50 do 600 nM i od 0.5 pM do 30 μM, odpowiednio dla sensorów PM i EIS). Ponadto, opracowana metoda modyfikacji powierzchni neutrawidyną została wykorzystana do przygotowania polimeru molekularnie wdrukowanego mioglobiną. Wytworzony chemosensor impidymetryczny charakteryzował się liniowym zakresem stężeń od 10 do 500 ng/mL.

Co więcej, zaprojektowano i zsyntetyzowano osiemnaście nowych FMów. Szesnaście spośród nich to pochodne (2,2'-bisbitienylo)metanu natomiast dwa pozostałe były pochodnymi [C60]fulerenu. Podstawniki tiofenowe i fulerenowe umożliwiły przygotowanie polimerów za pomocą elektropolimeryzacji w warunkach, odpowiednio, utleniających lub redukujących. Każdy z przygotowanych FMów zawierał również podstawnik rozpoznający, aby zapewnić możliwość oddziaływania z szablonem. Oddziaływania te to oddziaływania prowadzące do wytworzenia wiązań jonowych, wodorowych, jak również oddziaływania π-π, van der Waalsa i słabe oddziaływania dyspersyjne.

Na podstawie wykonanych obliczeń kwantowo-chemicznych oceniono zdolność FMów do wiązania szablonów. W tym celu zoptymalizowano struktury kompleksów FMów z wybranymni szablonami wykorzystując teorię funkcjonału gęstości. Następnie obliczono zysk entalpii swobodnej towarzyszący tworzeniu kompleksu FMa z szablonem. Okazało się, że kompleksy te są trwałe, a zatem można je zastosować do przygotowania MIPów, jako elementy rozpoznające chemosensorów.

Wybrane FMy zastosowano do przygotowania chemosensorów do oznaczania ważnych bioanalitów, w tym 6-tioguaniny (leku chemoterapeutycznego), nikotyny (trucizny) i związków nitroaromatycznych (związków wybuchowych). Ponadto, na podstawie wcześniejszych wyników badań przeprowadzonych w Grupie Badawczej Warstw Molekularnych w IChF PAN, przygotowano chemosensor do oznaczania melaminy w celu oceny możliwości jego zastosowania do oznaczania melaminy w próbkach pasz. W chemosensorze tym wykorzystano spektroskopię rezonansu plazmonów powierzchniowych jako metodę przetwarzania sygnału chemicznego rozpoznawania na użyteczny sygnał analityczny.

Contents

Chapter 1

Critical literature review

1.1 Conducting polymers

Conducting polymers (CPs) are organic macromolecules, composed of mers, that can conduct electricity. For their discovery and development, the Nobel Prize in Chemistry 2000 was awarded to Alan J. Heeger, Alan G. MacDiarmid, and Hideki Shirakawa. According to the mode of charge propagation, conducting polymers are calssified as redox conducting polymers (RCPs), electronically conducting polymers (ECPs), and ionically conducting polymers (ICPs) [1].

Redox conducting polymers, e.g., poly(vinyl ferrocene), contain electrostatically and spatially localized redox sites covalently bound to an electrochemically inactive polymer backbone [1]. This backbone is extensively conjugated. Hence, the charge is considerably delocalized. The charge is transported by electron hopping via sequential electron self-exchange mostly between neighboring redox sites. Two processes are involved in charge transporting across a redox polymer film. One is the charge transfer across the polymer-(support electrode) interface and the other is charge percolation via electron self-exchange or hopping through the film. In the former process, redox sites located close to the electrode surface are involved, while the latter is driven by the concentration gradient of the oxidized or reduced sites in the polymer bulk. These polymers conduct only in a limited potential range and this conduction attains maximum at potential equal to the standard potential of the redox sites of the polymer. At this potential, the concentration of the oxidized and reduced sites are equal. RCPs are either preformed, and subsequently deposited onto the support electrode via dip or spin coating, or deposited by electropolymerization. Moreover, other formation routes are also accessible for this type of polymers [1–4].

In ionically conducting polymers, redox-active species are electrostatically incorporated in an ionomer (ion-exchange polymer) matrix. In this case, redox active component is a counterion to a polyionic (anionic or cationic) polymer material.

Here, conductivity is due to local electron hopping between fixed redox sites that remain immobile, similarly as in CRPs, or via physical diffusion of the incorporated redox moieties followed by electron transfer. During an ICP preparation, usually the electrode surface is first coated with an ion-exchange polymer, and then redox active ions enter the film as counterions [3].

In electronically conducting polymers, the polymer backbone itself is electronically conducting. This conductivity is imparted by addition of redox dopants in a relatively large quantity into the polymer matrix. The term "doping" is originally referred to semiconductors. Noticeably, properties of semiconductors can be tuned by adding very small quantities of foreign atoms to the lattice of the host semiconductor. This semiconductor can be made either an n or p type depending on the nature of the added dopant atoms, i.e., whether the latter have an excess or deficit of electrons. New dopant energy levels are introduced into the band gap and conduction is facilitated. The conductivity level attained strongly depends on the concentration of the donor or acceptor species incorporated. However, the doping mechanism in ECPs significantly differs from that in semiconductors. Firstly, a redox species is used for doping. Secondly, the doping level is significant; it can be as high as 10 mole percent. Furthermore, charge is transferred between the incorporated dopant and the polymer chain. Hence, the latter is partially oxidized or reduced. The partial oxidation of the polymer chain results in p-type doping. It involves electron removal to form a positively charged repeat unit. The ECP partial reduction leads to n-type doping. ECPs can be doped either electrochemically by applying suitable potential or chemically by using appropriate oxidizing or reducing agents. Nature of charge carriers in ECPs depends on the type of the polymer. Charge is carried by defects that are delocalized over a number of repeat units on the polymer chain [2]. In contrast to RCPs, ECPs conduct over a wide potential range. To a large extent, the potential range of conductivity is governed by the chemical nature of the polymer and it can, therefore, be synthetically controlled. This type of conducting polymers is usually generated via in situ electrodeposition, although other paths of deposition are also available. By way of example, structural formulas of few conducting polymers are shown in Scheme 1.1.

The list of conducting polymer applications is long, starting from application of thin CP films to antistatic coatings, microwave absorption, parts for microelectronics, and corrosion protection through construction of electroluminescent and electrochromic devices, materials of membranes and ion exchangers, artificial muscles, materials for batteries and other energy technologies like supercapacitors ending on chemical sensors [3]. Basis for most applications is conductivity. But CPs have also other useful properties that differ them from metals, e.g., flexibility, ease of deposition on various surfaces, and possibility to tune their properties by synthesis of
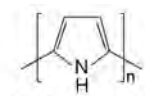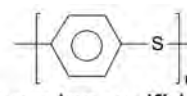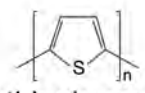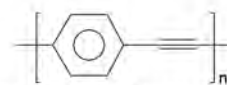
2
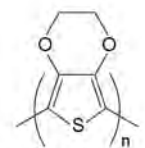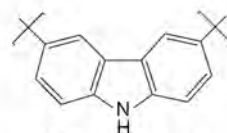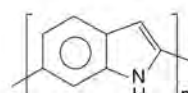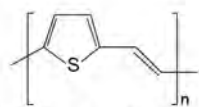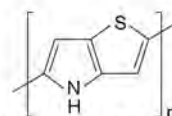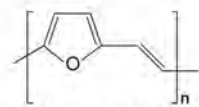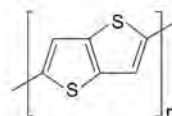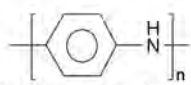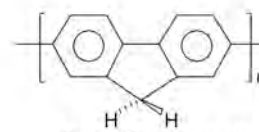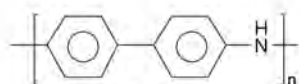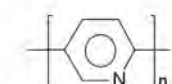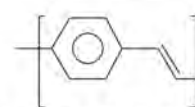
Scheme 1.1 Structural formulas of the most typical conducting polymers in their undoped forms. (Adapted from [4].)

dedicated monomers of desired properties.

ECPs of lower conductivity (100-200 S cm^{-1}) are used as electromagnetic shielding and electrostatic discharge materials [5]. ECPs of higher conductivity and those revealing electroactivity (CRPs) are used for charge storage in rechargeable batteries, supercapacitors, and fuel cells [6]. Moreover, these materials can be used in photovoltaic systems [7], displays as electrically stimulated light sources [8,9], and electrochromic devices [10]. One of the less obvious application is for the preparation of electromechanical actuators, so called artificial muscles [11]. Moreover, CPs can be utilized in membrane preparation for separation applications [12, 13] and controlled release devices [14], or coatings for corrosion protection [15].

Another wide application of conducting polymers involves preparation of chemical sensors [16,17]. Many different systems utilizing conducting polymers for sensing applications have been described so far. The SciFinder search of combination of key words 'conducting polymers' and 'sensors' results ins ~3400 hits. Those sensors can detect small species like simple ions [18, 19], small organic molecules [20, 21], and macromolecules, like proteins and enzymes [16, 22], as well. In herein described research, thiophene and fullerene derivatives were designed and synthesized for sensor preparation. Therefore, those two classes of compounds are shortly described below.

1.1.1 Thiophene based conducting polymers

Polythiophenes are formed from cyclopentadiene molecules that have the sulfur heteroatom in their structure. Because of high chemical and electrochemical stability both in dry air and in moisture in a doped and undoped state [23], polythiophene films have attracted considerable attention.

Thiophenes can be polymerized through oxidation initiated either chemically or electrochemically. In case of chemical polymerization, different initiators are used, e.g., copper(II) perchlorate, iron(III) chlorate, or molibdenium(V) chlorate [4]. Moreover, light-induced polymerization is possible. For instance, thiophenes dimerize after irradiation with 150 W xenon lamp [24]. In case of electrochemical formation of a thiophene polymer, anodic current or potential applied initiates the polymerization. This process involves formation of cation radicals, which then react with one another to form a polymer structure. Therefore, a counterion (anion) is incorporated into the polymer matrix during polymerization to balance the positive charge generated on the polymer backbone. Scheme 1.2 shows the mechanism of thiophene polymerization.

Several factors need to be taken into consideration while preparing polythiophene films of desired properties. The solvent nature is one of them. For instance, even small amount of water present in the solution for polymerization causes mislinkages
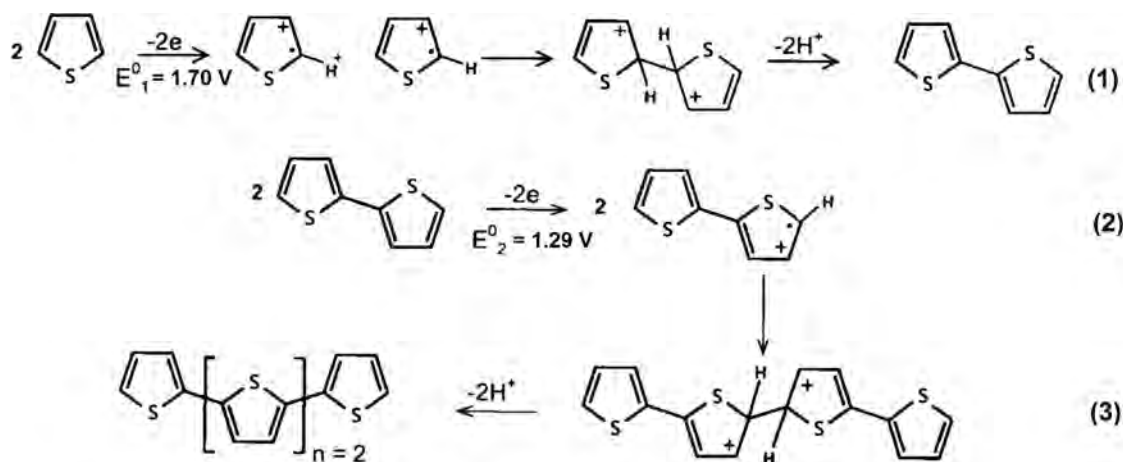
Scheme 1.2 The proposed mechanism of thiophene and oligothiophene polymerization. (Adapted from [25].)

deteriorating polymer properties. Moreover, a minimum thiophene concentration needed for polymerization depends on the solvent used. That is, if solvents of high electric permittivity are used the minimal monomer concentration needed for effective polymerization is lower than that if solvents of low electric permittivity are used. Another important factor is the nature of a counter ion. For example, the initial rate of oxidation was the highest for the ClO_4^- dopant compared to that for the PF_6^- and the BF_4^- dopants [26].

Apparently, the polymer itself is overoxidized at potentials required to oxidize the thiophene monomer [4]. This overoxidation results in deterioration of chemical and physical properties of the polythiophene obtained. Therefore, the polymer prepared is a mixture of polythiophene and overoxidized polythiophene if electropolymerization is performed under either galvanostatic or potentiostatic conditions. Fortunately, substitution of bithiophene in β position with certain functional groups can decrease its oxidation potential, thus allowing to avoid this overoxidation. Similarly, for bithiophenes or terthiophenes, used as starting materials for electropolymerization, this potential is much lower than that for thiophene. The influence of selected substituents on the monomer oxidation potential is presented in Figure 1.1 [23]. The cyclic voltammetry anodic potential shift for the monomers considered linearly correlates with the Hammet constant of the substituent. This shift depends upon three parameters, namely, the polar, steric, and mesomeric effect exerted by the substituents. Importantly, electrophilic substituents hinder the electropolymerization because the polymerization mechanism involves removal of the π electron from the thiophene ring.

Moreover, properties of polythiophenes strongly depend upon the nature of the polymerization starting material. Because of the above mentioned thiophene overoxidation during electropolymerization the use of substituted thiophenes, e.g., alkylated monomers, will result in polymers of much higher conductivity than that of
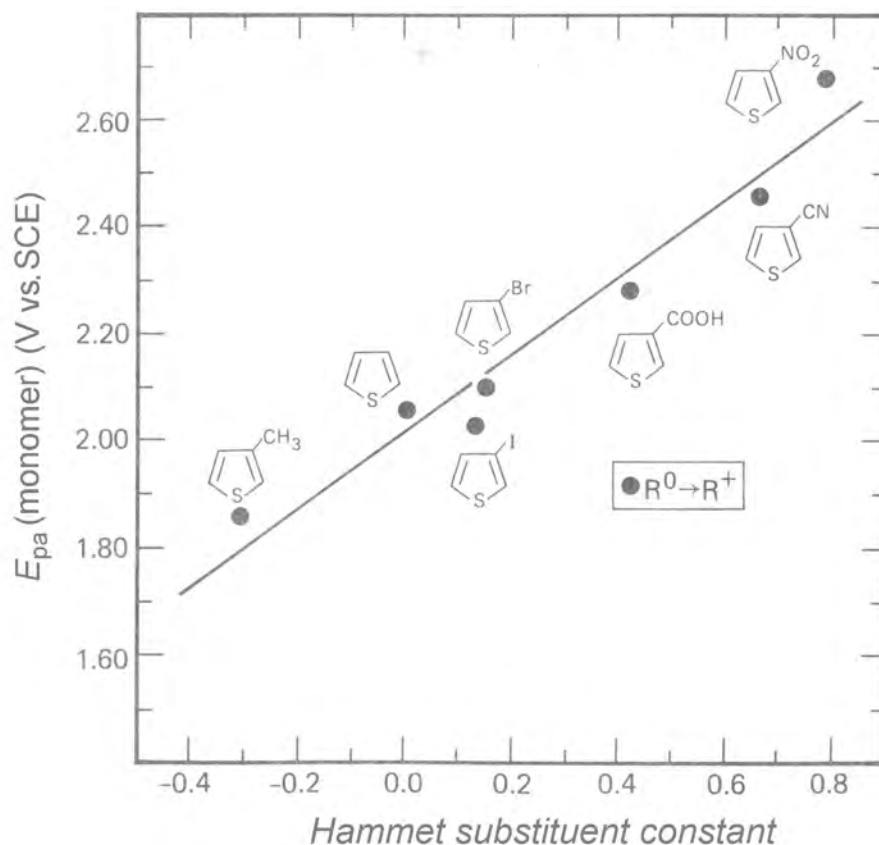
Figure 1.1 Cyclic voltammetry anodic peak of oxidation of substituted thiophene monomers versus the respective Hammet substituent constant [23].

the unsibstituted polythiophene. For instance, conductivity as high as 7 500 S cm^{-1} was reached for poly(methylthiophene) [27]. Moreover, thin polymer films are more conductive than those thicker [28]. Interestingly, conductivity of polymers prepared via chemical polymerization is lower than that prepared via electropolymerization because the counter ion doping level is, generally, lower for the former [4, 23].

1.1.2 [C60]Fullerene based conducting polymers

A lot of effort has been paid to incorporate fullerenes into a polymer matrix in hope that the resulting materials will retain useful properties as fullerenes themselves [29]. Polymers containing [C60]fullerene can be prepared using different synthetic strategies. That is [C60]fullerene can be a part of the main polymer chain or a pendant on the polymer chain. Possible structures of polymers containing [C60]fullerenes are shown in Scheme 1.3. These polymers can conduct electricity because of π electrons on the [C60]fullerenes cages. However, properties of a polymer chain in between fullerene molecules and distance between these molecules are another important factor determining conductivity of heteropolymers containing [C60]fullerenes.

Fullerene homopolymers (**1** in Scheme 1.3) can be formed through 2+2 cycloaddition induced by excitation with photons [32], electrons [33], plasma discharge [34],
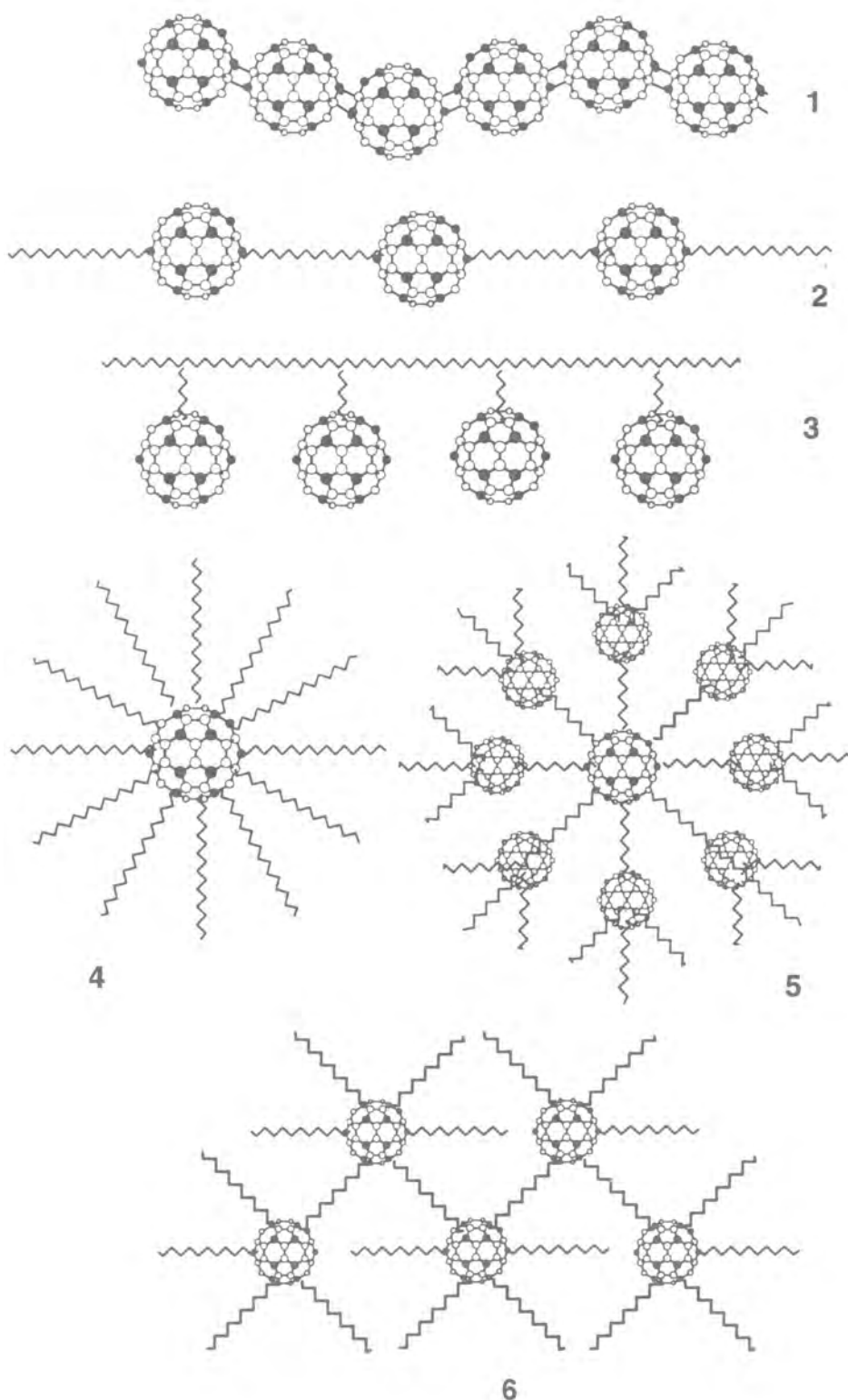
Scheme 1.3 Schematic view of the fullerene homopolymer **1**, the fullerene-derived main chain polymer "pearl necklace" **2**, the fullerene-grafted side-chain polymer **3**, "charm bracelet", the fullerene-derived starbust polymer **4**, the fullerene dendrimers **5**, and the fullerene-crosslinked polymer network **6**. (Adapted from [30] and [31].)

or application of high pressure [35]. However, stability of these homopolymers is relatively low [31].

Charm-bracelet polymers of [C60]fullerenes (**3** in Scheme 1.3) can be formed using two different methods. One involves reaction of a pre-formed polymer with [C60]fullerene and the other polymerization of a monomer containing C_{60} moieties [36].

Fullerene-derived starbust polymer (**4** in Scheme 1.3) can be prepared using many different ways. The one most often described in literature involves anionic reactions that can lead to formation of a six-arm star [37].

Another example of polymers containing [C60]fullerenes are polymers of dendrimeric architecture (**5** in Scheme 1.3); many examples of these polymers were described [38].

From the point of view of the polymer electric properties, namely, conductivity, the "pearl necklace" [C60]fullerenes polymers are of interest (**2** in Scheme 1.3). In this type of structures, fullerenes are interconnected with each other by either an aliphatic chain or a transition metal ion that can be complexed. Scheme 1.4 shows a layout of the structure of the [C60]fullerene derived polymer film with metal ions incorporated into this structure. This type of a polymer film can be formed chemically or via electroreduction of [C60]fullerenes in the presence of a suitable complex of a transition metal, e.g., platinum(II) or palladium(II). Because synthesis of the [C60]fullerene derived monomers presented herein aims at electroreductive polymerization with Pd(II) acetate, this polymerization method is shortly described below.

M = Pd, Pt, Ir, Rh, Au, Ag
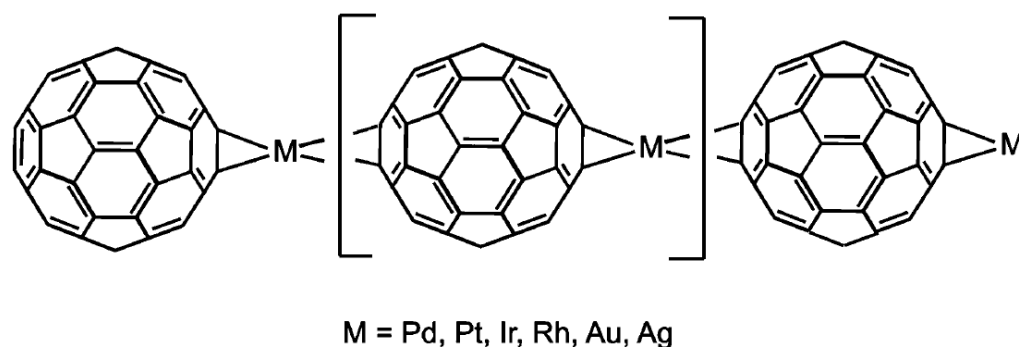
Scheme 1.4 Schematic structure of a two-component polymer formed from [C60]fullerenes and transition metals [31].

For deposition of polymer films of [C60]fullerene with transition metal ions, first, the fullerene needs to be dissolved in solution containing a transition metal complex and a supporting electrolyte. Next, the negative potential must be applied in order to form a zero-valent metal intermediate. This intermediate formation initiates the polymer film growth. During that process however, nanoclusters of a metallic phase may be simultaneously deposited if the ratio of [C60]fullerene to precursors, i.e.,

transition metal complexes is too low [39]. A list of precursors that can be used in this polymerization is presented in Table 1.1 [31].

Table 1.1 Complex precursors of electropolymerization of [C60]fullerene with transition metal ions [31].

Transition metal	Complex precursor
Pd	$[Pd(CH_3CO_2)_2]_3$ $Pd(CH_3CO_2)_2$ $Pd(PhCN)_2Cl_2$ *trans*-$PdCl_2(py)_2$
Pt	*cis*-$PtCl_2(py)_2$ *trans*-$PtCl_2(py)_2$ $PtI_2(py)_2$ $[Pt(\mu$-$Cl)Cl(C_2H_4)]_2$
Rh	$[Rh(CO)_2Cl_2]_2$ $[Rh(CF_3CO_2)]_2$ $Rh(1,5$-$COD)_2SO_3CF_3$ $RhCl_3(py)_3$
Ir	$[IrCl(cyclooctane)_2]_2$ $Ir(CO)_2Cl(p$-toluidine)
Au	$AuCl(AsPh_3)$ $(CH_3)_2SAuCl$
Ag	$Ag(CH_3CO_2)$

1.2 Molecularly imprinted polymers

The conducting polymer use for the preparation of molecularly imprinted polymers (MIPs) has already been well established as a field of research with hundreds of research papers published every year. The main goal of MIP preparation is to fabricate a cheap material that is capable of selective analyte binding. This selectivity is reached by imprinting molecular cavities within the polymer matrix that are compatible in shape, size, and orientation of their recognition sites to the template molecule. For the cavity formation, first, a pre-polymerization complex of the template with functional monomers (FMs) must be formed in solution. Then, the polymerization is induced, often in the presence of a cross-linking monomer in order to assure polymer rigidity. Next, the template is extracted from the polymer film leaving behind empty molecular cavities. At this step, the polymer is ready to use, i.e., it is capable of analyte binding. For compatibility of the molecular cavity and the analyte molecule, the template used in the first step of MIP preparation is either the analyte itself or its close structural analogue. Scheme 1.5 shows consecutive steps of MIP preparation exploiting different binding possibilities. Based on the binding mode used for the preparation of the pre-polymerization complex, the imprinting can be classified into three categories, namely, covalent, semi-covalent, and non-covalent imprinting. All of these methods of imprinting are shortly described below.

In case of covalent imprinting, the template molecule is covalently bound by FMs (for simplicity, the idea of FM is described below in the present Section). The most common ways of covalent imprinting involve formation of a reversible Schiff's base [41] and a boronate ester [42–44] for binding compounds, such as amines and
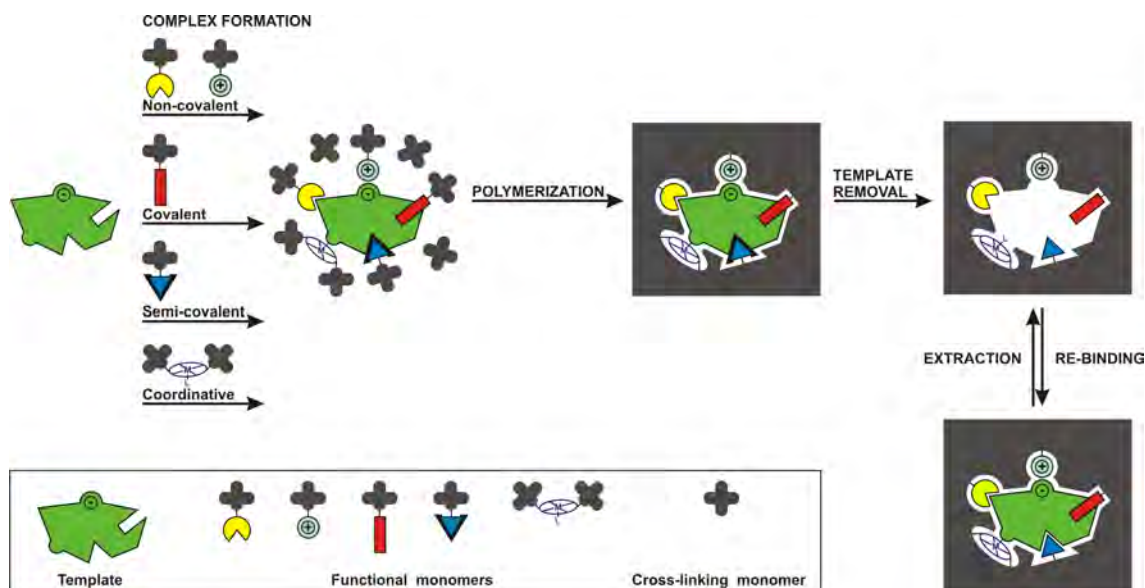
Scheme 1.5 Consecutive steps of MIP preparation utilizing different binding possibilities [40].

diols, respectively. The main advantage of covalent imprinting consists in strict control of stoichiometry of the template molecule binding with FMs, which results in formation of homogenous molecular cavities in the polymer and, therefore, limited non-specific binding. Moreover, strength of the covalent bond is independent of dielectric properties of the medium. This is a very important factor that needs to be considered if non-covalent binding is involved, as the strength of most interactions, e.g., hydrogen bonds, strongly depends upon nature of the solvent used. Still, covalent imprinting has its drawbacks, the most important one is a limited scope of functional groups that can be involved in this type of imprinting.

Another approach to MIP preparation involves the use of FMs that can form a covalent complex with the templates on the one hand and are capable of non-covalent interaction with the analyte after polymerization and template removal on the other. This approach, referred to as semi-covalent imprinting, was introduced by Whitcombe as early as in 1995 [45]. Most often, this imprinting involves formation of ester bonds. Then, these bonds yield free carboxylic groups in the polymer cavities that can bind the analyte through hydrogen bonds [46–50]. Moreover, this method can be used to generate cavities featuring recognition sites interacting with the analyte other than carboxylic group, e.g., the hydroxyl [51, 52] or amine group [53]. This imprinting, similarly to covalent imprinting, allows for formation of homogenous molecular cavities. Moreover, these cavities operate after template removal just as cavities prepared by non-covalent imprinting.

In the MIP literature, non-covalent imprinting is most often encountered [54]. This imprinting allows for easy and straightforward preparation of a pre-polymerization complex in solution. Then, both FMs and templates are dissolved in a solution

to form a pre-polymerization complex. Non-covalent interactions, i.e., hydrogen bonds, electrostatic interactions, hydrophobic interactions, and van der Waals interactions, all contribute to this complex formation. Therefore, no initiation of complex formation is necessary. This is the main advantage of this imprinting method. Another advantage is easy template removal from an MIP that does not require harsh conditions, which might influence the polymer structure.

Furthermore, preparation of MIPs utilizing coordination bonds is possible. In this case, FM contains a metal atom that can form a coordination bond with an atom of the template molecule [55–58]. Moreover, it is possible to use a combined approach by mixing monomers interacting with the template in different ways, e.g., in a combined semi-covalent and non-covalent way [59], or coordination binding and non-covalent binding [55].

A crucial step in the MIP design is selection of proper FMs. The FM is a compound that not only is capable of polymer formation but it bears functionalities that can interact with the template. So, the FM is typically composed of two parts, one being a polymerizing moiety and the other being a functional group or a site capable of analyte binding, this group is often called a recognizing moiety. Sometimes a spacer between polymerizing and recognizing moieties is introduced as well in order to assure formation of molecular cavities of pre-defined properties. Scheme 1.5 summarizes functional monomers used for different types of template-monomer interactions, and Scheme 1.6 shows parts of FM structure.
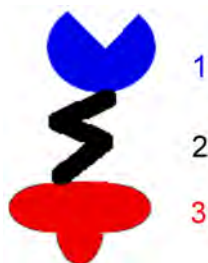
Scheme 1.6 Schematic view of a functional monomer FM and its parts (1) functional moiety, (2) spacer, and (3) polymeryzing moiety. (Adapted from [40].)

The role of the polymerizing moiety (3 on Scheme 1.6) is to assure polymer formation. Because of a large variety of recognizing sites that can be used for FM preparation, many types of polymers and many methods of polymerization are now available. From the point of view of sensor application, conducting polymers are of special interest. This is because they can easily be deposited on surfaces of conducting or semiconducting solids that can be then combined with different transduction schemes. Moreover, most monomers that can form conducting polymers can easily be modified with functional groups. Chemistry of monomers, such as pyrrole [60,61], thiophene [62], aniline [63], and phenols [64], have been widely studied. In order

to polymerize those monomers, two approaches are used, viz., a chemical and electrochemical approach. Chemical synthesis of polymers usually involves monomers that polymerize oxidatively and, therefore, oxidizing chemical agents need to be used for that, e.g., $FeCl_3$ or $(NH_4)_2S_2O_8$. In the case of electrochemical polymerization, the current or potential applied initiates the process. Advantageously, the rate of polymer nucleation and growth can readily be controlled in this approach by proper selection of the electropolymerization parameters. That is, the film thickness is controlled by the amount of charge passed during film deposition and the film morphology by suitable selection of an appropriate solvent and supporting electrolyte [65].

As mentioned above, the role of the FM recognizing moieties is to bind the analyte. In order to assure successful binding of many different analytes, many different functionalities are introduced into FM. For simplicity, the recognizing moieties described in literature are categorized according to the type of interaction of the FM with the analyte.

The first category of FMs include those binding an analyte via hydrogen bonds. For this type of binding, FMs should bear a donor or acceptor of the hydrogen bond. Therefore, FMs containing simple groups, such as hydroxyl [55,66,67], amino [68–70], carboxy [18, 71, 72], or amido [73, 74] groups fall into this category. Moreover, more complicated assemblies were proposed, e.g., FMs containing urea [75] and groups that mimick interactions encountered in natural receptors, e.g., interactions leading to the Watson-Crick nucleobase pairing. For that, FMs having, i.a., the uracil [73], cytosine [76,77], or guanine [78] recognition unit, were synthesized.
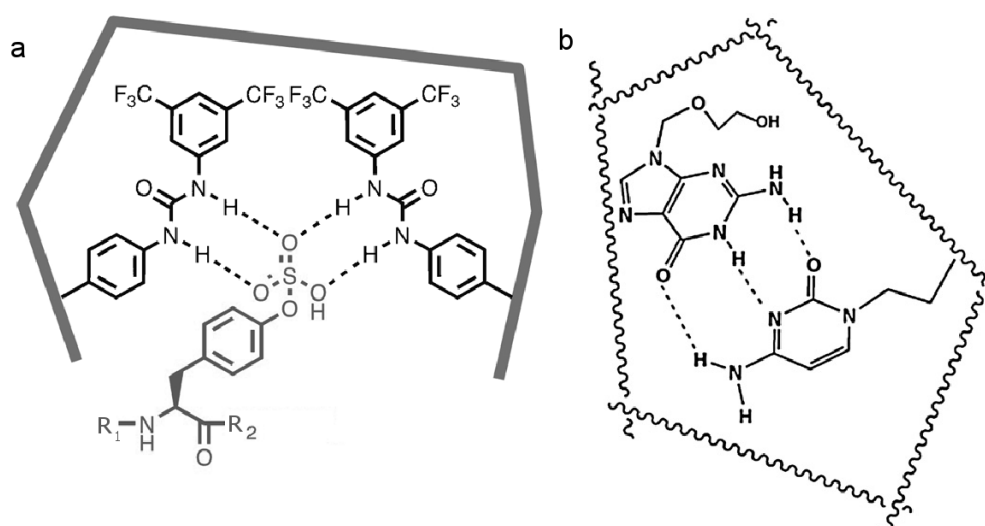
Figure 1.2 An example of analyte binding with a functional monomer via hydrogen bonds (a) short peptide containing sulfonated tyrosine interaction with the urea recognizing moiety [75] and (b) acyclovir interaction with the cytosine recognizing moiety [77].

Another type of FMs consists of monomers that bind an analyte through coordination bonds. Here, FMs containing a metal atom in their structure can serve as illustrative examples. This metal atom binds the electron-rich analyte atoms, e.g., nitrogen or oxygen atoms. Example of FMs using this interaction are those containing (i) the Tb(III) ion coordinating oxygen atoms of dipicolinic acid [79], (ii) the Pt and Fe atoms coordinating nitrogen and oxygen atoms of 8-hydroxy-2'-deoxyguanosine [58], and (iii) the Zn atom for coordination of the nitrogen atom of the nicotine analyte [55, 56]. Advantageously, these FMs interact with the analyte molecules more strongly than the FMs utilizing non-covalent interactions. However, selectivity of the MIP cavity cannot be justified solely on this interaction; selectivity can be assured by other parameters of the cavity too, e.g., its size. Moreover, introduction of another FM for the analyte binding can serve that purpose.
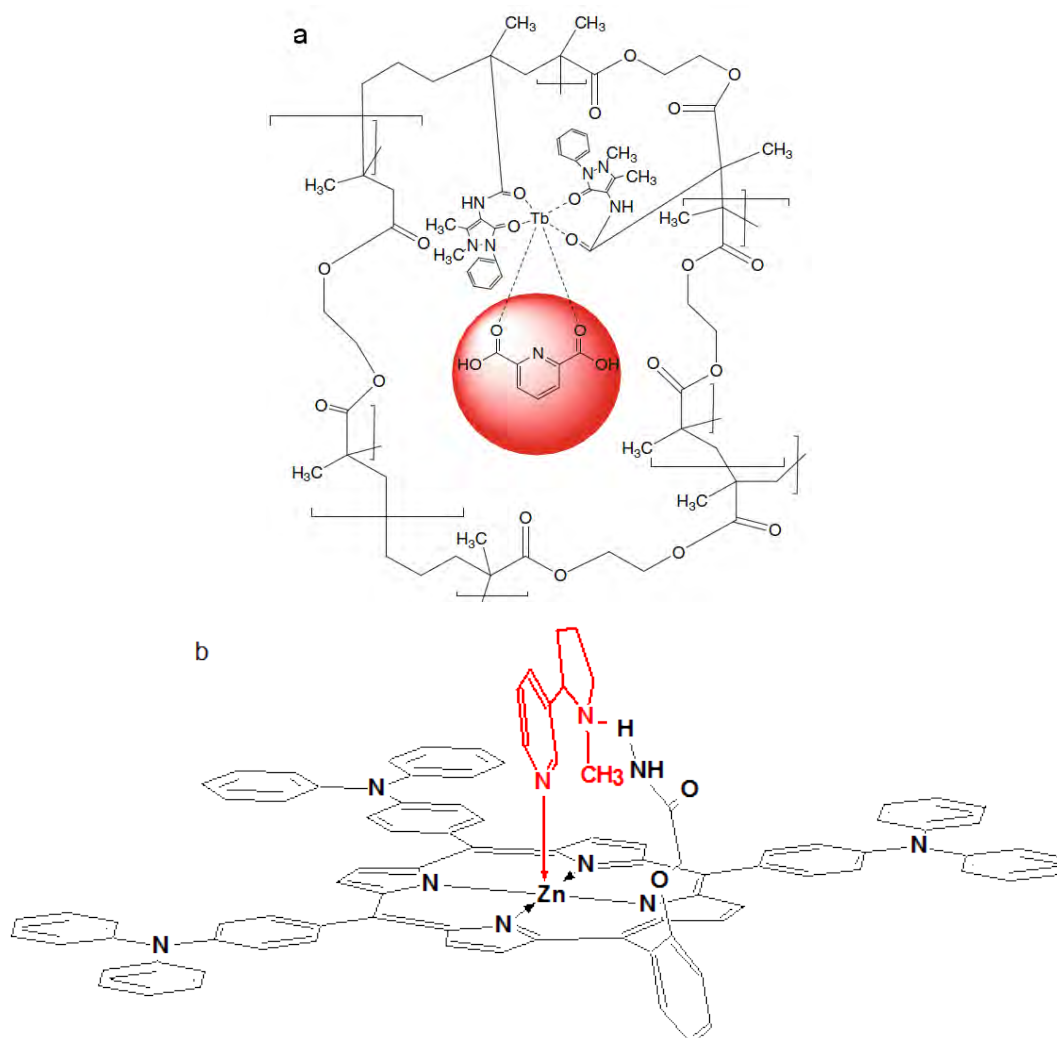
Figure 1.3 An example of an analyte binding with a functional monomer utilizing coordination bonds (a) dipicolonic acid analyte interaction with the recognizing moiety containing the Tb(III) atom [79] and (b) the nicotine analyte complex with the recognizing moiety containing the Zn(II) atom [56].

Interactions with ions, either anions or cations, can serve for designing another group of FMs. In this group, there are FMs containing cations and/or anions in their structures as well as those capable of interacting with ions. An example of a charged FM is the derivatized monomer of a zwitterionic betain structure. Because of that, it can bind analytes, such as carnosine [80]. Another example of the charge-bearing FMs is a monomer containing the SO_3^- group for fenbufen binding [81] and a monomer containing charged imidazolium group for caffeine binding [82]. Another approach is to design an FM that is capable of cation or anion binding. An illustrative example of such an FM is that containing a crown ether moiety in its structure because crown ethers bind cations [83].
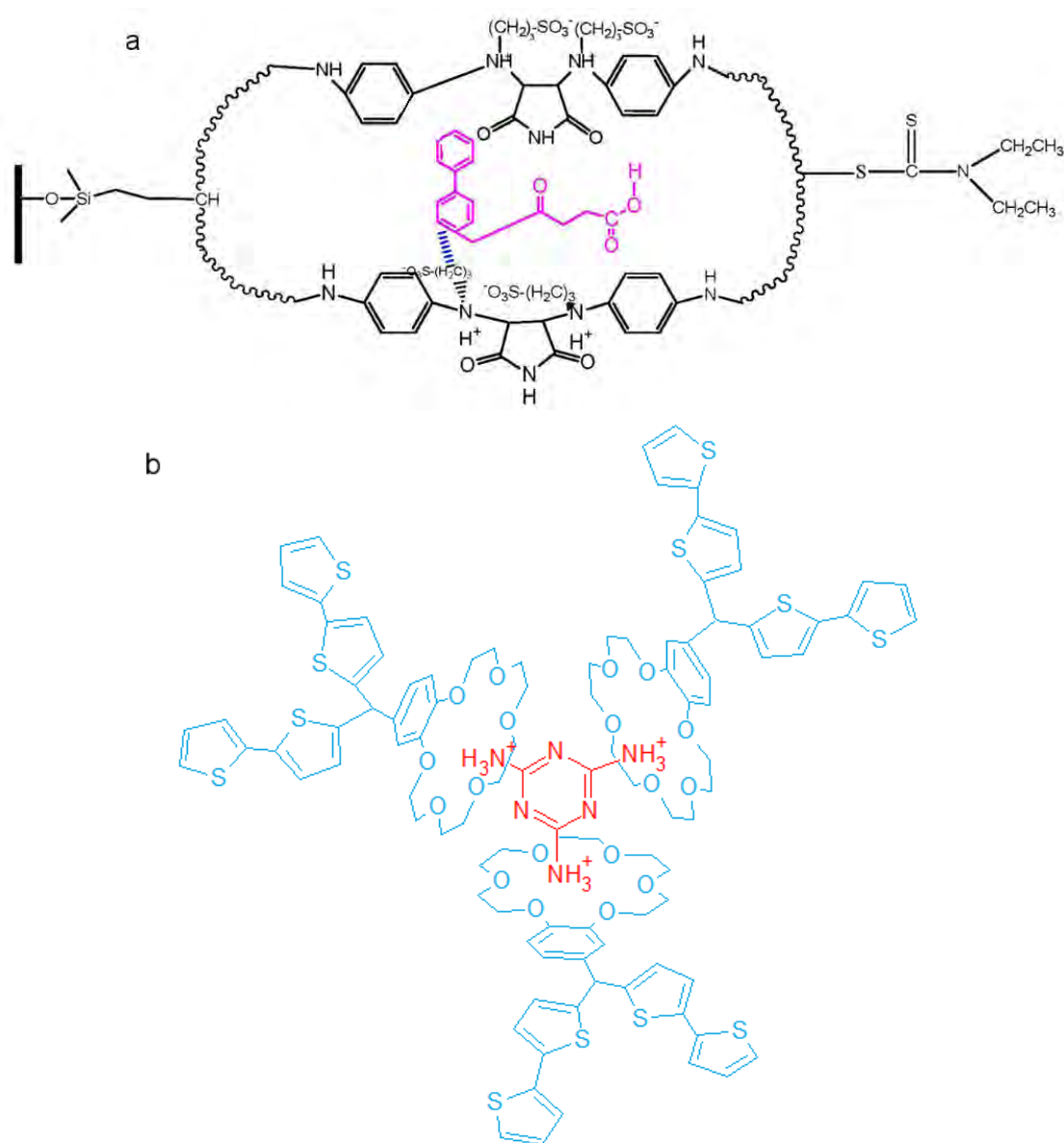
Figure 1.4 An example of analyte binding with a functional monomer via interactions of charged groups (a) fenbufen analyte binding with anionic groups of FM [81], (b) protonated melamine binding with FM containing crown ether moiety [83].

Another group of FMs consists of those that utilize weak interactions for analyte binding. These interactions include van der Waals interactions, π-π interactions, and hydrophobic interactions. 2-Mercaptobenzimidazole used to bind melamine through π - donor-acceptor interactions [84] and graphene oxide used as a part of an MIP for binding pentachlorophenol [85] may serve as examples of FMs utilizing this type of interactions.
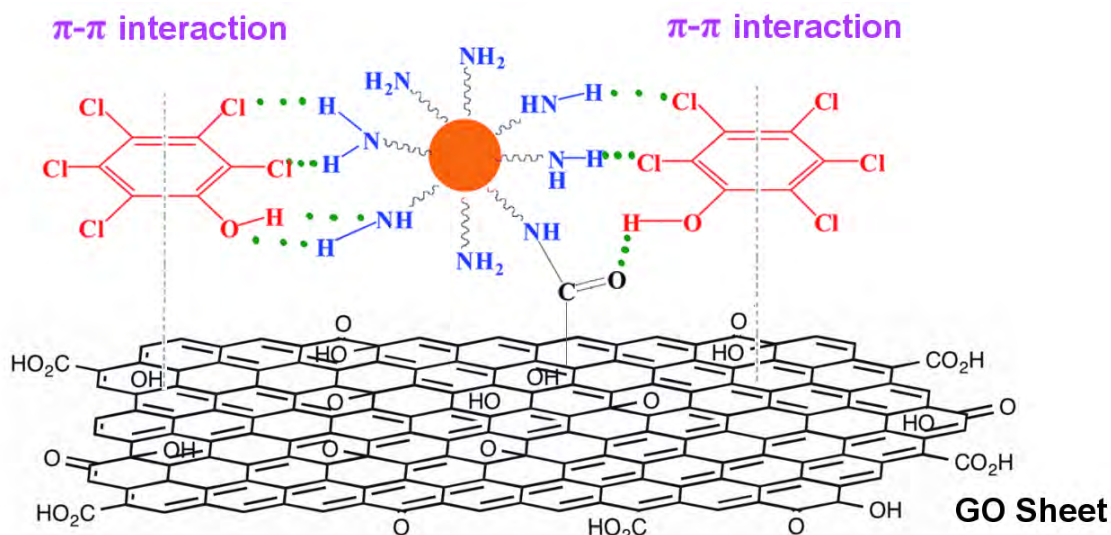
Figure 1.5 An example of analyte binding by an MIP via π-π interactions with pentachlorophenol by graphene oxide (GO). (Adapted from [85] and [86].)

Once a proper FM is designed and synthesized, it is then used for MIP preparation. In fact, this MIP can be utilized in many ways. Most popular MIP applications include preparation of materials for separations. Towards that, these materials are used as supports in the chromatography or solid phase extraction systems. Another widely discussed and studied MIP application involves chemical sensors. One more interesting emerging field of research is focused on MIP application in catalysis. Although other applications of MIPs are proposed, they are not discussed herein, because research presented in the present thesis focuses on preparation of chemical sensors.

The main idea behind MIP fabrication was to replace so far used biological recognition systems, e.g., antibodies and enzymes, in preparation of recognition units of biosensors. Therefore, initial target analytes of the MIP chemosensors include a variety of templates that are of biological significance. Moreover, analytes that are not naturally present in the environment can be detected using MIPs designed in the same way as those for naturally occurring analytes. Targets of imprinting for chemosensor applications are categorized in three groups. Each group is shortly described below. Moreover, two examples of working sensors prepared using molecular imprinting for the determination of targets selected from each group are provided.

The first group of targets consists of very small molecules, mostly simple ions. An illustrative example of such a sensor is the recently reported conductivity chemosensor for the determination of Cu^{2+}. This chemosensor was based on imprinting via coordination of Cu^{2+} with the *N*-vinyl-2-pyrrolidone FM [87]. Copper chloride was used for imprinting and detectability reached the level of 0.02 μM Cu^{2+}. Moreover, selectivity of this chemosensor with respect to other divalent cations, such as Ni^{2+}, Zn^{2+}, and Co^{2+}, was high. This chemosensor was tested for Cu^{2+} determination in real water samples. It allowed for a very fast measurement with the still acceptable response time of 1 min. Moreover, imprinting can be used for the determination of anions, e.g., phosphates. A chemosensor, prepared using the FM bearing thiourea for phosphate binding [88], can serve as an example. In the presented work, an MIP imprinted with phosphate was used for fabrication of a recognizing membrane incorporated into a conductivity chemosensor. The chemosensor proved to be useful for phosphate determination in waste water samples with the limit of detection equal to 0.16 mg L^{-1} phosphates and the linear concentration range extending to 60 mg L^{-1} phosphate. Since the EU directive specifies the maximum annual mean total phosphorus concentration of 1 mg L^{-1} in waters, the prepared chemosensor was useful for phosphate determination in real water samples.
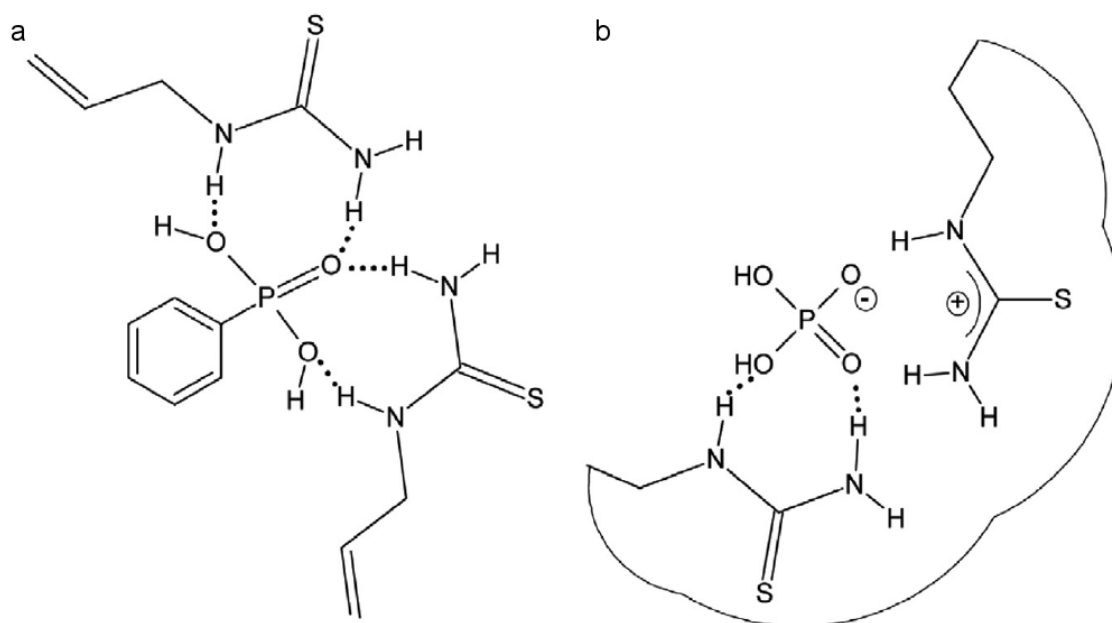
Figure 1.6 An example of ion imprinting (a) a pre-polymerization complex of the phospate anion interacting with two FM molecules bearing thiourea groups and (b) the cavity of an MIP interacting with the phosphate anion [88].

The second group includes analytes of low molecular weight (at the level of hundreds Da). Molecular imprinting of this group of analytes is most widely studied. This is because small molecules have limited number of binding sites that can interact with FMs and, therefore, they can easily be designed to fit a particular

molecule. Sometimes it is possible to use different FMs for each site available for binding, thus assuring high selectivity. An example of a chemosensor utilizing three binding sites of an analyte is an MIP sensor of atrazine [57]. Atrazine is a herbicide that must be quantified because of its toxicity. The chemosensor response was based on changes of fluorescence of functional monomers serving also as fluorescence probes of atrazine binding. The limit of detection reached was as low as 1.8 μM atrazine and selectivity with respect to other herbicides of similar molecular structure was high. These results proved that this chemosensor was suitable for atrazine determination in real samples. Another chemosensor utilizing multiple binding of an analyte is the chemosensor for metronidazole [89]. Importantly, metronidazole should be determined because it is a potential genotoxic agent. Therefore, its use is banned in many countries. However, metronidazole can still be found in meat. A chemosensor reported was based on a current signal of oxidation of metronidazole accumulated in the MIP cavities. Very high selectivity to interferences of similar structures, high detectability of few ng L^{-1}, and the linear dynamic concentration range of 9.9 to 130.0 ng L^{-1} atrazine were achieved.
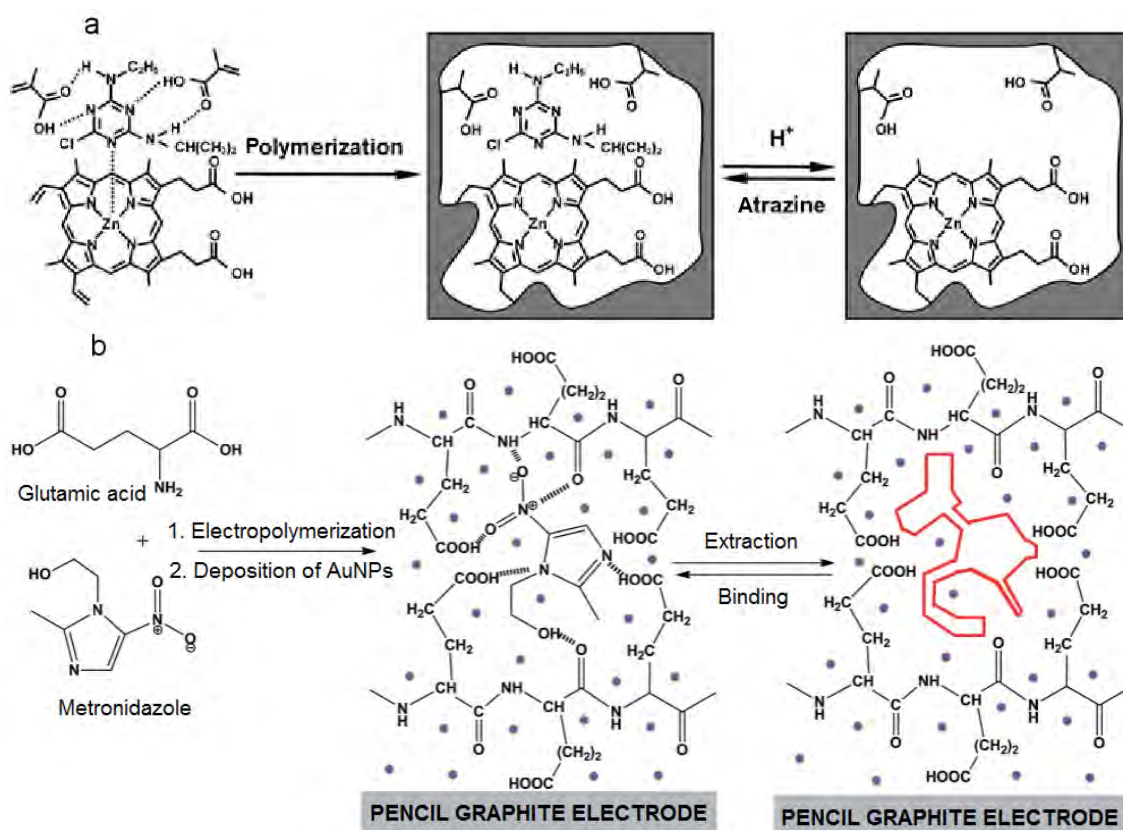
Figure 1.7 Examples of low-molecular-weight analytes used for MIP preparation. (a) An MIP with atrazine imprinted via three-point binding [57] and (b) an MIP with metronidazole imprinted via six-point binding [89].

The third group consists of high-molecular-weight biocompounds, such as peptides, proteins, oligonucleotides, and enzymes. Imprinting of these compounds i

still challenging because of complexed structure of the target molecules, their sensitivity to environmental conditions, and their low concentration in real samples. One way to approach this task is to imprint the so called epitope, i.e., a small, peripheral fragment of a protein. The idea of this way of imprinting is presented in Scheme 1.7. An example of an MIP prepared that way can be that of a chemosensor for the determination of glycoprotein 41 (gp41). This protein is related to human immunodeficiency virus type 1 (HIV-1) [90]. Since gp41 is an expensive biomacromolecule, a 34-peptide-long fragment of this protein, i.e., an epitope, was used as a template for imprinting. Dopamine served as both an electropolymerizable FM and a cross-linking monomer. After MIP film deposition on surface of a quartz crystal resonator, and then template removal, the chemosensor was used for gp41 determination. The chemosensor was capable of protein detection at the concentration level of single ng mL^{-1} gp41 at high selectivity with respect to other proteins of similar structure, namely, mutated gp41 protein with various number of aminoacids different from the template molecule. Moreover, the chemosensor was successfully used for gp41 determination in human urine.

Another approach involves imprinting of a whole protein [91–94]. A representative example of this imprinting is preparation of a chemosensor for concovalin A [91]. First, the protein was immobilized on an electrode surface through self assembly of mannose, bound to the surface, and concovalin A. Next, a film of the MIP templated with concovalin A was deposited through electropolymerization on the electrode surface. Subsequently, the concovalin A template was removed from the MIP. Consecutive steps of chemosensor preparation are shown in Scheme 1.8. The concovalin A binding to the MIP was real-time monitored by the QCM measurements. The chemosensor revealed high selectivity with respect to homologues of the target protein.
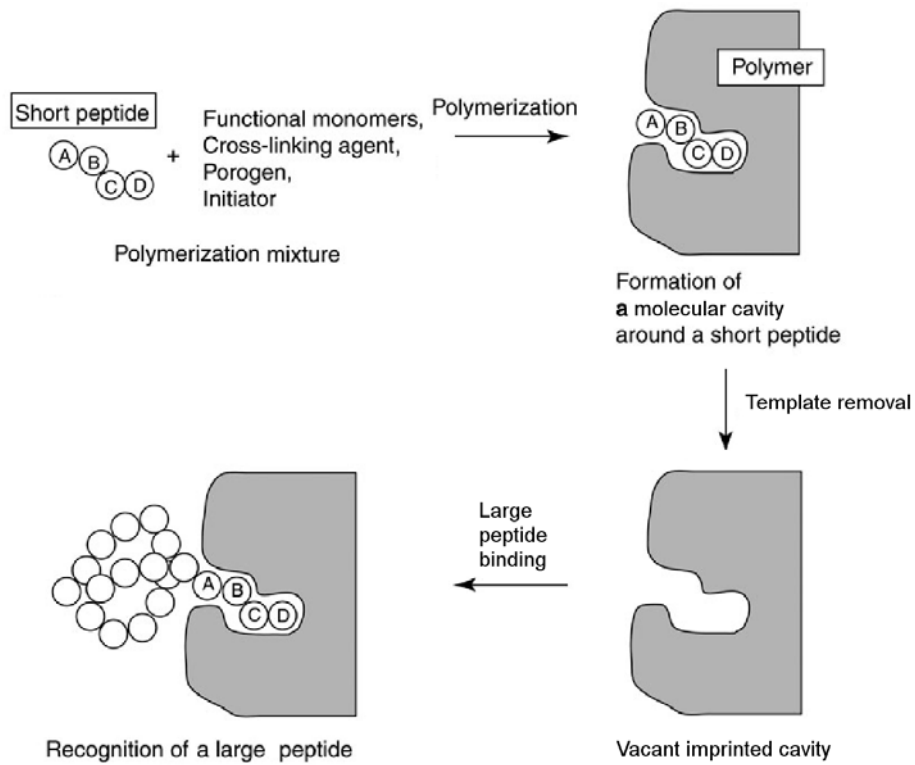
Scheme 1.7 Schematic diagram of epitope imprinting. (Adapted from [95].)
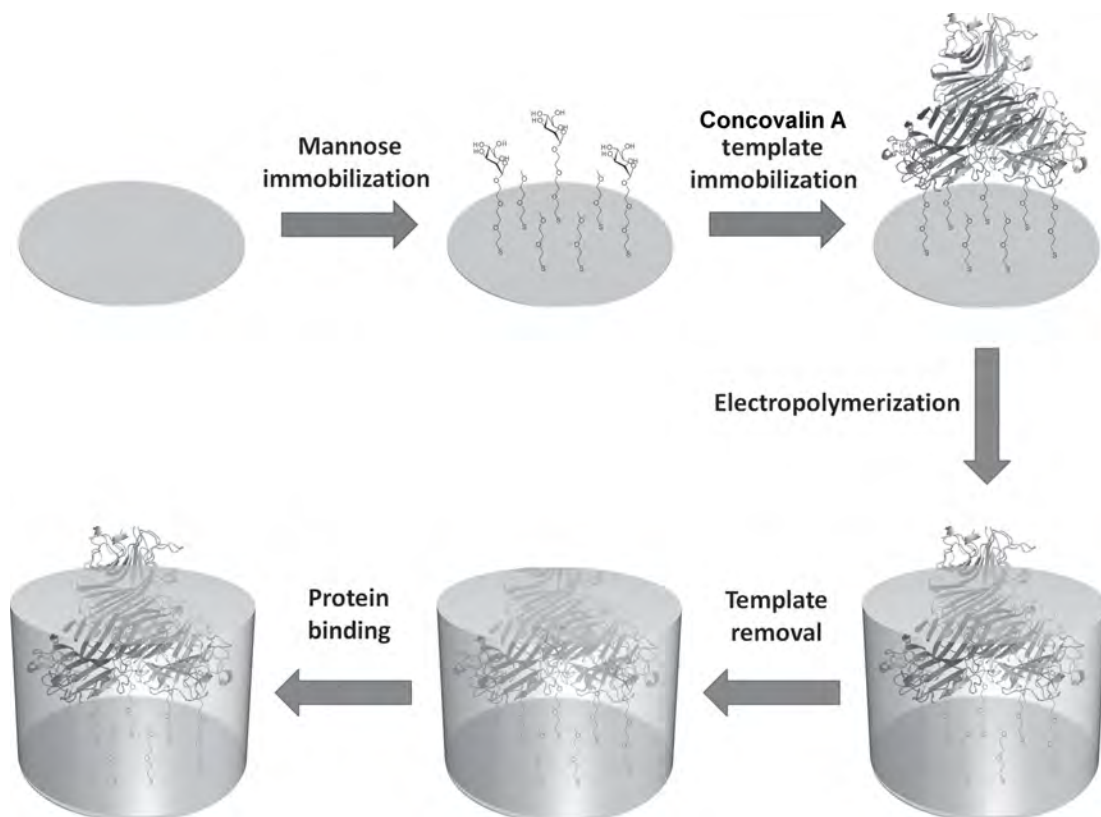
Scheme 1.8 Schematic representation of the concovalin A template oriented surface imprinting for the preparation of MIP films. (Adapted from [91].)

1.3 Oligonucleotide chemosensors

Oligonucleotides are short, single-stranded fragments of DNA or RNA, built of 50 or less nucleotides [96]. Oligonucleotides are capable of sequence-specific binding and formation of double strands with fragments of ssDNA or ssRNA of a complementary nucleobase sequences. This property allows them to be used as probes for DNA and RNA detection and to constitute a foundation of techniques of DNA or RNA sensing, such as Southern blotting [97], DNA microarrays [98] and other types of chemosensing [99].

The importance of the DNA determination is manifested by a broad application of DNA sensors varying from forensic uses and medical diagnostics to detection of toxins, whole bacteria, and viruses [99–104]. Many different transduction platforms were used for that purpose including optical sensors. Even though the limit of detection of sensors utilizing optical techniques was low, i.e., at the level of single nanomoles [105–108], those sensors required probes for signal collection or amplification. Other platform of detection that did not require using labels or probes utilizes the piezoelectric effect [109] including piezoelectric microgravimetry (PM) with the use of a quartz crystal microbalance (QCM) [102,110]. However, sensitivity of those sensors was lower in comparison to optical sensors, unless signal is amplified, e.g., by adding modified gold nanoparticles [111]. Another widely used methods employed electrochemical techniques. Electrochemical sensors could detect oligonucleotides directly or indirectly. Indirect sensors can be very sensitive, e.g., sensor utilizing enzymatic reduction of silver [112]. Despite that detectability of this sensor was appreciable, i.e., in the femtomolar range, its use was not simple because it required a multi-step measurement. A more straightforward measurement was based on the DNA quantification via electrochemical signal of electroactive DNA intercalation probes. However, the limit of detection exceeded nanomoles [113–115]. There are examples of this type of sensors with even lower detection limits, i.e., down to attomoles [116]. However, they required additional modification for signal amplification. In one example, a cascade of hybridization reactions was target-triggered that required the use of not only a probe but also an excess of long recognizing oligonucleotides. Out of electrochemical methods that did not require probes interacting with the target oligonucleotide, i.e., the so called label-free methods, electrochemical impedance spectroscopy (EIS) is most promising because of its high sensitivity and simplicity of measurement. The detection limit of most EIS sensors is at the level of single nanomoles [101,117–121].
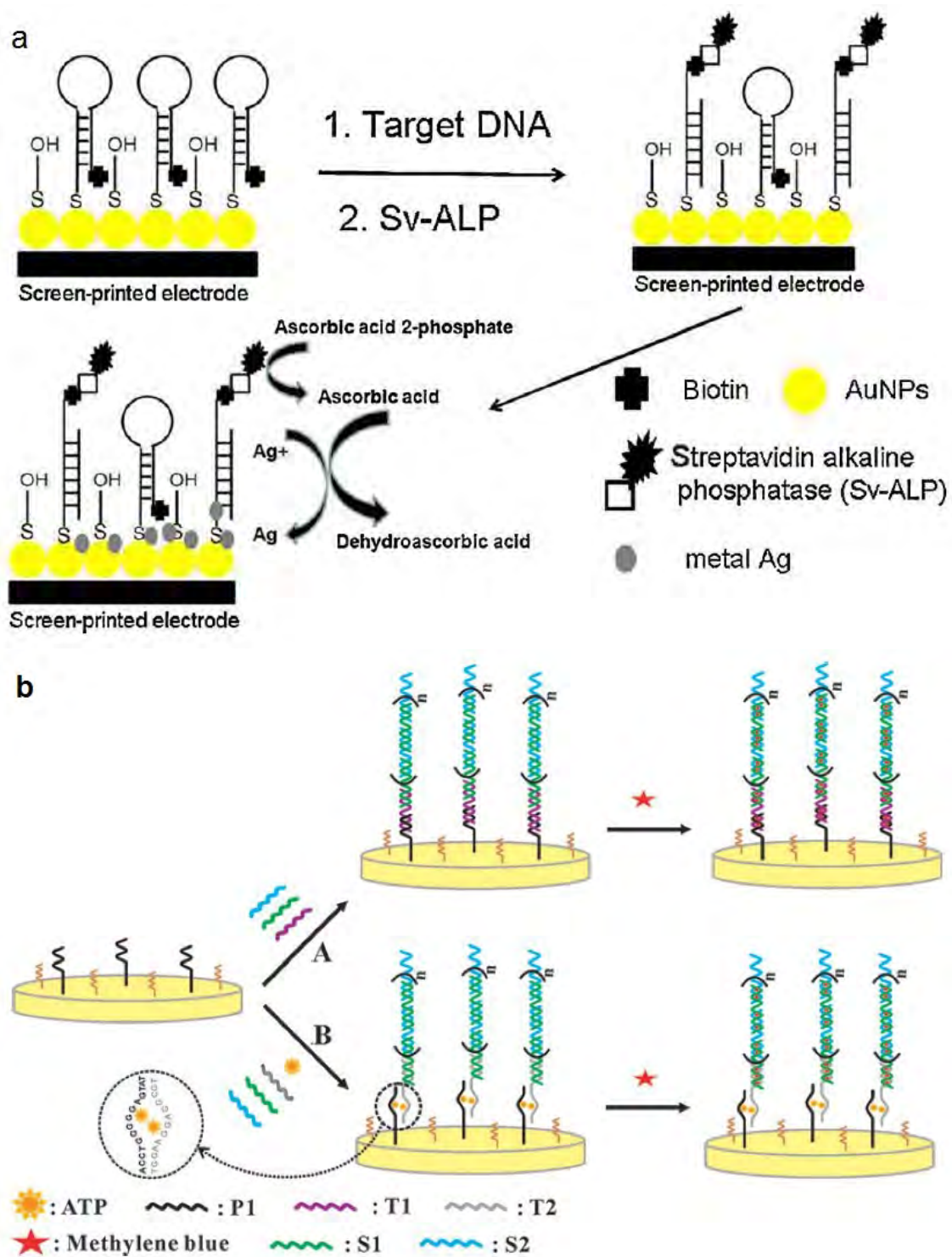
Figure 1.8 Performance of sensitive DNA sensors based on (a) coulometric measurement of enzymatic silver deposition on a gold nanoparticle modified electrode [112] and (b) ssDNA assisted cascade of hybridization for a sequence-specific DNA detection [116].

Chapter 2

Experimental Section

2.1 Chemicals and materials

The following chemicals and materials were used in the hereby described research.

- 4-Acetaminobenzaldehyde - Sigma-Aldrich
- Acetone - Fisher, POCh
- Biotin N-hydroxysuccinimide ester - Sigma-Aldrich
- 2,2'-Bisbithiophene - Sigma-Aldrich, Combi Blocks, Inc.
- Bromoethanol - Sigma-Aldrich
- 2-Bromoacetamide - Sigma-Aldrich
- 4-Carboxybenzaldehyde - Sigma-Aldrich
- Cytosine - Sigma-Aldrich
- D-biotin - Chempep
- Dibromoethane - Sigma-Aldrich
- 3,4-Dihydroxybenzaldehyde - Sigma-Aldrich
- 4-Dimethylaminopyridine - Sigma-Aldrich
- Dimethyl formamide, DMF - Fisher
- Dimethyl sulfoxide, DMSO - Fisher
- 1-Ethyl-3-(3-dimethylaminopropyl)carbodiimide, EDCI - Sigma-Aldrich
- Ethylene glycol - Sigma-Aldrich
- Ethylene carbonate - Sigma-Aldrich
- $[C_{60}]$fullerene - SES Research
- Guanine - Sigma Aldrich
- 4-Hydroxybenzaldehyde - Sigma-Aldrich
- 4-Methylbenzenesulfonyl chloride - Sigma-Aldrich
- 4-Methylbenzaldehyde - Sigma-Aldrich
- Myoglobin - Sigma-Aldrich

- *N*-hydroxysuccinimide - Sigma-Aldrich

- Neutravidin - Thermo Scientific

- 4-Nitrobenzaldehyde - Sigma-Aldrich

- Pentaethylene glycol - Sigma-Aldrich

- Perchloric acid (70%) - Sigma-Aldrich

- Pet feed samples - Lab Chem, Laboratorium Chemiczne Badania Podstawowe i Stosowane Hanna Kurcińska

- Potassium carbonate - Sigma-Aldrich

- Potassium chloride - Chempur and Sigma-Aldrich

- Potassium dihydrogen phosphate, KH_2PO_4- Sigma-Aldrich

- Potassium hexacyanidoferrate(II), $K_4Fe(CN)_6$ - Chempur and Fisher

- Potassium hexacyanoferrate (III), $K_3Fe(CN)_6$ - Chempur and Sigma-Aldrich

- Potassium hydroxide - Chempur and Sigma-Aldrich

- Sarcosine - Sigma-Aldrich

- Sodium bicarbonate - Sigma-Aldrich

- Sodium chloride - Fisher and POCh

- Sodium hydrogen phosphate, Na_2HPO_4 - Sigma-Aldrich

- Sodium hydroxide - Fisher and POCh

- Oligonucleotides of various sequences - AlphaDNA

- Tetrabutylammonium perchlorate - Sigma-Aldrich and Southwestern analytical inc.

- Tetrahydrofuran, THF - VWR

- Triethylamine - Sigma-Aldrich

- Thymine-1-acetic acid - Sigma-Aldrich

2.2 Instrumentation

The measurements involving electroanalytical techniques, namely, cyclic voltammetry (CV) and electrochemical impedance spectroscopy (EIS), were performed using a computerized PARSTAT2273 potentiostat/galvanostat controlled by the PowerSuite software both of Princeton Applied Research or an AUTOLAB computerized electrochemistry system of Eco Chemie equipped with expansion cards of the PGSTAT12 potentiostat and the FRA2 frequency response analyzer, and controlled by the GPES 4.9 software of the same manufacturer.

For herein presented research, a typical three-electrode setup was used with a V-shaped glass cell, (Scheme 2.1). A 3-mm diameter disk glassy carbon electrode, GCE, or gold coated glass slide were used as working electrodes and a Pt wire
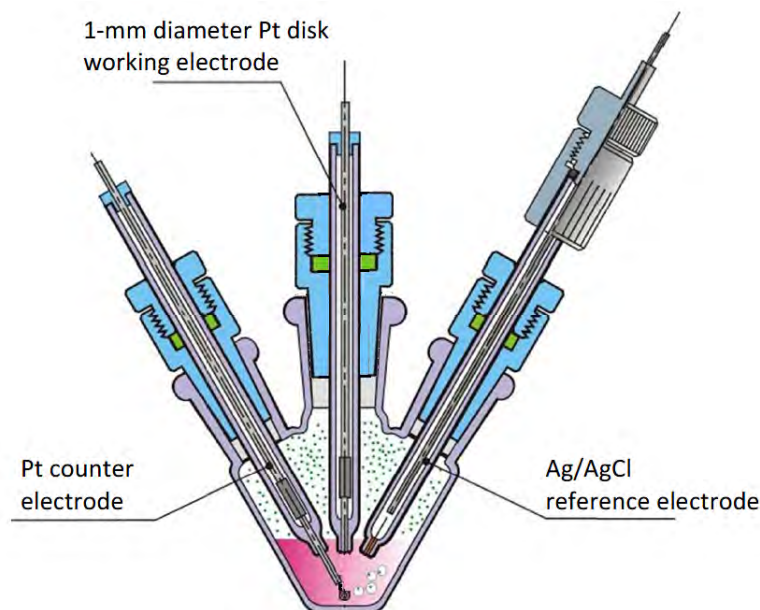
Scheme 2.1 Sketch of a three-electrode electrochemical cell used herein.

coil and an Ag wire coated with the AgCl film served as the counter and reference electrode, respectively.

A model EQCM 5610 [122] and EQCM 5710 [123] quartz crystal microbalance [124] controlled by the EQCM 5710-S2 software, all of IPC PAS, served to perform the PM experiments under either the batch or FIA conditions, respectively. The resonant frequency change, Δf, was measured with 0.1-Hz resolution using the 14-mm diameter AT-cut plano-plano 10-MHz resonant frequency QCRs with 5-mm diameter and $\sim$100-nm thick circular Au-film electrodes evaporated over Ti underlayers on both sides of QCRs. Experimental setup used is shown in Scheme 2.2.

The atomic force microscopy (AFM) imaging of polymer films was performed using a MultiMode$^\circledR$ 8 AFM under control of a Nanoscope V controller of Bruker. The ScanAsyst mode was utilized for sample imaging with the use of the ScanAsyst-Air-HR probes provided by Bruker. The films for imaging were deposited on the gold film coated glass slides.

The surface plasmon resonance (SPR) measurements as well as simultaneous SPR and electrochemical measurements were performed using an Autolab ESPRIT instrument of Eco Chemie coupled to a computerized PGSTAT128N potentiostat/galvanostat and controlled by the GPES 4.9 and AUTOLAB SPR Data Acquisition software of the same manufacturer.

The ^{1}H NMR spectra were recorded using the 500 MHz and 400 MHz NMR spectrometers of Varian. Data obtained were processed using the VNMRJ 2.2C software of Varian or the SpinWorks v.3.1.7 software developed by Kirk Marat at the University of Manitoba. Chemical shifts are given in parts per million (δ) relative to tetramethylsilane.
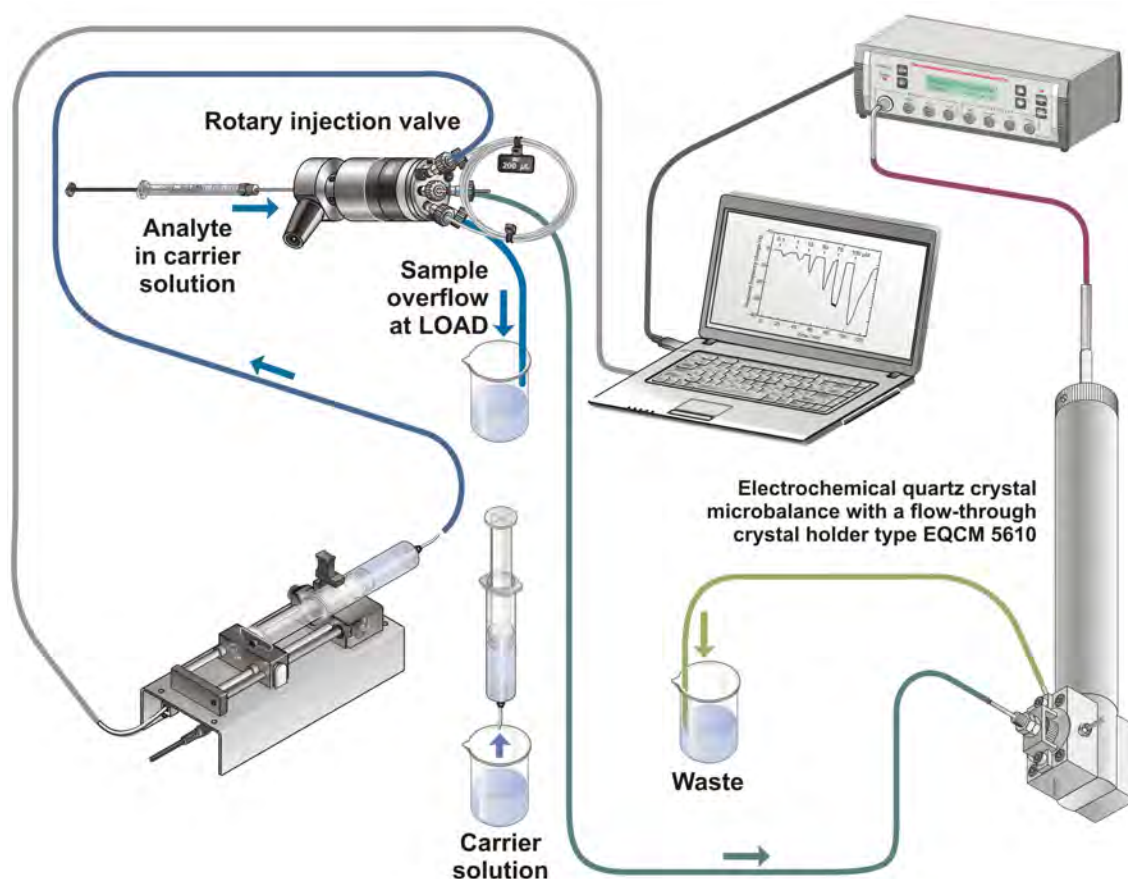
Scheme 2.2 The experimental set-up for silmultaneous measurement of the resonant frequency change and the dynamic resistance change during flow-injection analysis, FIA, by piezoelectric microgravimetry at the electrochemical quartz crystal microbalance EQCM 5610.

The quantum-chemistry calculations were performed using the Gaussian 2009 [125] software package installed within the operating system of Linux openSUSE 11.4 (x86-64) on a high performance computer (16 cores of processor Intel Xeon E5620 2.4 GHz and 24 GB of RAM). Structures of molecules and their complexes as well as values of the free Gibbs energy change due to complex formation, ΔG, were calculated using the density functional theory (DFT) method at either B3LYP or M062X level.

2.3 Experimental techniques

2.3.1 Cyclic voltammetry

Cyclic voltammetry (CV) is one of the most frequently used electroanalytical techniques where variation of current with the potential, applied to the working electrode, is measured. The potential applied is changed linearly with time from the initial value of E_i, to the final value of E_f, through E_v, which is the vertex potential,

as shown in Figure 2.1.
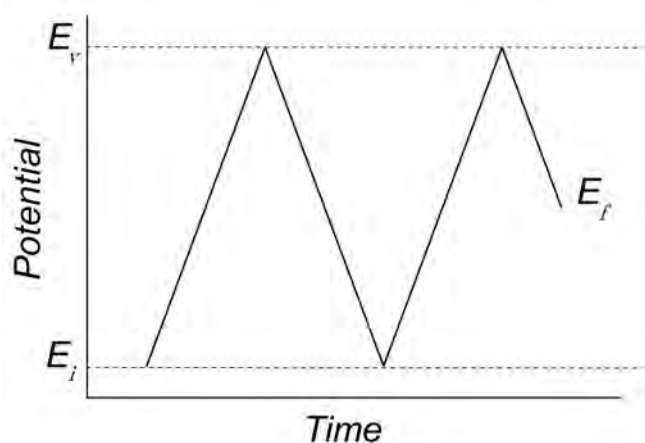
Figure 2.1 The potential change with time of the working electrode in cyclic voltammetry.

On a typical cyclic voltammogram (a curve of $I = f(E)$), recorded for solution containing a redox active analyte, current peaks are observed. With the increase of the working electrode potential, current increases (A-B in Fig. 2.2) until the analyte concentration at the electrode surface drops to zero (B on Fig. 2.2). Then, the current decreases as the concentration of the analyte is depleted in the electrode vicinity (B-C in Fig. 2.2). If the redox couple is reversible, then current will drop during the opposite potential scan until the cathodic peak potential of the oxidized species is reached (C-D in Fig. 2.2). This cathodic peak is formed because of depletion of the oxidized species in the electrode vicinity.

For a reversible redox process, the peak current is described by the Randles-Ševčik equation [127].

$$i_\mathrm{p} = 2.72 \times 10^5 n^{3/2} D^{1/2} A v^{1/2} c \tag{2.1}$$

In this equation n is the number of electrons exchanged in the elementary electrode process, A is the electrode surface area $\mathrm{cm^2}$, D is the diffusion coefficient of a redox species $\mathrm{cm^2/s}$, v is the potential scan rate $\mathrm{V/s}$, and c is the redox species concentration in bulk of the solution M.

Moreover, for this process the anodic and cathodic peak separation is described, as [127].

$$\Delta E = E_\mathrm{pa} - E_\mathrm{pc} = \frac{0.059}{n} \, [\mathrm{V}] \tag{2.2}$$

The situation is different for a quasi-reversible process, that is the process controlled by both the rate of the electrode process and the rate of diffusion. In this case, the peak separation is higher. For an irreversible process, solely controlled by the rate of the electrode process, the anodic and cathodic peak separation is even higher, or in many cases, only one peak is seen on the cyclic voltammogram. For an
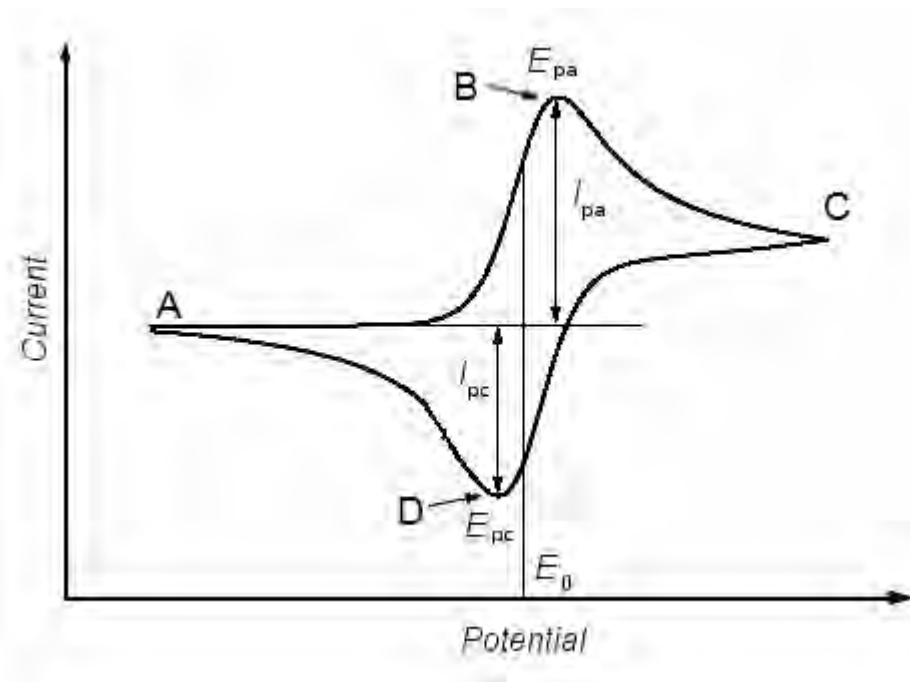
Figure 2.2 The change of current as a function of potential of the working electrode in cyclic voltammetry. (Adapted from [126].)

irreversible oxidation, the peak of anodic current is described by Equation 2.3 [127]

$$i_{pa} = 2.72 \times 10^5 \, \alpha_a^{1/2} \, D^{1/2} \, A \, v^{1/2} \, c \tag{2.3}$$

where α_a is the charge transfer coefficient of an anodic process.

2.3.2 Electrochemical impedance spectroscopy

In electrochemical impedance spectroscopy, EIS, an alternating voltage of a small amplitude, typically 10 mV, is applied to the working electrode. This potential is described by Equation 2.4 [128]

$$E(t) = E_0 sin(\omega t) \tag{2.4}$$

where E_0 is the potential amplitude, $\omega = 2\pi f$ is angular frequency of the alternating voltage applied, and t is time.

As a result, current is shifted in phase with respect to potential by the phase angle, φ. This behavior is depicted in Figure 2.3. Current is described by Equation 2.5

$$I(t) = I_0 sin(\omega t + \varphi) \tag{2.5}$$

where I_0 is the current amplitude.

In a complex plane, E and I are represented by vectors $\Delta \bar{E}$ and $\Delta \bar{I}$, respectively,
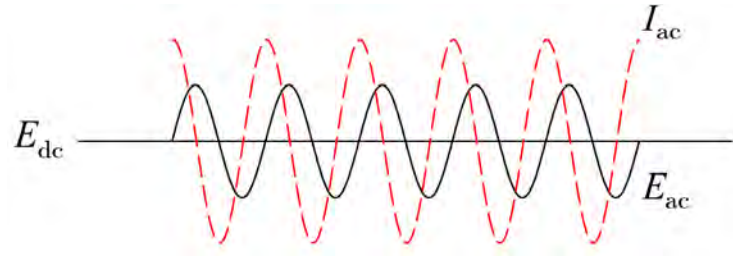
Figure 2.3 Changes of current incurred by application of a sinusoidal voltage change. (Adapted from [129].)

and are described by Equations 2.6 and 2.7, respectively.

$$\triangle \bar{E} = \triangle E_{\mathrm{Re}} + j\triangle E_{\mathrm{Im}} = E_0 cos(\omega t) + j sin(\omega t) = E_0 e^{-j\omega t} \tag{2.6}$$

$$\triangle \bar{I} = I_0 e^{(-j\omega t + \varphi)} \tag{2.7}$$

In these equations $j = \sqrt{-1}$.

Impedance, Z, of this system is described by Equation 2.8

$$Z = \frac{\triangle \bar{E}}{\triangle \bar{I}} = |Z| e^{-j\omega} = Z_{\mathrm{real}} - j Z_{\mathrm{im}} \tag{2.8}$$

where Z_{real} and Z_{im} is the real and imaginary component of impedance, respectively, and

$$|Z| = \frac{E_0}{I_0} \tag{2.9}$$

In a complex-plane representation, the impedance is often presented as a vector of the length equal to

$$|Z| = \sqrt{Z_{\mathrm{real}}^2 - j Z_{\mathrm{im}}^2} \tag{2.10}$$

with the real component of impedance defined as

$$Z_{\mathrm{real}} = |Z| cos\varphi, \tag{2.11}$$

the imaginary component of impedance defined as

$$Z_{\mathrm{im}} = |Z| sin\varphi, \tag{2.12}$$

and the phase angle, φ, defined as

$$\varphi = arctan\frac{Z_{\mathrm{im}}}{Z_{\mathrm{real}}} \tag{2.13}$$

Impedance at a certain ω value in the coordinate system of Z_{real} and Z_{im}, so called the Nyquist plot, is shown in Figure 2.4.

In general, an electrochemical cell can simply be considered as an impedance to
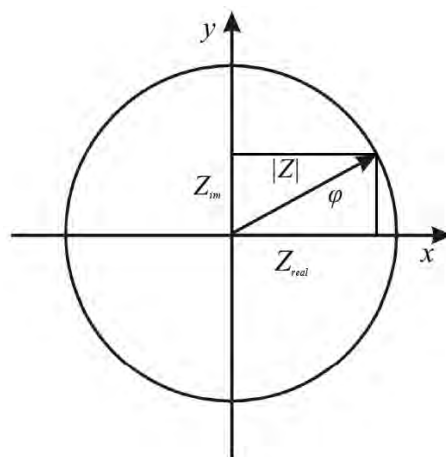
Figure 2.4 Vector projection of Z in a complex plane at constant ω. (Adapted from [129].)

a small sinusoidal excitation. Therefore, performance of this cell may be represented by an equivalent circuit of electrical elements characterized by the same amplitude and phase angle as the real cell under a given excitation. Mathematical representation of basic electric equivalent elements used for constructing equivalent circuits is given below.

Resistor

$$Z = R \tag{2.14}$$

Capacitor

$$Z = \frac{1}{j\omega C} \tag{2.15}$$

Inductor

$$Z = j\omega L \tag{2.16}$$

where R is resistance, C is capacitance, and L is inductance.

Figure 2.5 shows typical impedance spectra and corresponding equivalent circuits.

2.3.2.1 Impedance of polymer films deposited on electrodes in the redox probe presence in solution

For the electrodes coated with porous polymer films, a modified Randles-Ershler equivalent circuit is often applied (Scheme 2.3). In this circuit, the R_s element represents the solution resistance. Because polymer films rarely behave as ideal capacitors and, therefore, reveal a non-zero real component [131], the double-layer capacity, C_dl, used in the Randles circuit, is often replaced by the constant phase element (CPE). Equation (2.17) shows contribution of CPE, Z_CPE, to the total
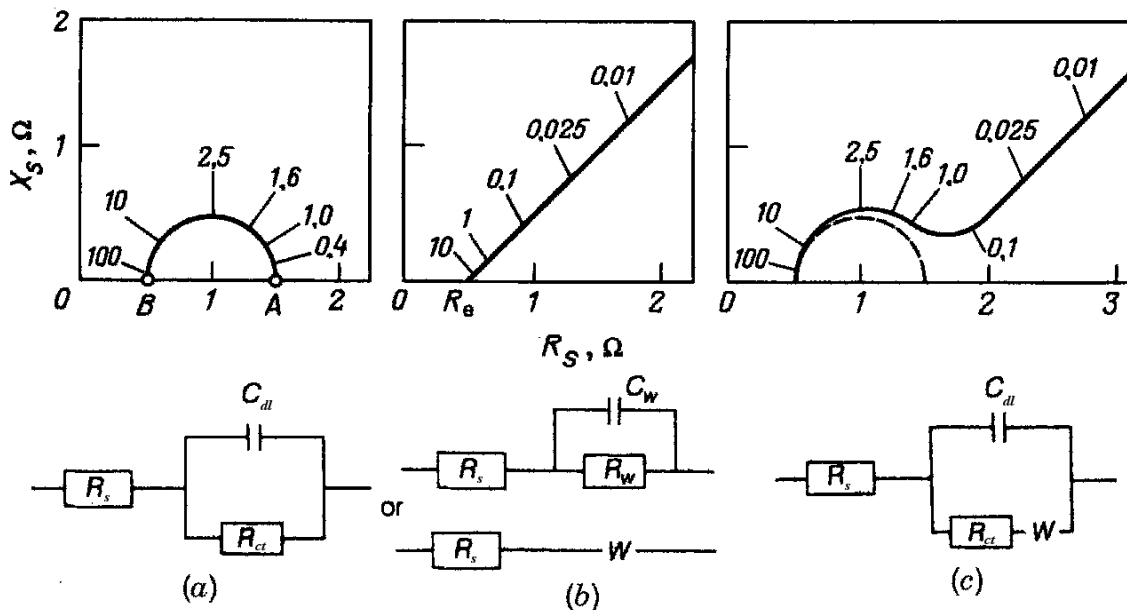
Figure 2.5 Impedance spectra of an electrode and the corresponding electric equivalent circuits for the electrode processes controlled by the rate of (a) charge transfer, (b) diffusion, and (c) charge transfer and diffusion [130]. Numbers on the graphs correspond to frequency values in kHz. W - the Warburg impedance, R_W - the resistance corresponding to Warburg impedance, R_{ct} - the charge transfer resistance, R_s - the solution resistance, C_w - the capacitance corresponding to Warburg impedance, C_{dl} - the double-layer capacitance.

impedance.

$$Z_{CPE} = \frac{1}{(i\omega)^{\phi}T} \tag{2.17}$$

In this equation, T is the frequency-independent proportionality factor. Its physical meaning is related to the diffusion coefficient. It is characteristic of a given electrochemical system. Symbol ϕ is an exponent. This exponent can take values, $0 \leq \phi \leq 1$. For $\phi = 1$, the system behavior is purely capacitive where the CPE impedance, Z_{CPE}, equals to C^{-1} while for $\phi = 0$ Z_{CPE} equals to pure resistance.
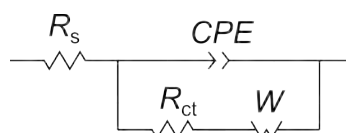
Scheme 2.3 The modified Randles-Ershler equivalent circuit used to fit experimental data. R_s - the solution resistance, R_{ct} - the charge transfer resistance, CPE - the constant phase element, W - the Warburg impedance.

The Warburg impedance, W, introduced to the equivalent modified Randles-Ershler circuit (Scheme 2.3) represents the mass transfer to the electrode accompanying the redox process. Contribution of the Warburg impedance to the total

impedance is described by Equation (2.18), as follows.

$$Z_{\text{W}} = \frac{B tanh(iT\omega)}{(iT\omega)^{\phi}} \tag{2.18}$$

In this equation, B is the fitted parameter. Herein, R_{ct} describes the charge transfer resistance, i.e., the resistance of the electron transfer between the electrode and the redox species in solution. Therefore, R_{ct} corresponds to the resistance of the electrode, on which a faradaic reaction proceeds. The value of this resistance is affected by any surface changes leading to blocking of the electrode, for instance by deposition of a less conducting film.

2.3.2.2 Impedance of polymer films under non-faradaic conditions

Under non-faradaic conditions, i.e., in the abscence of a redox active species, the imaginary component of impedance of the electrical double layer is inversely proportional to its capacity, C_{dl} (Eqn. 2.19).

$$Z_{\text{im}} = \frac{1}{\omega A C_{\text{dl}}} \tag{2.19}$$

For the (polymer film)-coated electrode in a supporting electrolyte solution, the equivalent circuit applied is composed of a solution resistor in series with an electrical double-layer capacitor (Scheme 2.4). For thin polymer films its capacitance and resistance is negligible in the equivalent circuit.
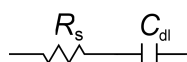
Scheme 2.4 The equivalent circuit of a cell wih a non-faradaic electrochemical process, for the (polymer film)-coated electrode in a supporting electrolyte solution. The R_{s} and C_{dl} symbol stands for the electric resistance of the solution and capacity of the electrical double layer, respectively.

Because of inverse proportionality of the imaginary component of impedance and ω or f (Eqn. 2.19), the capacity response is higher at low frequencies. The phase angle, φ, values can be calculated using Eqn. 2.20.

$$\varphi = tan^{-1}\left(\frac{Z_{im}}{Z_{real}}\right) \tag{2.20}$$

From Eqn. 2.20 it follows that the more negative the φ the more capacitive the nature of the equivalent circuit is. Ultimately, $\varphi = -90°$ for a purely capacitive process.

2.3.3 Piezoelectric microgravimetry

Piezoelectric microgravimetry is a technique that utilizes a converse piezoelectric effect. Piezoelectric effect is a physical phenomenon of electric charge generation while mechanical stress is applied to the piezoelectric material. Piezoelectricity occurs in crystals with no symmetry centers. The converse effect is observed when alternating voltage is applied to the electrical contacts mounted to the sides of such a crystal. Then, the crystal mechanically oscillates at the natural resonance frequency proportional to its thickness [124]. When mass is deposited on an AT-cut quartz crystal resonator (QCR) surface, a drop in oscillation frequency is observed. The change of frequency is correlated with the mass change by the Sauerbray relation, Equation (2.21) [132]

$$\Delta f_{\mathrm{mass}} = -\frac{2\, f_0^2\, \Delta m}{A_{\mathrm{acoust}}\, (\mu_{\mathrm{q}}\rho_{\mathrm{q}})^{1/2}} \tag{2.21}$$

where f_0 is the fundamental frequency of the resonator (here 10 MHz), A_{acoust} is the acoustically active area of the resonator (here 0.1963 cm^2), μ_{q} is the shear modulus of quartz (2.947 $\times$ 10^{11} g s^{-2} cm^{-1}), and ρ_{q} is the quartz density (2.648 g cm^{-3}).

The Sauerbray equation holds if several assumptions are fulfilled. An important one requires that the film deposited on a resonator was perfectly elastic, i.e., as rigid as the resonator material itself. If the resonator is contacted with a liquid, then the frequency change is described by Equation (2.22) [124].

$$\Delta f_{\mathrm{mass}} = -\left[\frac{2\, f_0^2}{(\mu_{\mathrm{q}}\rho_{\mathrm{q}})^{1/2}}\right]\left[\left(\frac{\Delta m}{A}\right) + \left(\frac{\mu_{\mathrm{L}}\rho_{\mathrm{L}}}{4\pi f_0}\right)^{1/2}\right] \tag{2.22}$$

where μ_{L} and ρ_{L} are the shear modulus and density of the contacting liquid, respectively. This formalism has been extended to resonators coated with viscous films. In this case, contribution of the frequency change due to the change of viscosity of the film is [124]

$$\Delta f = -f_0^{3/2}\left(\frac{\mu_{\mathrm{L}}\rho_{\mathrm{L}}}{\pi\mu_{\mathrm{q}}\rho_{\mathrm{q}}}\right)^{1/2} \tag{2.23}$$

This change can indirectly be measured by the dynamic resistance, R_{D},

$$R_{\mathrm{D}} = \frac{A}{k_{\mathrm{QCR}}^2}\left(2\pi f_0\mu_{\mathrm{L}}\rho_{\mathrm{L}}\right)^{1/2} \tag{2.24}$$

where $k_{\mathrm{QCR}}^2 = 7.74 \times 10^{-3}\mathrm{A}^2$ s m^{-2} is the electromechanical coupling factor of QCR. From Eqns. (2.23) and (2.24), a relation between the frequency change with R_{D} can be derived

$$\Delta f = \frac{k^2 R_{\mathrm{D}} f_0}{\pi A \left(2\mu_{\mathrm{q}}\rho_{\mathrm{q}}\right)^{1/2}} \tag{2.25}$$

Therefore, the mass change can be calculated from a simultaneously recorded resonant frequency and dynamic resistance change.

2.3.4 Atomic force microscopy

Atomic force microscopy, AFM, is a technique of high-resolution imaging of materials surfaces. In AFM, the tip of a flexible cantilever is brought very close to the sample surface, so that a force acts between them. The measurement of this force allows for sample imaging [133]. The force acting between the AFM tip and the sample can be measured by registration of the cantilever deflection. This measurement can be accomplished by shining a laser light beam on the cantilever and measuring position of the reflected beam (Scheme 2.5).
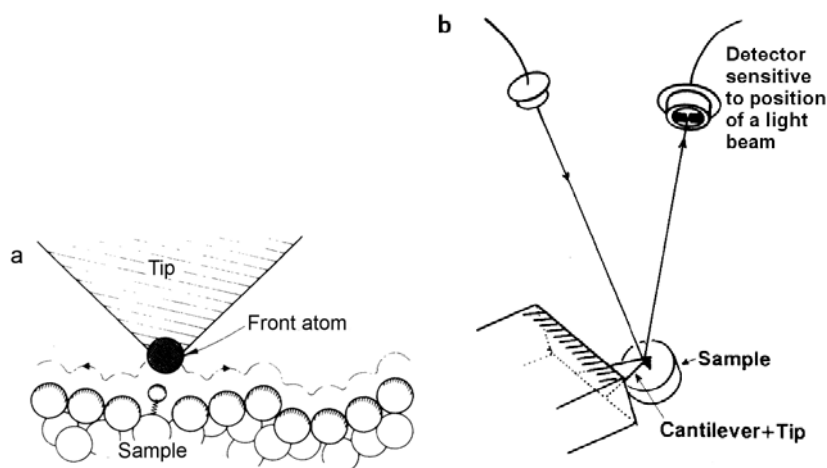
Scheme 2.5 A simplified view of (a) the AFM tip interacting with the sample surface [133] and (b) the measurement setup of cantilever deflection. (Adapted from [134].)

There are at least two modes of AFM operation, namely, the contact mode and the tapping mode [135]. In the contact mode, the force between the AFM tip and the sample is kept constant using a feedback signal to keep the cantilever deflection constant. In the tapping mode, the AFM tip oscillates with its resonance frequency. The oscillation frequency is affected by tip interaction with the sample. The instrument adjusts the tip position, so that the oscillation frequency of the AFM tip stays constant. Herein, the tapping mode AFM was used.

2.3.5 Surface plasmon resonance

Electrons of the conduction band in the metal bulk are in continuous motion and move freely through the crystal lattice. However, the electrons at the metal surface can move out of the bulk to the point where the charge distribution is altered sufficiently to pull the electrons back into the lattice. Therefore, there is an oscillation

of electrons at the metal surface, known as surface plasmon wave, perpendicular to the motion of the wave. The parameter of this oscillation, vis. frequency is defined by dielectric properties of the metal and its surroundings. This is because surface plasmon oscillation partially extends beyond the metal boundary [136].

The surface plasmon resonance is a phenomenon that can be observed as a drop of intensity of polarized light reflected from the metal surface under certain conditions including certain angle of incidence of the light beam, light wavelength, and the measurement setup. This phenomenon happens when the angular frequency and phase velocity of the incident light beam matches those of the surface plasmons [137]. However, normally, there is no angle of light beam incidence, for which the horizontal component of light wave matches the value of the angular frequency of the surface plasmon wave. Therefore, the wave vector and, in consequence, the phase velocity of light must be changed. This velocity can be changed by two configurations. One of them was used herein, namely, by using an attenuated total reflection, ATR, coupler [138].

In the ATR coupler, the incident light is passed through a dielectric medium (usually quartz or glass) in the form of a prism whose refractive index η exceeds 1. Such a medium decreases the phase velocity of photons. Therefore, the incident light can come into resonance with the surface plasmons. Two possible configurations of the ATR setups are shown in Scheme 2.6 [138]. For sensor application, the Kretschmann configuration is used. This is because surface plasmons are in direct contact with the environment in this setup.
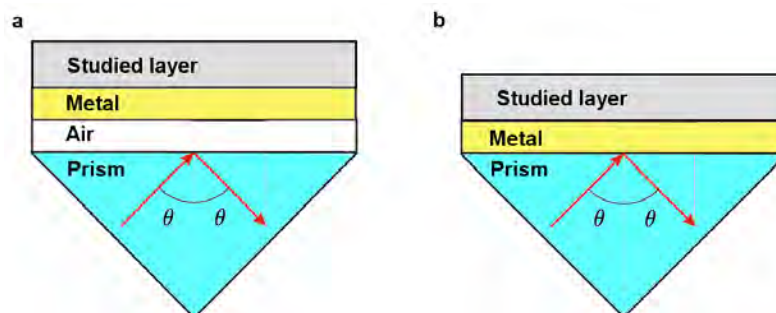
Scheme 2.6 Schematic view of the ATR couplers in two possible configurations, that is, the (a) Otto and (b) Kretschmann configuration. (Adapted from [138].)

As mentioned above, the reflected light intensity drops at a certain angle of incidence. Herein, this angle is referred to as the SPR angle. At this SPR angle, the light energy is transformed into energy of surface plasmons. Since parameters of surface plasmons depend on the dielectric properties of the medium in the vicinity of the metal surface, any change of this medium results in a change of the SPR angle. Therefore, deposition of a polymer film from solution, and then changes in structure of this film can be measured. Exemplary curve recorded during measurement of

SPR angle is shown in Scheme 2.7.
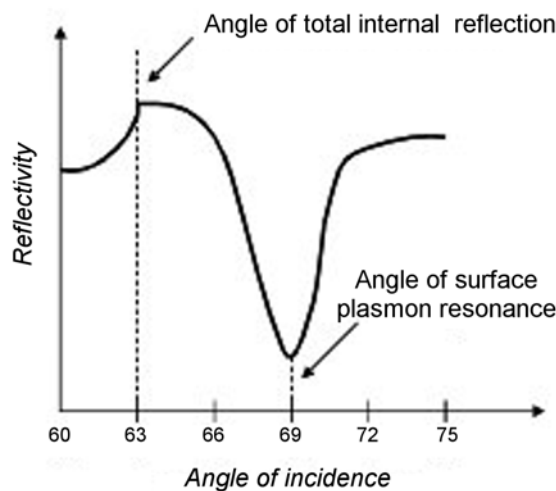
Scheme 2.7 Exemplary plot of reflectivity vs. angle of light beam incidence showing typical surface plasmon resonance experiment. (Adapted from [139].)

2.4 Procedures of syntheses

For each compound used as a functional monomer, a number was assigned. If synthesis of a certain functional monomer required several steps, the intermediates were labeled with a number of the final product and a letter. For clarity, the NMR and MS spectra as well as crystallographic data are provided in Appendix.

2.4.1 Syntheses of new thiophene derivatives

Within the present research, sixteen new bis(2,2'-bithiophene) and two new [C60]fullerene derivatives were designed and synthesized to serve as functional monomers (FMs). Their recognition sites varied from simple functional groups, such as hydroxyl, amino, nitro, carboxyl, or amide groups, to bigger assemblies containing naturally occuring recognizing moieties, such as biotin, thymine, cytosine, or guanine. Other FMs contained succinimide, 4-tertbutylcalix[6]arene, and pentaethyleneglycol as recognizing sites. Each of the newly prepared FM contained one recognition site.

4-Bis(2,2'-bithiophen-5-yl)methylphenol **1** (Scheme 2.8). First, 2,2'-bithiophene (2.045 g, 12.3 mmol) and 4-hydroxybenzaldehyde (500 mg, 4.1 mmol) were mixed with ethylene glycol (80 mL) and the mixture was stirred for 30 min under N_2. Then, 70% $HClO_4$ (12 mL, 184.5 mmol) was added and the resulting solution was stirred

for 16 h at 60 °C. Next, the reaction mixture was cooled to room temperature and the excess of methylene chloride was added in order to dissolve the desired product. Subsequently, the mixture was treated with the saturated solution of Na_2CO_3 to neutralize the excess acid. The collected organic liquid layer was washed with water and dried with anhydrous Na_2SO_4. After the evaporation of the organic layer solvent, a crude product was purified by liquid chromatography on a silica gel column using the hexane : $CHCl_3$ (1 : 1 to 1 : 9, $v : v$) eluent. Yield: 1.13 g (63%). ^{1}H NMR ($CHCl_3$-d), Fig. A.1: (δ in ppm) 7.22–7.18 (d, 2H, bithiophene H), 7.16–7.13 (dd, 2H, bithiophene H), 7.08-7.06 (dd, 2H, bithiophene H), 7.00–6.97 (d, 2H, phenyl H), 6.96-6.93 (dd, 2H, phenyl H), 6.83–6.79 (d, 2H, bithiophene H), 6.77–6.75 (dd, 2H, bithiophene H), 5.68 (s, 1H, –CH–). Product molecular mass calcd.: 436.6.
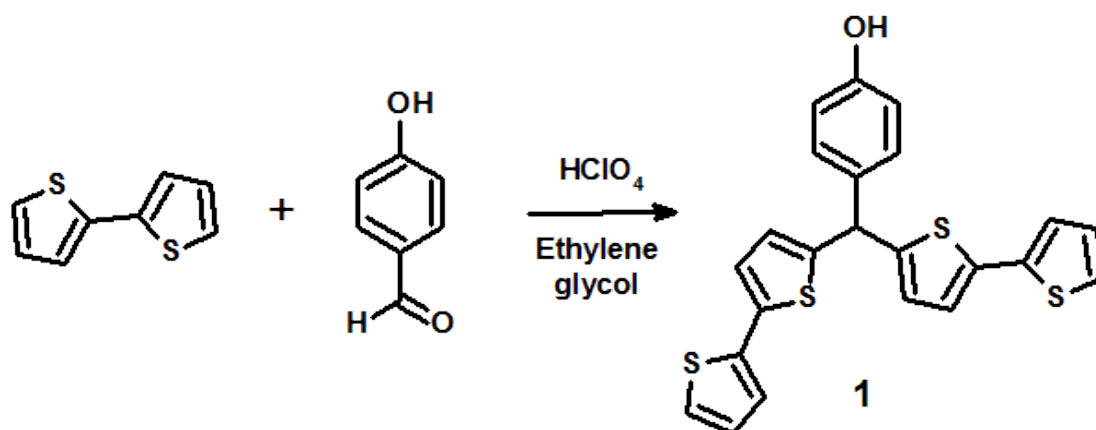
Scheme 2.8 Synthesis of 4-bis(2,2'-bithiophen-5-yl)methylphenol **1**.

4-Bis(2,2'-bithien-5-yl)methylphenol biotin ester **2** (Scheme 2.9). First, D-biotin (366 mg, 1.5 mmol) was dissolved in DMF (40 mL) and cooled to 0 °C by keeping in an ice bath. Then, EDCI (466 mg, 3 mmol) was added and the mixture stirred for ~30 min under N_2. Next, **1** (655mg, 1.5 mmol) dissolved in 20 mL of DMF was added dropwise for 10 min. After that, the reaction mixture was stirred in an ice bath for 1 h. The reaction was continued for another 45 h at room temperature. Then, the reaction solvent was evaporated under reduced pressure. The residue was purified by lyquid chromatography on a silica gel column using first the hexane : $CHCl_3$ (1 : 1 to 0 : 1, $v : v$), and then $CHCl_3$: MeOH (9 : 1, $v : v$) eluent. Yield: 110 mg (11%). ^{1}H NMR ($CHCl_3$-d), Fig. A.2: δ (in ppm) 7.36-7.32 (d, 2H, bithiophene H), 7.16-7.14 (dd, 2H, bithiophene H), 7.08-7.02 (m, 4H, overlapped bithiophene and phenyl H), 7.00-6.97 (d, 2H, phenyl H), 6.96-6.92 (dd, 2H, bithiophene H), 6.74-6.70 (dd, 2H, bithiophene H), 6.24 (s, 1H, biotin -NH-), 5.74 (s, 1H, -CH-) 5.62 (s, 1H, biotin -NH-), 4.42-4.38 (m, 1H, biotin), 4.25-4.21 (m, 1H, biotin), 3.12-3.08 (q, 1H, biotin), 2.84-2.80 (dd, 1H, biotin), 2.68-2.64 (d, 1H, biotin H), 2.58-2.52 (t, 2H, biotin H), 1.80-1.60 (m, 4H, biotin H), 1.52-1.45 (m, 2H, biotin

H). ESI-MS m/z calcd. for $C_{32}H_{28}N_2O_3S_5+2H_2O$: 684.9, found: 685.1 (Fig. A.4).
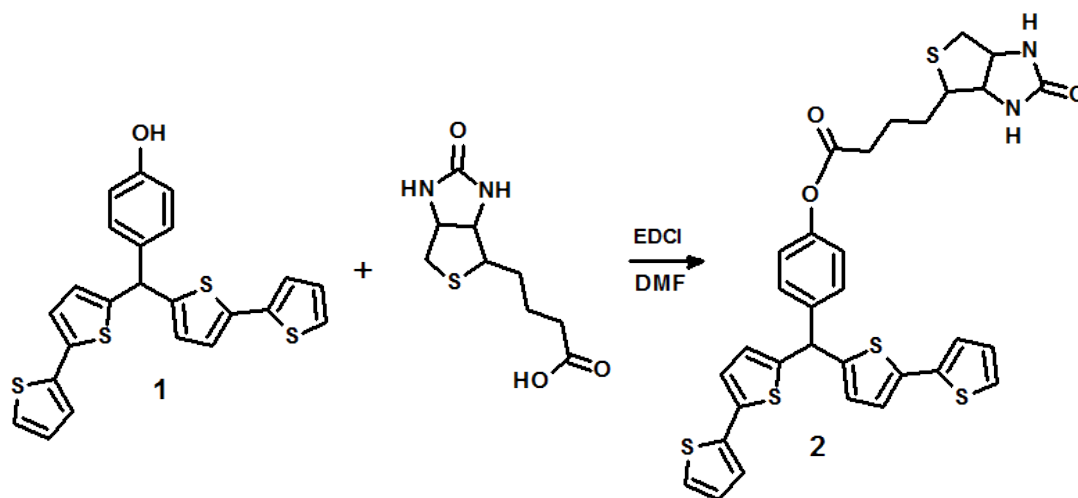
Scheme 2.9 Synthesis of 4-bis(2,2'-bithien-5-yl)methylphenol biotin ester **2**.

4-(2-Hydroxyethoxy)benzaldehyde **3a** (Scheme 2.10). First, 4-hydroxybenzaldehyde (3 g, 24.6 mmol) was dissolved in acetone. Then, K_2CO_3 (20 g, 144.6 mmol) was added and the mixture stirred for 30 min under N_2. Next, bromoethanol (5.22 mL, 73.7 mmol) was added dropwise and the resulting mixture stirred for 20 h at 80 °C. After cooling at room temperature, the reaction mixture was filtered and the filtrate solvent evaporated. The yellow oily residue left was diluted with dichloromethane, and then washed with water. The organic layer was dried with anhydrous Na_2SO_4, and then the solvent evaporated. A crude product left was purified by liquid chromatography on a silica gel column using the $CHCl_2$: MeOH (100 : 0 to 95 : 5, $v : v$) eluent. Yield: 1.96g (48%). ^{1}H NMR ($CHCl_3$-d), Fig. A.3: δ (in ppm) 9.82 (s, 1H, CHO), 7.81-7.79 (d, 2H, phenyl H), 7.04–6.98 (d, 2H, phenyl H), 4.16-4.10 (t, 2H, -CH2-), 4.00-3.96 (t, 2H, -CH2-). Product molecular mass calcd.: 166.2.

4-Bis(2,2'-bithien-5-yl)methylphenol glycol ether **3** (Scheme 2.10). First, 2,2'-bithiophene (3.6 g, 21.7 mmol) and 4-(2-hydroxyethoxy)benzaldehyde (1.44 g, 8.7 mmol) were mixed with ethylene glycol (120 mL), and then the mixture was stirred for 30 min under N_2. Next, 70% $HClO_4$ (12 mL, 184.5 mmol) was added and the resulting solution was stirred for 16 h at 60 °C. Afterwards, the reaction mixture was cooled to room temperature and the excess of methylene chloride was added in order to dissolve the desired compound. Subsequently, the mixture was treated with the saturated solution of Na_2CO_3 to neutralize the excess acid. The collected organic liquid layer was washed with water, and then dried with anhydrous Na_2SO_4. After solvent evaporation out of the organic layer, the compound was purified by liquid chromatography on a silica gel column using the hexane : $CHCl_3$ (1 : 1 to

0 : 1, *v* : *v*) eluent. Yield: 1.13g (1.714 g, 41%). ^{1}H NMR (CHCl$_3$-d), Fig. A.5: δ (in ppm) 7.30–7.25 (d, 2H, bithiophene H), 7.18–7.14 (dd, 2H, bithiophene H), 7.10-7.07 (dd, 2H, bithiophene H), 7.03-7.00 (d, 2H, phenyl H), 6.98-6.95 (dd, 2H, phenyl H), 6.92–6.88 (d, 2H, bithiophene H), 6.77–6.74 (dd, 2H, bithiophene H), 5.71 (s, 1H, −CH−), 4.08-4.04 (t, 2H, -CH2-), 3.96-3.92 (t, 2H, -CH2-). Product molecular mass calcd.: 480.7.
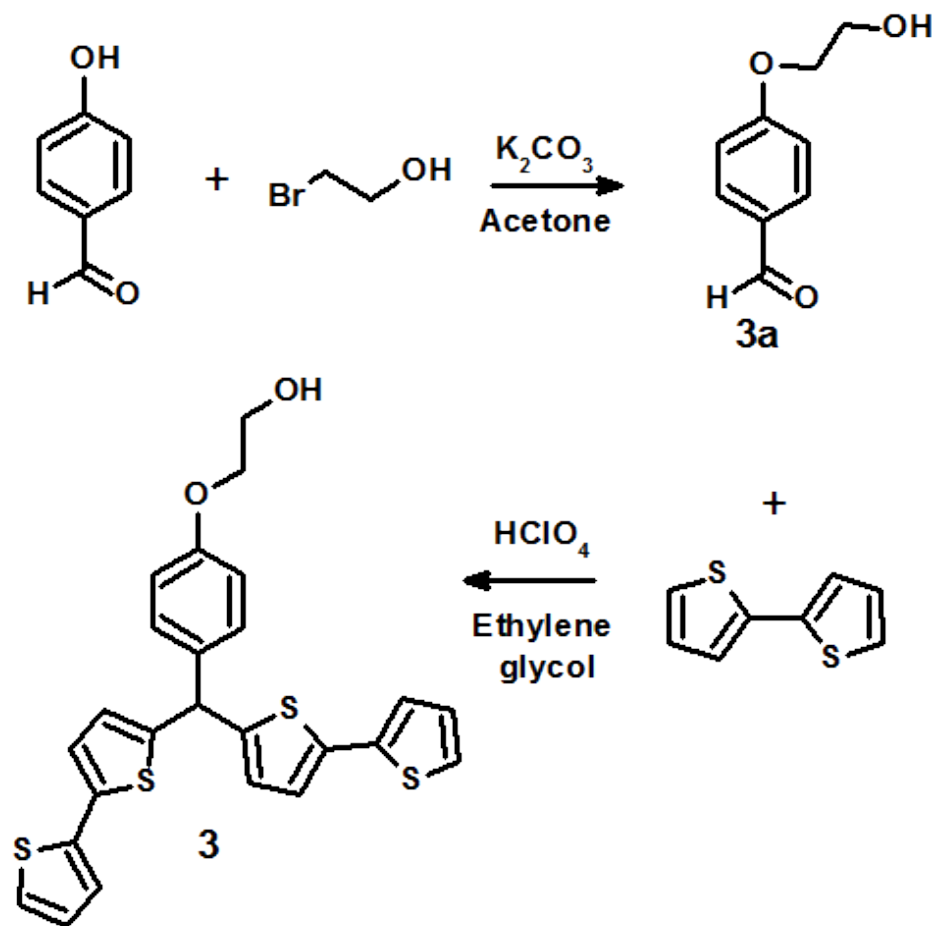
Scheme 2.10 Syntheses of 4-(2-hydroxyethoxy)benzaldehyde **3a** and 4-bis(2,2'-bithien-5-yl)methylphenol glycol ether **3**.

4-Bis(2,2'-bithienyl)-(4-[2-tosyl]ethoxy)methane **4a** (Scheme 2.11). First, **3** (1.5 g, 3.12 mmol), 4-dimethyloaminopyridine (19 mg, 0.16 mmol) and triethylamine (435 μL, 3.12 mmol) were dissolved in dichloromethane, and then stirred under N$_2$ for 1 h. Next, 4-methylbenzenesulfonyl chloride (595 mg, 3.12 mmol) dissolved in dichloromethane was added dropwise for 10 min. After that, the reaction mixture was stirred for 16 h. Subsequently, the solvent was evaporated, and then the residue was dissolved in CHCl$_3$ followed by washing with water, and then the NaHCO$_3$ solution. Subsequently the organic layer was dried with anhydrous Na$_2$SO$_4$, and then the solvent evaporated. The residue was purified by liquid chromatography on a

silica gel column using the hexane : CHCl$_3$ (1 : 1 to 8 : 2, v : v) eluent. Yield: 1.37g (69%). ^{1}H NMR (CHCl$_3$-d), Fig. A.6: δ (in ppm) 7.85–7.80 (d, 2H, tosylate phenyl H), 7.34–7.29 (d, 2H, tosylate phenyl H), 7.28-7.24 (d, 2H, bithiophene H), 7.18-7.14 (dd, 2H, bithiophne H), 7.12-7.08 (dd, 2H, bithiophene H), 7.04-7.00 (d, 2H, phenyl H), 6.98-6.94 (dd, 2H, phenyl H), 6.78–6.74 (dd, 2H, bithiophene H), 5.71 (s, 1H, –CH–), 4.38-4.32 (t, 2H, -CH2-), 4.12-4.08 (t, 2H, -CH2-), 2.41 (s, 3H, tosylate -CH3). Product molecular mass calcd.: 634.9.

4-Bis(2,2'-bithien-5-yl)methylphenol 2-O-(4-tertbutylcalix[6]arene) ethoxyl ether **4** (Scheme 2.11). First, 4-terbutylcalix[6]arene (1.91 g, 2 mmol) was dissolved in DMF (80 mL). Then, K$_2$CO$_3$ (667 mg, 4.9 mmol) was added, and then the mixture was stirred under N$_2$ for 1 h. Next, **4a** (308 mg, 0.49 mmol) dissolved in DMF was added dropwise. After that, the reaction mixture was heated to 60 °C and stirred for 48 h. Then, K$_2$CO$_3$ was filtered out, and then the filtrate solvent was evaporated under reduced pressure. The resulting solid was purified by liquid chromatography on a silica gel column using the hexane : CHCl$_3$ (9 : 1 to 1 : 1, v : v) eluent. Yield: 150 mg (21%). ^{1}H NMR (CHCl$_3$-d), Fig. A.7: δ (in ppm) 9.89 (s, 2H, ca-lixarene OH), 9.34 (s, 1H, calixarene OH), 9.03 (s, 2H, calixarene OH), 7.34–7.30 (d, 2H, bithiophene H), 7.20–7.14 (m, 4H, bithiophene H overlapped with calixarene phenyl H), 7.20-7.02 (dd, 4H, overlapped with calixarene phenyl H), 7.09-7.02 (m, 8H, bithiophene H overlapped with calixarene phenyl H), 6.99-6.96 (dd, 2H, phenyl H), 6.95–6.92 (d, 2H, phenyl H), 6.73–6.70 (dd, 2H, bithiophene H), 5.72 (s, 1H, –CH–), 4.60-4.49 (m, 6H, calixarene -CH2- overlapped with –CH2-), 3.60-3.42(d, 2H, calixarene –CH2-) 3.50-3.36 (m, 4H, calixarene-CH2-overlapped with –CH2-). ESI(-)-MS m/z calcd. for C$_{91}$H$_{104}$O$_7$S$_4$: 1436.0, found: 1433.6 (Fig. A.8).

4-(2-Bromoethoxy)benzaldehyde **5a** (Scheme 2.12). First, 4-hydroxybenzaldehyde (5 g, 40.9 mmol) was dissolved in acetone. Next, K$_2$CO$_3$ (28 g, 202.5 mmol) was added, and then the mixture was stirred for 30 min under N$_2$. Subsequently, dibro-moethane (10.6 mL, 122.7 mmol) was added dropwise and the resulting mixture was stirred for 20 h at 80 °C. After that, K$_2$CO$_3$ was filtered out, and then the filtrate sol-vent was evaporated. The yellow oily residue left was diluted with dichloromethane, and then washed with water in order to remove the K$_2$CO$_3$ residue. The organic layer was dried with anhydrous Na$_2$SO$_4$, and then evaporated. Finally, a crude compound was purified by liquid chromatography on a silica gel column using the hexane : CHCl$_3$ (1 : 1 to 8 : 2, v : v) eluent. Yield: 4.09 g (44%). ^{1}H NMR (CHCl$_3$-d), Fig. A.9: δ (in ppm) 9.89 (s, 1H, CHO), 7.86-7.80 (d, 2H, phenyl H), 7.04–6.98 (d, 2H, phenyl H), 4.38-4.32 (t, 2H, -CH2-), 3.68-3.60 (t, 2H, -CH2-). Product molecular mass calcd.: 228.2.

Scheme 2.11 Syntheses of 4-bis(2,2'-bithienyl)-(4-[2-tosyl]ethoxy)methane **4a** and 4-bis(2,2'-bithien-5-yl)methylphenol 2-O-(4-tertbutylcalix[6]arene) ethoxyl ether **4**.

4-Bis(2,2'-bithien-5-yl)methylphenol 2-bromoethyl ether **5** (Scheme 2.12). First, 2,2'-bithiophene (1.63 g, 9.8 mmol) and **5a** (753 mg, 3.3 mmol) were mixed with ethylene glycol (120 mL), and then the mixture was stirred for 30 min under N_2. Then, 70% $HClO_4$ (8.6 mL, 132 mmol) was added and the resulting solution was stirred for 16 h at 60 °C. Next, the reaction mixture was cooled to room temperature and the excess of methylene chloride was added in order to dissolve the desired compound. Subsequently, the mixture was treated with the saturated solution of Na_2CO_3 to neutralize the excess acid. The collected organic liquid layer was washed with water, and then dried with anhydrous Na_2SO_4. After the evaporation of the organic layer, the compound was purified by liquid chromatography on a silica gel column using the hexane : $CHCl_3$ (100 : 100 to 95 : 5, v : v) eluent. Yield: 1.08 g (1.714 g, 60%). ^{1}H NMR ($CHCl_3$-d), Fig. A.10: δ (in ppm) 7.30–7.26 (d, 2H, bithiophene H), 7.20–7.16 (dd, 2H, bithiophene H), 7.10-7.07 (dd, 2H, bithiophene

H), 7.02-7.00 (d, 2H, phenyl H), 6.98-6.96 (dd, 2H, phenyl H), 6.90–6.86 (d, 2H, bithiophene H), 6.76–6.72 (dd, 2H, bithiophene H), 5.71 (s, 1H, –CH–), 4.30-4.26 (t, 2H, -CH2-), 3.64-3.60 (t, 2H, -CH2-). Product molecular mass calcd.: 543.6.
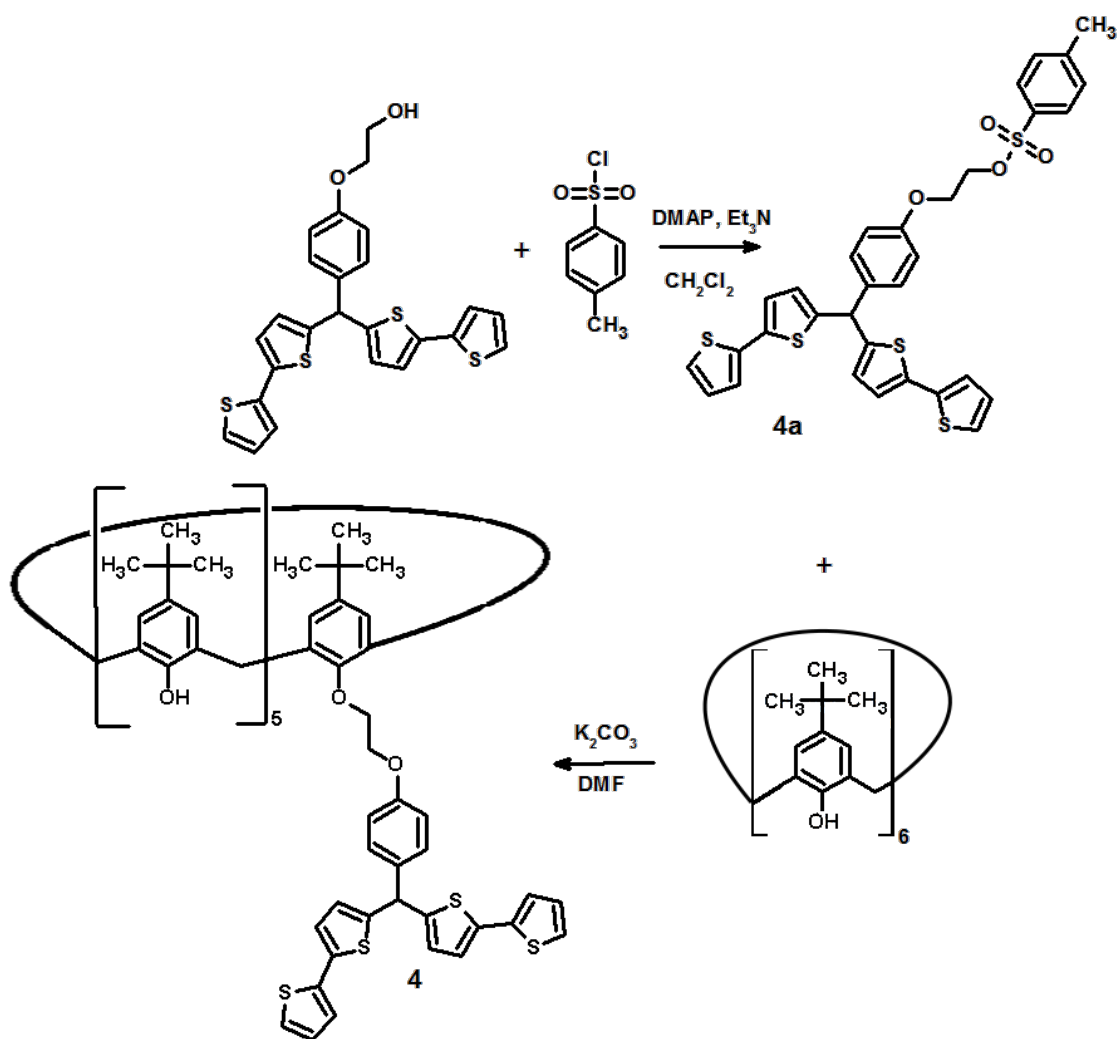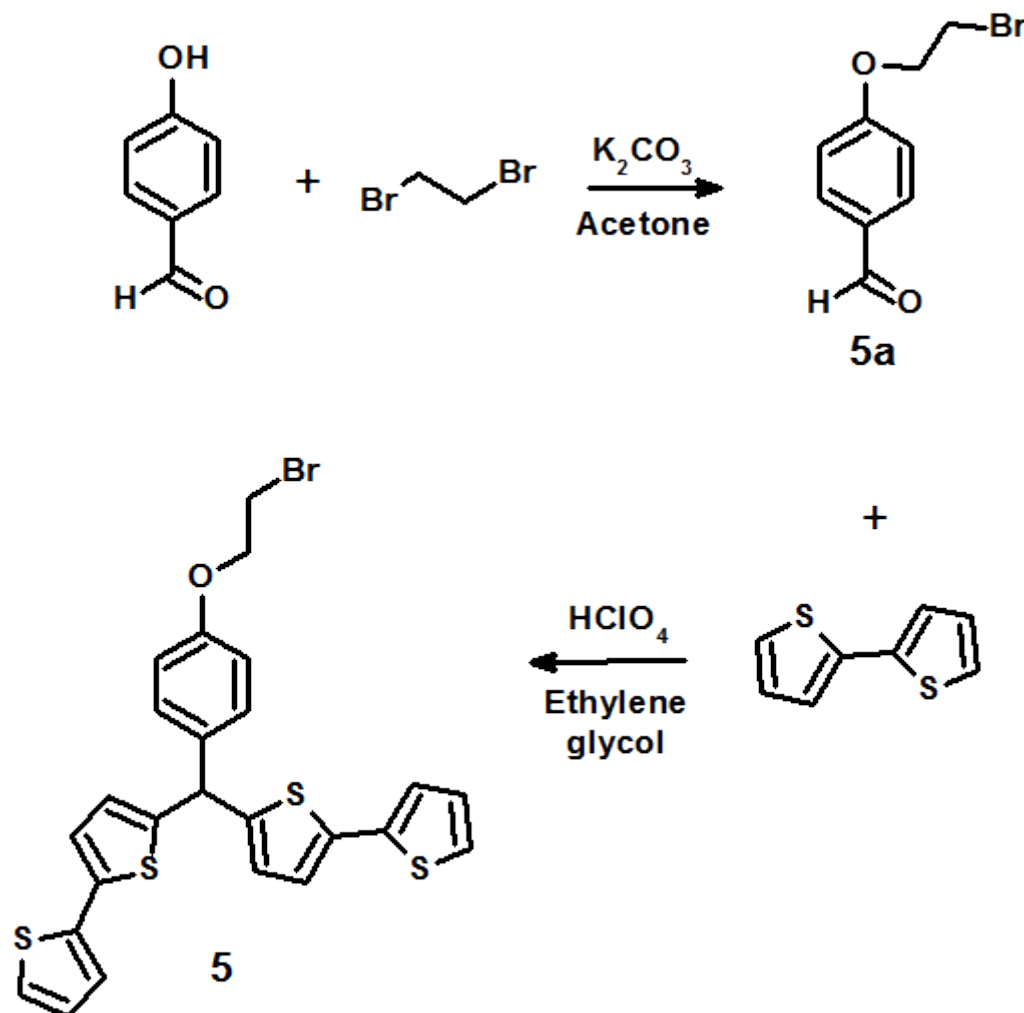

Scheme 2.12 Syntheses of 4-(2-bromoethoxy)benzaldehyde **5a** and 4-bis(2,2'-bithien-5-yl)methylphenol 2-bromoethyl ether **5**.

4-Bis(2,2'-bithien-5-yl)methylphenol 2-(1-N-succinimidoxy)ethyl ether **6** (Scheme 2.13). First, N-hydroxysuccinimide (58 mg, 0.5 mmol) was dissolved in acetone. Next, K_2CO_3 (700 mg, 10 mmol) was added, and then the mixture was stirred for 30 min under N_2. After that, **5** (544 mg, 1 mmol) dissolved in 10 ml of acetone was added dropwise, and then the resulting mixture was stirred for 48 h at 80 °C. Next, K_2CO_3 was filtered out and then the filtrate solvent evaporated. A crude dark blue product was purified by liquid chromatography on a silica gel column using the hexane : CH_3 (3 : 1 to 0 : 1, $v : v$) as eluent. Yield: 100 mg (35%). ^{1}H NMR (CHCl$_3$-d), Fig. A.11: δ (in ppm) 7.26–7.22 (d, 2H, bithiophene H), 7.16–7.13 (dd, 2H, bithiophene H), 7.09-7.07 (dd, 2H, bithiophene H), 7.02-7.00

(d, 2H, phenyl H), 7.00-6.97 (d, 2H, phenyl H), 6.97–6.93 (dd, 2H, phenyl H), 6.85-6.81 (d, 2H, bithiophene H), 6.74–6.71 (dd, 2H, bithiophene H), 5.69 (s, 1H, –CH–), 4.48-4.44 (t, 2H, -CH2-), 4.28-4.24 (t, 2H, -CH2-), 2.74 (s, 4H, succinimide –CH2-). Product molecular mass calcd.: 577.8.
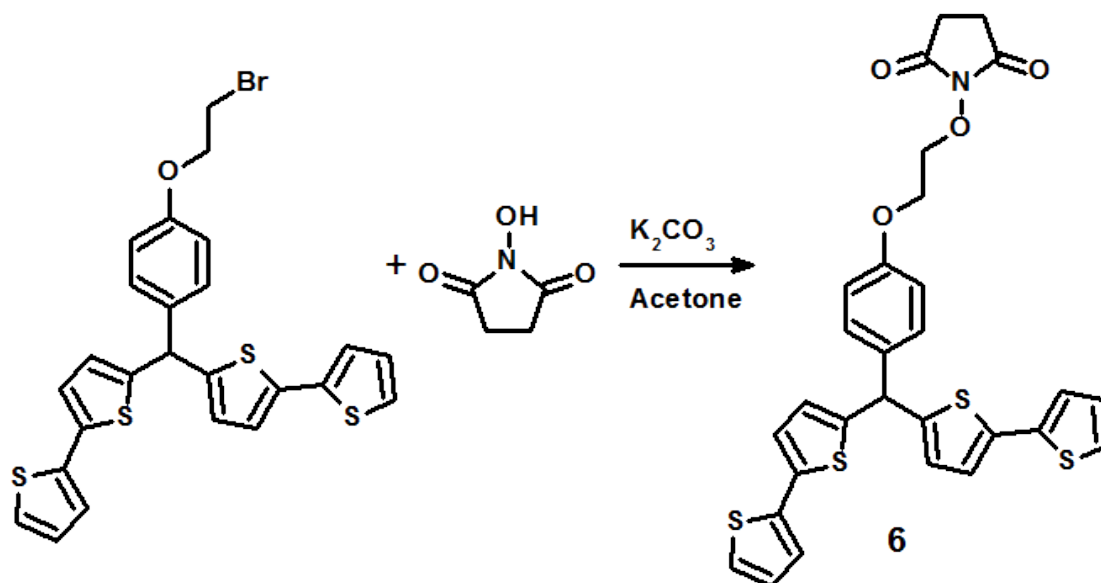
Scheme 2.13 Synthesis of 4-bis(2,2'-bithien-5-yl)methylphenol 2-(1-*N*-succinimidoxy)ethyl ether **6**.

4-Bis(2,2'-bithien-5-yl)methylalanine **7** (Scheme 2.14). First, 2,2'-bithiophene (2.54 g, 15.3 mmol) and 4-acetaminobenzaldehyde (1.0 g, 6.13 mmol) were mixed with ethylene glycol (80 mL), and then the mixture was stirred for 30 min under N_2. Next, 70% $HClO_4$ (16 mL, 245.2 mmol) was added, and then the resulting solution was stirred for 16 h at 60 °C. After that, the reaction mixture was cooled to room temperature and the excess of methylene chloride was added in order to dissolve the desired compound. Subsequently, the mixture was treated with the saturated solution of Na_2CO_3 to neutralize the excess acid. The collected organic liquid layer was washed with water, and then dried with anhydrous Na_2SO_4. After solvent evaporation out of the organic layer, a crude product left was purified by lyquid chromatography on a silica gel column using the hexane : $CHCl_3$ (1 : 1 to 0 : 1, *v* : *v*), and then CH_2Cl_2 : MeOH (8 : 0, *v* : *v*) eluent. Yield: 1.53g (57%). ^{1}H NMR ($CHCl_3$-d), Fig. A.12: δ (in ppm) 7.18–7.16 (dd, 2H, bithiophene H), 7.16–7.13 (d, 2H, bithiophene H), 7.11-7.08 (dd, 2H, bithiophene H), 7.03–7.00 (m, 2H, bithiophene H), 6.98-6.95 (dd, 2H, phenyl H), 6.77–6.74 (dd, 2H, phenyl H), 6.68–6.64 (d, 2H, bithiophene H), 5.66 (s, 1H, –CH–), 3.7-3.3 (s, 2H, -NH2). ESI(-)-MS *m/z* calcd. for $C_{23}H_{17}NS_4$: 435.7, found: 434.0 (Fig. A.13).

For crystallization, first, **7** was dissolved in CH_2Cl_2, and then spiked with concentrated HCl, in a 5 mL vial. After that, the vial was tightly capped so that the solvent
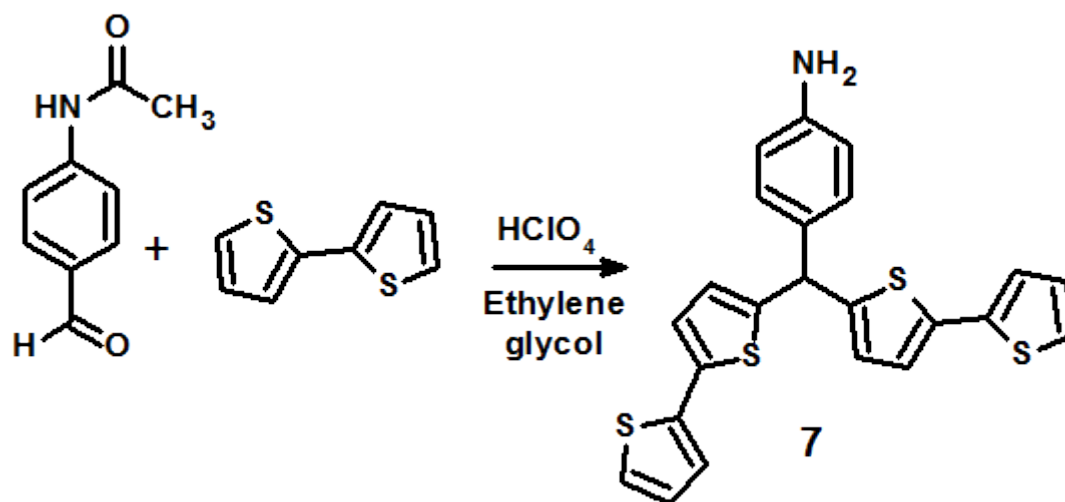
Scheme 2.14 Synthesis of 4-bis(2,2'-bithien-5-yl)methylalanine **7**.

only slowly evaporated. After few weeks, a dark-green needle-shaped crystals were formed in the solution. Details on the atomic coordinates, bond lengths, and angles between bonds for **7** are summarized in Tables B.1 through B.4 in Appendix B. This crystal structure has been deposited at the Cambridge Crystallographic Data Centre (CCDC) and allocated the deposition number CCDC 923045 (Scheme 2.15).
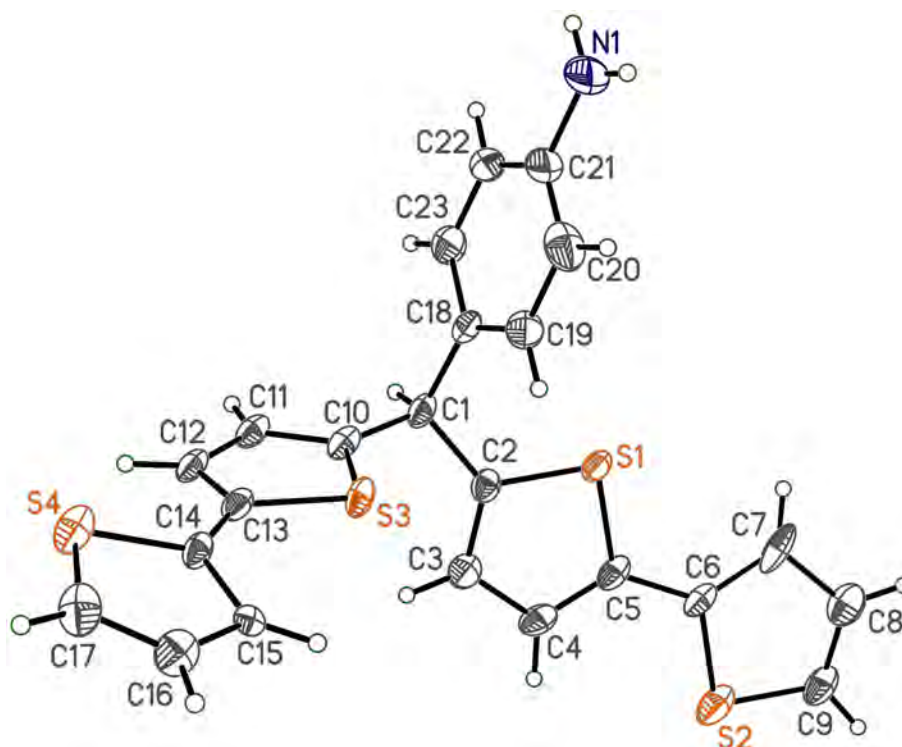
Scheme 2.15 Crystal structure of 4-bis(2,2'-bithien-5-yl)methylalanine **7**.

4-Bis(2,2'-bithien-5-yl)methyl-nitrobenzene **8** (Scheme 2.16). First, 2,2'-bithiophene (1.0 g, 6 mmol) and 4-nitrobenzaldehyde (363 mg, 2.4 mmol) were mixed with ethylene glycol (60 mL) and the mixture was stirred for 30 min under N_2. Then,

70% $HClO_4$ (6.3 mL, 96 mmol) was added, and then the resulting solution was stirred for 16 h at 60 °C. Next, the reaction mixture was cooled to room temperature and the excess of methylene chloride was added in order to dissolve the desired compound. Subsequently, the mixture was treated with the saturated solution of Na_2CO_3 to neutralize the excess acid. The collected organic liquid layer was washed with water, and then dried with anhydrous Na_2SO_4. After the evaporation of solvent of the organic layer, the compound was purified by liquid chromatography on a silica gel column using the hexane : $CHCl_3$ (100 : 100 to 75 : 25, $v : v$) eluent. Yield: 470 mg (42%). ^{1}H NMR ($CHCl_3$-d), Fig. A.14: δ (in ppm) 8.22-8.17 (d, 2H, bithiophene H), 7.53–7.48 (d, 2H, bithiophene H), 7.20-7.17 (dd, 2H, bithiophene H), 7.12–7.08 (dd, 2H, bithiophene H), 7.04-7.01 (d, 2H, phenyl H), 7.00–6.96 (dd, 2H, phenyl H), 6.77–6.74 (dd, 2H, bithiophene H), 5.85 (s, 1H, –CH–). ESI(-)-MS m/z calcd. for $C_{23}H_{15}NO_2S_4$: 465.6, found 464.0 (Fig. A.16).

Scheme 2.16 Synthesis of 4-bis(2,2'-bithien-5-yl)methyl-nitrobenzene **8**.

For crystallization, first, **8** was dissolved in few drops of CH_2Cl_2. Next, methanol was slowly added on top of CH_2Cl_2 in such a way that the two solvents would not mix. After that, the vial was tightly capped so that the solvent only slowly evaporated. After few weeks, a dark-blue needle-shaped crystals were formed in the solution. Details on the atomic coordinates, bond lengths, and angles between bonds for **8** are summarized in Tables B.5 through B.8 in Appendix B. The crystal structure of **8** is shown in Scheme 2.17.

4-Bis(2,2'-bithien-5-yl)methylbenzoic acid glycol ester **9** (Scheme 2.18). First, 2,2'-bithiophene (3.32 g, 20 mmol) and 4-carboxybenzaldehyde (1.0 g, 6.7 mmol) were mixed with ethylene glycol (100 mL), and then the mixture was stirred for 30 min under N_2. Then, 70% $HClO_4$ (19.5 mL, 300 mmol) was added, and then the resulting solution was stirred for 16 h at 60 °C. Next, the reaction mixture was cooled
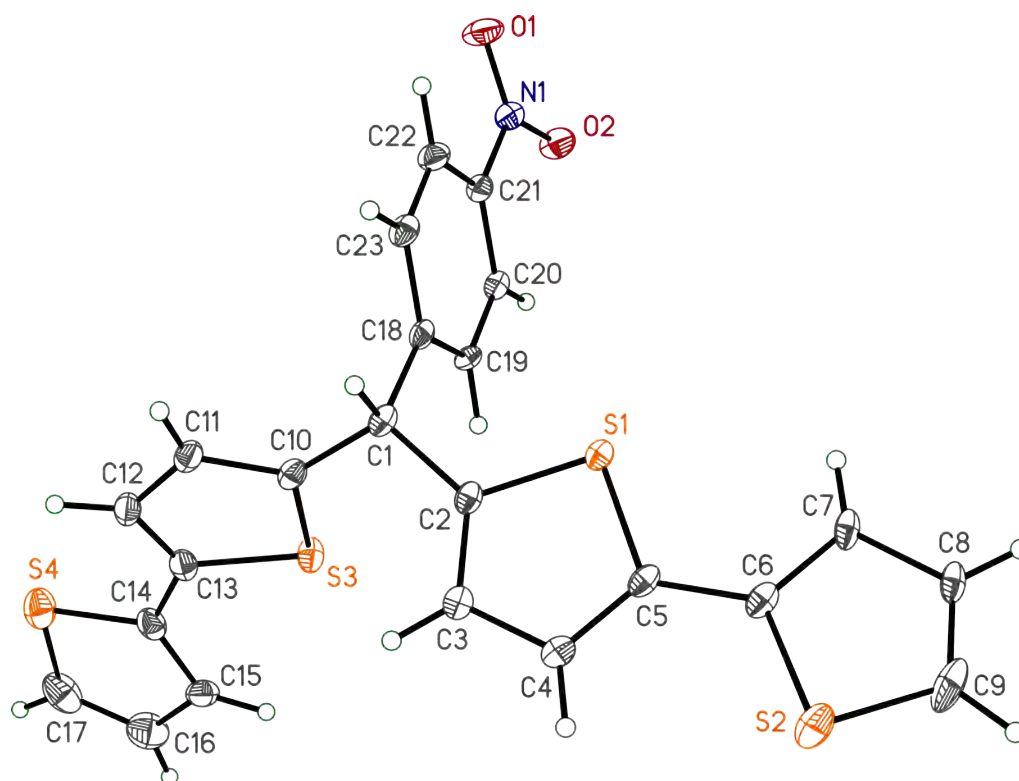
Scheme 2.17 Crystal structure of 4-bis(2,2'-bithien-5-yl)methyl-nitrobenzene **8**.

to room temperature and the excess of methylene chloride was added in order to dissolve the desired compound. Subsequently, the mixture was treated with the saturated Na_2CO_3 solution to neutralize the excess acid. The collected organic liquid layer was washed with water, and then dried with anhydrous Na_2SO_4. After the evaporation of solvent of the organic layer, the compound was purified by liquid chromatography on a silica gel column using the hexane : $CHCl_3$ (1 : 1 to 1 : 9, $v : v$), and then $CHCl_3$: MeOH (9 : 1, $v : v$) eluent. Yield: 2.14 g (63%). ^{1}H NMR ($CHCl_3$-d), Fig. A.15: δ (in ppm) 8.10-8.06 (d, 2H, bithiophene H), 7.46–7.42 (d, 2H, bithiophene H), 7.19-7.16 (d, 2H, bithiophene H), 7.13–7.09 (d, 2H, bithiophene H), 7.04-7.02 (d, 2H, phenyl H), 7.00–6.96 (m, 2H, phenyl H), 6.76–6.73 (d, 2H, bithiophene H), 5.80 (s, 1H, −CH−), 4.49-4.46 (t, 2H, -CH2-), 3.97-3.94 (t, 2H, -CH2-). Product molecular mass calcd.: 508.6.

For crystallization, **9** was dissolved in methanol and the vial was tightly capped so that the solvent only slowly evaporated. After few weeks, a dark-violtet needle-shaped crystals were formed in the solution. Details on the atomic coordinates, bond lengths, and angles between bonds for **9** are summarized in Tables B.9 through B.12 in Appendix B. The crystal structure of **9** is shown in Scheme 2.19.

4-Bis(2,2'-bithien-5-yl)methylbenzoic acid **10** (Scheme 2.20). First, **9** (1.02 g, 2 mmol) was dissolved in THF. Then, KOH (5.6 g, 100 mmol) dissolved in 30 mL of water was added, and then the resulting solution was stirred under N_2 for
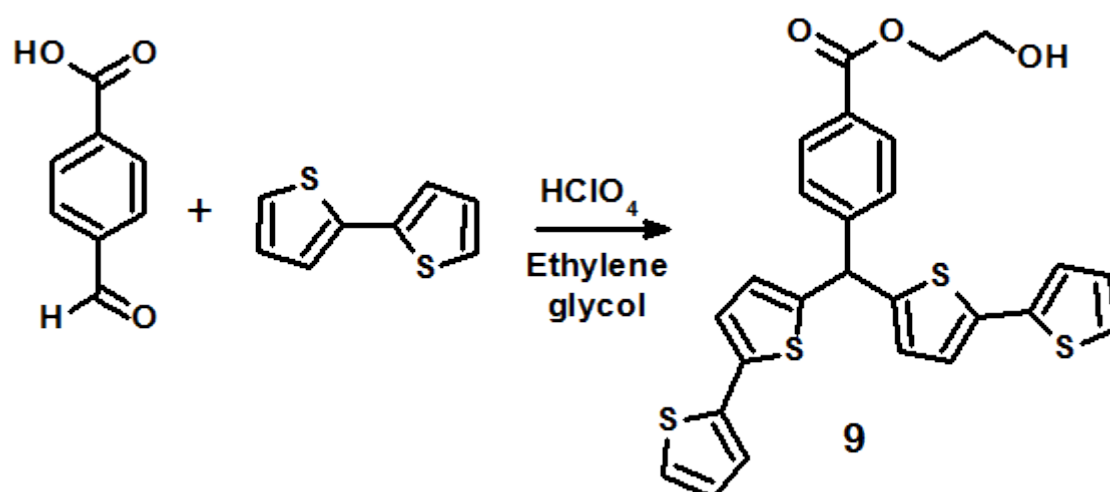
Scheme 2.18 Synthesis of 4-bis(2,2'-bithien-5-yl)methylbenzoic acid glycol ester **9**.
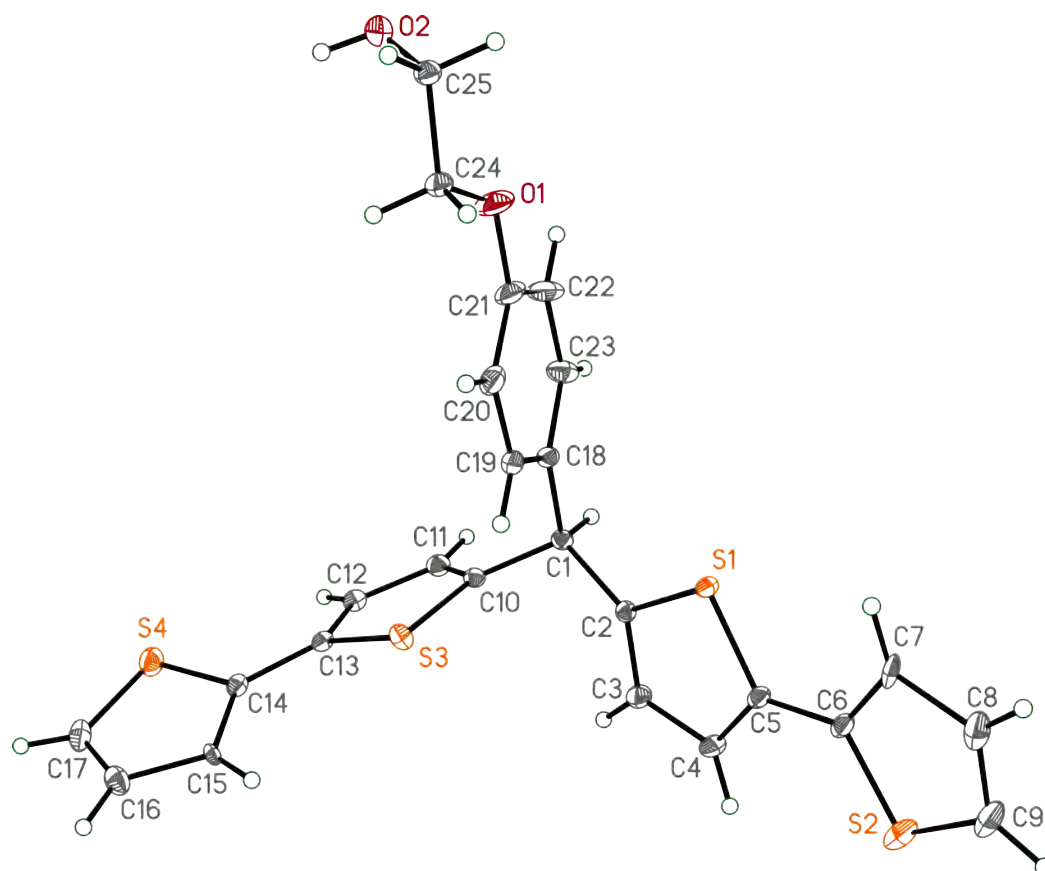
Scheme 2.19 Crystal structure of 4-bis(2,2'-bithien-5-yl)methylbenzoic acid glycol ester **9**.

18 h at 70 °C. Next, THF was evaporated from the reaction mixture and the remaining water solution was acidified with HCl. Subsequently, the product was extracted with the excess of methylene chloride. The collected organic layer was neutralized with the saturated solution of Na_2CO_3, and then washed with water followed by drying with anhydrous Na_2SO_4. After the evaporation of solvent of the organic layer, a crude product left was purified by liquid chromatography on a silica gel column using the hexane : $CHCl_3$ (1 : 1 to 0 : 1, v : v) eluent. Yield: 780 mg (84%). ^{1}H NMR ($CHCl_3$-d), Fig. A.17: δ (in ppm) 8.16-8.10 (d, 2H, bithiophene H), 7.50–7.46 (d, 2H, bithiophene H), 7.21-7.17 (d, 2H, bithiophene H), 7.14–7.08 (d, 2H, bithiophene H), 7.06-7.00 (d, 2H, phenyl H), 7.00–6.96 (m, 2H, phenyl H), 6.78–6.74 (d, 2H, bithiophene H), 5.84 (s, 1H, –CH–). ESI(-)-MS m/z calcd. for $C_{24}H_{16}O_2S_4$: 464.6, found: 463.0 (Fig. A.19).
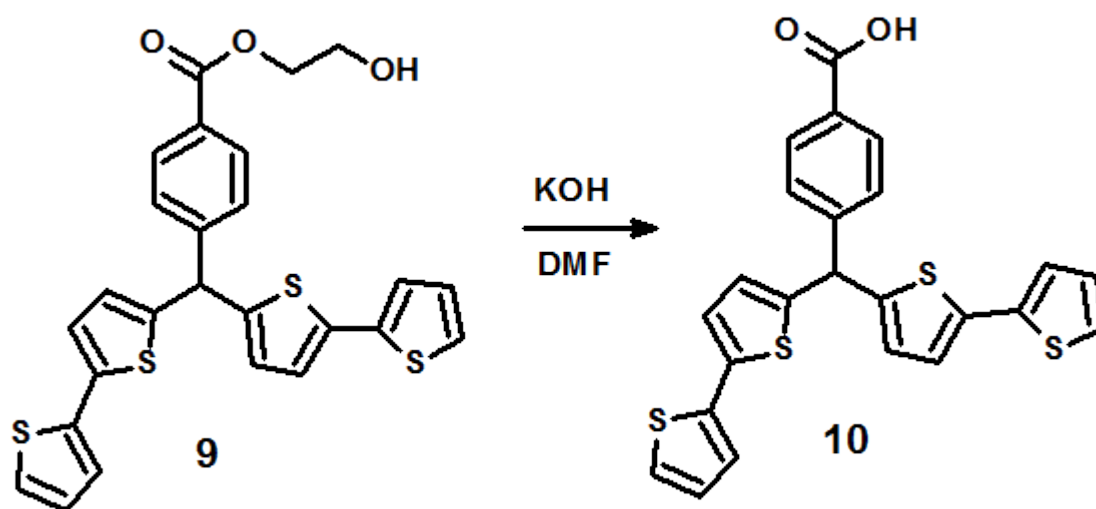
Scheme 2.20 Synthesis of 4-bis(2,2'-bithien-5-yl)methylbenzoic acid **10**.

For crystallization, first, **10** was dissolved in few drops of CH_2Cl_2. Next, THF was slowly added on top of CH_2Cl_2 in such a way that the two solvents would not mix. After that, the vial was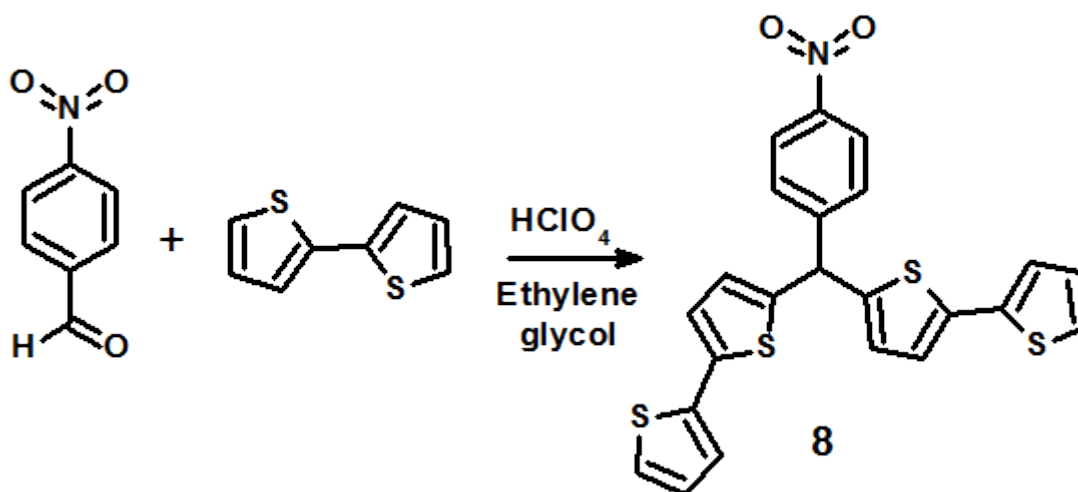 tightly capped so that the solvent only slowly evaporated. After few weeks, a transparent needle-shaped crystals were formed in the solution. Details on the atomic coordinates, bond lengths, and angles between bonds for **10** are summarized in Tables B.13 through B.16 (Appendix B). The crystal structure of **10** is shown in Scheme 2.21.

1-(2'-Hydroxyethyl)cytosine **11a** (Scheme 2.22). The synthesis procedure adapted from literature [140]. That is, cytosine (1.5 g, 13.5 mmol) and ethylene carbonate (1.19 g, 13.5 mmol) were dissolved in DMF (60 mL) slightly alkalized with NaOH. The mixture was stirred under N_2 for 20 h at 70 °C. After reaction solvent was evaporated under reduced pressure, the residue was purified by liquid chromatography on a silica gel column using the hexane : $CHCl_3$ (1 : 1 to 1 : 9, v : v), and then
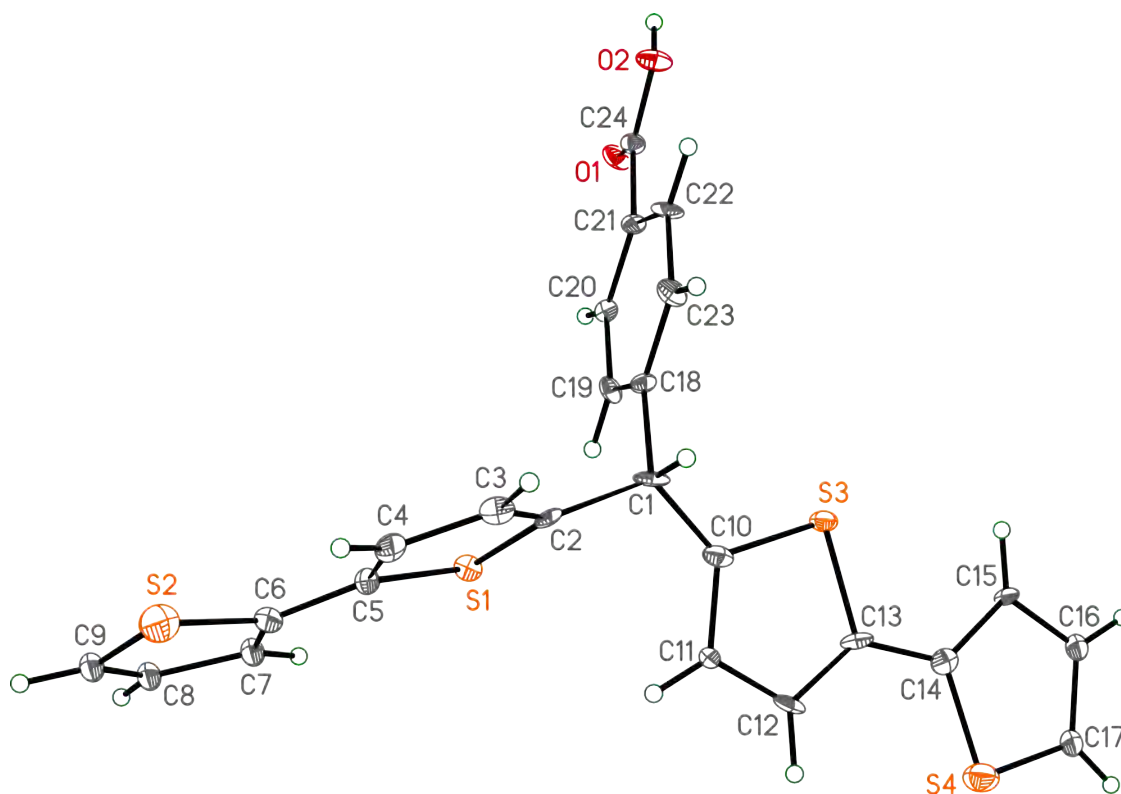
Scheme 2.21 Crystal structure of 4-bis(2,2'-bithien-5-yl)methylbenzoic acid **10**.

CHCl$_3$: MeOH (9 : 1 to 1 : 1, *v* : *v*) eluent. Yield: 110 mg (11%). ^{1}H NMR (methanol-d4), Fig. A.18: δ (in ppm) 7.55-7.51 (d, 1H, -CH=), 5.84-5.80 (dd, 1H, -CH=) 3.88-3.82 (t, 2H, CH2), 3.79-3.72 (t, 2H, CH2). Product molecular mass calcd.: 155.2.

2-(Cytosin-1-yl)ethyl 4-bis(2,2'-bithien-5-yl)methylbenzolate **11** (Scheme 2.22). First, **10** (410 mg 0.88 mmol) was dissolved in DMF (50 mL), and then cooled to 0 °C in an ice bath. Then, EDCI (273 mg, 1.76 mmol) was added, and then the mixture was stirred for ~30 min under N$_2$. Next, **11a** (136.5 mg, 0.88 mmol), dissolved in DMF 20 mL, was added dropwise for 10 min. Afterwards, the reaction mixture was stirred in an ice bath for 1 h. The reaction was continued for another 72 h at room temperature. After that, the reaction solvent was evaporated under reduced pressure. The oily residue was purified by a liquid chromatography on a silica gel column using the CHCl$_3$: MeOH (9 : 1 to 1 : 5, *v* : *v*) eluent. Yield: 143 mg (27%). ^{1}H NMR (CHCl$_3$-d), Fig. A.20: δ (in ppm) 9.32-9.26 (d, 1H, cytosine –CH=), 7.50-7.36 (m, 4H, bithiophene H), 7.16-7.11 (d, 2H, overlapped bithiophene and phenyl H), 7.10-7.04 (d, 2H, phenyl H), 7.02-6.90 (m, 4H, bithiophene H), 5.78 (s, 1H, -CH-) 3.80-3.72 (t, 2H, CH2), 3.32-3.24 (t, 2H, CH2). ESI-MS *m/z* calcd. for C$_{30}$H$_{23}$O$_3$N$_3$S$_4$+H$_2$O: 619.8, found: 620.1 (Fig. A.22).

4-Bis(2,2'-bithienyl)-(4-hydroxyphenyl)methane thymine-1-acetate **12** (Scheme 2.23).
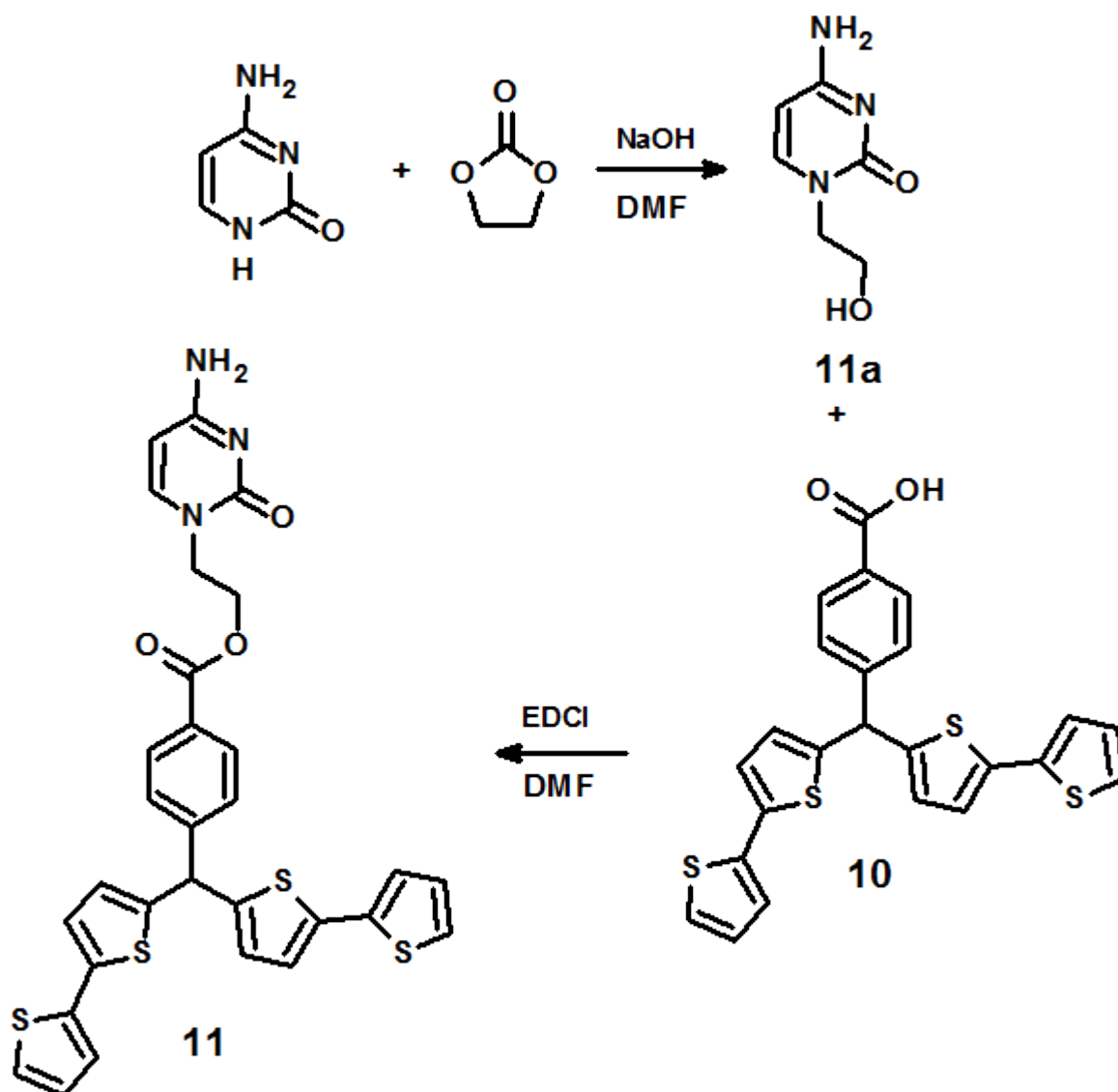
Scheme 2.22 Syntheses of 1-(2'-hydroxyethyl)cytosine **11a** and 2-(cytosin-1-yl)ethyl 4-bis(2,2'-bithien-5-yl)methylbenzolate **11**.

First, thymine-1-acetic acid (72 mg 0.4 mmol) was dissolved in DMF (30 mL) and cooled to 0 °C in an ice bath. Then, EDCI (121 mg, 0.8 mmol) was added and the mixture was stirred for ~30 min under N_2. Next, **1** (170 mg, 0.4 mmol) dissolved in 10 mL of DMF, was added dropwise for 10 min. Subsequently, the reaction mixture was stirred in an ice bath for 1 h. The reaction continued for another 46 h at room temperature. After that, the reaction solvent was evaporated under reduced pressure. The residue was purified by liquid chromatography on a silica gel column using the $CHCl_3$: MeOH (9 : 1 to 1 : 2, v : v) eluent. Yield: 75 mg (31%). ^{1}H NMR ($CHCl_3$-d), Fig. A.21: δ (in ppm) 9.04 (s, 1H, thymine -NH-), 7.33-7.28 (d, 2H, phenyl H), 7.12-7.09 (m, 2H, bithiophene H), 7.07-7.04 (d, 2H, phenyl H), 7.03-7.01 (m, 2H, phenyl H), 6.97-6.89 (m, 5H, overlapped bithiophene H, phenyl H, and thymine -CH2=), 6.68-6.66 (m, 2H, bithiophene H), 5.75 (s, 1H, -CH-) 4.67

(s, 2H, -CH2-), 1.25 (s, 3H, thymine CH3). Product molecular mass calcd.: 602.8.
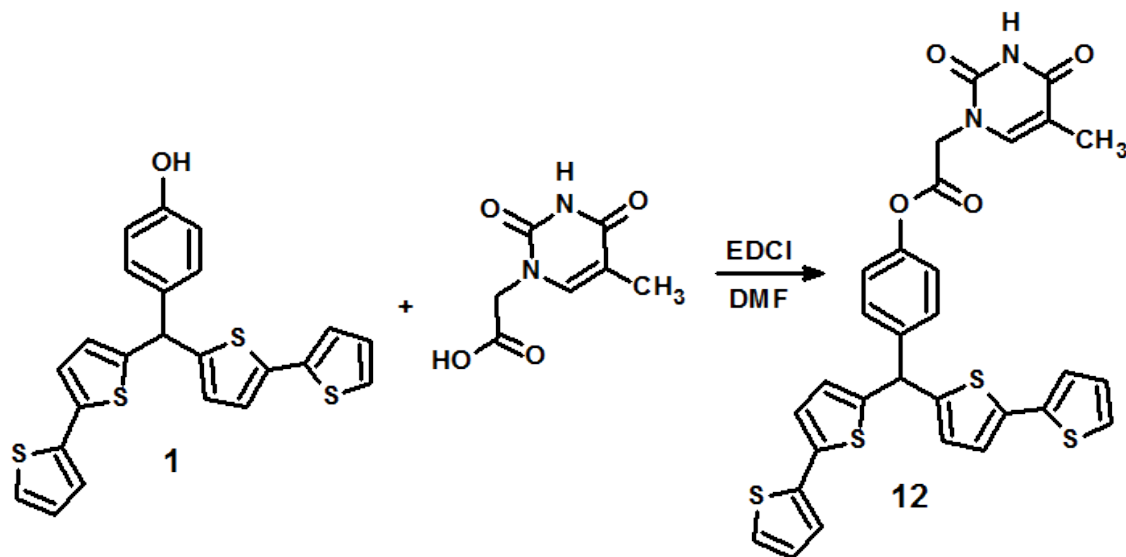
Scheme 2.23 Synthesis of 4-bis(2,2'-bithienyl)-(4-hydroxyphenyl)methane thymine-1-acetate **12**.

4-[2-(Guanin-9-yl)ethoxy]benzaldehyde **13a** (Scheme 2.24). First, guanine (916 mg, 4 mmol) and K_2CO_3, were mixed in DMF (100 mL) in a round bottom flask for 1 h under N_2. Next, **5a** (916 mg, 4 mmol) was added, and then the reaction mixture stirred for another 69 h at 120 ^{o}C. Then, DMF was evaporated under reduced pressure. The resulting yellow oily residue was pre-purified by liquid chromatography on a silica gel column using the CH_2Cl_2 : MeOH (95 : 5 to 80 : 20, *v* : *v*) eluent. Crude product was used for further syntheses without additional purification.

4-Bis(2,2'-bithien-5-yl)methylphenol 2-(guanin-9-yl)ethyl ether **13** (Scheme 2.24). First, 2,2'-bithiophene (499 g, 3 mmol) and 4-carboxybenzaldehyde (300 mg, 1.3 mmol) were mixed with ethylene glycol (50 mL), and then the resulting mixture was stirred for 30 min under N_2. Then, 70% $HClO_4$ (19.5 mL, 300 mmol) was added, and then the resulting solution was stirred for 16 h at 60 °C. Next, the reaction mixture was cooled to room temperature, and then the excess of methylene chloride was added in order to dissolve the desired compound. Subsequently, the mixture was neutralized with the saturated Na_2CO_3 solution. The collected organic liquid layer was washed with water, and then dried with anhydrous Na_2SO_4. After the evaporation of the organic layer solvent, a crude product was purified by liquid chromatography on a silica gel column using the CH_2Cl_2 : MeOH (95 : 5 to 60 : 50, *v* : *v*) eluent. Yield: 2.14 g (63%). ^{1}H NMR (CHCl$_3$-d), Fig. A.23: δ (in ppm) 7.70-7.53 (d, 1H, NH), 7.18–7.12 (d, 2H, bithiophene H), 7.10–7.05 (m, 2H, bithiophene H), 7.01-6.95 (m, 2H, bithiophene H), 6.94–6.89 (m, 2H, phenyl H), 6.89-6.83 (d, 2H, phenyl H), 6.77–6.69 (d, 2H, bithiophene H), 6.66–6.59 (m, 2H, bithiophene

H), 5.59 (s, 1H, –CH–), 4.55 (s, 1H, -CH=), 4.29-4.18 (m, 2H, -CH2-), 4.14-4.05 (m, 2H, -CH2-). ESI(-)-MS m/z calcd. for $C_{30}H_{23}O_2N_5S_4+2CH_3OH$: 677.9, found: 678.1 (Fig. A.25).
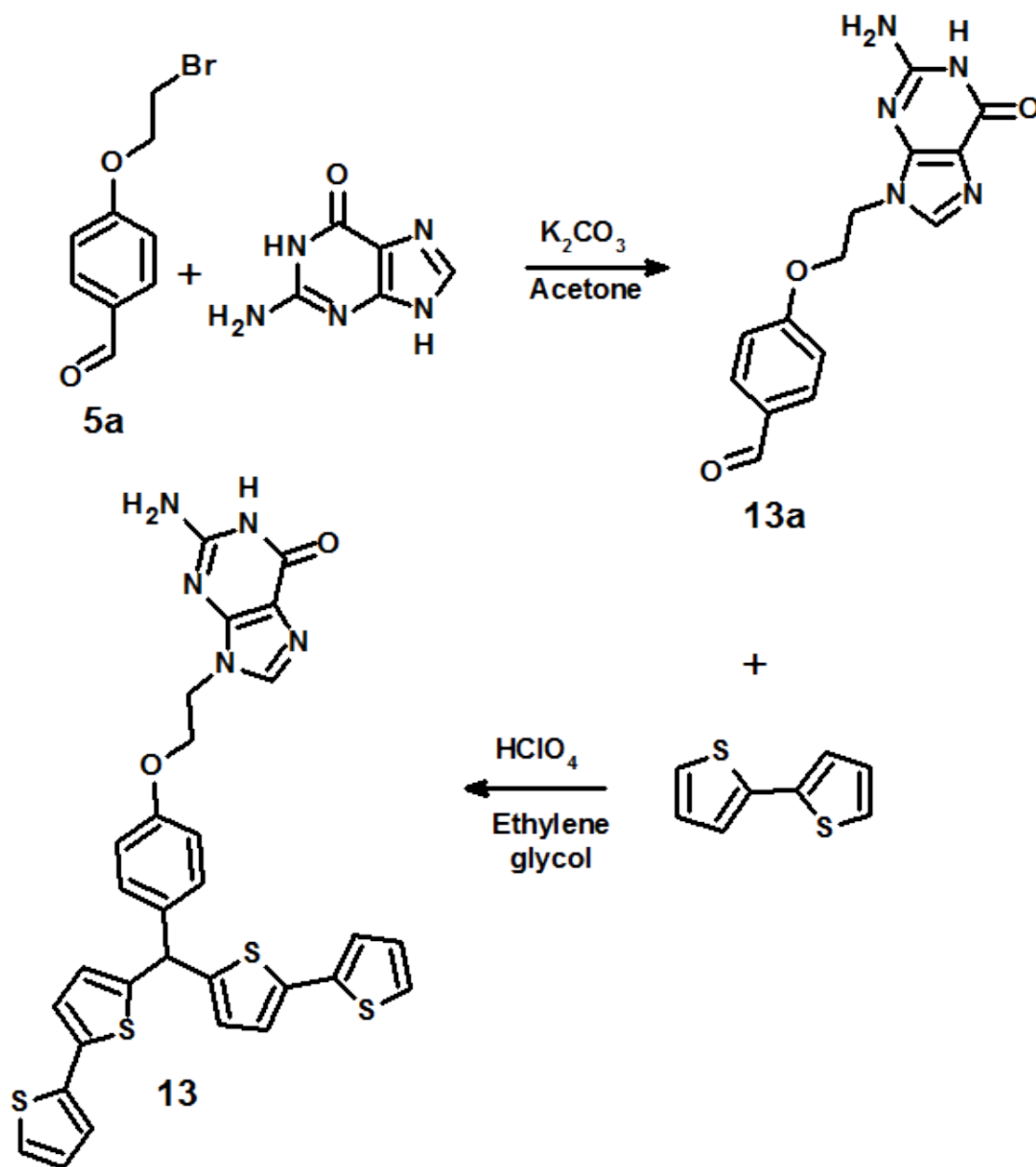
Scheme 2.24 Syntheses of 4-[2-(guanin-9-yl)ethoxy]benzaldehyde **13a** and 4-bis(2,2'-bithien-5-yl)methylphenol-2-(guanin-9-yl)ethyl ether **13**.

4-Bis(2,2'-bithien-5-yl)methylphenol-2-hydroxyacetamide ether **14** (Scheme 2.25). First, **1** (570 mg, 1.3 mmol) and K_2CO_3 (1.81 g, 13.1 mmol), were mixed in acetone (80 mL) in a round bottom flask for 30 min under N_2. Next, 2-bromoacetamide (542 mg, 4 mmol) was added, and then the reaction mixture stirred for another 16 h at 60 °C. After cooling at room temperature the reaction mixture was filtered and solvent of the filtrate was evaporated. A crude product was purified by liquid

chromatography on a silica gel column using hexane : CHCl$_3$ (1 : 1 to 1 : 9, $v : v$) eluent. Yield: 297 mg (46%). ^{1}H NMR (CHCl$_3$-d), Fig. A.24: (δ in ppm) 7.35–7.30 (d, 2H, bithiophene H), 7.20–7.17 (dd, 2H, bithiophene H), 7.11-7.08 (dd, 2H, bithiophene H), 7.03–7.00 (d, 2H, phenyl H), 6.99-6.96 (dd, 2H, phenyl H), 6.93–6.89 (d, 2H, bithiophene H), 6.77–6.74 (dd, 2H, bithiophene H), 5.74 (s, 1H, –CH–), 4.50 (s, 2H, -CH2-). Product molecular mass calcd.: 493.68.
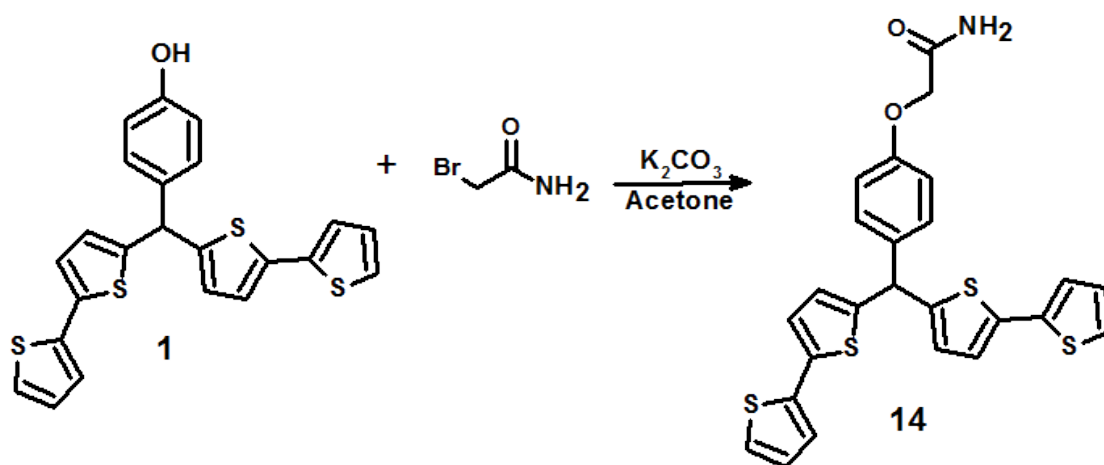
Scheme 2.25 Synthesis of 4-bis(2,2'-bithien-5-yl)methylphenol-2-hydroxyacetamide ether **14**.

Pentaethylene glycol p-toluenesulfonate **15a** (Scheme 2.26). First, pentaethylene glycol (1 mL, 4.73 mmol), 4-dimethyloaminopyridine (59.8 mg, 0.47 mmol) and triethylamine (1.318 mL, 9.46 mmol) were dissolved in dichloromethane, and then stirred under N$_2$ for 1 h. Then, 4-methylbenzenesulfonyl chloride (2.255 g, 11.83 mmol), dissolved in dichloromethane, was added dropwise for 20 min. After that, the reaction mixture was stirred for 16 h. Next, the solvent was evaporated. Subsequently, the residue was dissolved in CHCl$_3$, and then washed with water followed by the NaHCO$_3$ solution. The collected organic layer was dried with anhydrous Na$_2$SO$_4$, and then its solvent was evaporated. The residue was purified by liquid chromatography on a silica gel column using the hexane : CHCl$_3$ (9 : 1 to 3 : 2, $v : v$) eluent. Yield: 517 mg (27%). ^{1}H NMR (CHCl$_3$-d), Fig. A.26: δ (in ppm) 7.83–7.78 (d, 2H, tosylate phenyl H), 7.38–7.33 (d, 2H, tosylate phenyl H), 4.20-4.14 (m, 2H, -CH2-), 3.75-3.57 (overlapped m, 18 H, -CH2-), 2.46 (s, 3H, -CH3). Product molecular mass calcd.: 392.46.

3,4-Bis(pentaethyleneglycol)benzaldehyde **15b** (Scheme 2.26). First, 3,4-dihydroxy benzaldehyde (166 mg, 1.2 mmol) was dissolved in acetone (80 mL). Next, K$_2$CO$_3$ (3.318 g, 24 mmol) was added, and then the mixture stirred under N$_2$ for 1 h. Then, **15a** (1.412 g, 3.6 mmol), dissolved in acetone, was added dropwise. After that,

the reaction mixture was refluxed under stirring for 23 h. Subsequently, K_2CO_3 was filtered out, and then solvent of the filtrate was evaporated. The resulting yellow oil was purified by liquid chromatography on a silica gel column using the hexane : $CHCl_3$ (1 : 1 to 1 : 9, v : v), and then $CHCl_3$: MeOH (9 : 1, v : v) eluent. Yield: 498 mg (72%). ^{1}H NMR ($CHCl_3$-d), Fig. A.27: δ (in ppm) 9.83 (s, 1H, -CHO), 7.46-7.43 (m, 2H, overlayed phenyl H), 7.03-7.00 (d, 1H, phenyl H), 4.27-4.21 (m, 6H, -CH2-), 3.93-3.88 (m, 6H, -CH2-), 3.77-3.57 (m, 28 H, overlapped -CH2-). Product molecular mass calcd.: 578.6.

4-Bis(2,2'-bithien-5-yl)methyl-o-catechol pentaethyleneglycol diether **15** (Scheme 2.26). First, 2,2'-bithiophene (429 mg, 2.6 mmol) and **15b** (498 mg, 0.86 mmol) were mixed in ethylene glycol (60 mL), and then the mixture was stirred for 30 min under N_2. Next, 70% $HClO_4$ (2.24 mL, 34.4 mmol) was added, and then the resulting solution was stirred for 16 h at 60 °C. After that, the reaction mixture was cooled to room temperature, and then the excess of methylene chloride was added in order to dissolve the desired compound. Subsequently, the mixture was treated with the saturated Na_2CO_3 solution to neutralize the excess acid. The collected organic liquid layer was washed with water, and then dried with anhydrous Na_2SO_4. After the evaporation of solvent of the organic layer, a crude product left was purified by liquid chromatography on a silica gel column using the hexane : $CHCl_3$ (1 : 1 to 1 : 1, v : v), and then $CHCl_3$: MeOH (95 : 5 to 80 : 20, v : v) eluent. Yield: 678 mg (76%). ^{1}H NMR ($CHCl_3$-d), Fig. A.28: δ (in ppm) 7.10-6.97 (m, 2H, bithiophene H), 6.93-6.86 (m, 2H, bithiophene H), 6.84-6.79 (m, 4H, overlapped bithiophene and phenyl H), 6.71-6.59 (m, 6H, overlapped bithiophene and phenyl H), 5.54 (s, 1H, –CH–), 4.09-3.99 (m, 4H, -CH2-), 3.79-3.71 (m, 4H, -CH2-), 3.67-3.47 (m, 32 H, overlapped -CH2-). Product molecular mass calcd.: 893.2.
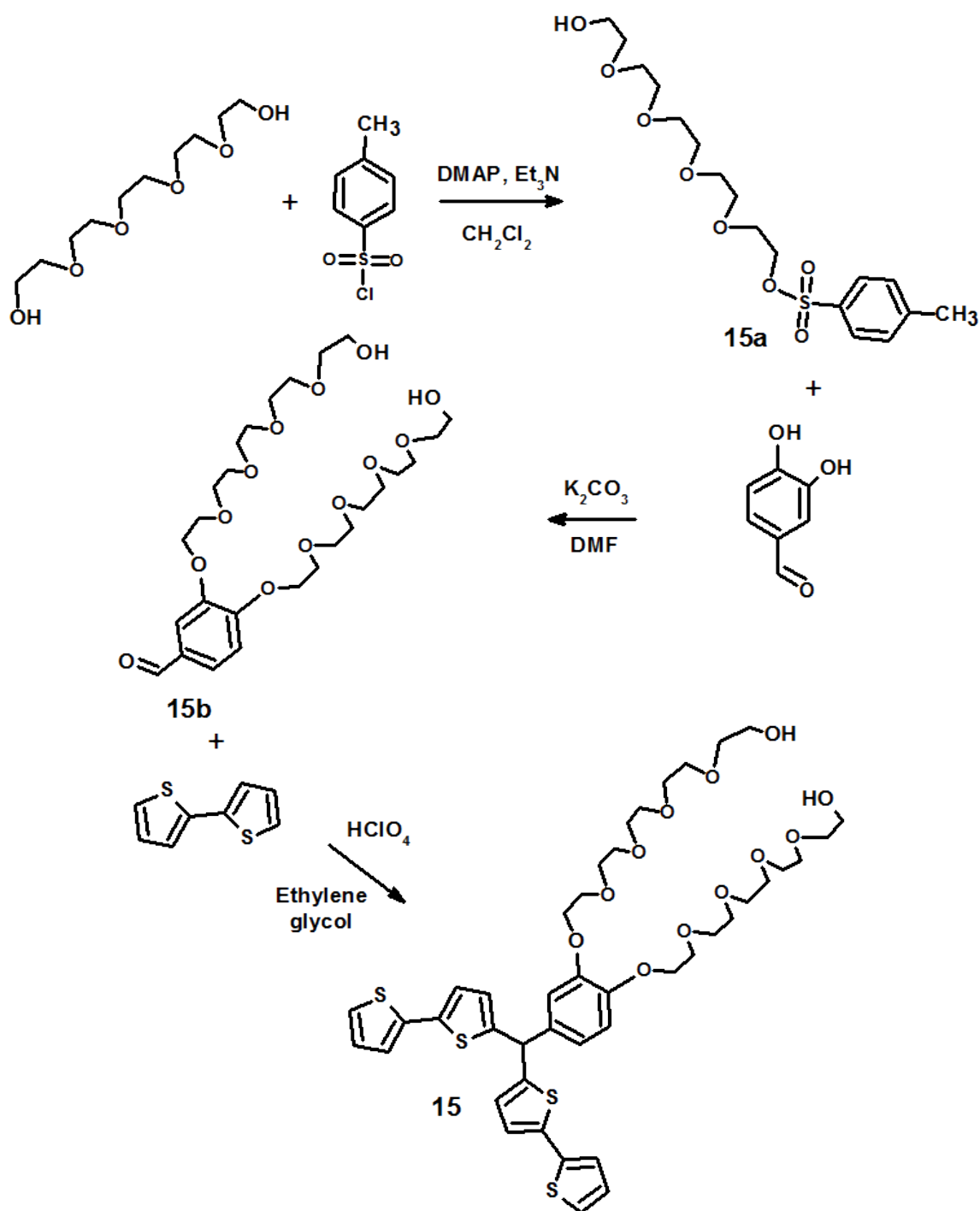
Scheme 2.26 Syntheses of pentaethylene glycol p-toluenesulfonate **15a**, 3,4-bis(pentaethyleneglycol)benzaldehyde **15b**, and 4-bis(2,2'-bithien-5-yl)methyl-*o*-catechol pentaethyleneglycol diether **15**.

4-Bis(2,2'-bithiophen-5-yl)methyltoluene **16** (Scheme 2.27). First, 2,2'-bithiophene (1.6 g, 10 mmol) and 4-methyl benzaldehyde (240 mg, 3.33 mmol) were mixed in ethylene glycol (70 mL), and then the mixture was stirred for 30 min under N_2. Then, 70% $HClO_4$ (6 mL, 90 mmol) was added and the resulting solution stirred for 16 h at 60 °C. Next, the reaction mixture was cooled to room temperature, and then the excess of methylene chloride was added in order to dissolve the desired product. Subsequently, the mixture was neutralized with the saturated Na_2CO_3 solution. The collected organic liquid layer was washed with water, and then dried with anhydrous Na_2SO_4. After solvent evaporation of the organic layer, a crude product was purified by liquid chromatography on a silica gel column using the hexane : $CHCl_3$ (8 : 2 to 1 : 1, v : v) eluent. Yield: 810 mg (56%). ^{1}H NMR ($CHCl_3$-d), Fig. A.29: (δ in ppm) 7.17–7.14 (d, 2H, bithiophene H), 7.10–7.07 (m, 4H, overlayed bithiophene H), 6.92-6.84 (m, 4H, overlayed bithiophene and phenyl H), 6.67–6.62 (d, 2H, phenyl H), 5.62 (s, 1H, –CH–), 2.26 (s, 3H, -CH3). Product molecular mass calcd.: 434.7.
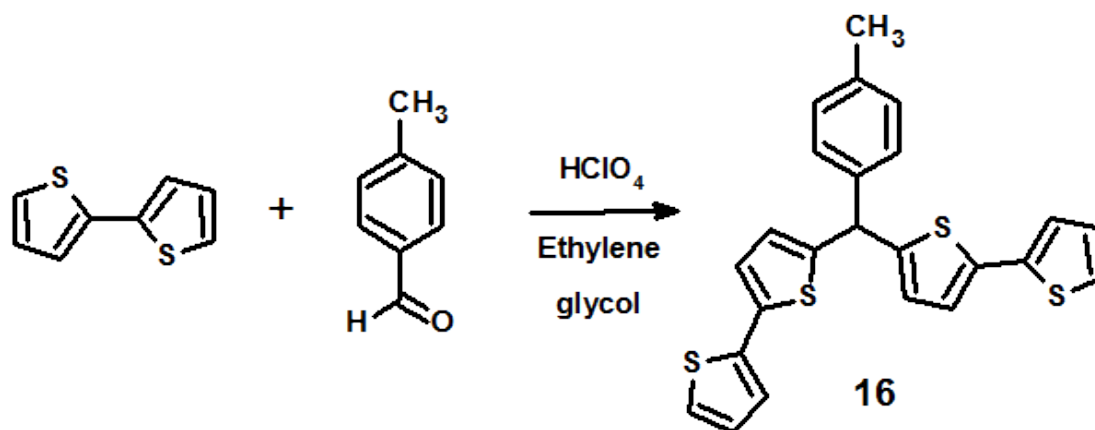
Scheme 2.27 Synthesis of **16**, 4-bis(2,2'-bithiophen-5-yl)methyltoluene.

Out of those FMs synthesized, some have already been used for the preparation of chemosensors. These include the chemosensors for oligonucleotide and myoglobin determination using **2** [141], the MIP chemosensor for nicotine determination using **3** [55], the MIP chemosensor for nitroaromatic explosive determination using **7** [142], the MIP chemosensor for nicotine determination using **9** [55, 143], and the MIP chemosensor for 6-thioguanine determination using **11** [76, 143]. Other research includes preparation of MIP for the determination of a short oligomer TATAAA involving **12** as FM [144]. FMs **10** and **11** are used for the preparation of MIP selective to inosine [145]. Moreover **10** is used for the preparation of a polymer imprinted with carnosine [146].

2.4.2 Syntheses of new fullerene derivatives

Two new fullerene derivatives were designed and synthesized to serve as FMs. Each of them consists of the [C60]fullerene polymerizing moiety, the spacer, and the recognizing site. Those recognizing sites are 18-crown-6-ether and the amide group. Novelty of these two FMs is that their recognizing sites are linked to the C_{60} moiety via flexible spacers in contrast to the previously reported fullerene derivatives [147, 148]. For syntheses of these derivatives, application of multi-step procedure was necessary.

Pentaethylene glycol di(p-toluenesulfonate) **17a** (Scheme 2.28). First, pentaethylene glycol (1 mL, 4.73 mmol), 4-dimethyloaminopyridine (59.8 mg, 0.47 mmol), and triethylamine (1.318 mL, 9.46 mmol) were dissolved in dichloromethane, and then stirred under N_2 for 1 h. Then 4-methylbenzenesulfonyl chloride (2.255 g, 11.83 mmol), dissolved in dichloromethane was added dropwise for 20 min. After that, the reaction mixture was stirred for 16 h. Next, the solvent was evaporated. Subsequently, the residue was dissolved in $CHCl_3$, and then washed with water and $NaHCO_3$ solution. The collected organic layer was dried with anhydrous Na_2SO_4, and then its solvent evaporated. The residue was purified by liquid chromatography on a silica gel column using the hexane : $CHCl_3$ (9 : 1 to 5 : 1, $v : v$) eluent. Yield: 959 mg (37%). ^{1}H NMR ($CHCl_3$-d), Fig. A.30: δ (in ppm) 7.81–7.78 (d, 4H, tosylate phenyl H), 7.36–7.32 (d, 4H, tosylate phenyl H), 4.18-4.13 (m, 4H, -CH2-), 3.71-3.66 (m, 4H, -CH2-), 3.62-3.57 (m, 12H, overlapped -CH2-), 2.44 (s, 6H, -CH3). Product molecular mass calcd.: 546.65.

4'-Formylbenzo-[18-crown-6] **17b** (Scheme 2.28). The synthesis procedure was adapted from literature [149]. That is first, a mixture of 3,4-dihydroxybenzaldehyde (323 mg, 2.34 mmol) and the excess of K_2CO_3 (3.236 g, 23.4 mmol) in DMF (~60 mL) was stirred at ~80 °C under N_2 for 30 min. Then, **17a** (1.278 g, 2.34 mmol), dissolved in DMF (20 mL) was added to the reaction mixture during 20 min, and then the mimxture wass stirred at ~80 °C under N_2 for 23 h. After cooling to room temperature, the mixture was filtered. Subsequently, the filtrate solvent was evaporated to dryness, and then the residue extracted with dichloromethane. The extract solvent was evaporated to yield a viscous oil, which was then purified by liquid chromatography on a silica gel column using the hexane : $CHCl_3$ (1 : 1 to 0 : 1, $v : v$), and then $CHCl_3$: MeOH (9 : 1, $v : v$) eluent. Evaporation of the solvent yielded a pale-yellow oil. Yield: 75%. ^{1}H NMR ($CHCl_3$-d), Fig. A.31: δ (in ppm) 9.76 (s, 1H), 7.38-7.35 (dd, 1H, phenyl H), 7.31-7.30 (d, 1H, phenyl H), 6.89-6.87 (d, 1H, phenyl H), 4.19-4.13 (m, 4H, crownethylene H), 3.91-3.84 m, 4H, crownethylene H), 3.72-3.54 (m, 12H, crownethylene H). Product molecular mass

calcd.: 340.4.

Benzo[18-crown-6]methanol **17c** (Scheme 2.28). The synthesis procedure was adapted from literature [150]. That is first, sodium borohydride (104.8 mg, 2.77 mmol) was dissolved in ethanol. Then, **17b** (564 mg, 1.86 mmol) was added and the resulting mixture stirred for 2 h in room temperature under N_2. After that, the solvent was evaporated. Then, the resulting yellow oily product was dissolved in dichloromethane, and then washed with water. An organic layer was dried with anhydrous Na_2SO_4, and then the solvent evaporated. The product was used for further syntheses without purification. Yield: 4.09 g (44%).

2-Chloromethylbenzo[18-crown-6] **17d** (Scheme 2.28). The synthesis procedure was adapted from literature [151]. That is first, **17c** (693 mg, 1,92 mmol) was dissolved in dichloromethane. Next, K_2CO_3 (1.106 g, 8.0 mmol) was added, and then the mixture cooled to 0 °C. After that, $SOCl_2$ was added to the reaction mixture, and then the mixture stirred for 1 h. Subsequently, the solution was filtered, and then the solvent of the filtrate evaporated. The resulting yellow oily product was used for the next synthetic step without further purification.

3-([18-Crown6]benzyl]oxy)benzaldehyde **17e** (Scheme 2.28). First, 4-hydroxybenzaldehyde was dissolved in DMF. Then, K_2CO_3 (1.062 g, 7.7 mmol) was added, and then the mixture heated to 80 °C and stirred for 30 min. After that, **17d** (693 mg, 1.9 mmol) was added and the reaction mixture stirred for 13 h. Next, the solution was filtered out, and then washed with water. The collected organic layer was dried with anhydrous Na_2SO_4, and then the solvent evaporated. A yellow viscous oil left was purified by liquid chromatography on a silica gel column with the hexane : CH_2Cl_2 (1 : 1 to 1 : 9, $v : v$), and then CH_2Cl_2 : MeOH (9 : 1, $v : v$) eluent. Yield: 150 mg (18%). ^{1}H NMR (CHCl$_3$-d), Fig. A.32: δ (in ppm) 9.79 (s, 1H, CHO), 7.77-7.72 (d, 2H, phenyl H), 7.00–6.96 (d, 2H, phenyl H), 6.89-6.83 (m, 3H, overlapped phenyl H), 4.96 (s, 2H, -CH2-), 4.12-4.04 (m, 2H, crownethylene H), 3.85-3.81 (m, 2H, crownethylene H), 3.68-3.51 (m, 16H, crownethylene H). Product molecular mass calcd.: 464.49.

4-(1-Methylfulleropyrrolidin-2-yl)phenol-3,4-[18-crown-6]benzyl ether **17** (Scheme 2.28). The synthesis procedure was adapted from literature [152]. That is first, **17d** (150 mg, 0.24 mmol), sarcosine (61 mg, 0.68 mmole), and [C60]fullerene (490 mg, 0.68 mmole) were placed in a 250-mL round bottom flask containing dry toluene (100 mL). Then, the resulting mixture was refluxed for 16 h. After cooling at room temperature, the solvent was evaporated and a brown crude solid product was purified by liquid chromatography on a silica gel column with the hexane : toluene

(1 : 1 to 1 : 9, v : v), and then toluene : MeOH (95 : 5 to 80 : 20, v : v) eluent. Yield: 63 mg (22%). ^{1}H NMR (CDCl$_3$-d with few drops of CS$_2$), Fig. A.33: δ (in ppm) 7.19-7.16 (m, 2H, phenyl H), 7.12-7.08 (m, 4H, phenyl H), 6.83-6.77 (d, 1 H, phenyl H), 4.35 (s, 2H, -CH2-), 4.11-4.06 (m, 2H, crownethylene H), 3.88-3.84 (m, 4H, crownethylene H), 3.72-3.62 (m, 5H, overlapped crownethylene H and pyrrolidyne H), 3.63 (s, 4 H, crownethylene H), 3.60-3.56 (m, 4H, crownethylene H), 2.28 (s, 3H, -CH3). Product molecular mass calcd.: 1220.2.
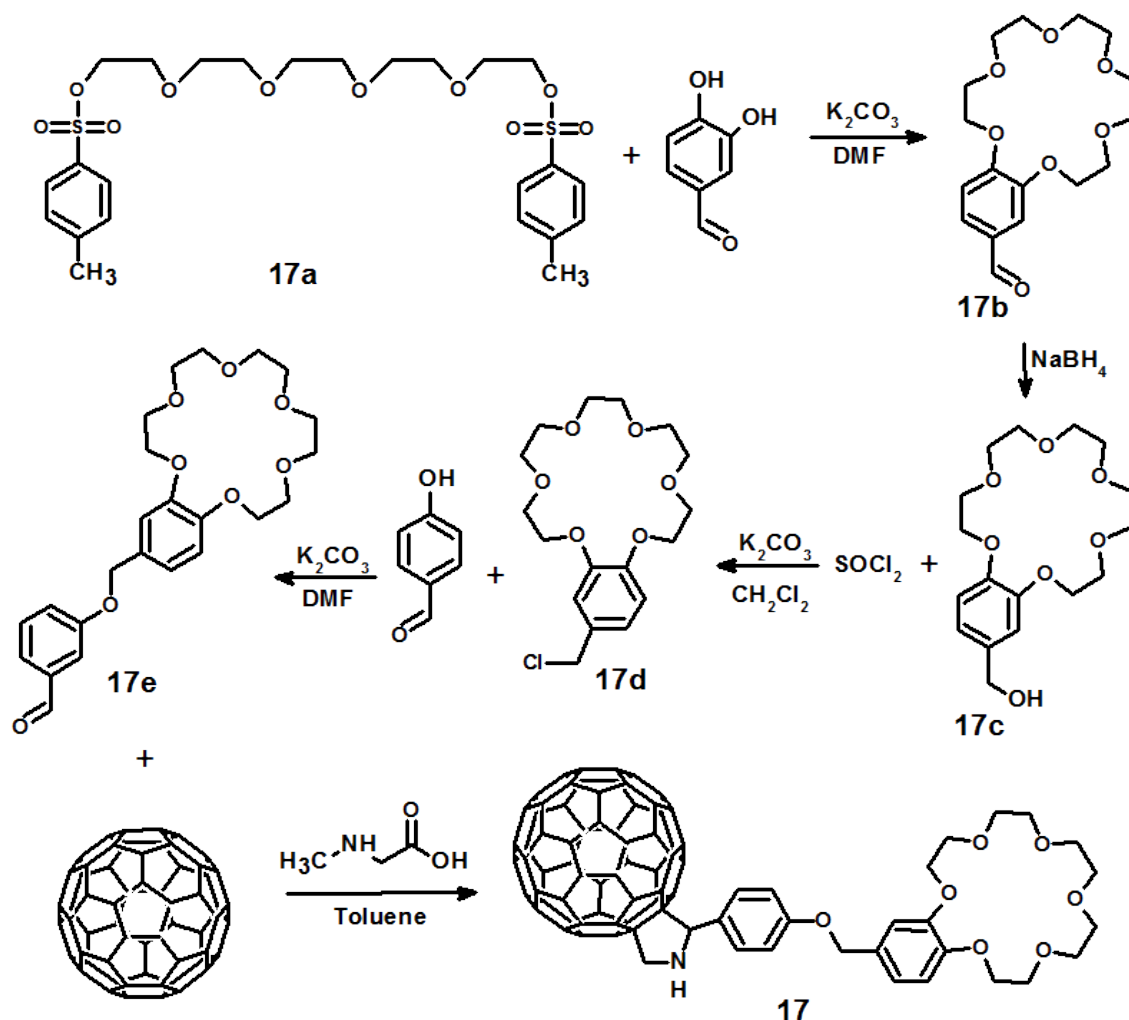
Scheme 2.28 Syntheses of pentaethylene glycol di(p-toluenesulfonate) **17a**, 4'-formylbenzo[18-crown-6] **17b**, benzo[18-crown-6]methanol **17c**, 2-Chloromethylbenzo[18-crown-6] **17d**, 3-([18-crown6]benzyl]oxy)benzaldehyde **17e**, and p-(1-methylfulleropyrrolidin-2-yl)phenol-o,p-[18-crown-6]benzyl ether **17**.

2-(Acetylamino)ethyl-3-formylbenzoate **18a** (Scheme 2.29). First, 4-carboxybenzaldehyde (405 mg, 3 mmol) was dissolved in DMF (40 mL) and cooled to 0 °C by keeping in an ice bath. Then, EDCI (931 mg, 6 mmol) was added, and then the mixture stirred for 30 min under N$_2$. Next, N-acetylethanolamine (276 µL,

3 mmol) was added dropwise for 10 min. After that, the reaction mixture was stirred in an ice bath for 1 h. The reaction was continued for another 36 h at room temperature. Next, the reaction solvent was evaporated under reduced pressure. The residue was pre-purified by liquid chromatography on a silica gel column using the hexane : CH_2Cl_2 (1 : 1 to 1 : 9, $v : v$), and then CH_2Cl_2 : MeOH (9 : 1, $v : v$) eluent. The product was used for the subsequent syntheses without purification. ^{1}H NMR ($CHCl_3$-d), Fig. A.34: δ (in ppm) 9.81 (s, 1H, -CHO), 7.72-7.68 (d, 2H phenyl H), 7.43-7.39 (d, 2H, phenyl H), 6.8 (broad s, 1H, -NH-), 3.59-3.54 (t, 2H, -CH2-), 3.03-2.95 (q, 2H, -CH2-), 2.23 (s, 3H, -CH3). Product molecular mass calcd.: 235.2.

2-Acetamidethyl 4-(1-methylfulleropyrrolidin-2-yl)benzolate **18** (Scheme 2.29). First, **18a** (220 mg, 0.9 mmole), sarcosine (178 mg, 1.8 mmol), and [C60]fullerene (1.3 g, 1.8 mmol) were placed in a 500-mL RB flask containing dry toluene (300 mL). Then, the resulting mixture was refluxed for 16 h. After cooling at room temperature, the solvent was evaporated and a brown crude solid product purified by liquid chromatography on a silica gel column with the hexane : toluene (1 : 1 to 1 : 9, $v : v$), and then toluene : MeOH (95 : 5 to 80 : 20, $v : v$) eluent. Yield: 71 mg (22%). ^{1}H NMR ($CDCl_3$-d with few drops of CS_2), Fig. A.35: δ (in ppm) 7.05-7.01 (d, 2H phenyl H), 6.97-6.94 (d, 2H, phenyl H), 5.92 (broad s, 1H, -NH-), 3.53-3.49 (t, 2H, -CH2-), 3.26 (s, 1H, pyrolidine H), 3.22-3.17 (q, 2H, -CH2-), 2.14 (s, 3H, -CH3), 1.80 (s, 3H, -CH3). Product molecular mass calcd.: 1009.0.
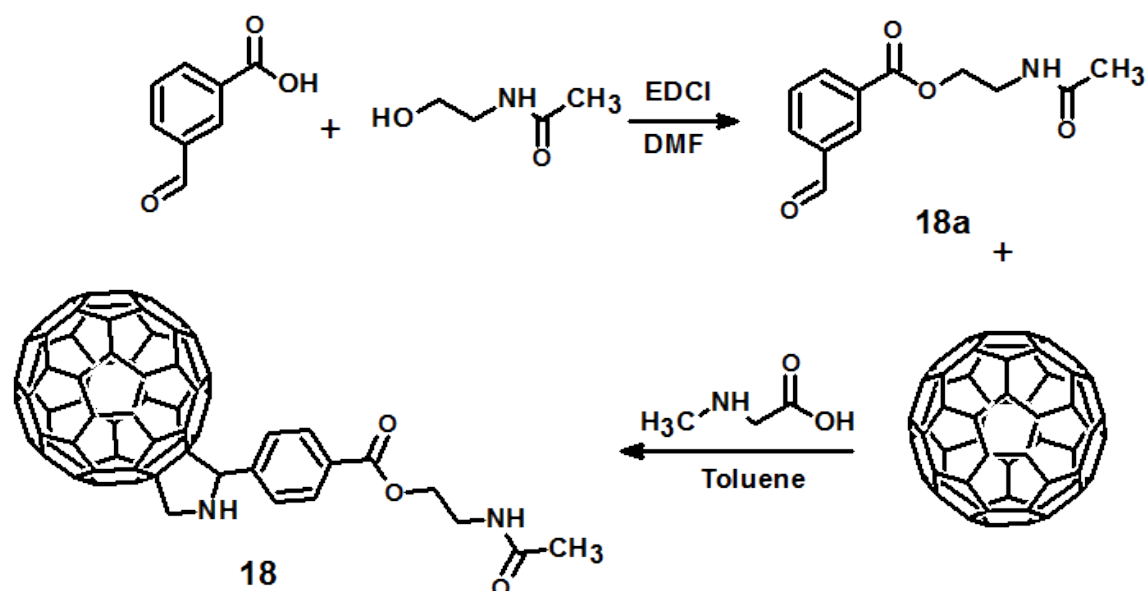
Scheme 2.29 Syntheses of 2-(acetylamino)ethyl 3-formylbenzoate **18a** and 2-acetamidethyl-*p*-(1-methylfulleropyrrolidin-2-yl)benzolate **18**.

2.4.3 Biotinylated myoglobin

The procedure of myoglobin biotinylation used herein was adapted from literature [153]. First, 8.73 mg of myoglobin was dissolved in 876 μL of PBS of pH=7.4, in order to prepare a 10 mg/mL myoglobin solution. Next, 1.7 mg of biotinylation agent, namely, biotin N-hydroxysuccinimide ester B-NHS, was dissolved in 500 μL of DMSO, yielding 0.01 M B-NHS. After that, a sample of 476 μL of 0.01 M B-NHS was added to the above myoglobin solution. The mixture was left at room temperature for 1 h. Subsequently, a sample of 476 μL of 0.01 M glycine was added to the mixture in order to cease the biotinylation reaction. Then, the reaction product was purified using the Zeba Spin Desalting Columns for size exclusion chromatography. The extent of biotinylation was not investigated, therefore, a resulting 2.6 mg/mL solution of biotinylated myoglobin consisted of the myoglobin molecules modified with different numbers of biotin substituents.

Chapter 3

Results and discussion

3.1 Design of new functional monomers

3.1.1 Guide to functional monomers

One of the most important features of a chemosensor is its selectivity. As mentioned in the previous chapter, one way of achieving high selectivity of a chemosensor is to prepare an MIP layer serving as a recognition element. For MIP preparation, functional monomers (FMs) containing polymerizable moiety and recognizing moiety are needed (Scheme 1.6 in Section 1.2). In hereby presented work, we focused on preparation of new FMs containing bis(2,2'-bithienyl) and [C60]fullerene as polymerizing moieties. Reason for that is their proven capability of polymerization under potentiodynamic conditions and high stability of the resulting polymer films [142,149,154,155]. In order to introduce various binding capabilities, functional groups were introduced.

Predominantly, interactions between molecules in nature were mimicked for designing functional groups. Weak interactions are the key means by which biomolecules interact with one another, e.g., enzymes with their substrates, hormones with their receptors, antibodies with their antigens. Those interactions include electrostatic interactions, hydrogen bonds, π-π interactions, van der Waals interactions, and weak dispersion interactions. Out of those three types, hydrogen bonds play a very important role, crucial in events such as DNA double strand formation and protein folding. Therefore, several FMs were herein designed in a way to contain recognition sites (including just a few atoms) that would be capable of hydrogen bond formation. This FM class consists of **1** and **3** both having the -OH group, **7** having the -NH$_2$ group, **8** bearing the -NO$_2$ group, **9** and **10** both containing the -COOH group, and **14** and **18** both bearing the -CONH$_2$ group.

Moreover, the second FM class with binding sites of a more complicated structure utilizes hydrogen bonding. For instance, **15** has two long arm-like substituents.

Other FMs were directly copied from nature. That is, they contain nucleobases capable of Watson-Crick pairing. Accordingly, three FMs, i.e., **11**, **12**, and **13**, bearing cytosine, thymine, and guanine, respectively, were synthesized. Another bioinspired monomer was **2**, having biotin in its structure and, therefore, capable of strong interaction with avidin and its analogues, like streptavidin and neutravidin.

Monomers inspired by supramolecular chemistry belong to the third FM class. In this field of chemistry, crown ethers and calixarenes are amongst molecules of the highest interest [156,157]. Therefore, two monomers, including that bearing the 4-tertbutylcalix-6-arene moiety **4** and the other having 18-crown-6 ether substituent **17** were synthesized.

Finally, a monomer containing succinimide group, **6**, and the monomer with no functional group, **16**, offering just a toluene ring for π-π stacking interactions were prepared. The goal of synthesis of **6** was to use it for protein immobilization on top of an underlayer polymer film, as succinimide is known as a protein binding agent [158–160]. The **16** was synthesized in order to utilize π-π interactions for the preparation of a recognition polymer as well as to have a control compound in order to test the effect of functional groups on binding properties of FMs.

3.1.2 Quantum-chemical calculations

Because of limited time of the present research, not all monomers designed and synthesized within its scope have already been used for chemosensor preparation. Quantum-chemical calculations can provide information on usefulness for binding of the FMs prepared without engaging into time and resource consuming experiments. Three examples, one for each class of FMs, of complex formation between FMs and selected analytes are presented below. Calculations were mainly performed by Dr. Tan-Phat Huynh.

Information that allows for assessment of the extent of binding between the FM and the analyte molecules is the free Gibbs energy gain (ΔG) due to complex formation. That is, the more negative its value the stronger complex is formed. In order to calculate ΔG of complex formation of selected analyte with FM, first, structure of each molecule involved in complex formation was optimized and free energy of its formation was calculated. Then, FM molecules were placed near the analyte molecule and allowed to approach each other freely until the optimized complex structure was reached. Finally, the free energy difference between the energy of formation of the complex and the sum of energies of formation of the individual complex components was calculated.

3.1.2.1 Interaction of 4-bis(2,2'-bithien-5-yl)methylbenzoic acid 10 with carnosine

Carnosine, (2S)-2-[(3-Amino-1-oxopropyl)amino]-3-(3H-imidazol-4-yl)propanoic acid (Scheme 3.1), is a dipeptide built of L-histidine and β-alanine. It naturally occurs in human organism, mainly in muscles, but it is also present in other tissues. It reveals antioxidant properties [161] and its main role is to keep acid-base hemoestasis in muscles [162, 163]. For many years, carnosine has been used by professional athletes as a dietary supplement [164]. Deficiency of carnosine in human body results in the carnurosemia illness [165, 166]. Apparently, there is a need to detect and quantify carnosine in body fluids (e.g., urine) and dietary supplements. Therefore, carnosine was targeted as an analyte and different FMs out of those synthesised herein, where examined in order to find if any of them can be useful for carnosine imprinting.
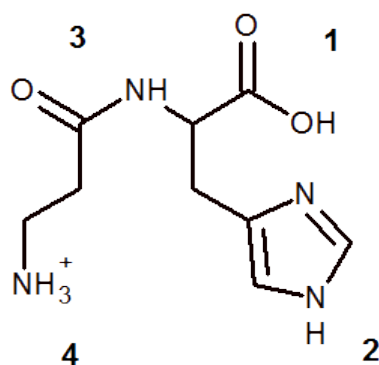
Scheme 3.1 Carnosine structural formula with numbered binding sites.

Carnosine (Scheme 3.1) has four recognition sites. For each of those sites, different FMs were inspected for possible binding. Apparently, the most appropriate for carnosine binding was **10** out of herein reported FMs. That was because **10** contains the carboxyl group allowing for binding with three out of four carnosine binding sites. For binding the site left unbound, the FM previously synthesised by R. Chitta [149] appeared to be the most efficient. Calculation results are summarized in Table 3.1. The negative ΔG of complex formation of carnosine with all four FMs was as high as -227.37 kJ mol^{-1} suggesting that those monomers can be used for the preparation of a molecularly imprinted polymer selective to carnosine.

Table 3.1 The free Gibbs energy change (ΔG) due to complex formation of carnosine with different functional monomers.

FM functional group and number	Binding site number (Scheme 3.1)	ΔG / kJ mol^{-1}
COOH, **1**	1	-42.77
	2	-22.16
	3	-35.66
18-crown-6 ether	4	-178.20
Total		-227.37
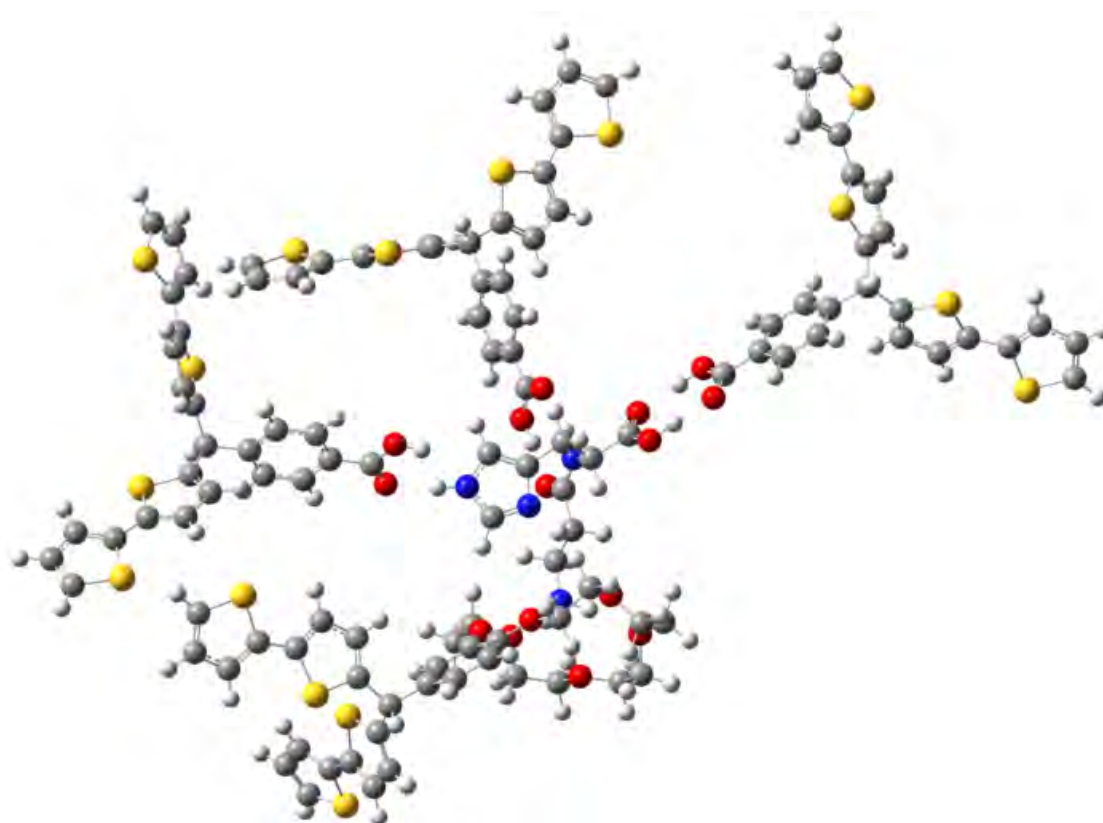
Figure 3.1 The optimized structure of a complex of the 4-bis(2,2'-bithien-5-yl)methylbenzoic **10** functional monomer and the 4-bis(2,2'-bithienyl)-benzo-[18-crown-6]methane **19** functional monomer with carnosine.

3.1.2.2 Interaction of 2-(cytosin-1-yl)ethyl 4-bis(2,2'-bithien-5-yl)methyl-benzolate 11 with 6-thioguanine

6-Thioguanine, 2-amino-1H-purine-6(7H)-thione, is used as a drug for leukemia treatment, similarly to 6-mercaptopurine [167]. Apart from undesired accumulation in liver of the 6-thiogunanine active metabolite, 2-amino-6-methylmercaptopurine [168], an excessive drug dose administered during clinical treatment may cause more side toxic effects, e.g., bone marrow depression and gastrointestinal effect, than those caused by 6-mercaptopurine [169]. Therefore, there is a need to fabricate a receptor capable of selective capture of excessive 6-thioguanine in a patient body that could be used for the preparation of a recognition unit of a chemosensor.

A sound example of application of FM of the second class is nature-mimicking interaction of **11** with 6-thioguanine [76,143]. This complex resembles the cytosine-guanine Watson-Crick type nucleobase pairing in double-stranded DNA or RNA [170]. However, the present interaction was weaker because the highly electronegative oxygen atom in guanine was replaced by the sulfur atom of lower electronegativity in 6-thioguanine. Neverthless, the total negative Gibbs free energy gain, ΔG, of formation of the complex in DMF was as high as -53.40 kJ mol^{-1}.
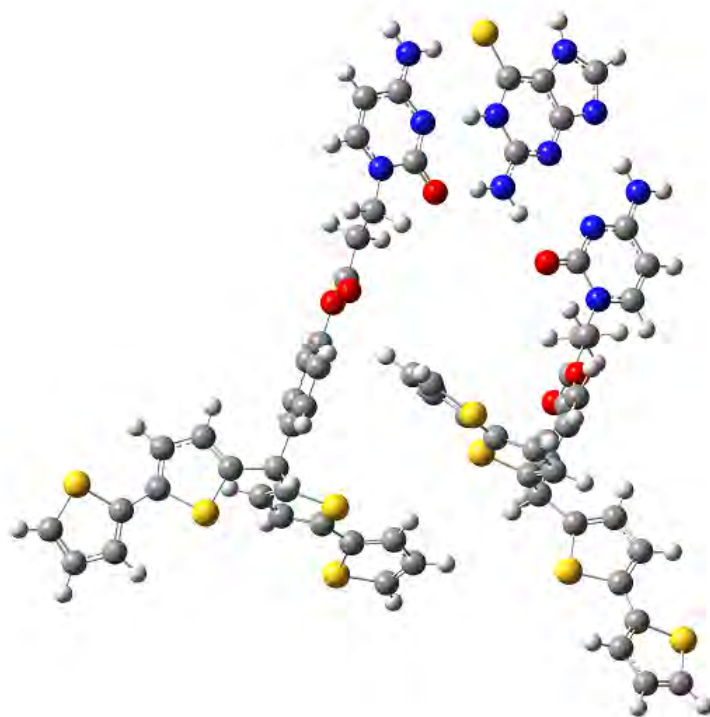
Figure 3.2 The optimized structure of the complex of 6-thioguanine with the 2-(cytosin-1-yl)ethyl-4-bis(2,2'-bithien-5-yl)methylbenzolate **11** functional monomer.

3.1.2.3 Interaction of 4-(1-methylfulleropyrrolidin-2-yl)phenol-3,4-[18-crown-6]benzyl ether 17 and 2-acetamidethyl 4-(1-methylfulleropyrrolidin-2-yl)benzolate 18 with serotonin

Serotonin, 5-hydroxytryptamine, (Scheme 3.2) is a neurotransmitter present in vertabrates organisms. Its concentration in human blood is linked to depression [171]. Since serotonin-involved depression is one of the most frequently occurring mental diseases in modern civilized life [172], monitoring the serotonin level becomes increasingly important. Therefore, there is a demand for sensitive and selective serotonin sensors.

Serotonin (Scheme 3.2) has three sites available for binding. The first, primary amine site, may be bound, after quarternation, by crown ether while two others by any moiety capable of formation of a hydrogen bond. Serotonin is electroactive, it undergoes electrooxidation at the potential of ~0.4 V [173]. Therefore, it is impossible to imprint it electrochemically using bithiophene based monomers. Simply, serotonin would simultaneously be oxidized during oxidative electropolymerization of the bithiophene moiety and, in effect, the polymer deposited would be imprinted with the product of serotonin oxidation instead. In order to overcome this difficulty, [C60]fullerene adducts **17** and **18** were designed and synthesized to serve as FMs. The DFT/B3LYP/6-31G* calculation results are summarized in Table 3.2. The total ΔG of formation of the complex of the serotonin molecule with three FM molecules is as high as -363.38 kJ mol^{-1} suggesting that these monomers can be used for the preparation of a molecularly imprinted polymer selective to serotonin.

Table 3.2 The free Gibbs energy change (ΔG) due to complex formation of serotonin with functional monomers **17** and **18**.

FM functional group and number	Binding site number (Scheme 3.2)	ΔG / kJ mol^{-1}
18-crown-6 ether, **17**	1	-311.08
amide, **18**	2 and 3	-52.3
Total		-363.38
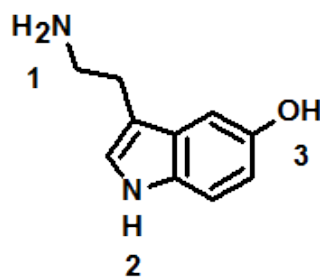
Scheme 3.2 Serotonin structural formula with numbered binding sites.
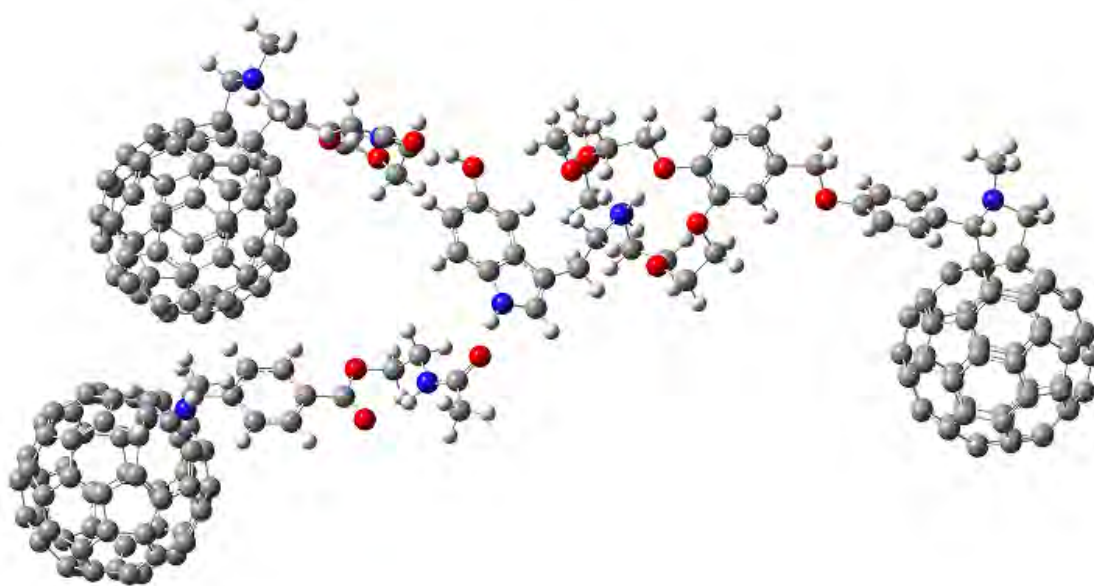
Figure 3.3 The optimized structure of the complex of the fulleropyrrolidine functional monomers **17** and **18** with serotonin.

3.2 Chemical sensor for an HIV oligonucleotide

For the present study, an oligonucleotide of the 5'-ACT GCT AGA GAT TTT CCA CAT-3' sequence, reported as the single-stranded DNA fragment characteristic for the HIV-1 virus [174] was selected as the target analyte.

Films of a new conducting polymer, prepared by electropolymerization of 4-bis(2,2'-bithien-5-yl)methylphenol biotin ester **2**, were applied as the recognition units of two different biosensors for selective HIV oligonucleotide determination using electrochemical impedance spectroscopy (EIS) in one of them and piezoelectric microgravimetry (PM) in the other for a label-free analytical signal transduction.

In these biosensors, the target oligonucleotide was recognized with the recognizing, called 'probe', oligonucleotide of the sequence complementary to that of the target. For immobilization of the recognizing oligonucleotide, a well known biotin-avidin interaction was utilized. First, the polymer film of a newly prepared FM **2** was deposited on the surface of an electrode (glassy carbon electrode, GCE or a gold electrode of QCR). The resulting polymer film was then modified with neutravidin. Neutravidin is a deglycosilated analogue of avidin that binds biotin as strongly as avidin, however, it advantageously reveals higher binding selectivity [175,176]. Neutravidin immobilization on top of the polymer film allowed for subsequent immobilization of a recognizing biotinylated oligonucleotide. This prepared layer-by-layer assembly consisted a working recognition platform of both biosensors. Consecutive steps of recognition film preparation are shown in Scheme 3.3 and described in

details in the Section 3.2.1, below.
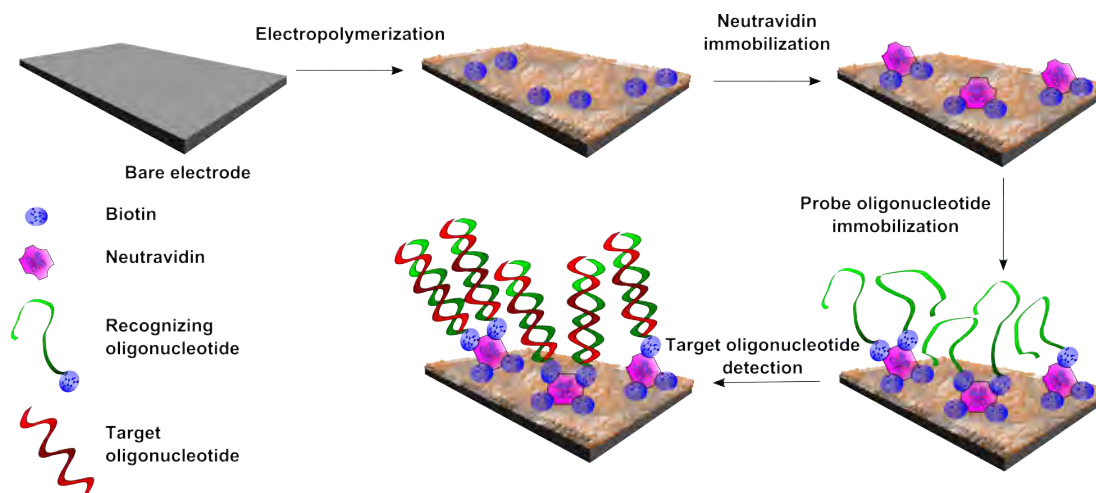
Scheme 3.3 Consecutive steps of preparation of the film for oligonucleotide recognition.

For efficient label-free signal transduction, EIS and PM were used. In the former, the charge transfer resistance of an electrode film was utilized as the analytical signal. That was possible because the film properties changed after binding the target oligonucleotide. In the latter case, the resonant frequency change was used as the signal. This change resulted from the mass change of the electrode film because of immobilization of the target oligonucleotide.

3.2.1 Preparation of a recognition film

Polymer film deposition. The first step of preparation of the recognition film involved deposition of the polymer film from the FM **2** solution by linear cycling of the potential in the range of 0.50 to 1.50 V vs. Ag|AgCl (Figures 3.5 and 3.4). That was possible because thiophenes are capable of electrochemical polymerization in the positive potential range via cation radical formation. The solution for electropolymerization was 1 mM in **2** and 0.1 M in $(TBA)ClO_4$ containing a mixture of ethanol and acetonitrile (1 : 1, $v : v$). Ethanol was used to facilitate dissolution of **2**. An anodic peak observed between 1.20 and 1.30 V vs. Ag|AgCl (Figures 3.5 and 3.4a) resulted from oxidation of the bisbithiophene moiety of the FM **2** leading to the polymer film formation. This film formation was confirmed by the resonant frequency decrease of QCR (Figure 3.4b) indicating the mass increase of the film deposited on the surface of the QCR, in accord with Equation (2.21). A positive anodic peak potential shift of the bisbithiophene moiety electro-oxidation can be attributed to the increase of the electrode charge-transfer resistance due to the growth of the film, which was much less conductive than the bare electrode. Moreover, this effect was confirmed by the behavior of the dependence of the frequency change on the num-

ber of the current-potential (*I-E*) cycles. That is, the frequency change was smaller in each consecutive cycle indicating deposition of a smaller mass of the polymer in each cycle. A similar behavior has already been reported for polymerization of other monomers of the bis(2,2'-bithien-5-yl)methane polymerizing moiety [73, 177]. After deposition, the polymer was rinsed with ethanol to remove the excess of the supporting electrolyte solution. Further preparation of the recognition film was different for the EIS and PM biosensor.
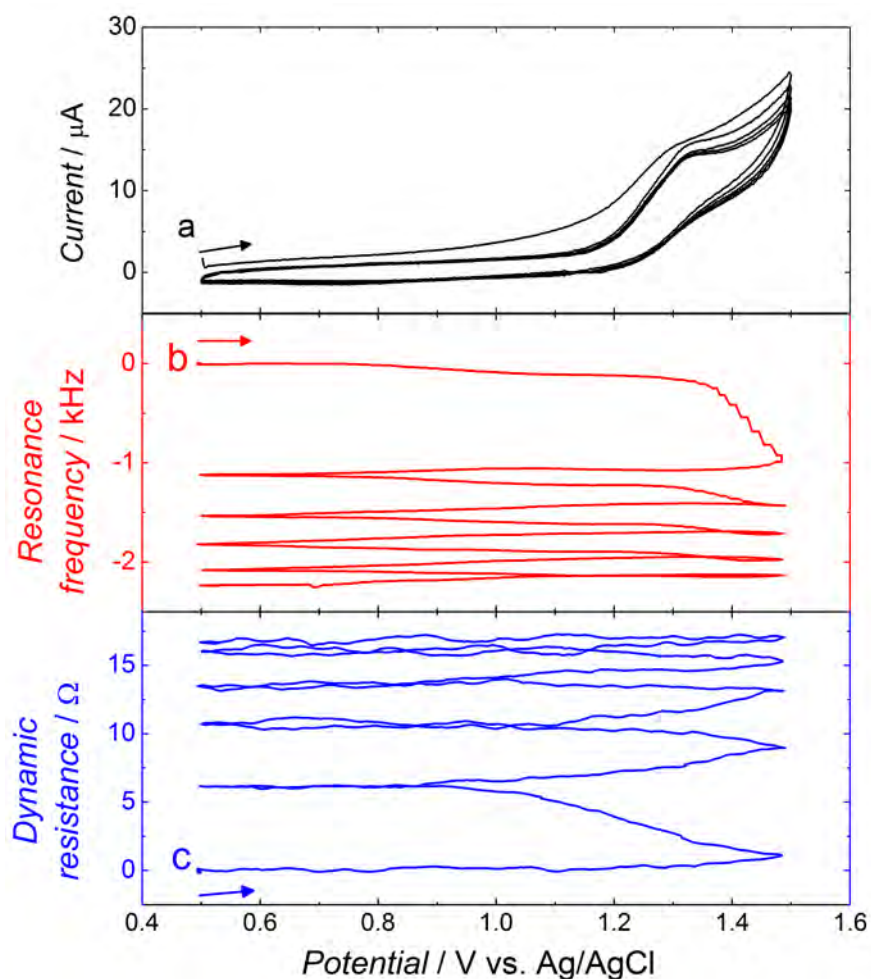
Figure 3.4 Potentiodynamic electropolymerization of the functional monomer **2** in 0.1 M (TBA)ClO$_4$ in acetonitrile : ethanol (1 : 1, *v* : *v*). Simultaneously recorded curves of the potential dependence of (a) current, (b) resonance frequency change, and (c) dynamic resistance change for the Au-QCR. The potential scan rate was 50 mV/s.
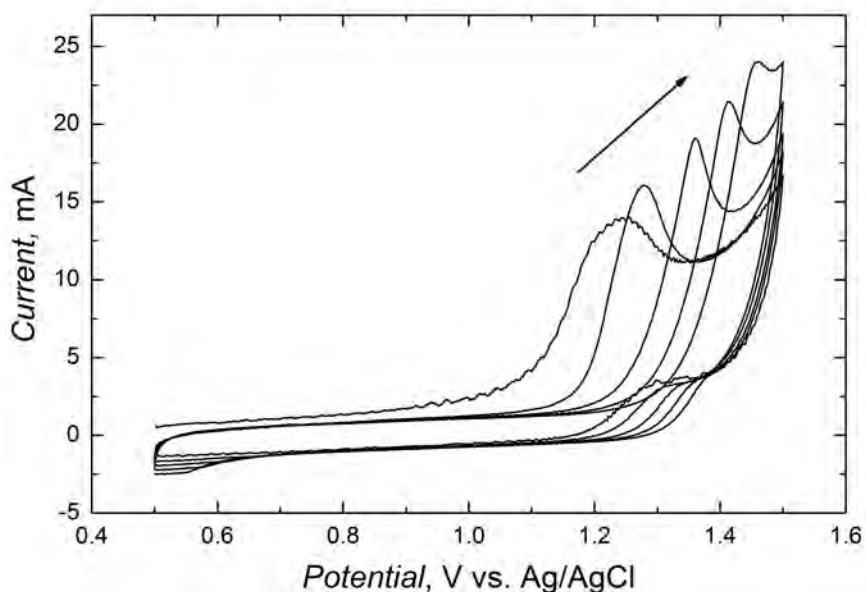
Figure 3.5 Potentiodynamic electropolymerization of the functional monomer **2** in 0.1 M (TBA)ClO$_4$ in acetonitrile : ethanol (1 : 1, v : v) on the GCE surface. The potential scan rate was 50 mV/s.

Preparation of a recognition film for the EIS chemosensor. After deposition of the polymer film on GCE, the potential was cycled in the range of -0.20 and 0.60 V vs. Ag|AgCl in the redox probe aqueous solution (0.1 M K$_3$Fe(CN)$_6$ and 0.1 M K$_4$Fe(CN)$_6$) in order to improve repeatability of the subsequent impedimetric measurements [118]. Next, this GCE was immersed in the 1 mg/mL neutravidin solution for 15 min. After that, it was rinsed with PBS (pH=7.4) in order to remove the unbound neutravidin. Then, the modified that way GCE was exposed to potential cycling again in the range indicated above until repeatable EIS spectra were recorded. Subsequently, the electrode was immersed in the 30 μM solution of the recognizing biotinylated oligonucleotide for 15 min. Afterwards, it was rinsed with PBS (pH=7.4), and then potential was cycled again until the EIS spectra were repeatable. The EIS spectra recorded after each preparation step are shown in Figure 3.6.

Each EIS curve consists of a flatten semicircle and a straight line segment in the high and low frequency range, respectively, typical of a simple redox process under the charge-transfer rate control at a porous electrode [130, 178]. In order to determine the value of the charge transfer resistance, R_{ct}, the experimental data were fitted with electric parameters of the modified Randles-Ershler circuit (Scheme 2.3). This circuit provided an adequate fit of the impedance data, in agreement with fits of impedance of other films used for DNA sensing [118, 119, 121]. Parameters of this circuit were described in details in the experimental section. Herein, the R_s element represents the solution resistance; its value was constant (22.3 Ω, 6.3 Ω cm^2 for the bare GCE) for all measured films, while R_{ct} describes the charge transfer resistance
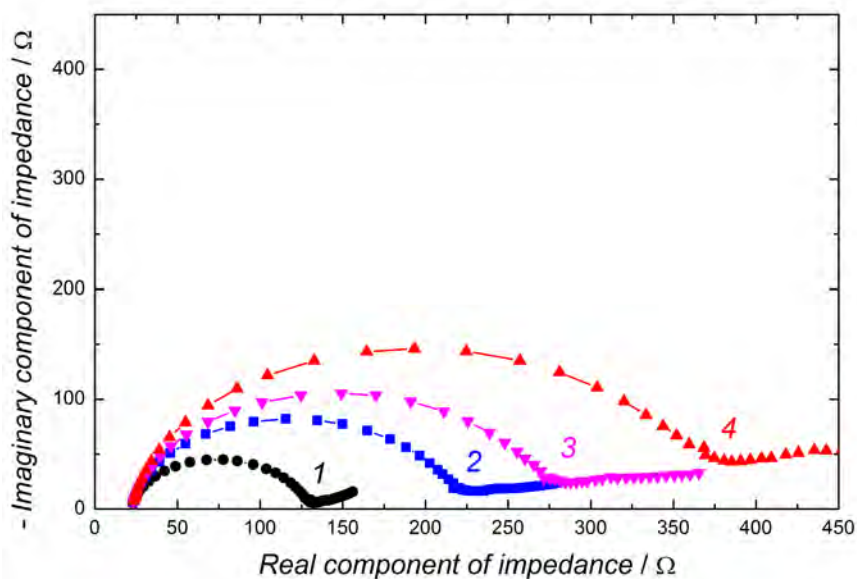
Figure 3.6 Exemplary Nyquist plots for GCE (*1*) coated with the polymer film of the monomer **2**, and then after consecutive immobilization of (*2*) neutravidin, (*3*) biotinylated oligonucleotide, and (*4*) equilibration with 50 pM target oligonucleotide for 6 min. Measurements were performed for 0.1 M $K_3Fe(CN)_6$ and 0.1 M $K_4Fe(CN)_6$ at the open circuit potential. An Ag|AgCl electrode and a platinum plate served as the pseudo-reference and counter electrode, respectively. Frequency was varied in the range of 1 MHz to 500 mHz.

of the electron transfer between the electrode and the $K_3Fe(CN)_6/K_4Fe(CN)_6$ redox probe in solution. Here, R_{ct} was calculated for each step of the recognition film preparation (Table 3.3), and then after interaction of this film with the target oligonucleotide. As expected, both the exponent ϕ and R_{ct} increased after immobilization of each layer of the recognition film. This increase indicated that the film became more insulating after each layer immobilization and its electrical double-layer properties remained close to those of an ideal capacitor. Moreover, the T value changed only slightly suggesting that diffusion of the electroactive species was not much affected by modification of the film (Table 3.3). Our present results are close to those reported for a similar system [118].

Table 3.3 Parameters calculated from the data presented in Figure 3.6 using the modified Ershler-Randles equivalent circuit presented in Scheme 2.3. T – capacitive parameter, ϕ – exponential factor of the constant phase element (CPE), R_{ct} – charge-transfer resistance.

No.	Polymer film	$T \ / \ \mu\text{F s}^{1-\phi}$	ϕ	$R_{\text{ct}} \ / \ \Omega$
1	As deposited	0.93±0.02	0.905±0.002	101.9±0.2
2	After neutravidin immobilization	0.81±0.03	0.912±0.003	169.0±0.5
3	After recognizing oligonucleotide immobilization	0.69±0.03	0.919±0.004	205.9±0.8
4	After interaction with 50 pM target oligonucleotide	0.59±0.02	0.925±0.004	271.5±1.5

Preparation of a recognition film for the QCM chemosensor. Once the QCR was coated with the polymer recognition film, it was mounted in the flow-through holder of the EQCM 5610 microbalance. The PBS (pH=7.4) carrier solution was flown over the QCR until the frequency readings became stable. Then, a 100-μL sample of 1 mg/mL neutravidin in PBS (pH=7.4) was injected. As soon as the frequency reading stabilized after neutravidin binding, a 100-μL sample of 15-μM recognizing oligonucleotide in PBS (pH=7.4) was injected. For both immobilization steps, the carrier solution flow rate was 35 μL/min. The resonant frequency and dynamic resistance changes during recognition film preparation are shown in Figure 3.7.

Almost every solution injection caused a frequency decrease (curve a in Figure 3.7) corresponding to consecutive irreversible immobilization of a different species. From this decrease, the mass of the immobilized species was calculated according to the Sauerbray Equation (2.21). The frequency decrease was accompanied by a small dynamic resistance increase in the range of few ohms (curve b in Figure 3.7), proving that the viscosity of the film did not change much. Apparently, rigidity of the film remained practically unchanged after each step of its preparation. The mass of neutravidin immobilized on the polymer film, calculated from the frequency decrease (Figure 3.7), was 276 ng (4.6 pmoles). The mass of the recognizing oligonucleotide subsequently immobilized was 87 ng (13.5 pmoles). Hence, the immobilized neutravidin-to-(recognizing oligonucleotide) mole ratio was 2.9 being close to that of 3, expected. The reason for it was that neutravidin had four biotin binding sites, at least one of which was occupied by the biotin moiety of the polymer film. Hence, the recognition film was fully modified with the recognizing oligonucleotide. At this step, the recognition film was ready for use. Subsequent injection of the 15 μM target oligonucleotide solution resulted in the mass decrease by 63 ng (9.8 pmoles). Apparently, hybridization of the recognizing oligonucleotide with the target oligonu-
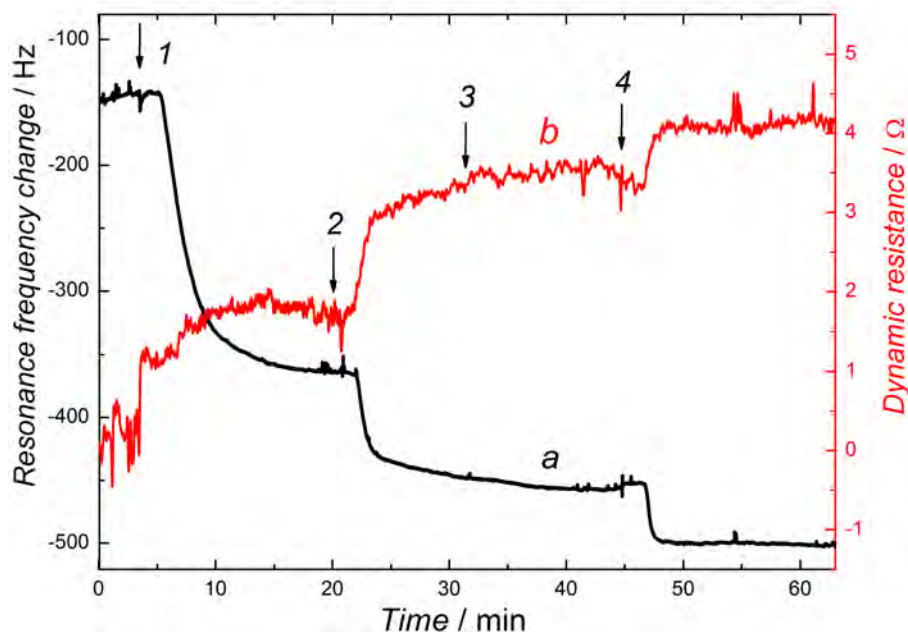
Figure 3.7 Changes with time of (*a*) the resonance frequency and (*b*) the dynamic resistance accompanying consecutive injections of (1) 1 mg/mL neutravidin, (2) 15 μM biotinylated oligonucleotide, (3) 15 μM non-complementary oligonucleotide, and (4) 15 μM target oligonucleotide under flow-injection analysis (FIA) conditions for the recognition polymer film. The injected volume of the sample of the target oligonucleotide in PBS (pH=7.4) was 100 μL; the flow rate of the PBS (pH=7.4) carrier solution was 35 μL/min.

cleotide was incomplete by 3.7 pmoles after the first injection. That was most likely because of significantly lower stability of the hybridization complex compared to that of the neutravidin-biotin complex.

Recognition film analysis by AFM imaging. The films for AFM imaging were deposited on the gold film coated glass slides using the same procedure as that for polymer deposition on GCE and QCR. The slides were cleaned with acetone, and then dried in an Ar stream before use. Scheme 3.4 shows the AFM images of the biosensor recognition film taken after each step of its preparation, i.e., the polymer film deposited using three *I-E* cycles (layer a and image a), the polymer film with immobilized neutravidin (layer b and image b), then modified with the recognizing oligonucleotide (layer c and image c), and then after binding the target oligonucleotide (layer d and image d). As a result of the film modification with neutravidin, morphology of the film changed distinctly. That is, small, 12±2 nm in diameter, grains (Scheme 3.4a) were replaced by clusters of 25±1 nm in diameter (Scheme 3.4b). This grain aggregation may indirectly suggest that neutravidin was complexed by biotin. The consecutive immobilization of recognizing oligonucleotide made the film more rigid with well seen pores of 17±4 nm in diameter (Scheme 3.4c). Moreover, flat terraces that appeared may suggest aggregation of

the oligonucleotides, indicating that the oligonucleotide structure was responsible for the film solidification. Hybridization of the target oligonucleotide negligibly changed morphology of the film (Scheme 3.4d).
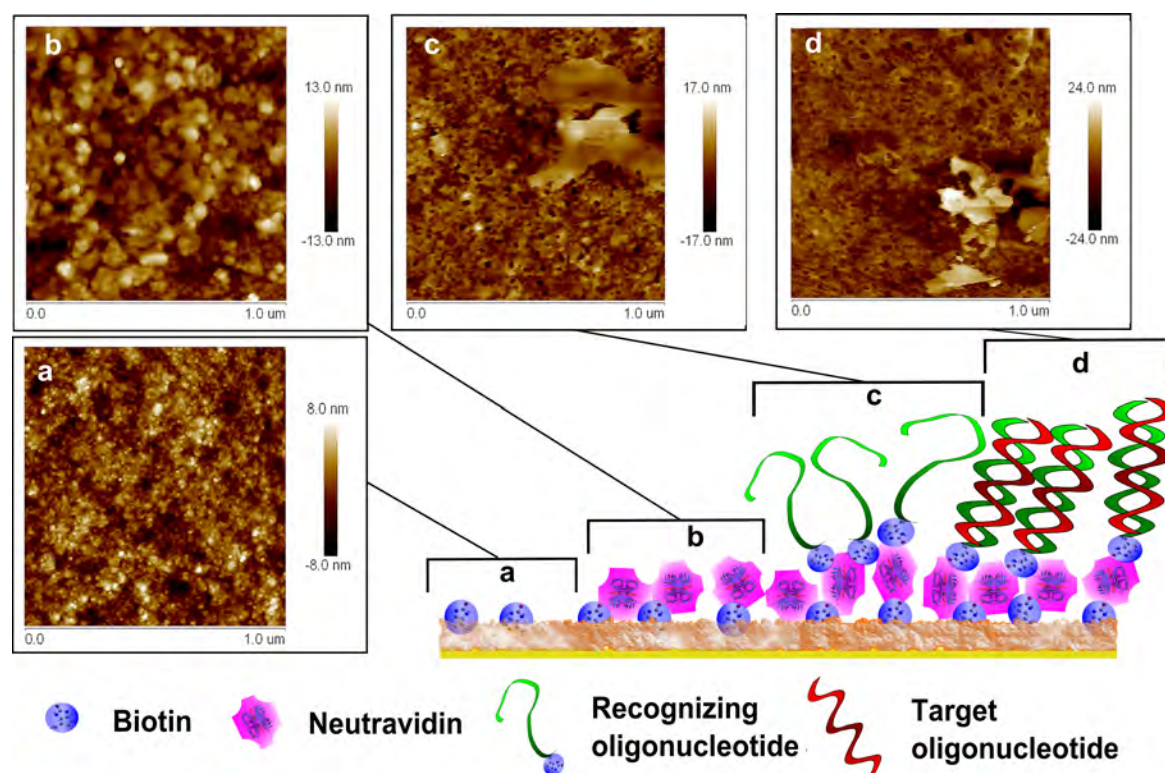
Scheme 3.4 The AFM images of (a) the polymer film deposited on a gold film coated glass slide using three *I-E* cycles and this film afer immobilization of (b) neutravidin, (c) recognizing oligonucleotide, and (d) target oligonucleotide.

3.2.2 Optimization of the recognition film preparation

In order to prepare biosensors of appreciable analytical performance, i.e., low LOD and high sensitivity, several parameters of preparation of the recognition polymer films were optimized. First, the influence of the polymer film thickness on sensor performance was examined. This thickness was controlled with the number of *I-E* cycles [83]. For that, AFM imaging provided useful information. Figure 3.8 shows AFM images of the polymer film deposited during one (Fig. 3.8a), three (Fig. 3.8b), five (Fig. 3.8c), and seven *I-E* cycles (Fig. 3.8d). The film deposited during one *I-E* cycle was uniform, covering the entire surface of the Au coated glass slide (Figure 3.8a). The film consisted of merged polymer grains of 12±2 nm in diameter (Figure 3.8b). With the increase of the number of *I-E* cycles, the film thickness and roughness increased. Apparently, the film became more porous with holes indicated by arrows in Figures 3.8c and 3.8d. The rate of the film growth was lower the higher was the number of the *I-E* cycle, in line with the PM measurements. That means

that the mass of the deposited polymer increased for the consecutive *I-E* cycles. However, this increase was smaller for each consecutive cycle, in accord with the resonance frequency changes.
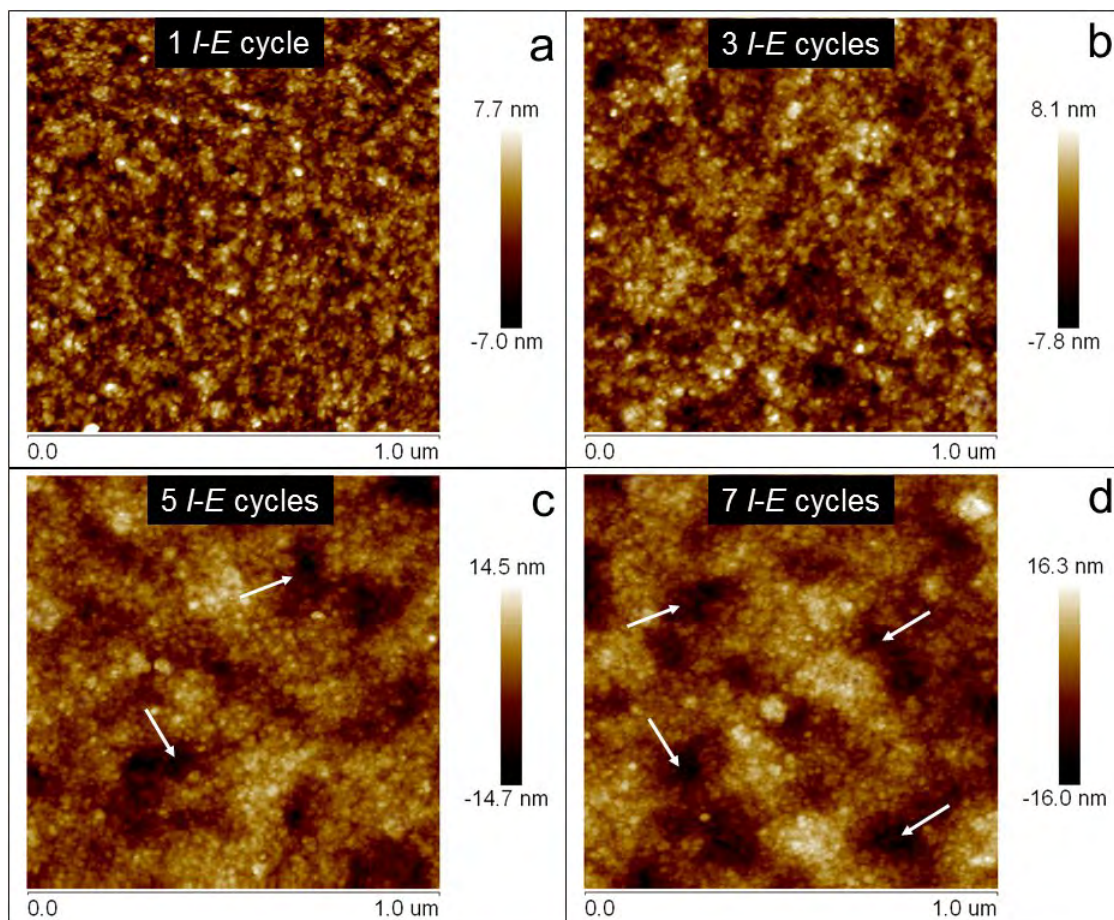
Figure 3.8 The AFM images of the polymer films deposited by potentiodynamic electropolymerization on the gold coated glass slide using (a) 1, (b) 3, (c) 5, and (d) 7 *I-E* cycles.

Moreover, deposition of a thicker film resulted in the increase of both its roughness and R_{ct} (data summarized in Table 3.4). It means that the electron transfer through the polymer film between the electrode substrate and the electroactive species in the solution could be significantly hindered due to the increase of the film resistivity. In consequence, the R_{ct} change due to immobilization of neutravidin, and then the recognizing oligonucleotide, would be indistinguishable. This behavior was confirmed experimentally. That is, immobilization of neutravidin and the recognizing oligonucleotide caused merely a small R_{ct} increase for thicker films. In effect, the sensitivity to the target oligonucleotide was low. In order to determine optimum film thickness, calibration plots were constructed for the recognition films prepared by applying different numbers of *I-E* cycles during electropolymerization (Figure 3.9). Apparently, the optimum number of cycles for the 1 mM monomer was 3, providing effective resistivity and surface roughness (or porosity) of the resulting

polymer film. Further deposition of the polymer increased porosity of the film on the one hand and increased its resistivity (Table 3.4) and, in consequence, decreased its LOD on the other.
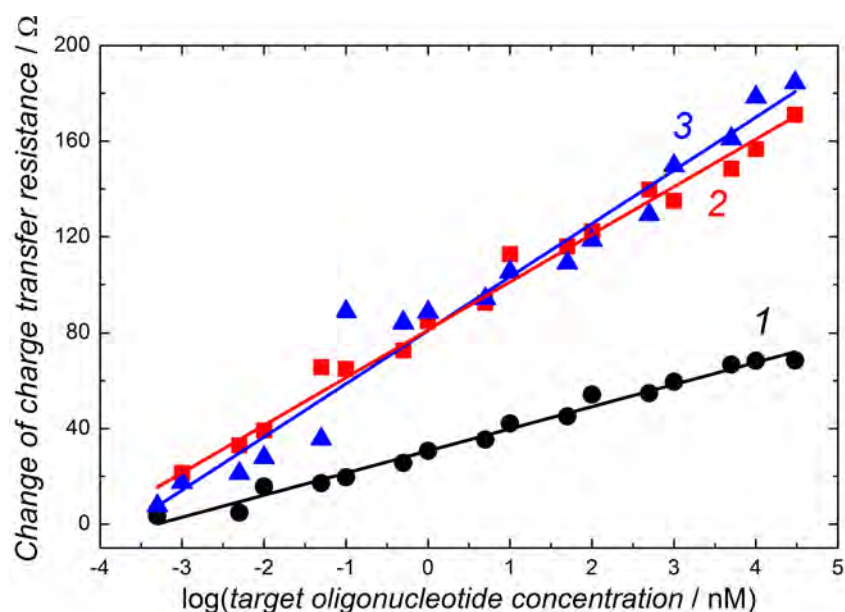
Figure 3.9 Calibration curves, constructed using the experimental data fitted with electrical parameters of the equivalent circuit (Scheme 2.3), for the target oligonucleotide determined by the film deposited by potentiodynamic electropolymerization in the course of (*1*) 1, (*2*) 3, and (*3*) 5 *I-E* cycles. Measurements were performed for 0.1 M $K_3Fe(CN)_6$ and 0.1 M $K_4Fe(CN)_6$ at the applied potential equal to the open circuit potential. An Ag|AgCl electrode and a platinum plate served as the pseudo-reference and counter electrode, respectively. Frequency was varied in the range of 1 MHz to 500 mHz.

Table 3.4 Parameters of the polymer film prepared by potentiodynamic electropolymerization using different number of *I-E* cycles.

No. of *I-E* cycles	Mean thickness / nm	Thickness increase / nm	Roughness nm	R_{ct} / Ω
1	36±2	—	2.18	76.5±0.4
3	57±4	20.6	2.95	101.9±0.2
5	74±5	17.2	7.33	108.3±6.4
7	83±3	8.6	8.95	206.5±28.4

Other parameters affecting the analytical performance of the biosensors include time of the electrode immersion in the neutravidin solution, and then in the recognizing oligonucleotide solution. Seemingly, the larger the amount of the recognizing oligonucleotide immobilized on the electrode, the larger the amount of the target oligonucleotide that could be bound. Hence, detectability could be higher. Therefore, the dependence of R_{ct} on the immersion time was investigated. For that, the

electrode coated with the polymer film was immersed in the 1 mg/mL neutravidin solution for 2, 5, 7, 10, 15, and 20 min. It appeared that the R_{ct} value was higher the longer was the immersion time up to 10 min, and then it remained constant suggesting saturation of the polymer active sites responsible for the biotin-neutravidin complexation. Similarly, the immobilization time of the recognizing oligonucleotide was optimized. Apparently, the R_{ct} reached its maximum steady value after 10-min immersion of the modified electrode in the 30-μM recognizing oligonucleotide solution.

3.2.3 Analytical performance of the impedimetric chemosensor HIV

After deposition of a complete recognition film, the electrode was immersed, consecutively, in the target oligonucleotide solutions of increasing concentrations for 6 min. Then, the electrode was rinsed with 0.1 M PBS (pH=7.4) and the potential linearly cycled between -0.20 and 0.60 V vs. Ag|AgCl. This biosensor treatment resulted in generating repeatable impedimetric data. Next, the experimental impedance data (Fig. 3.10) were fitted with electric parameters of the equivalent circuit presented in Scheme 2.3. The determined R_{ct} values were used to construct the calibration plot (curve *1* in Figure 3.11). The biosensor response was linear with respect to the logarithm of the target oligonucleotide concentration in a quite wide concentration range (0.5 pM to 30 μM). The linear regression equation and the correlation coefficient of the calibration plot was $(R_{ct,f} - R_{ct,i})/\Omega = 19.91(\pm 0.59) + 81.18(\pm 1.48)$ $\log(c_{target}/nM)$ and 0.99, respectively. In this equation, c_{target} is the concentration of the target oligonucleotide, while $R_{ct,i}$ and $R_{ct,f}$ is the charge-transfer resistance of the initial recognition film and that of the recognition film after immersion in the target oligonucleotide solution, respectively.

The recognition films, prepared under the same conditions, were used to compare the biosensor selectivity with respect to oligonucleotides containing 2- and 7-nucleobase mismatches (curve *2* and *3*, respectively, in Figure 3.11). The sensitivity with respect to the target oligonucleotide, 19.91($\pm$0.59) Ω, was nearly twice that to the 2-nucleobase mismatched oligonucleotide, 10.87($\pm$0.56) Ω, and seven times that to the 7-nucleobase mismatched oligonucleotide, 2.83($\pm$1.47) Ω indicating a pronounced biosensor selectivity.
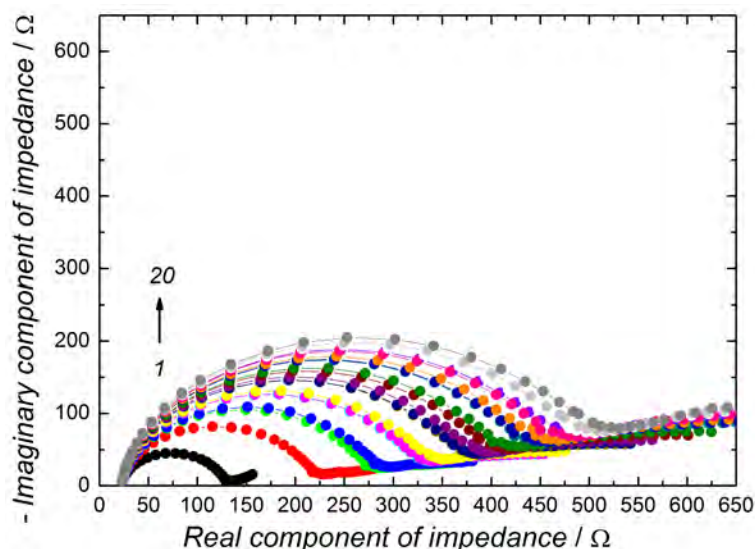
Figure 3.10 The Nyquist plots for the glassy carbon electrode (*1*) coated by the film of the electropolymerized biotinylated bis(2,2'-bithien-5-yl)methane, and then after consecutive immersions in solutions of (*2*) 1 mg/mL neutravidin for 15 min, next (*3*) 30 μM recognizing oligonucleotide for 15 min, and then in (*4*) 0.5, (*5*) 1, (*6*) 5, (*7*) 10, (*8*) 50, (*9*) 100, (*10*) 500 pM, (*11*) 1, (*12*) 5, (*13*) 10, (*14*) 50, (*15*) 100, (*16*) 500 nM, (*17*) 1, (*18*) 5, (*19*) 10, (*20*) 30 μM solution of the target oligonucleotide for 6 min. Measurements were performed for 0.1 M $K_3Fe(CN)_6$ and 0.1 M $K_4Fe(CN)_6$ at the applied potential equal to the open circuit potential. An Ag|AgCl electrode and a platinum plate served as the pseudo-reference and counter electrode, respectively. Frequency was varied in the range of 1 MHz to 500 mHz.
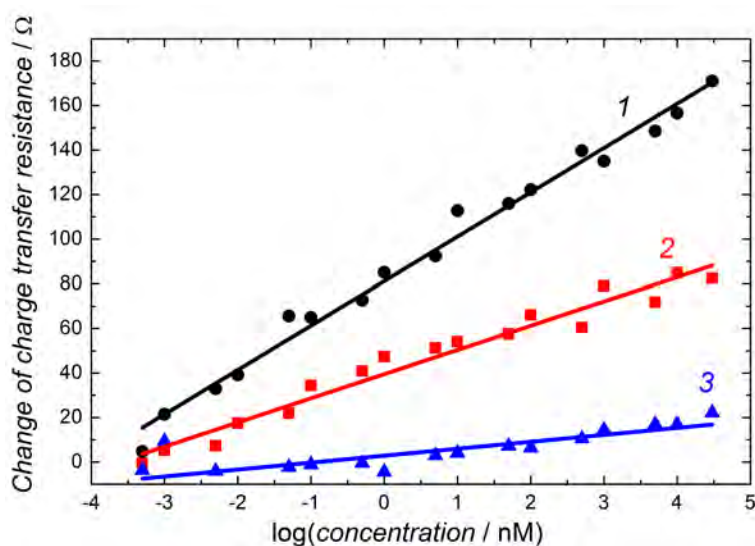
Figure 3.11 Calibration curves, constructed using the experimental data obtained by fitting electrical parameters of the equivalent circuit, shown in Scheme 2.3, for (*1*) the target oligonucleotide, (*2*) 2-nucleobase mismatched target oligonucleotide, and (*3*) 7-nucleobase mismatched target oligonucleotide determined for the recognition film. Measurements were performed for 0.1 M $K_3Fe(CN)_6$ and 0.1 M $K_4Fe(CN)_6$ at the applied potential equal to the open circuit potential. An Ag|AgCl electrode and a platinum plate served as the pseudo-reference and counter electrode, respectively. Frequency was varied in the range of 1 MHz to 500 mHz.

3.2.4 Analytical performance of the piezoelectric microgravimetry HIV chemosensor

After the preparation of the recognition film, the calibration curve was constructed by performing FIA injections of the target oligonucleotide solutions of different concentrations. After each injection, a sample of the 0.1 M NaOH solution was injected in order to de-hybridize the oligonucleotides, thus regenerating the biosensor. Figure 3.12 shows five consecutive injections of solutions of 600-nM target oligonucleotide. After each injection, frequency expectedly dropped to reach a constant value. Evidently, the oligonucleotides were permanently hybridized under the FIA conditions. After the injection of the 0.1 M NaOH sample, however, the frequency abruptly dropped, which was mirror imaged by the raise of the dynamic resistance. When the PBS carrier solution reached the flow-through cell, (~3 min after the initial frequency drop) the frequency returned to its initial baseline level. This behavior indicates a complete elution of the target oligonucleotide from the recognition film by 0.1 M NaOH. Supposedly, the abrupt frequency drop and subsequent increase to its baseline level was due to the change in the polymer swelling, which accompanied switching of the flow of the PBS carrier solution (pH=7.4) to that of the 0.1 M NaOH solution (pH=13.0). Signal repeatability was estimated from the data shown in Figure 3.12. The determined standard deviation of the target oligonucleotide quantification was 13%. The calibration curve (Figure 3.13) was constructed from the frequency change with time during consecutive FIA injections of the target oligonucleotide of different concentrations, each followed by injection of 0.1 M NaOH. The biosensor response to the target oligonucleotide was linear in the concentration range of 50 to 600 nM. The linear regression equation of the calibration plot and the correlation coefficient of the calibration plot was $\Delta f/\mathrm{Hz} = 0.028(\pm 0.003) + 4.74(\pm 0.66)$ $c_{\mathrm{target}}/\mathrm{nM}$ and 0.94, respectively; Δf being the resonant frequency change due to the injection of the target oligonucleotide.
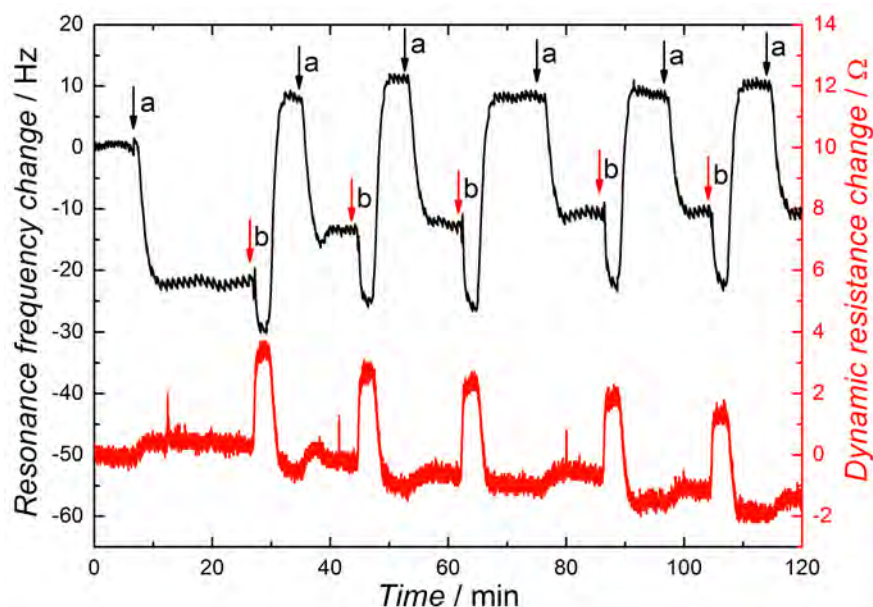
Figure 3.12 Simultaneous resonance frequency and dynamic resistance changes with time accompanying (a) consecutive injections of 600 nM target oligonucleotide, (marked with black arrows) followed by (b) injections of 0.1 M NaOH for de-hybridization, (marked with red arrows) measured under flow-injection analysis (FIA) conditions. The injected sample volume was 100 μL. PBS (pH=7.4) served as the carrier solution. Its flow rate was 35 μL/min.
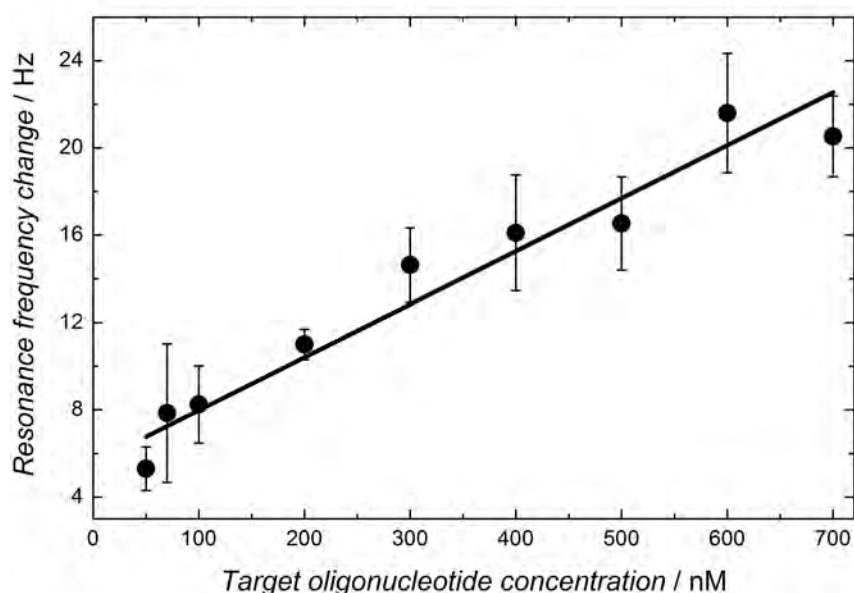
Figure 3.13 The resonance frequency change against the target oligonucleotide concentration during the flow-injection analysis (FIA) PM measurements. After each injection of the target oligonucleotide, 0.1 M NaOH was injected. Volume of the injected sample solution was 100 μL. PBS (pH=7.4) served as the carrier solution. Its flow rate was 35 μL/min.

3.3 Chemical sensor for myoglobin

A two-layer polymer film was prepared on a gold electrode for recognition of myoglobin. The method of modification of conducting surfaces with neutravidin, developed in the present study and described in Section 3.2, above, was utilized for construction of the inner polymer layer. After immobilization of neutravidin on the polymer surface, the electrode was further modified with biotinylated myoglobin. At this stage, myoglobin served as the template. Next, the electrode modified that way was transferred to a solution of the FM **10**, bearing the carboxylic group capable of hydrogen bond formation with the groups present on the myoglobin surface, e.g., the amino and hydroxyl groups. Then, the outer polymer layer was deposited by potentiodynamic electropolymerization, yielding the MIP imprinted with myoglobin. Finally, the myoglobin template was extracted from the MIP film resulting in a ready-to-use sensing platform capable of myoglobin recognition. The change of the impedance of the chemosensor accompanying binding of the myoglobin analyte was used for signal transduction. Consecutive steps of preparation of the recognition film are shown in Scheme 3.5 and described in details in Section 3.3.1, below.
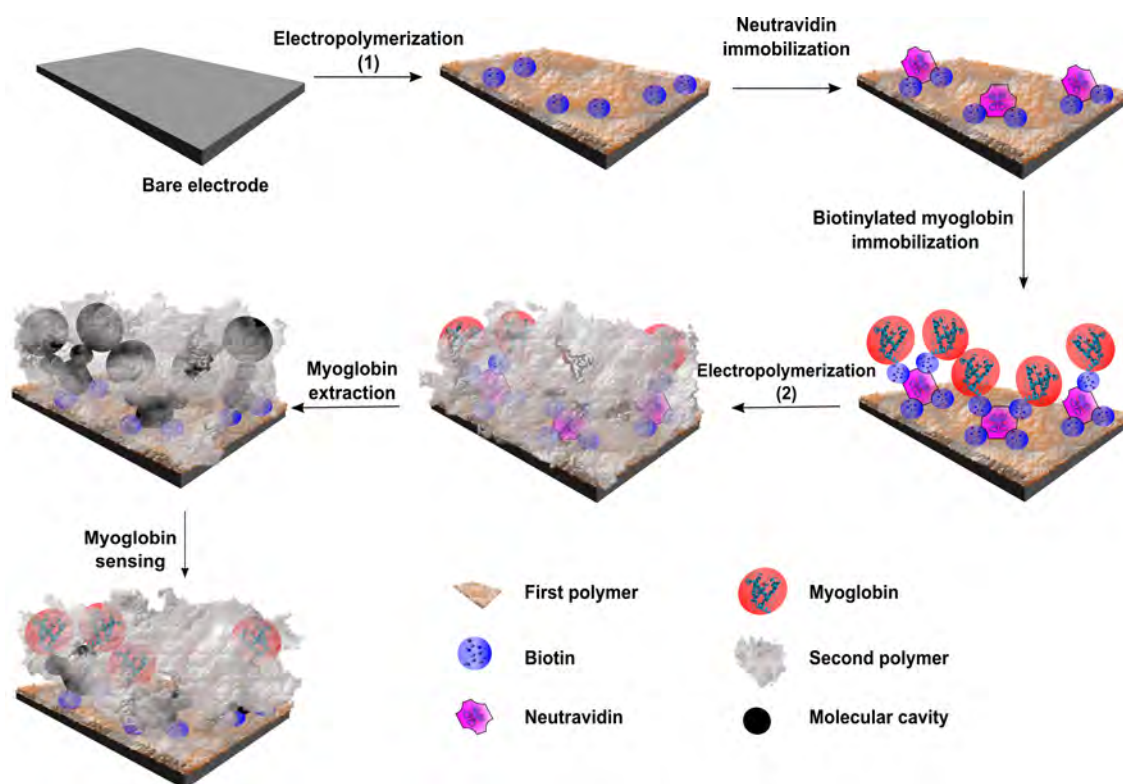
Scheme 3.5 Consecutive steps of preparation of the molecularly imprinted polymer film for myoglobin recognition.

3.3.1 Preparation of the myoglobin molecularly imprinted polymer film

3.3.1.1 Deposition of the inner polymer film

The first step of preparation of the myoglobin recognition film involved polymer deposition from the FM **2** solution by linear cycling of the potential in the range of 0.50 to 1.30 V vs. Ag|AgCl (Figure 3.14). The dichloromethane solution for electropolymerization was 1 mM in **2** and 0.1 M in (TBA)ClO$_4$. The solvent for this electropolymerization was different from that used previously for biotinylated polymer film deposition (Section 3.2, above). This solvent change allowed for polymerization at lower potentials, thus avoiding the undesired oxidation of the Au electrode surface. An anodic peak observed ~1.0 V vs. Ag|AgCl (Figure 3.14) resulted from oxidation of the bisbithiophene moiety of the FM **2** leading to the polymer film formation. This electropolymerization was similar to that described above in Section 3.2. That is, the anodic peak potential of the bisbithiophene moiety electrooxidation was shifted positively. After deposition, the polymer film was rinsed with dichloromethane to remove the excess of the supporting electrolyte.

Figure 3.14 Potentiodynamic electropolymerization of the functional monomer **2** in 0.1 M (TBA)ClO$_4$ in dichloromethane on the gold electrode surface. The potential scan rate was 50 mV/s. Scan numbers are indicated at curves.

3.3.1.2 Myoglobin immobilization

The procedure of electrode surface modification with myoglobin used herein was adapted from the procedure of preparation of a recognition film for oligonucleotide determination described above (Section 3.2). The method of biotinylation of myo-

globin was described in Chapter 2, Section 2.4.3, above. After inner polymer film deposition on the Au electrode, the potential was cycled in the range of -0.20 and 0.60 V vs. Ag|AgCl in the redox probe aqueous solution (0.1 M $K_3Fe(CN)_6$ and 0.1 M $K_4Fe(CN)_6$) in order to improve repeatability of the subsequent impedimetric measurements [118]. Next, this electrode was immersed in the 1 mg/mL neutravidin solution for 15 min. After that, the electrode was rinsed with PBS (pH=7.4) in order to remove the unbound neutravidin. Then, the modified that way electrode was exposed to potential cycling again in the range indicated above until repeatable EIS spectra were recorded. Subsequently, the electrode was immersed in the 1 mg/mL solution of the biotinylated myoglobin for 20 min. Afterwards, the electrode was rinsed with PBS (pH=7.4), and then potential was cycled again until the EIS spectra were repeatable. The EIS spectra recorded after each preparation step are shown in Figure 3.15.
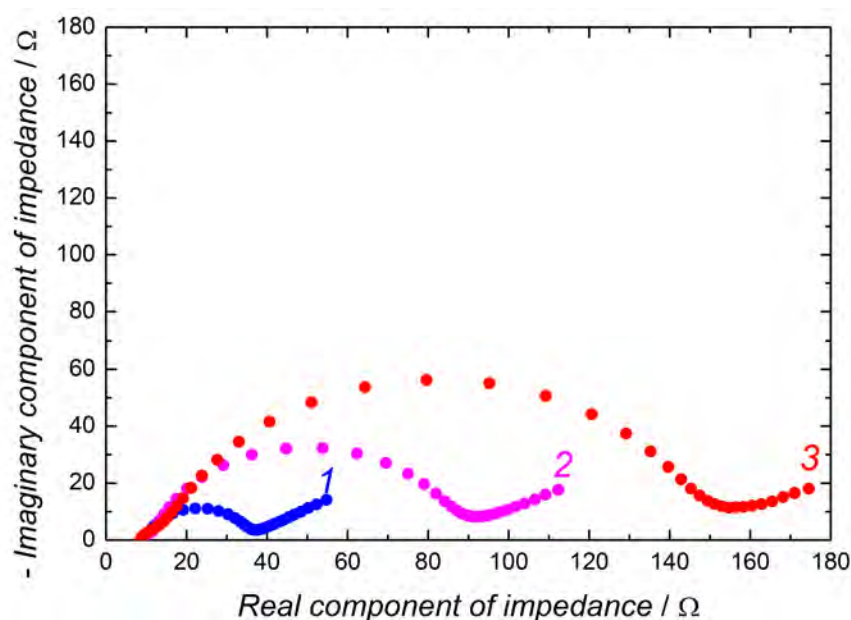
Figure 3.15 Exemplary Nyquist plots for GCE (*1*) coated with the inner polymer film of the monomer **2**, and then after consecutive immobilization of (*2*) neutravidin and (*3*) biotinylated myoglobin. Measurements were performed for 0.1 M $K_3Fe(CN)_6$ and 0.1 M $K_4Fe(CN)_6$ at the open circuit potential. An Ag|AgCl electrode and a platinum plate served as the pseudo-reference and counter electrode, respectively. Frequency was varied in the range of 1 MHz to 200 mHz.

The present EIS curves were similar to those for the oligonucleotide recognition film, because the preparation procedure involved similar steps. Therefore, a modified Randles-Ershler equivalent circuit was used for data interpretation (Scheme 2.3). The solution resistance, R_s, was constant (8.7 Ω, for the bare Au electrode) for all measured films. The film properties changed after each step of preparation, similarly as for the film for the oligonucleotide detection (Section 3.2.1, above). The fitted parameters of the film, such as the exponent ϕ, capacitive parameter T, and R_{ct},

are summarized in Table 3.5. After each preparation step, both the exponent ϕ and R_{ct} increased indicating that the film became more insulating and its electrical double-layer properties remained close to those of an ideal capacitor while the T value changed only slightly.

Table 3.5 Parameters determined from the data presented in Figure 3.15 using the modified Ershler-Randles equivalent circuit (Scheme 2.3). T – capacitive parameter, ϕ – exponential factor of the constant phase element (CPE), R_{ct} – charge-transfer resistance.

No.	Polymer film	$T \ / \ \mu Fs^{1-\phi}$	ϕ	$R_{ct} \ / \ \Omega$
1	As deposited	$5.9 \ (\pm 0.6) \times 10^{-5}$	0.785 ± 0.010	28.2 ± 0.5
2	After neutravidin immobilization	$6.3 \ (\pm 0.6) \times 10^{-5}$	0.750 ± 0.010	86.8 ± 2.1
3	After myoglobin immobilization	$6.9 \ (\pm 0.6) \times 10^{-5}$	0.707 ± 0.009	156.8 ± 3.4

In order to confirm immobilization of neutravidin, and then biotinylated myoglobin, the PM measurements were performed. For that, the polymer film was deposited on surface of the Au-QCR under the same conditions as those used for such a film deposition on the Au disk electrode. Then, the flow-injection analysis measurement was performed under the same conditions as those previously used for characterization of the oligonucleotide chemosensor (100-μL sample volume, the PBS (pH=7.4) carrier solution, and the 35 μL/min carrier solution flow rate). First, the 1 mg/mL neutravidin solution sample was injected followed by injection of the 1 mg/mL biotinylated myoglobin solution. The resonance frequency and dynamic resistance changes for this experiment are shown in Figure 3.16.

Importantly, both solution injections caused a frequency decrease (curve a in Figure 3.16) corresponding to consecutive irreversible immobilization of neutravidin, and then myoglobin. The frequency decrease was accompanied by only a small dynamic resistance change in the range of few ohms (curve b in Figure 3.16), proving that the viscosity and density of the film did not change significantly. Therefore, the mass of the immobilized species could be determined from the frequency decrease, according to the Sauerbray Equation (2.21). The mass of neutravidin immobilized on the polymer film was 272 ng (4.5 pmoles). The mass of subsequently immobilized myoglobin was 62 ng (3.6 pmoles). Hence, the immobilized neutravidin-to-myoglobin mole ratio was 0.8. Since the myoglobin molecule is smaller than that of neutravidin, it can be concluded that not all of the sites available for biotin binding were occupied after the first biotinylated myoglobin injection. This inference was confirmed by measuring the frequency change after one more injection of the biotinylated myoglobin solution. This second injection resulted in the further frequency decrease. After the fourth injection of the biotinylated myoglobin sample, no
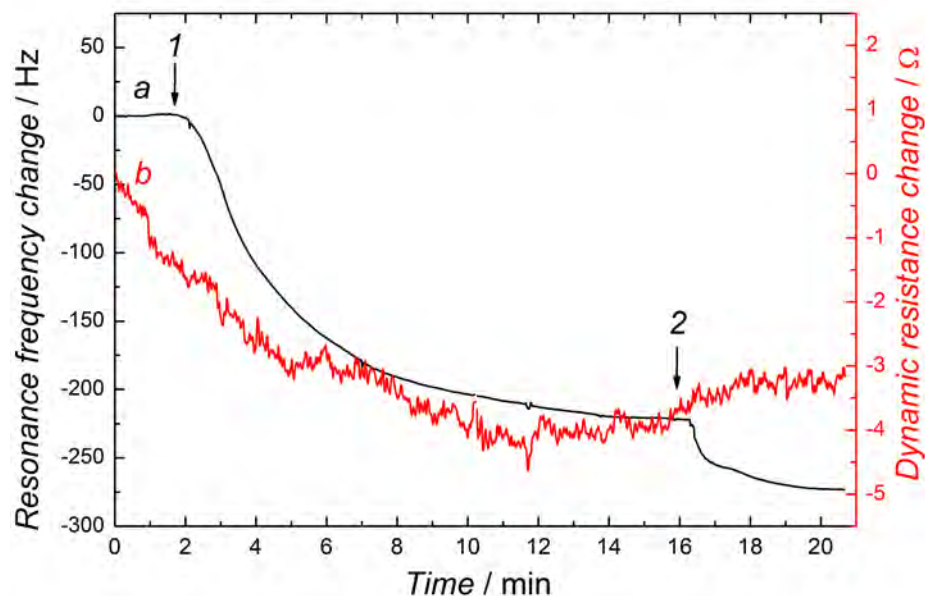
Figure 3.16 Changes with time of (*a*) the resonance frequency and (*b*) the dynamic resistance accompanying consecutive injections of (*1*) 1 mg/mL neutravidin, and then (*2*) 1 mg/mL biotinylated myoglobin under flow-injection analysis (FIA) conditions for the polymer film of FM **2**. The injected volume of the sample in PBS (pH=7.4) was 100 μL; the flow rate of PBS (pH=7.4), used as the carrier solution, was 35 μL/min.

change in the measured parameters was observed. Apparently, no more myoglobin molecules could be immobilized on the polymer surface. However, it would not be advantageous to coat the electrode surface with myoglobin completely, because the outer polymer film should be deposited around the myoglobin molecules. Therefore, the modification with only one biotinylated myoglobin injection was used for further studied.

3.3.1.3 Deposition of the outer polymer film

After myoglobin was bound to the polymer film, the electrode was transferred to the dichloromethane solution of 1 mM FM **10** and 0.1 M (TBA)ClO$_4$. Dichloromethane is water immiscible. Therefore, the myoglobin molecules kept their hydration shells, thus preventing changes in their conformation. Then, the potential was linearly cycled in the range of 0.50 to 1.30 V vs. Ag|AgCl (Figure 3.17). An anodic peak observed between 1.05 and 1.20 V vs. Ag|AgCl (Figure 3.17) was assigned to electro-oxidation of the bisbithiophene moiety of the FM **10**. This electro-oxidation led to deposition of the polymer film. Similarly to the previously described deposition of the inner polymer (Section 3.3.1.1, above), potential of the anodic peak of the bisbithiophene moiety electro-oxidation was shifted positively. After deposition, the MIP film imprinted with myoglobin was rinsed with dichloromethane to remove the

excess of the supporting electrolyte. Then, the film was immersed in acetone for few hours to extract myoglobin and neutravidin from the MIP.

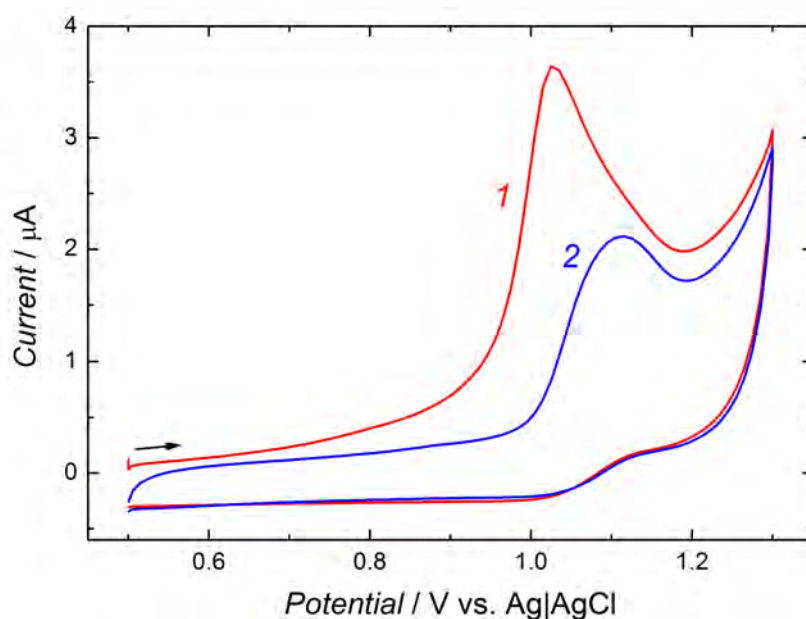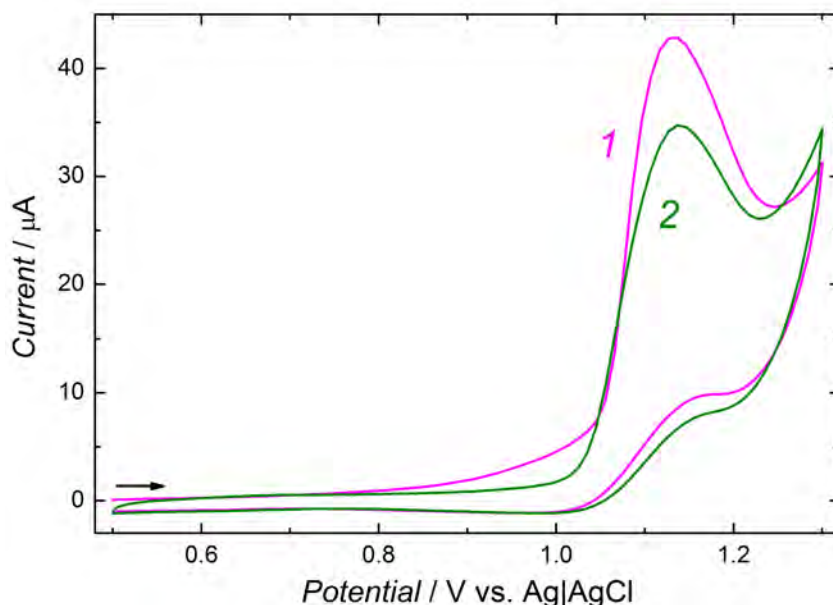**Figure 3.17** Two first consecutive curves of potentiodynamic electropolymerization of the 1 mM functional monomer **10** in 0.1 M (TBA)ClO$_4$, in dichloromethane, on the gold electrode surface. The potential scan rate was 50 mV/s. Scan numbers are indicated at curves.

The EIS spectra of a freshly prepared MIP film, and those of the MIP film after the myoglobin template extraction were recorded consecutively. Unfortunately, deposition of the outer polymer layer appeared to be not much repeatable. Figure 3.18 shows few EIS spectra recorded after template extraction from different MIP films prepared using the same preparation procedure. This low reproducibility might arise from different amounts of water introduced into the polymerization solution with the immobilized myoglobin molecules. The presence of water hinders bithiophene polymerization and results in the polymer films of low conductivity [4]. Apparently, this last step of MIP preparation bears further scrutiny. Nevertheless, the myoglobin extracted MIP film was used for the determination of myoglobin in order to verify the developed procedure of preparation of the chemosensor. The results obtained for one of the MIP films prepared are presented in Section 3.3.2, below.
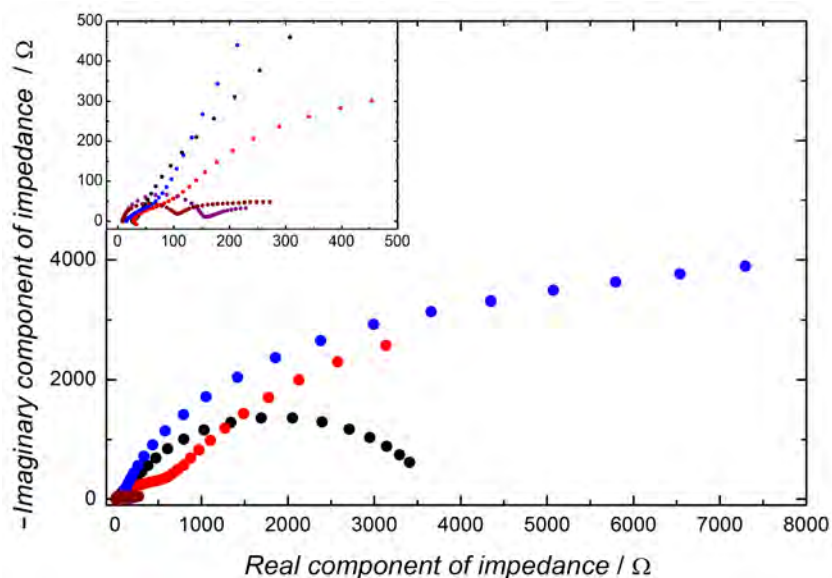
Figure 3.18 Exemplary Nyquist plots for the Au electrode coated with different MIP films imprinted with myoglobin. Inset shows the enlarged region of high frequency. Measurements were performed for 0.1 M $K_3Fe(CN)_6$ and 0.1 M $K_4Fe(CN)_6$ at the applied potential equal to the open circuit potential. An Ag|AgCl electrode and a platinum plate served as the pseudo-reference and counter electrode, respectively. Frequency was varied in the range of 1 MHz to 200 mHz.

3.3.1.4 Testing acetone as the myoglobin template extraction solvent

For myoglobin extraction from the MIP film, it was important to develop a method for breaking the covalent bond between biotin and neutravidin without damaging the film. For that, acetone was tested. Acetone is fully miscible with water. Therefore, water-dissolved proteins exposed to it change their conformation. This change causes the biotin-neutravidin bond to break and, hence, to break the bond between the polymer film and the immobilized species, thus allowing the myoglobin molecules to diffuse away from the electrode surface. In order to confirm this hypothesis, neutravidin solutions and acetone were alternately injected and the relevant data summarized in Table 3.6. After deposition of the polymer film from solution of FM **2**, first, the neutravidin solution was injected. In effect, frequency changed by -162 Hz. Subsequent injection of the neutravidin solution resulted in the frequency change of merely -15 Hz suggesting that the polymer film was fully coated with neutravidin just after the first injection. Next, biotinylated myoglobin was immobilized causing frequency to decrease by 36 Hz. The consecutive neutravidin solution injection resulted in neutravidin binding and the frequency drop of 133 Hz because the myoglobin molecule can be modified with more than one biotin molecule. The next injection of the neutravidin solution caused only a small frequency decrease of 12 Hz confirming full modification of the film with neutravidin after the first injection. After that, acetone was injected. This injection resulted in an abrupt

change in frequency in a form of the peak. This was caused by difference in viscosity of acetone and that of the PBS carrier solution. After this injection, frequency nearly returned to its value from before this injection after 5 min. The subsequent neutravidin solution injection caused the frequency drop of 130 Hz proving that the polymer was available for neutravidin binding again. After that, acetone, and then the neutravidin solution were injected consecutively, resulting in the frequency decrease of 105 Hz. This decrease proved that acetone cleaved the biotin-neutravidin bond and, therefore, could be used for myoglobin extraction from the polymer film.

Table 3.6 The resonance frequency drop after injections of different solutions for myoglobin immobilization and release.

Stage No.	Event	Frequency change / Hz
1	Nuetravidin solution injection	-162
	Nuetravidin solution injection	-15
	Myoglobin solution injection	-36
	Nuetravidin solution injection	-133
	Nuetravidin solution injection	-12
2	Acetone injection	—
	Nuetravidin solution injection	-130
3	Acetone injection	—
	Nuetravidin solution injection	-105

3.3.2 Analytical performance of the exemplary impidimetric chemosensor for myoglobin

Myoglobin was determined using the same procedure as that developed herein for oligonucleotide determination described above in Section 3.2. That is, after deposition of a complete MIP recognition film and extraction of the myoglobin template, the electrode was immersed in the test solutions of different myoglobin concentrations for 6 min. Then, the electrode was rinsed with 0.1 M PBS (pH=7.4) and the potential linearly cycled between -0.20 and 0.60 V vs. Ag|AgCl with the 50 mV/s scan rate. Next, the experimental impedance data (Figure 3.19) were fitted with electric parameters of the equivalent circuit presented in Scheme 2.3. The determined R_{ct} values were used to construct the calibration plot (Figure 3.20). The biosensor response was linear with respect to the myoglobin concentration in the concentration range of 10 to 500 ng/mL. The linear regression equation and the correlation coefficient of the calibration plot was $(R_{ct,f} - R_{ct,i})/\Omega = 0.09(\pm 0.01) + 15.11(\pm 2.20)\ c_{Myo}/$ ng/mL and 0.96, respectively. In this equation, c_{Myo} is the concentration of the myoglobin while $R_{ct,i}$ and $R_{ct,f}$ is the charge-transfer resistance of

the initial recognition film and that of the recognition film after its immersion in the solution of a given myoglobin concentration, respectively. The linear concentration range was appropriate for the determination of myoglobin in blood, because the myoglobin physiological concentration in healthy individuals ranges from 0 to 85 ng/mL. Higher myoglobin concentration indicates muscle damage, i.a., heart attack [179]. Therefore, further work on optimization of MIP preparation to reach high repeatability as well as studies of the chemosensor response to interferences are needed.
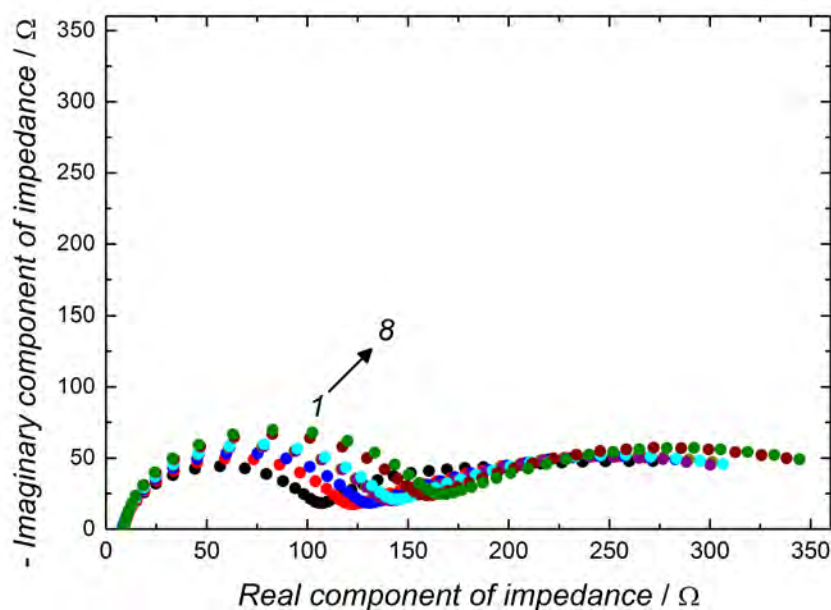
Figure 3.19 The Nyquist plots for the Au electrode (*1*) coated with an MIP film after template myoglobin extraction, and then after consecutive immersions in solutions of (*2*) 10, (*3*) 75, (*4*) 100, (*5*) 200, (*6*) 300, (*7*) 500, (*8*) 750 ng/mL solution of myoglobin for 6 min. Measurements were performed for 0.1 M $K_3Fe(CN)_6$ and 0.1 M $K_4Fe(CN)_6$ at the applied potential equal to the open circuit potential. An Ag|AgCl electrode and a platinum plate served as the pseudo-reference and counter electrode, respectively. Frequency was varied in the range of 1 MHz to 200 mHz.
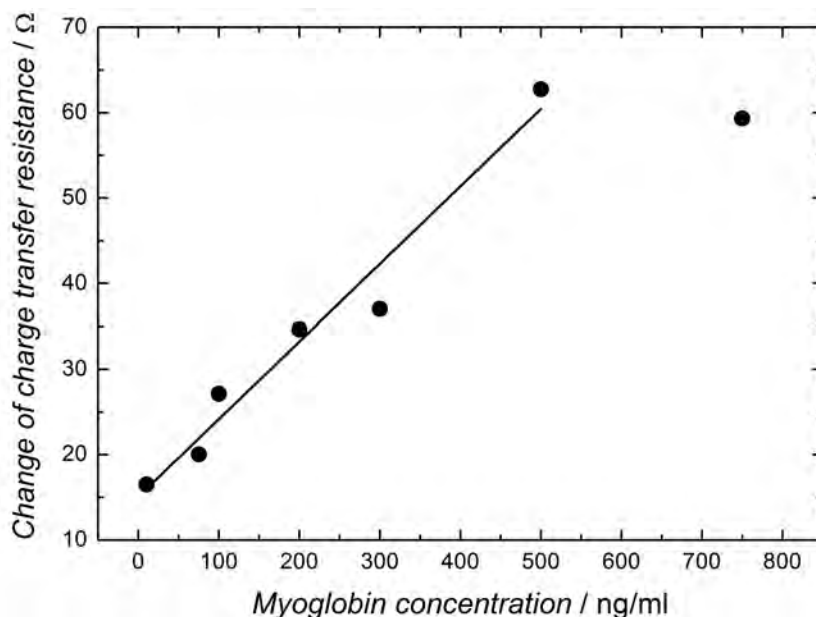
Figure 3.20 Calibration curve, constructed using the experimental data fitted with electrical parameters of the equivalent circuit (Scheme 2.3), for myoglobin determined by the MIP film coated Au electrode. Measurements were performed for 0.1 M $K_3Fe(CN)_6$ and 0.1 M $K_4Fe(CN)_6$ at the applied potential equal to the open circuit potential. An Ag|AgCl electrode and a platinum plate served as the pseudo-reference and counter electrode, respectively. Frequency was varied in the range of 1 MHz to 200 mHz.

3.4 Chemical sensor for melamine

Melamine is a small aromatic compound (Scheme 3.6a) containing 66.7% of nitrogen by mass. Therefore, it is used by dishonest manufacturers of food products in order to artificially inflate protein level. This is because this level is determined based on the nitrogen content. Repeated intake of melamine can cause formation of the kidney stones, and fatal renal failure after intaking it for prolonged time [180–182]. Therefore, investigation of the melamine concentration in food products and pet feed is necessary. It is estimated that melamine causes kidney diseases when its content in feed exceeds 200 mg per 1 kg of feed [183].

A piezomicrogravimetric melamine chemosensor has already been fabricated in our laboratory [83]. In the present work, usefulness of this chemosensor for melamine determination in real feed samples was assessed. Moreover, a sensor testing a new transduction platform, namely, surface plasmon resonance (SPR) spectroscopy was prepared. The functional monomer bearing 18-crown-6 ether moiety, vis., 4-bis(2,2'-bithienyl)benzo[18-crown-6]methane **19**, (Scheme 3.6b) was used for melamine imprinting in mildly acidified solutions becuase of strong 18-crown-6-ether interaction with protonated primary amine groups. This interaction was confirmed by quantum-

chemical calculations. The energy gain due to formation of the complex between three protonated primary amine groups of melamine and three FM molecules was as high as -1924 kJ mol^{-1}. This strong interaction allowed for formation of stable complexes that were incorporated in the structure of MIP via potentiodynamic electropolymerization deposition. Detectability of the PM chemosensors and their selectivity with respect to main interferences like ammeline, cyanuric acid, and cyromazine, were assessed in the previously reported research performed in our lab [83].
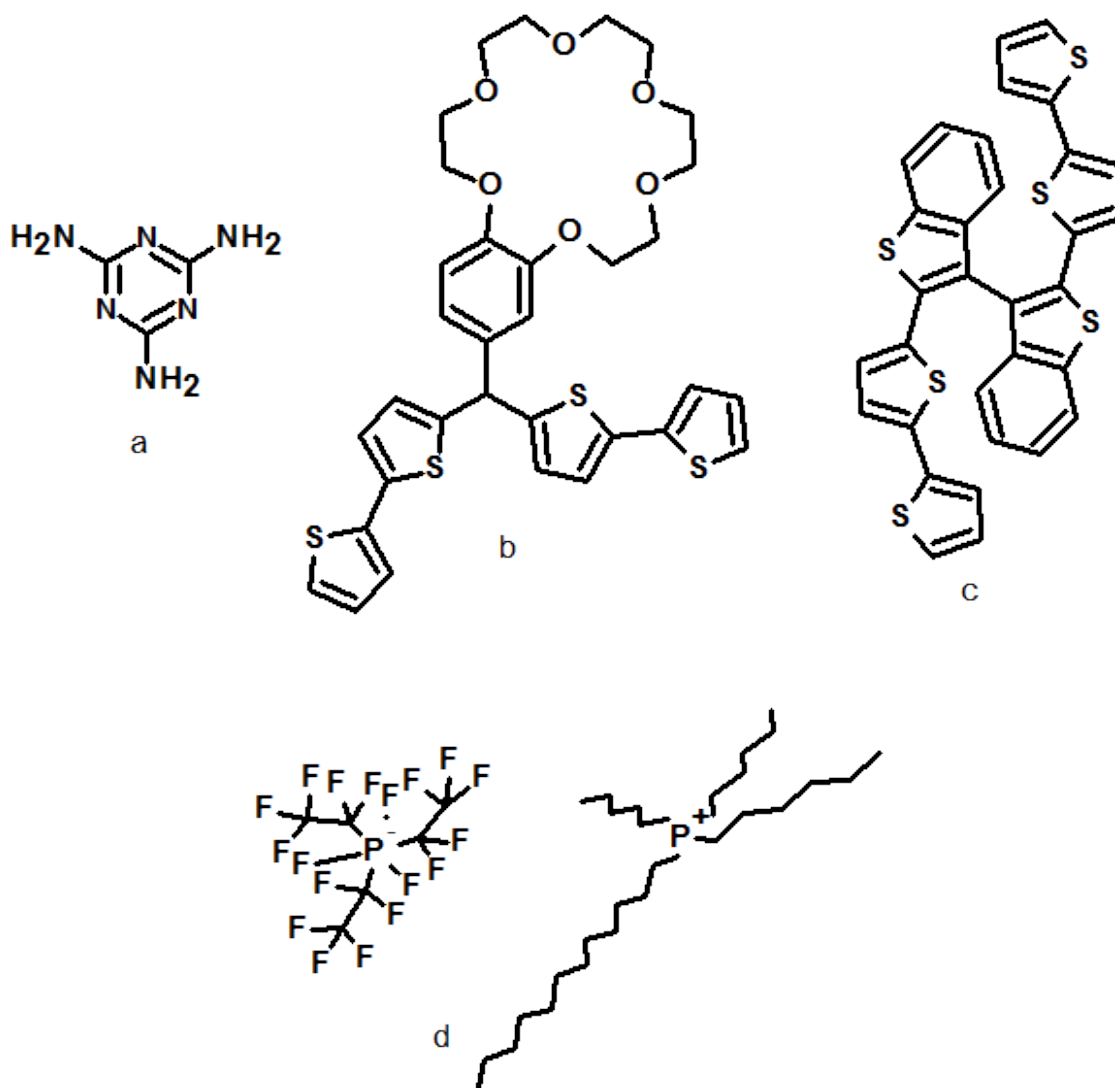
Scheme 3.6 Structural formula of (a) melamine, (b) functional monomer bis(2,2'-bithienyl)benzo[18-crown-6]methane **19**, (c) the cross-linking monomer 3,3'-bis[2,2'-bis(2,2'-bithiophene-5-yl)]thianaphthene **20**, and (d) trihexyl(tetradecyl)phosphonium tris(pentafluoroethyl)-trifluorophosphate ionic liquid.

3.4.1 Preparation of an MIP-melamine film

The procedure of MIP preparation was adapted from previously reported research [83]. Parameters of MIP preparation, namely, composition of the solution for electropolymerization, the potential range and scan rate, were optimized thereof and used herein without further modification.

The PM chemosensor for melamine. Potentiodynamic MIP deposition was carried out in the potential range of 0.50 to 1.50 V vs. Ag|AgCl (Figure 3.21). The solution for electropolymerization was 0.3 mM in **19**, 0.3 mM in the cross-linking monomer **20**, 0.1 mM in melamine, and 0.1 M in (TBA)ClO$_4$, in the mixture of acetonitrile and ionic liquid (1 : 1, v : v). The ionic liquid, trihexyl(tetradecyl)phosphonium tris(pentafluoroethyl)-trifluorophosphate (structural formula d in Scheme 3.6), was used in order to increase porosity of the MIP film and, hence, the melamine detectability [83]. Similarly to the electropolymerization of **2** (Section 3.2.1, above), an anodic peak of electro-oxidation of the bisbithiophene moiety was observed at ~1.0 V vs. Ag|AgCl (Figure 3.21a). The MIP film formation was confirmed by the resonant frequency decrease of QCR (Figure 3.21b). After deposition, the MIP was rinsed with acetonitrile in order to remove the excess of the supporting electrolyte solution. Next, the melamine template was extracted from the film by dipping the QCR/MIP in 0.1 M NaOH. Extraction under these conditions was efficient. That was because the melamine amine groups were deprotonated at the high pH value of the extracting solution. This deprotonation weakened interactions of the melamine molecules with the MIP cavities.

The SPR chemosensor for melamine. The electropolymerization conditions of MIP deposition on a gold film coated glass disk (i.e., an SPR chip) had to be adjusted. Firstly, this Au film was deposited directly on the glass surface, in contrast to the gold film of QCR that was deposited on a Ti underlayer. Therefore, the Au film on a glass disk was less stable with respect to positive potential polarization and could be damaged at potentials exceeding 1.35 V vs. Ag|AgCl. Therefore, the potential range applied was kept at 0.50 to 1.35 V vs. Ag|AgCl (Figure 3.21). Moreover, the measurable angle range of the incident light beam of the SPR spectroscope used was quite limited. Therefore, there was a certain limit of film thickness, which could not be exceeded. That was because film deposition caused the increase of the angle at which the surface plasmon resonance occurred (the SPR angle). Therefore, concentration of the solution for polymerization was adjusted and MIP films were deposited to reach the maximum SPR angle change of 6 °. The mixed acetonitrile and the ionic liquid (1 : 1, v : v) solution, optimized for electropolymerization, was 60 μM in **19**, 60 μM in the cross-linking monomer **20**, 20 μM in melamine,
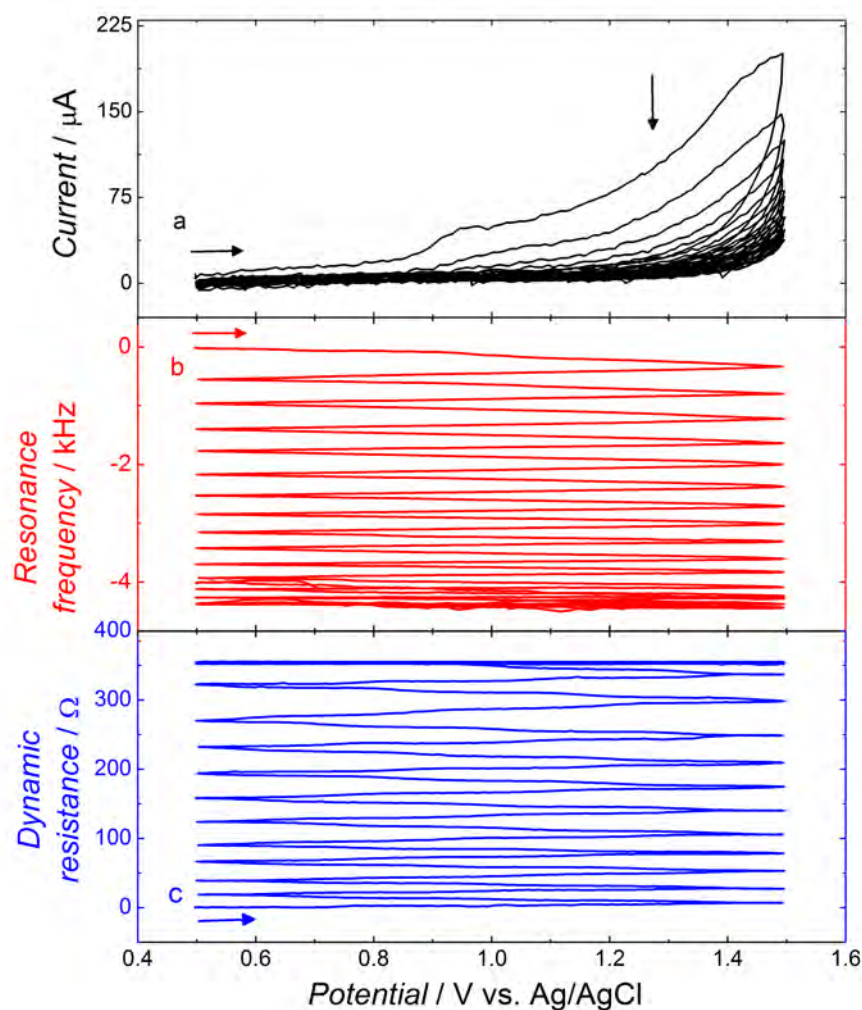
Figure 3.21 Simultaneously recorded curves of the potential dependence of (a) current, (b) the resonance frequency change, and (c) the dynamic resistance change for the Au-QCR accompanying potentiodynamic electropolymerization from solution of 0.3 mM functional monomer **19**, 0.3 mM cross-linking monomer **20**, 0.1 mM melamine in 0.1 M (TBA)ClO$_4$ and the acetonitrile-to-(ionic liquid) volume ratio of 1 : 1, acidified with trifluoroacetic acid. The potential scan rate was 50 mV/s.

and 0.1 M in (TBA)ClO$_4$. Electropolymerization with the MIP film deposition on the gold surface of the glass disk was very similar to that on the gold surface of QCR (Fig. 3.22a). From the PM measurements it followed that the MIP film was steadily growing during potential cycling, as confirmed by the increase of the SPR angle (Fig. 3.22b). Moreover, a recurring oscillation of the SPR angle was observed for each *I-E* cycle (Fig. 3.22c). This behavior could be attributed to changes in the dielectric property of the polymer film as it was switched from its oxidized to reduced state [184]. After deposition, the MIP film was rinsed with acetonitrile in order to remove the excess of the supporting electrolyte solution, and then the film was washed with 0.1 M NaOH solution in order to extract the melamine template.
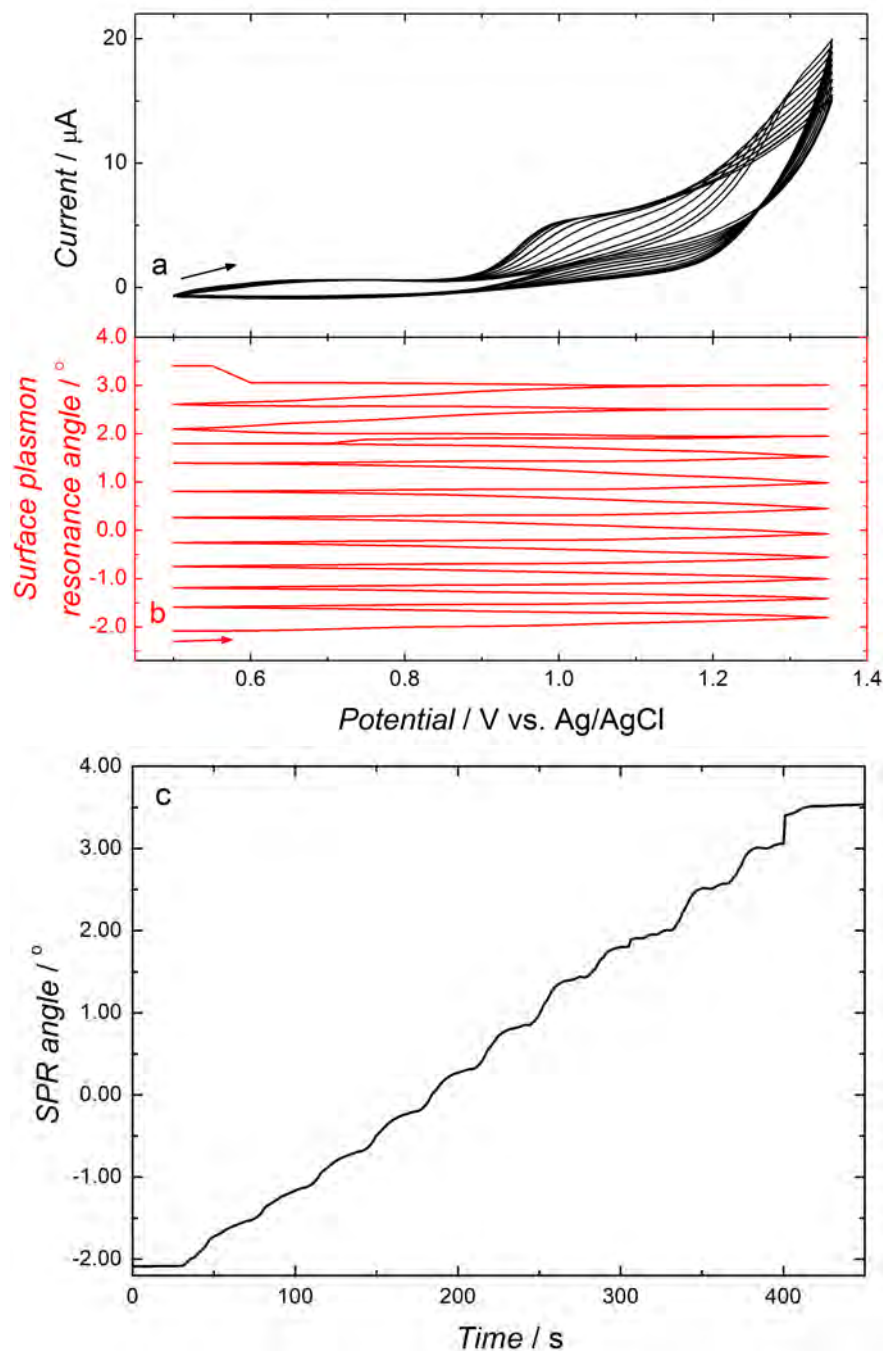
Figure 3.22 Simultaneously recorded curves of the potential dependence of (a) current and (b) the SPR angle for the Au coated glass disk, as well as (c) the SPR angle change with time accompanying MIP deposition by potentiodynamic electropolymerization from the 60 μM functional monomer **19**, 60 μM cross-linking monomer **20**, 20 μM melamine and 5 mM (TBA)ClO$_4$ solution of acetonitrile and ionic liquid (1 : 1, v : v) acidified with trifluoroacetic acid. The potential scan rate was 50 mV/s.

3.4.2 Performance of the SPR chemosensor for melamine

Once the composition of the solution for electropolymerization was optimized and the potential range of potentiodynamic electropolymerization defined, the only parameter left to be adjusted was thickness of the MIP film. Similarly to previously presented research [83, 149], this thickness was controlled by the number of potential cycles applied. The films prepared by applying different number of potential cycles were characterized by different SPR angle changes. Each film prepared was used for melamine determination. For that, the films were immersed in a 20-μL sample of 1 mM HCl. After the SPR angle stabilized, an 80-μL sample of the 1 mM HCl solution of melamine of known concentration was injected. In effect, the SPR angle increased (Fig. 3.23). The 10-min time of equilibration of the MIP film in the melamine solution appeared to be sufficient for signal stabilization. After each measurement, the MIP film was washed with 10 mM NaOH for 15 min for melamine extraction.
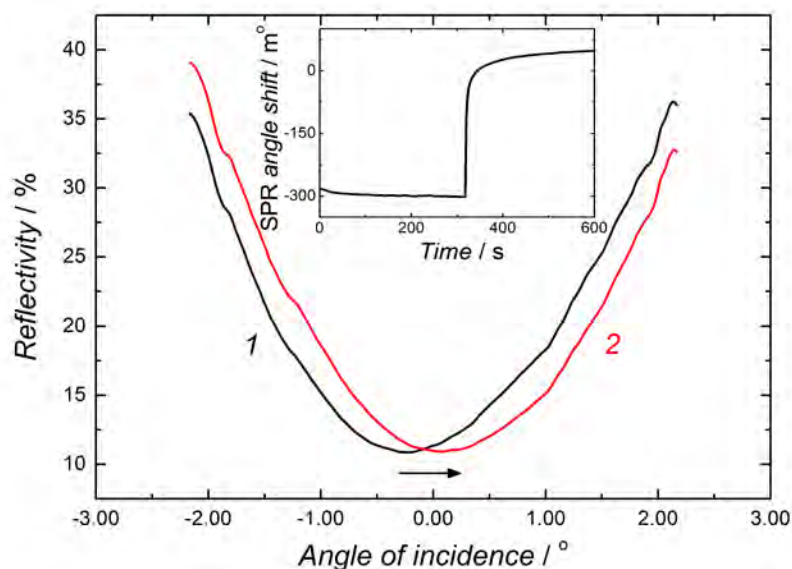
Figure 3.23 Reflectivity against angle of incidence of polarized light beam measured (*1*) before injection of the melamine sample solution and (*2*) after 10 min of equilibration of the MIP film in this solution. Inset shows the SPR angle shift with time.

Then, the calibration plots were constructed using values of the SPR angle change recorded for different melamine concentrations. Parameters of chemosensors prepared using different numbers of *I-E* cycles and, therefore, of different thickness, are summarized in Table 3.7. Evidently, the film exhibiting the highest SPR angle change during electropolymerization is that revealing the highest sensitivity and detectability. Since the SPR angle changed because of analyte binding by the MIP [184–186], the thicker the film, the more melamine was bound to it and, hence, the higher the change of the SPR angle was. Still, film thickness is low due to

instrumental limitation of the measurable SPR angles. Therefore, thickness of the film was still smaller than that of 200 nm reported previously [83] even though the thickest possible film was chosen in the present study. Therefore, melamine could freely diffuse in and out of the MIP film.

The data collected for the MIP film, prepared under optimum conditions, and the corresponding calibration plot is shown in Figure 3.24a and 3.24b, respectively. Apparently, the MIP film became saturated, typically, after the melamine concentration exceeded 1 mM. This effect is widely known in MIPs [187].

Table 3.7 Analytical parameters of the SPR chemosensor for melamine characterized by different values of the SPR angle change during electropolymerization corresponding to thickness of the MIP film.

The SPR angle change due to MIP film deposition / m°	Sensitivity / m° mM^{-1}	LOD / mM
400	4.5	2
1400	8.2	1
3200	18.7	0.6
3800	44.1	0.8
6000	124.5	0.032

Moreover, stability of the MIP film with time was also tested. For that, a series of measurements was performed immediately after film preparaion (*1* in Fig. 3.24a), one day after film preparation (*2* in Fig. 3.24a) and four days after film preparation (*3* on Fig. 3.24a). The MIP film was stored in 1 mM HCl in between measurements. The signal recorded after four days dropped by ~20% indicating that the MIP film was fairly stable.
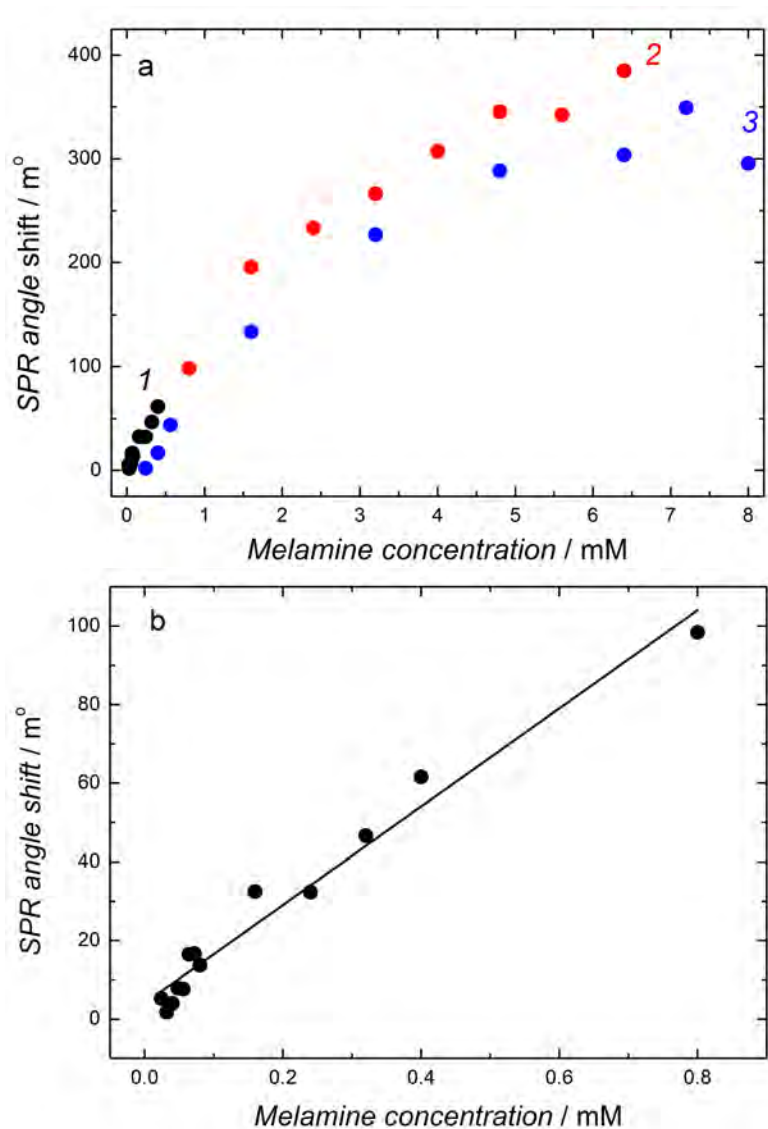
Figure 3.24 The SPR angle change against the melamine concentration measured after exposing the gold coated glass disk, covered with the MIP film, to melamine solutions of different concentrations for 5 min. (a) Three series of measurements; series (*1*) and (*2*) were recorded during consecutive days while series (*3*) was recorded after 2 days. After each determination, the MIP film was rinsed with 1 mM NaOH for 15 min for melamine removal.

3.4.3 Performance of the QCM chemosensor for melamine

Analytical performance of the QCM chemosensor was described in details previously [83]. Therefore, here, the only aspect considered was determination of melamine in the pet feed extracts. The melamine free pet feed samples were obtained from Lab Chem company (Warsaw, Poland). First, extracts were prepared by treating a sample of 1 g of the feed with 0.1 M HCl. The feed was kept in this acid solution under vigorous stirring for 2 h. Next, samples were centrifuged and filtered. Finally, the filtrate was diluted five times. The resulting solution was used as

the sample solution for melamine determination under FIA conditions. Expectedly, injection of this solution did not cause any change of frequency of the chemosensor. Then, the sample solution was spiked with melamine to reach a defined concentration in order to check if the chemosensor is capable of melamine detection. Figure 3.25 shows the response to consecutive injections of the sample solutions spiked with melamine to reach concentrations indicated above arrows. The first few injections of solutions of the same melamine concentration proved that the chemosensor response was repeatable. From the subsequent points, of increasing melamine concentration, the calibration plot was constructed. Apparently, saturation of MIP film was reached at the melamine concentration of ~1.0 mM. Therefore, the dynamic linear concentration range was limited to 0.8 mM. Since melamine solubility in water at 20 °C is 0.32 g per 100 g (25.7 mM) [188] and the melamine concentration in pet feed reaches toxicity at the level of hundreds mg per kg [183], the melamine concentration in the contaminated pet feed extracted with the method described above would be equal to hundreds of μM. Therefore, we safely concluded that the chemosensor was suitable for melamine determination in real samples of the feed. Noticeably, however, melamine is much more toxic if intaken together with cyanuric acid. Therefore, in the case of samples that have been tested positive with respect to the presence of cyanuric acid, the herein presented chemosensor would not be appropriate. This is because the harmful level of the melamine concentration is a few mg per kg of the feed being below LOD of our chemosensor. So, preconcentration of the melamine samples tested would be required.
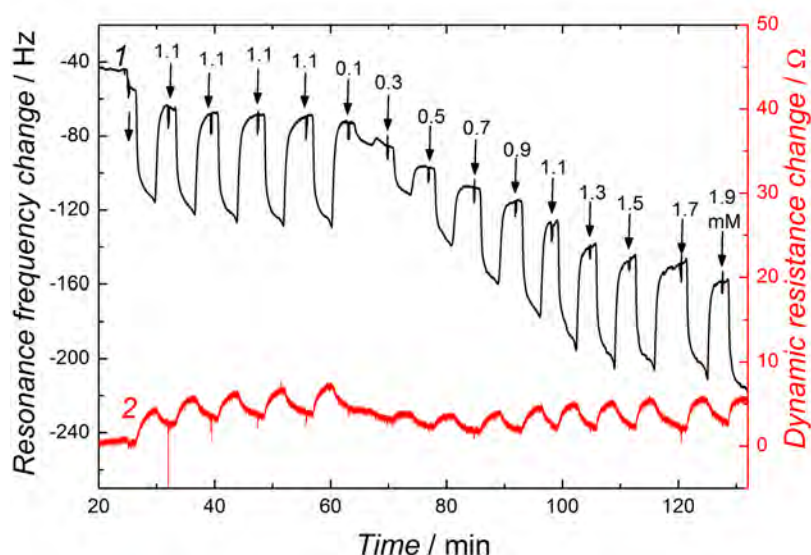
Figure 3.25 Simultaneously recorded the (*1*) resonance frequency and (*2*) dynamic resistance changes with time accompanying consecutive injections of the pet feed extract spiked with melamine to reach a predefined concentration in the range of 0.1 to 1.9 mM under flow-injection analysis (FIA) conditions. The injected sample volume was 100 μL, the carrier solution was 0.1 M HCl and its flow rate was 35 μL/min.
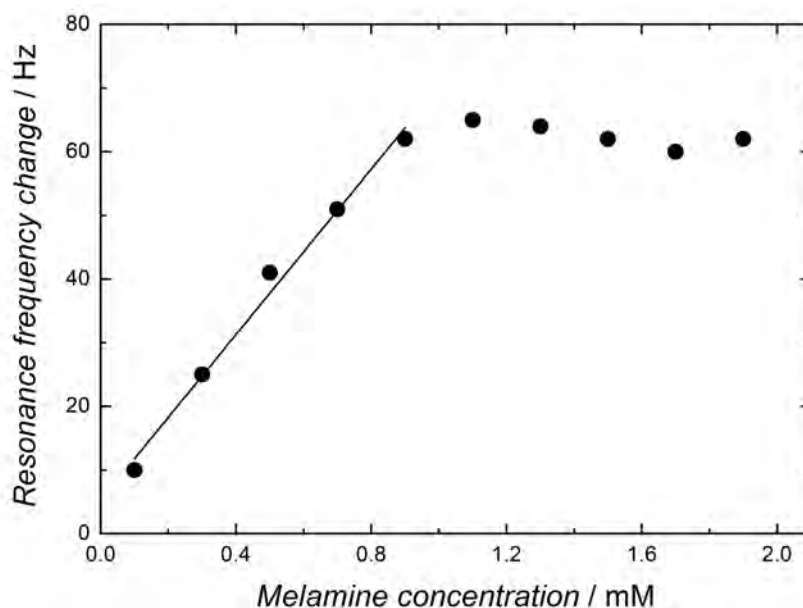
Figure 3.26 The resonance frequency change against the melamine concentration in solution of the pet feed spiked with melamine during flow-injection analysis (FIA) PM determination. Volume of the injected sample solution was 100 μL, the carrier solution was PBS (pH=7.4) and its flow rate was 35 μL/min.

3.5 Chemical sensor for 6-thioguanine

The chemosensor presented in this section was prepared and described in details before [76,143]. Therefore, it is briefly described here as an example of application of the FMs synthesized herein.

The MIP imprinted with 6-thioguanine (6-TG, Scheme 3.7) was prepared and used for construction of an impedimetric chemosensor. Quantum-chemical calculations confirming formation of a pre-polymerization complex of the 6-TG analyte with the FM **11** are described in Section 3.1.2.2, above. The 6-TG complexation in solution was confirmed by the fluorescence titration of **11** with 6-TG. From the fluorescence data it followed that the complex stoichiometry of 1 : 2 for 6-TG : **11** was confirmed and the stability constant of complex formation calculated was $2.17(\pm0.07)\times 10^7$ M^{-2}. This value is much lower than that calculated from the $\triangle G$ obtained from the quantum-chemical calculations, equal to 1.08×10^{10} M^{-2}. The reason for this apparent discrepancy might be that the calculations were performed for the complex in vacuum while the complex is mainly formed via hydrogen bonds that are weaker the higher the electric permittivity of the medium is.

After confirmation of interaction of **11** with 6-TG, the MIP was prepared via potentiodynamic electropolymerization. This electropolymerization resulted in deposition of the MIP film on the 1-mm diameter Pt disk electrode from the 0.2 mM 6-TG, 0.4 mM **11**, 1.2 mM cross-linking monomer **20**, and 0.1 M (TBA)ClO$_4$ solu-
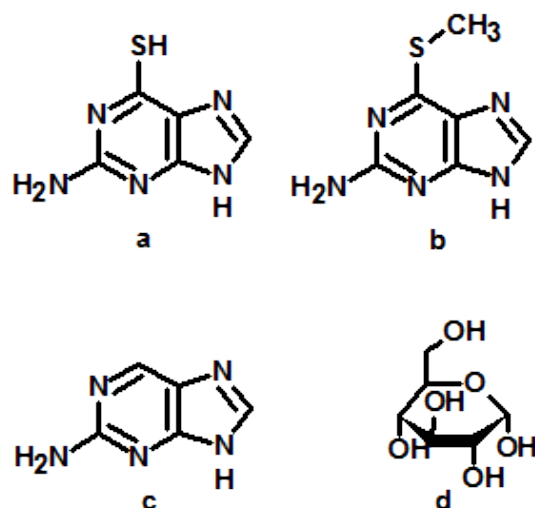
Scheme 3.7 Structural formula of (a) 6-thioguanine as well as its interferents (b) 2-amino-6-methylmercaptopurine, (c) 2-aminopurine, and (d) glucose.

tion of acetonitrile : DMF (9 : 1, v : v). A relatively high cross-linking monomer **20** concentration used afforded extensive polymer cross-linking to form a rigid 3-D matrix.

After MIP preparation, the 6-TG template was extracted with 0.1 M HCl for 3 h under vigorous magnetic stirring conditions.

The measurement of the capacity change of the electrical double layer of the MIP film coated electrode was adopted herein as an indirect method for 6-TG determination. The capacity was measured with EIS at a constant low-frequency (20 Hz) low-amplitude (10 mV) ac voltage for the 0.5 M KF supporting electrolyte solution. Both capacitance and resistance of the MIP film were negligible because the MIP film used was thin and, therefore, the equivalent circuit shown in Scheme 2.4 was used for data interpretation.

Expectedly, an FIA peak of the electrical double-layer capacity of the MIP film was lower the lower was the 6-TG concentration in the consecutively injected solution samples of the 6-TG solution (Fig. 3.27). The linear dynamic concentration range extended from 10 to 600 μM (curve *1* in Fig. 3.28) obeying the linear regression equation of C_{dl} / nF cm^{-2} = 2.95$\pm$(0.17) + 200.76($\pm$52.10) $c_{\mathrm{thioguanine}}$ / μM. The sensitivity and correlation coefficient was (2.95$\pm$0.17) nF cm^{-2} μM^{-1} and 0.99, respectively. At the signal-to-noise ratio, S/N = 3, the LOD of this chemosensor was 10 μ6-TG.
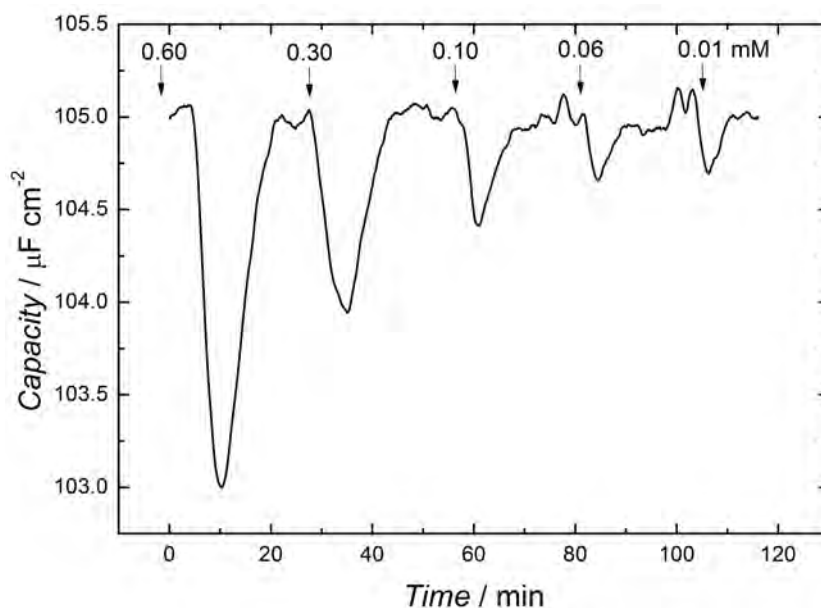
Figure 3.27 The capacity change with time during injection of 100-μL samples of 0.5 M KF solutions of 6-thioguanine of different concentrations (indicated with numbers above arrows), under the FIA conditions, for the template-extracted MIP film-coated 1-mm diameter Pt disk electrode. The flow rate of 0.5 M KF, used as the carrier solution, was 20 μL/min.
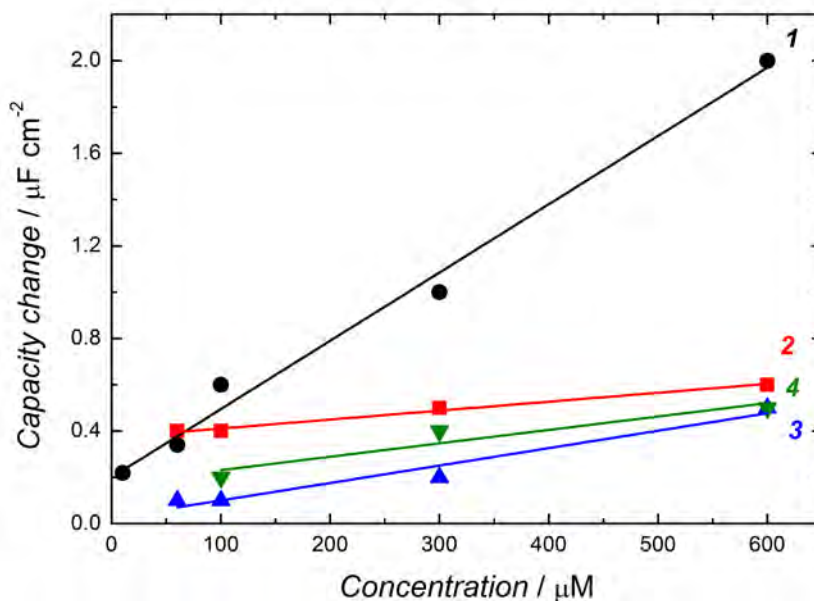
Figure 3.28 The capacity change with the analyte or interference concentration change after injections of 100-μL samples of 0.5 M KF solutions of different concentrations of (*1*) 6-thiogunanie, (*2*) 2-aminopurine, (*3*) glucose, and (*4*) 2-amino-6-methylmercaptopurine under FIA conditions for the (6-thioguanine template)-extracted MIP film-coated Pt disk electrode. The flow rate of 0.5 M KF, used as the carrier solution, was 20 μL/min.

3.6 Chemical sensor for nicotine

The chemical sensor presented in this section was prepared and described in details before [55, 143]. Therefore, it is shortly described here as an example of application of the synthesized FM **9**.

The FM **9** together with the zinc phthalocyanine derivative of bis(2,2'-bithienyl)-methane **21**, were used for biomimetic recognition of nicotine. First, the structure of the complex of nicotine with FMs was optimized (Scheme 3.9) and the total Gibbs free energy gain due to complex formation was calculated, being -115.95 kJ mol^{-1}. Next, binding of FM **21** with nicotine was confirmed with the UV-vis titration in chloroform. During FM **21** titration with nicotine, the Soret absorption band of FM **21** increased and red-shifted by ~2 nm. From those titration data, the complex stability constant was calculated to amount $K_s = 6.9 \times 10^{-5}$ M^{-1}.

Table 3.8 Detectability (LOD) and selectivity of the MIP chemosensing, determined under the FIA conditions for the 0.1 M NaClO$_4$ carrier solution, by injecting 200-μL solution samples of the Nic analyte or interference of different concentrations.

		LOD	Selectivity to	
		μM	cotinine	myosmine
Chemosensor	CA	40	15.5	8.4
	PM	12	3.8	1.8

After confirmation of formation of the pre-polymerization complex, the MIP film was deposited by potentiodynamic electropolymerization on the Au-QCR from a solution containing nicotine (Scheme 3.8), FM **9,** FM **21**, and the cross-linking monomer **20**, in the mole ratio of 1 : 1 : 1 : 3. After deposition of the MIP film, nicotine was extracted from this film with methanol. Then, this film was used for simultaneous PM and CA nicotine determination. The CA determination was possible due to oxidative electroactivity of nicotine. In order to obtain the current signal, a constant potential of 1.10 V vs. Ag|AgCl was applied. The simultaneously recorded frequency change and current during consecutive injections of the nicotine sample solutions are shown in Figure 3.29. These data allowed for construction of the calibration curve. The LOD of the PM chemosensing was as low as 12 μM while that of the CA chemosensing was 40 μM. Selectivity data are summarized in Table 3.8.
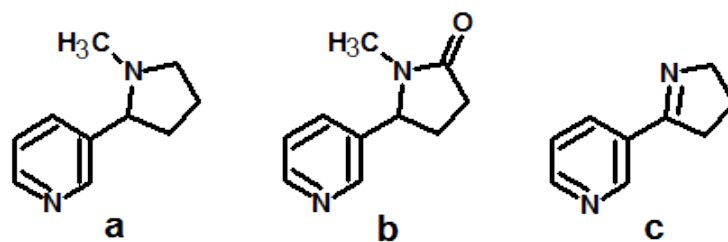
Scheme 3.8 Structural formula of (a) nicotine and its interferences (b) cotinine and (c) myosmine.
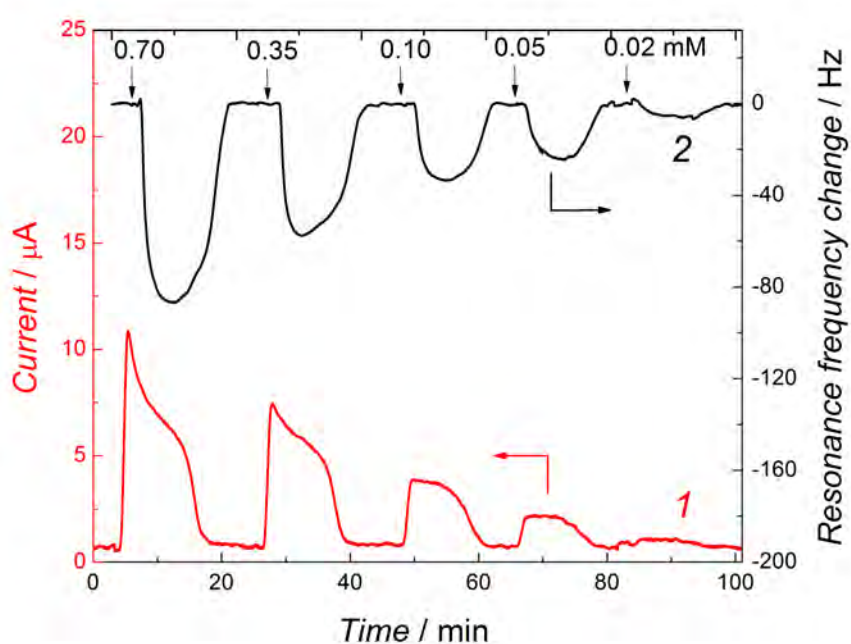
Figure 3.29 The simultaneous change with time, at 1.10 V vs. Ag/AgCl, of (*1*) anodic current and (*2*) resonant frequency during injection of 200-μL samples of 0.1 M NaClO$_4$ solutions of nicotine of different concentrations (indicated with numbers at peaks), under FIA conditions, for the nicotine-template extracted MIP film-coated Au-QCR. The flow rate of 0.1 M NaClO$_4$, used as the carrier solution, was 20 μL/min.
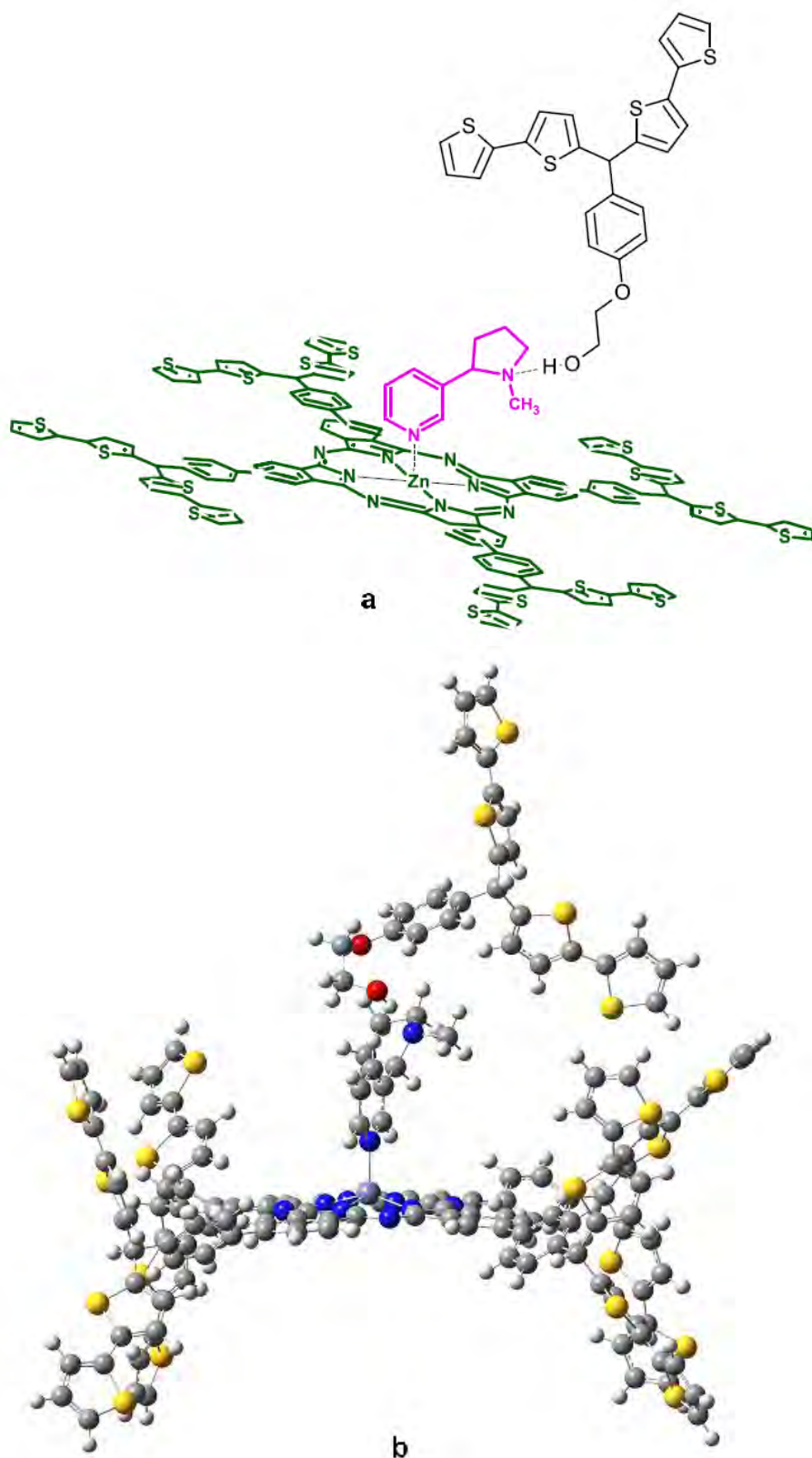
Scheme 3.9 (a) Structural formula and (b) optimized structure of the complex of nicotine with the zinc phtalocyanine containing functional monomer **21** and **9**, optimized by the DFT method at the B3LYP level using the 3-21G* basis set.

3.7 Chemical sensors for nitroaromatic explosives

The chemosensors presented in this section were prepared and described in details before [142, 143]. Therefore, they are only briefly described herein as examples of application of the synthesized FM **7**.

The FM **7** was used for the preparation of MIP films for the determination of nitroaromaticexplosive compounds including 2,4,6-trinitrophenol (TNP), 2,4,6-trinitrotoluene (TNT), 1,3,5-trinitrobenzene (TNB), and 2,4-dinitrotoluene (DNT) Scheme 3.10. FM **7** interacted with analytes via π-π stacking allowing formation of molecular cavity in the polymer film. Before preparation of the MIP film, interaction of **7** with analytes was confirmed by quantum-chemical calculations and fluorescence titration (data summarized in Table 3.9). Calculations performed using the DFT method at the M062X level with the 3-21G* basis set allowed for complex visualisation (Figure 3.30) and estimation of ΔG of complex formation of **7** with different analytes (Table 3.9). During fluorescence titration of **7**, separately with each analyte in toluene, the fluorescence band of bis(2,2'-bithienyl)methane moiety was quenched. From the titration data, stochiometry of the complex of **7** with each analyte was estimated to be 1 : 1. Moreover, the stability constant of each complex was determined (Table 3.9). Details of these calculations are given in literature [142, 143]. These results confirmed possibility of MIP formation.
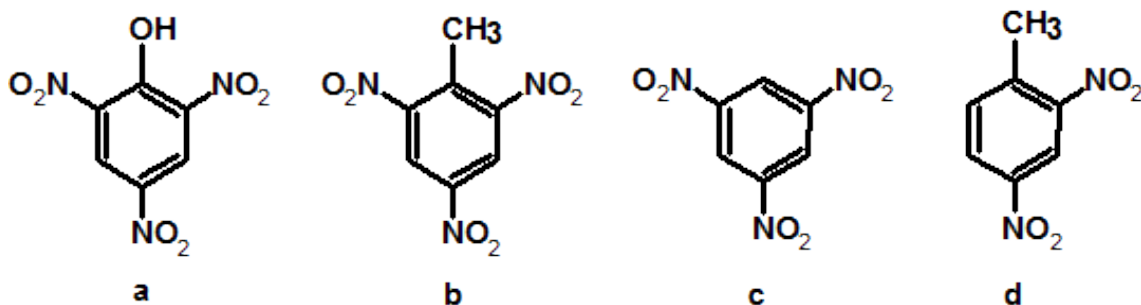
Scheme 3.10 Structural formulas of four common explosive nitroaromatic compounds (a) 2,4,6-trinitrophenol (TNP), (b) 2,4,6-trinitrotoluene (TNT), (c) 1,3,5-trinitrobenzene (TNB), and (d) 2,4-dinitrotoluene (DNT).

Next, an MIP film for each of analytes was deposited by potentiodynamic electropolymerization on the Au-QCR. The solutions for electropolymerization were made 0.5 mM in one of the analytes, 0.5 mM in the functional monomer **7**, 1.5 mM in the cross-linking monomer **20**, and 0.1 M in (TBA)ClO$_4$, in the acetonitrile and dichlorobenzene mixture (1 : 1, v : v), in order to meet the 1 : 1 stoichiometry of the complexes. The cross-linking monomer was added in the large excess in order to fix the MIP-NT matrix rigidly. After that, a mixed solution of methanol and acetonitrile (1 : 1, v : v) was used for extraction of the nitroaromatic explosive tem-

Table 3.9 The Gibbs free energy gain, ΔG, due to formation of the 1 : 1 complexes of **7** with different NTs and the complex stability constant, K_s, calculated using DFT at the M602X/3-21G* level and determined from the fluorescence titration, respectively.

NT	ΔG, kJ mol^{-1}	K_s, M^{-1}
TNP	-58.1	3000
TNT	-51.8	2044
TNB	-48.7	1596
DNT	-36.4	858
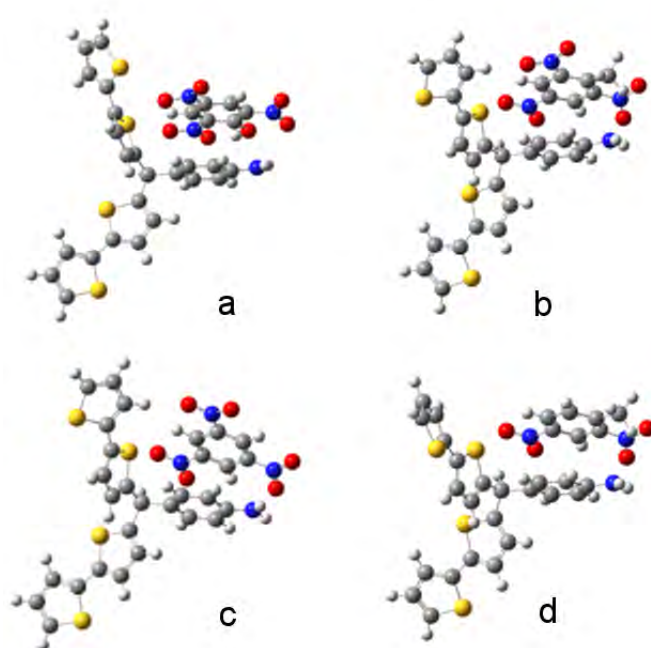
Figure 3.30 Molecular structure of the 1 : 1 complexes of **7** with (a) TNP, (b) TNT, (c) TNB, and (d) DNT, optimized using DFT at the M062X level with the 3-21G* basis set.

plate under vigorous magnetic stirring conditions. Then, the MIP films were used for simultaneous PM and CA determination of the nitroaromatic explosive analytes. Expectedly, both the cathodic current and resonant frequency, recorded using the MIP film-coated Au-QCR, changed producing peaks after each injection of the 0.2 M NaCl solution of the analyte of different concentration indicating reversible analyte binding, and then releasing by molecular cavities of the MIP film. As an example, the signal measured for the MIP imprinted with TNT is shown in Figure 3.31.

From the CA and PM curves measured for MIPs imprinted with different analytes during injections of analytes and interferences, the LOD and selectivity of each chemosensor was determined. These data are presented in Table 3.10.
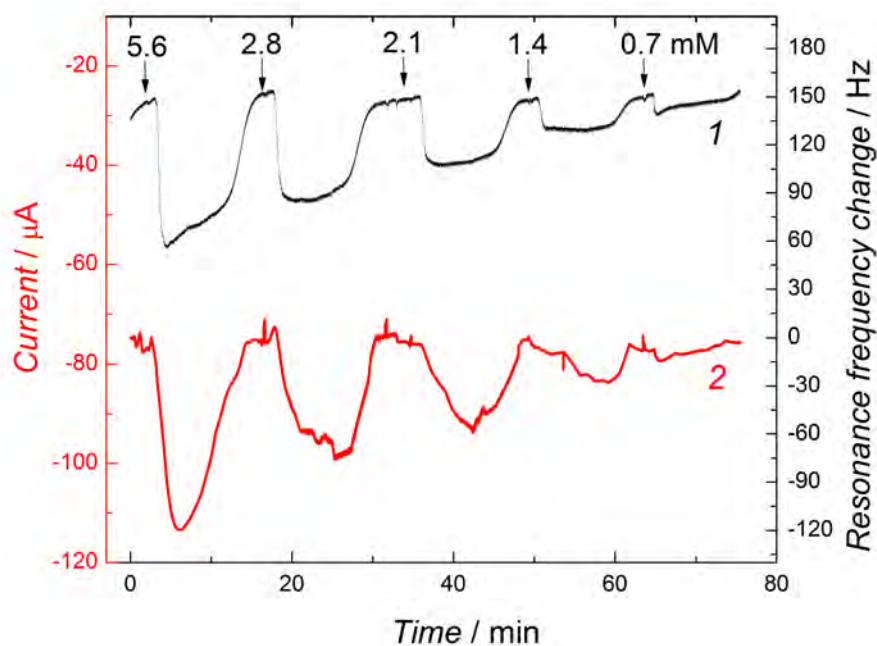
Figure 3.31 The simultaneous change, at -0.80 V vs. Ag/AgCl, of (*1*) cathodic current and (*2*) resonance frequency with time during injection of 0.2 M NaCl in the water : acetonitrile (1 : 1, *v* : *v*) solutions of TNT of different concentrations (final TNT concentrations in solution are indicated with numbers above arrows) under FIA conditions for the TNT-extracted MIP film-coated Au-QCR.

Table 3.10 Detectability (LOD) and selectivity of the MIP chemosensors, determined for the 0.2 M NaCl solutions of water : acetonitrile (1 : 1, *v* : *v*), by injecting the analyte or interference solutions of different concentrations.

Chemosensor	LOD / mM		Selectivity	
	CA	PM	CA	PM
MIP-TNP	0.69	0.02	2.6 (to TNT)	4.8 (to TNT)
MIP-TNT	0.62	0.07	2.1 (to TNP)	3.1 (to TNP)
MIP-TNB	0.29	0.15	2.4 (to TNT)	2.7 (to TNT)
MIP-DNT	—	0.76	—	3.0 (to TNB)

Chapter 4

Conclusions

Eighteen new functional monomers (FMs) were designed and synthesized. One of them, biotinylated bis(2,2'-bithien-5-yl)methane **2**, was electropolymerized under potentiodynamic conditions. The biotin-containing resultant polymer film irreversibly bound neutravidin. This binding enabled preparation of a label-free biosensor for the determination of (nucleobase sequence)-specific HIV oligonucleotide. Detectability of the devised and fabricated herein PM chemosensor for oligonucleotides was lower than that of the impedimetric chemosensor (50 nM and 0.5 pM, respectively). Advantageously, however, the former operated under the flow-injection analysis conditions and in the absence of an electrolyte. Moreover, it was capable of reversible binding of the target oligonucleotide. The PM and EIS biosensors were appreciably selective with respect to mismatched target oligonucleotides. The LOD and linear dynamic concentration range of the herein reported impedimetric chemosensor advantageously compared to other oligonucleotide biosensors using EIS for signal transduction. Our EIS results showed that the resistance of the recognition film changed because of binding of the target oligonucleotide thus indicating that other less sophisticated electrochemical techniques, e.g., differential pulse voltammetry (DPV), could be used for transduction. Moreover, results of the PM experiments proved a significant mass change because of binding of the target oligonucleotide. Hence, other techniques based on the mass change of the surface confined film, e.g., SPR spectroscopy could be applied for the transduction. Justifiably, therefore, it is to claim that the monomer **2** opens a new avenue of biosensor preparation, as the same film preparation procedure can be extended for the preparation of biosensors of different properties. So, the biosensor properties, such as detectability and the linear concentration range, can be tuned to meet particular sensing needs by selection of the most appropriate transduction technique. Moreover, there are many analytes whose determination can be elaborated using the hereby developed procedures since the biotin-avidin chemistry and procedures of biotinylation of different species are well established.

As an illustration of usefulness of the procedure of surface modification with

neutravidin described above an MIP imprinted with myoglobin was prepared utilizing FM **2**. After neutravidin immobilization, the polymer surface was decorated with biotinylated myoglobin. After that, a second polymer layer of FM **10** was deposited by potentiodynamic polymerization yielding an MIP imprinted with myoglobin. After template removal, the MIP was applied to detect myoglobin using EIS as the transduction method. So prepared chemosensor had the linear dynamic concentration range of the chemosensor prepared ranged from 10 to 500 ng/mL. Unfortunately, the second polymerization step was not studied thoroughly enough to get repeatably operating polymer films. Therefore, studies on this chemosensor bear further scrutiny. Nevertheless, this result has proved that the herein developed procedure of surface modification with neutravidin can be extended for the preparation of chemosensors other than those for oligonucleotide detection.

Moreover, quantum-chemical calculations were performed. The results revealed that the **7**, **9**, **10**, **11**, **17**, and **18** FMs were capable of formation of stable complexes with selected analytes, including nitroaromatic explosives, nicotine, carnosine, 6-thioguanine, and serotonin, respectively. Conclusively, these FMs could be used for the preparation of chemosensors utilizing the molecular imprinting technology. For the nitroaromatic explosives, nicotine, and 6-thioguanine, the respective chemosensors have already been prepared proving that calculations used were suitable for prediction of stability of the pre-polymerization complexes of FMs with templates. Presumably, these FMs formed stable complexes also with other compounds featuring recognizing sites similar to those of the already investigated templates. Moreover, other FMs that were not used for calculations might be useful for the preparation of chemosensors for analytes featuring the binding sites compatible to the recognizing sites of molecular cavities of the respective FMs.

Furthermore, a molecularly imprinted polymer (MIP) film for melamine determination was prepared using the previously described procedure. The limit of detection of the PM chemosensor equal to 0.1 mM, determined for pet feed extracts, allowed for the use of this chemosensor for melamine quantification in real feed samples. Moreover, a melamine chemosensor, utilizing SPR spectroscopy as the transduction technique, was prepared. The limit of detection and dynamic linear concentration range of this chemosensor was close to that of the PM chemosensor. Analytical performance of both chemosensors was similar because both transduction techniques were based on the mass change of the surface confined MIP film. For the PM chemosensor, the increase of the film mass resulted in the decrease of the resonant frequency of a quartz crystal resonator. For the SPR chemosensor, electric permittivity of the film changed if the analyte entered the film and, therefore, the angle of the incident polarized light beam causing the resonance of surface plasmons was changed.

Bibliography

[1] Freund, M. S.; Deore, B. A. *Self-doped conducting polymers;* John Wiley and Sons: New Jersey, 2007.

[2] Albery, W. J.; Doblhofer, K.; Lyons, M. E. G.; Mount, A. R.; Vorotyntsev, M. *Electroactive polymer electrochemistry;* Plenum Press: New York, 1994.

[3] Inzelt, G. *Conducting polymers: A new era in electrochemistry;* Springer-Verlag: Berlin, 2012.

[4] Wallace, G. G.; Spinks, G. M.; Kane-Maguire, L. A. P.; Teasdale, P. R. *Conductive electroactive polymers;* CRC Press: Boca Raton, 2009.

[5] Kim, S. H.; Jang, S. H.; Byun, S. W.; Lee, J. Y.; Joo, J. S.; Jeong, S. H.; Park, M. J. *J. Appl. Polym. Sci.* **2003,** *83,* 1969-1974.

[6] Holze, R.; Wu, Y. P. *Electrochim. Acta* **2014,** *122,* 93-107.

[7] Kim, J. G.; Walker, J.; Samuelson, L. A.; J., K. *Nano Lett.* **2003,** *3,* 523-525.

[8] Marmisolle, W. A.; Posadas, D.; Florit, I. M. *Electrochim. Acta* **2013,** *109,* 894-900.

[9] Kwak, K.; Cho, K.; Kim, S. *Appl. Phys. Lett.* **2014,** *104,.*

[10] Hyodo, K. *Electrochim. Acta* **1994,** *39,* 265-272.

[11] Otero, T. F.; Martínez, J. G.; B., Z. *Smart Mater. Struct.* **2013,** *22,* 104019.

[12] Almeida Junior, J. H. S.; Bertuol, D. A.; Meneguzzi, A.; Ferreira, C. A.; Amado, F. D. R. *Mater. Res.* **2013,** *16,* 860-866.

[13] Stolarczyk, A.; Turczyn, R.; Januszkiewicz-Kaleniak, A.; Domagala, W.; Imach, S. *Acta Phys. Pol., A* **2013,** *124,* 563-566.

[14] Wallace, G. G.; Lin, Y. *J. Controlled Release* **1994,** *30,* 137-142.

[15] Spinks, G. M.; Dominis, A. J.; Wallace, G. G.; Tallman, D. E. *J. Solid State Electrochem.* **2002,** *6,* 85-100.

[16] Travas-Sejdic, J.; Aydemir, N.; Kannan, B.; Williams, D. E.; Malmstrom, J. *J. Mater. Chem., B* **2014,** *2*, 4593-4609.

[17] Yoon, H. *Nanomaterials* **2013,** *3*, 524-549.

[18] Lou, B.; Chen, C.; Zhou, Z.; Zhang, L.; Wang, E.; Dong, S. *Talanta* **2013,** *105*, 40-45.

[19] Gholami, M.; Ghasemi, A. B.; Loghavi, M. M.; Behkami, S.; Ahamdi-Dokht-Faraghe, A. *Chem. Pap.* **2013,** *67*, 1079-1086.

[20] Lei, W.; Si, W.; Xu, Y.; Gu, Z.; Hao, Q. *Microchim. Acta* **2014,** *181*, 707-722.

[21] Kesik, M.; Kanik, F. E.; Hizalan, G.; Kozanoglu, D.; Esenturk, M. N.; Timur, D.; Toppare, L. *Polymer* **2013,** *54*, 4463-4471.

[22] Minamiki, T.; Minami, T.; Kurita, R.; Niwa, O.; Wakida, S.; Fukuda, K.; Kumaki, D.; S., T. *Appl. Phys. Lett.* **2014,** *104*, 243703.

[23] Skotheim, T. A., Ed.; *Handbook of conducting polymers;* Marcel Dekker, Inc.: New York, 1986.

[24] Huisman, C. L.; Huijser, A.; Donker, H.; Schoonman, J.; Goossens, A. *Macromolecules* **2004,** *37*, 5557-5564.

[25] Heinze, J.; Frontana-Uribe, A.; Ludwigs, S. *Chem. Rev.* **2010,** *110*, 4724-4771.

[26] Tanaka, K.; Shichiri, T.; Wang, S.; Yamabe, T. *Synth. Met.* **1988,** *24*, 203-215.

[27] Sato, M.; Tanaka, S.; Ama, K. J. *Synth. Met.* **1983,** *87*, 22789.

[28] Yassar, A.; Roncali, J.; Garnier, F. *Macromolecules* **1989,** *22*, 804-809.

[29] Mirkin, C. A.; Caldwell, W. B. *Tetrahedron* **1996,** *52*, 5113-5130.

[30] Chiang, L. Y.; Wang, L. Y. *Fullerenes chemsitry, physics, and technology;* Chapter 7, pp. 331-356, ed. Kadish, K. M. and Ruoff, R. S., John Wiley and Sons: New York, 2000.

[31] Winkler, K.; Balch, A. L.; Kutner, W. *J. Solid State Electrochem.* **2006,** *10*, 761-784.

[32] Yamamoto, H.; Iwata, N. *Trans. Mater. Res. Soc. Japan* **2010,** *35*, 461-466.

http://rcin.org.pl

[33] Zhao, Y. B.; Poirier, D. M.; Pechman, R. J.; Weaver, J. H. *Appl. Phys. Lett.* **1994,** *64*, 577-579.

[34] Ramm, M.; Ata, M.; Gross, T.; Unge, W. *Mater. Phys. Mech.* **2001,** *4*, 8-12.

[35] Meletov, K. P.; Davydov, V. A.; Arvanitidis, J.; Christofilos, D.; Andrikopou-los, K. S.; Kourouklis, G. A. *J. Exp. Theor. Phys.* **2008,** *107*, 620-631.

[36] Chen, Y.; Huang, Z. L.; Cai, R. F.; Yu, B. C. *Eur. Polym. J.* **1998,** *34*, 137-151.

[37] Vinogradova, L. V. *Russ. Chem. Bull.* **2012,** *61*, 907-925.

[38] He, Z.; Ishizuka, T.; Jiang, D. *Polym. J.* **2007,** *39*, 889-922.

[39] Winkler, K.; Balch, A. L. *C. R. Chim.* **2006,** *9*, 928-943.

[40] Sharma, P. S.; Dabrowski, M.; F., D.; Kutner, W. *TrAC Trends Anal. Chem.* **2013,** *51*, 146-157.

[41] Huang, Y. P.; Liu, Z. S.; Zheng, C.; Gao, R. Y. *Electrophoresis* **2009,** *30*, 155-162.

[42] Yang, W. L.; Huang, S. M.; Wu, Q. Z.; He, J. H. *J. Polym. Res.* **2014,** *21*, 383.

[43] Okutucu, B.; Onal, S. *Talanta* **2011,** *87*, 74-79.

[44] Rajkumar, R.; Warsinke, A.; Möhwald, H.; Scheller, F. W.; Katterle, M. *Biosens. Bioelectron.* **2007,** *22*, 3318-3325.

[45] Whitcombe, M. J.; Rodriguez, M. E.; Villar, P.; Vulfson, E. N. *J. Am. Chem. Soc.* **1995,** *117*, 7105-7111.

[46] Hashim, S. N. N. S.; Boysen, R. I.; Schwarz, L. J.; Danylec, B.; Hearn, M. T. W. *J. Chromatogr. A* **2014,** *13590*, 35-43.

[47] Wang, S.; Xu, J.; Tong, Y.; Wang, L.; He, C. *Polym. Int.* **2005,** *54*, 1268-1274.

[48] Rosengren-Holmberg, J. P.; Karlsson, J. G.; Svenson, J.; Andersson, H. S.; Nicholls, I. A. *Org. Biomol. Chem.* **2009,** *7*, 3148-3155.

[49] Dubey, L.; Chianella, I.; Dubey, I.; Piletska, E.; Whitcombe, M. J.; Pilet-sky, S. *Open Anal. Chem. J.* **2012,** *6*, 15-21.

[50] da Silva, M. S.; Viveiros, R.; Aguiar-Ricardo, A.; Bonifacio, V. D. B.; Casimiro, T. *RSC Adv.* **2012,** *2,* 5075-5079.

[51] Qi, P.; Wang, J.; Wang, L.; Li, Y.; Jin, J.; Su, F.; Tian, Y.; Chen, J. *Polymer* **2010,** *51,* 5417-5423.

[52] Ikegami, T.; Lee, W. S.; Nariai, H.; Takeuchi, T. *J. Chromatog. B* **2004,** *804,* 197-201.

[53] Wang, X.; Wang, L.; He, X.; Zhang, Y.; Chen, L. *Talanta* **2009,** *78,* 327-332.

[54] Kandimalla, V. B.; Ju, H. *Anal. Bioanal. Chem.* **2004,** *380,* 587-605.

[55] Huynh, T.-P.; KC, C. B.; Sosnowska, M.; Sobczak, J. W.; Nesterov, V. N.; D'Souza, F.; Kutner, W. *Biosens. Bioelectron.* **2015,** *64,* 657-663.

[56] Noworyta, K.; Kutner, W.; Wijesinghe, C. A.; Srour, S. G.; D'Souza, F. *Anal. Chem.* **2012,** *84,* 2154-2163.

[57] Liu, R.; Guan, G.; Wang, S.; Zhang, Z. *Analyst* **2011,** *136,* 184-190.

[58] Say, R.; Gultekin, A.; Ozcan, A. A.; Denizlid, A.; Ersoz, A. *Anal. Chim. Acta* **2009,** *640,* 82-86.

[59] Puzio, K.; Delepee, R.; Vidal, R.; Agrofoglio, L. A. *Anal. Chim. Acta* **2013,** *790,* 47-55.

[60] Maeda, H. *Bull. Chem. Soc. Jpn.* **2013,** *86,* 1359-1399.

[61] Berlin, A.; Vercelli, B.; Zotti, G. *Polym. Rev.* **2008,** *48,* 493-530.

[62] Huynh, T.-P.; Sharma, P. S.; Sosnowska, M.; D'Souza, F.; Kutner, W., **2014**, submitted.

[63] Boeva, Z. A.; Sergeyev, V. G. *Polym. Sci., C* **2014,** *56,* 144-153.

[64] Ates, M. *Mater. Sci. Eng. C* **2013,** *33,* 1853-1859.

[65] Sharma, P. S.; Pietrzyk-Le, A.; D'Souza, F.; Kutner, W. *Anal. Bioanal. Chem.* **2012,** *402,* 3177-3204.

[66] Qian, T.; Yu, C.; Zhou, X.; Ma, P.; Wu, S.; Xu, L.; Shen, J. *Biosens. Bioelectron.* **2014,** *58,* 237-241.

[67] Lv, Y. K.; Liu, X. H.; Yan, S. L.; Zhang, Y.; Sun, H. W. *J. Porous Mater.* **2013,** *20,* 1345-1352.

[68] Zhang, X.; Peng, Y.; Bai, J.; Ning, B.; Sun, S.; Hong, X.; Liu, Y.; Liu, Y.; Gao, Z. *Sens. Actuators, B* **2014,** *200,* 69-75.

[69] Melo, L. P.; Queiroz, M. E. C. *Anal. Methods* **2013,** *5,* 3538-3545.

[70] Kan, X.; Liu, T.; Li, C.; Zhou, H.; Xing, Z.; Zhu, A. *J. Solid State Electrochem.* **2012,** *16,* 3207-3213.

[71] Ren, Y. M.; Yang, J.; Ma, W. Q.; Ma, J.; Feng, J. amd Liu, X. L. *Water Res.* **2014,** *50,* 90-100.

[72] Vergara, A. V.; Pernites, R. B.; Pascua, S.; Binag, C. A.; Advincula, R. C. *J. Polym. Sci., Part A: Polym. Chem.* **2012,** *50,* 675-685.

[73] Huynh, T.-P.; Pietrzyk-Le, A.; KC, C. B.; Noworyta, K.; Sobczak, J. W.; Sharma, P. S.; D'Souza, F.; Kutner, W. *Biosens. Bioelectron.* **2013,** *41,* 634-641.

[74] Zheng, N.; Li, Y. Z.; Chang, W. B.; Wang, Z. M.; Li, T. J. *Anal. Chim. Acta* **2002,** *452,* 277-283.

[75] Shinde, S.; Bunschoten, A.; Kruijtzer, J. A. W.; Liskamp, R. M. J.; B., S. *Angew. Chem., Int. Ed.* **2012,** *51,* 8326-8329.

[76] Huynh, T.-P.; Wojnarowicz, A.; Sosnowska, M.; Srebnik, S.; Benincori, T.; Sannicolo, F.; D'Souza, F.; Kutner, W., **2014,** submitted.

[77] Wu, S.; Tan, L.; Wang, G.; Peng, G.; Kang, C.; Tang, Y. *J. Chromatogr. A* **2013,** *1285,* 124-131.

[78] Diltemiz, S. E.; Hur, D.; Ersoz, A.; Denizli, A.; Say, R. *Biosens. Bioelectron.* **2009,** *25,* 599-603.

[79] Gultekin, A.; Ersoz, A.; Sariozlu, N. Y.; Denizli, A.; Say, R. *J. Nanopart. Res.* **2010,** *12,* 2069-2079.

[80] Singh, L. K.; Singh, M.; Singh, M. *Mater. Sci. Eng., C* **2014,** *45,* 383-394.

[81] Singh, M.; Tarannum, N.; Kumar, A. *J. Porous Mater.* **2014,** *21,* 677-684.

[82] Luo, X.; Dong, R.; Luo, S.; Zhan, Y.; Tu, X.; Yang, L. *J. Appl. Polym. Sci.* **2013,** *127,* 2284-2890.

[83] Pietrzyk, A.; Kutner, W.; Chitta, R.; Zandler, M. E.; D'Souza, F.; Sannicolo, F.; Mussini, P. R. *Anal. Chem.* **2009,** *81,* 10061-10070.

[84] Wu, B. amd Wang, Z.; Zhao, D.; Lu, X. *Talanta* **2012,** *101,* 374-381.

[85] Pan, S. D.; Shen, H. Y.; Zhou, L. X.; Chen, X. H.; Zhao, Y. G.; Cai, M. Q.and Jin, M. C. *J. Mater. Chem., A* **2014,** *2,* 15345-15356.

[86] Rourke, P. J. "Graphene oxide's solubility disappears in the wash", Press release 23, University of Warwick, Coventry, United Kingdom, 8 March 2011.

[87] Bajwa, S. Z.; Dumler, R.; Lieberzeit, P. A. *Sens. Actuators, B* **2014,** *192,* 522-528.

[88] Warwick, C.; Guerreiro, A.; Gomez-Caballero, A.; Wood, E.; Kitson, J.; Robinson, J.; Soares, A. *Biosens. Bioelectron.* **2014,** *52,* 173-179.

[89] Roy, E.; Maity, S. K.; Patra, S.; Madhuri, R.; Sharma, P. K. *RSC Adv.* **2014,** *4,* 32881-32893.

[90] Lu, C. H.; Zhang, Y.; Tang, S. F.; Fang, Z. B.; Yang, H. H.; Chen, X.; Chen, G. N. *Biosens. Bioelectron.* **2012,** *31,* 439-444.

[91] Dechtrirat, D.; Gajovic-Eichelmann, N.; Bier, F. F.; Scheller, F. W. *Adv. Funct. Mater.* **2014,** *24,* 2233-2239.

[92] Deng, Q.; Wu, J.; Zhai, X.; Fang, G.; Wang, S. *Sensors* **2013,** *13,* 12994-13004.

[93] El-Sharif, H. F.; Aizawa, H.; Reddy, S. M. *Sens. Actuators, B* **2015,** *206,* 239-245.

[94] Inoue, Y.; Kuwahara, A.; Ohmori, K.; Sunayama, H.; Ooya, T.; Takeuchi, T. *Biosens. Bioelectron.* **2013,** *48,* 113-119.

[95] Whitcombe, M. J.; Chianella, I.; Larcombe, L.; Piletsky, S. A.; Noble, J.; Porter, R.; Horgan, A. *Chem. Soc. Rev.* **2011,** *40,* 1547-1571.

[96] Nelson, D. L.; Cox, M. M. *Lehninger principles of biochemistry;* W. H. Freeman and Company: New York, 2008.

[97] Southern, E. *J. Mol. Biol.* **1975,** *98,* 503-517.

[98] Schena, M.; Heller, R. A.; Theriault, T. P.; Konrad, K.; Lachenmeier, E.; Ronald, W. D. *Trends Biotechnol.* **1998,** *16,* 301-306.

[99] Peng, H.; Zhang, L.; Soeller, C.; Travas-Sejdic, J. *Biomaterials* **2009,** *30,* 2132-2148.

[100] Ferguson, B. S.; Buchsbaum, S. F.; Wu, T.-T.; Hsieh, K.; Xiao, Y.; Sun, R.; Soh, H. T. *J. Am. Chem. Soc.* **2011,** *133,* 9129-9135.

[101] Hassen, W. M.; Chaia, C.; Abdelghani, A.; Bessueille, F.; Leonard, D.; Jaffrezic-Renault, N. *Sens. Actuators, B* **2008,** *134,* 755-760.

[102] Nowicka, A. M.; Kowalczyk, A.; Stojek, Z.; Hepel, M. *Biophys. Chem.* **2010,** *146,* 42-53.

[103] Palchetti, I.; Mascini, M. *Anal. Bioanal. Chem.* **2008,** *391,* 455-471.

[104] Carey, L.; Mitnik, L. *Electrophoresis* **2002,** *23,* 1386-1397.

[105] Indrawattana, N.; Promptmas, C.; Wat-Aksorn, K.; Soontornchai, S. *Anal. Methods* **2014,** *6,* 7634-7639.

[106] Zhang, Z.; Sharon, E.; Freeman, R.; Liu, X.; Willner, I. *Anal. Chem.* **2012,** *84,* 4789-4797.

[107] Wang, Q.; Wang, W.; Lei, J.; Xu, N.; Gao, F.; Ju, H. *Anal. Chem.* **2013,** *85,* 12182-12188.

[108] Holthausen, D.; Vasani, R. B.; McInnes, S. J. P.; Ellis, A. V.; Voelcker, N. H. *ACS Macro Lett.* **2012,** *1,* 919-921.

[109] Mukhopadhyay, R.; Lorentzen, M.; Kjems, J.; Besenbacher, F. *Langmuir* **2005,** *21,* 8400-8408.

[110] Dupont-Filliard, A.; Billon, M.; Livache, T.; Guillerez, S. *Anal. Chim. Acta* **2004,** *515,* 271-277.

[111] Liu, T.; Tang, J.; Han, M.; Jiang, L. *Biochem. Biophys. Res. Commun.* **2003,** *304,* 98-100.

[112] Liu, J.; Yuan, X.; Gao, Q.; Qi, H.; Zhang, C. *Sens. Actuators, B* **2012,** *162,* 384-390.

[113] Shiddiky, M. J. A.; Torriero, A. A. J.; Zeng, Z.; Spiccia, L.; Bond, A. M. *J. Am. Chem. Soc.* **2010,** *132,* 10053-10063.

[114] Liu, M.; Luob, C.; Peng, H. *Talanta* **2012,** *88,* 216-221.

[115] Zhang, L.; Sun, H.; Li, D.; Song, S.; Fan, C.; Wang, S. *Macromol. Rapid Commun.* **2008,** *29,* 1489-1494.

[116] Yin, B.-C.; Guanz, Y.-M.; Ye, B.-C. *Chem. Commun.* **2012,** *48,* 4208-4210.

[117] Wang, M.; Gong, W.; Meng, Q.; Zhang, Y. *Russ. J. Electrochem.* **2011,** *47,* 1464-1470.

[118] Kowalczyk, A.; Nowicka, A. M.; Jurczakowski, R.; Fau, M.; Krolikowska, A.; Stojek, Z. *Biosens. Bioelectron.* **2011,** *26*, 2506-2512.

[119] Booth, M. A.; Harbison, S. A.; Travas-Sejdic, J. *Biosens. Bioelectron.* **2011,** *28*, 362-367.

[120] Xu, Y.; Ye, X.; Yang, L.; He, P.; Fang, Y. *Electroanalysis* **2006,** *18*, 1471-1478.

[121] Wang, W.; Yuan, X.; Zhang, W.; Gao, Q.; Qi, H.; Zhang, C. *Electrochim. Acta* **2012,** *78*, 377-383.

[122] Kochman, A.; Krupka, A.; Grissbach, J.; Kutner, W.; Gniewinska, B.; Nafalski, L. *Electroanalysis* **2006,** *18*, 2168-2173.

[123] Koh, W.; Kutner, W.; Jones, M. T.; Kadish, K. M. *Electroanalysis* **1993,** *5*, 209-214.

[124] Buck, R. P.; Lindner, E.; Kutner, W.; Inzelt, G. *Pure Appl. Chem.* **2004,** *76*, 1139-1160.

[125] Frisch, M. J.; et al. Gaussian 09, Gaussian, Inc.: Wallingford CT, 2009.

[126] Cyganski, A. *Podstawy metod elektroanalitycznych;* Wydawnictwa Naukowo Techniczne: Warszawa, 1999.

[127] Galus, Z. *Fundamentals of electrochemical analysis;* Polish Scientific Publishers PWN: Warsaw, 1994.

[128] Orazem, M. E.; Tribollet, B. *Electrochemical impedance spectroscopy;* John Wiley and Sons: New Jersey, 2008.

[129] Lasia, A. "Introduction to electroanalytical methods", Lecture course, Institute of Physcial Chemistry, Polish Academy of Sciences, Warsaw, Poland, 2011.

[130] Bard, A. J.; Faulkner, L. R. *Electrochemical methods: Fundamentals and applications. 2nd ed.;* John Wiley and Sons: New York, 2000.

[131] Lasia, A. in, *Modern aspects of electrochemistry;* Vol. 43 Springer-Verlag: New York, 2009.

[132] Sauerbrey, G. *Zeit. Phys.* **1959,** *155*, 206-222.

[133] Binnig, G. K.; Quate, C. F. *Phys. Rev. Lett.* **1986,** *56*, 930-933.

[134] Nakayam, K. *Rev. Laser Eng.* **1991,** *19*, 147-158.

[135] Binnig, G. K. *Phys. Scr.* **1987,** *T19,* 53-54.

[136] Homola, J.; Yee, S. S.; Gauglitz, G. *Sens. Actuators, B* **1999,** *54,* 3-15.

[137] Davies, J. *Surface analytical techniques for probing biomaterial processes;* CRC Press: Boca Raton, 1996.

[138] Nuster, R.; Paltauf, G.; Burgholzer, P. *Opt. Express* **2007,** *15,* 6087-6095.

[139] Kolomenskii, A. A.; Gershon, P. D.; Schuessler, H. A. *Appl. Opt.* **1997,** *36,* 6539-6547.

[140] Cowie, J.; Love, C. *Polymer* **2001,** *42,* 4783-4789.

[141] Sosnowska, M.; Pieta, P.; Sharma, P.; Chitta, R.; KC, C.; Bandi, V.; D'Souza, F.; Kutner, W. *Anal. Chem.* **2013,** *85,* 7454-7461.

[142] Huynh, T.-P.; Sosnowska, M.; Sobczak, J.; KC, C. B.; Nesterov, V.; D'Souza, F.; Kutner, W. *Anal. Chem.* **2013,** *85,* 8361-8368.

[143] Huynh, T-P., *Bis(2,2'-bithienyl)methane-derived functional monomers: from molecular recogntion to sensing applications*, PhD thesis, Institute of Physical Chemistry, Polish Academy of Sciences, Warsaw, Poland, 2014.

[144] Bartold, K.; Pietrzyk-Le, A.; Huynh, T.-P.; Iskierko, Z.; Noworyta, K.; Sosnowska, M.; Lisowski, W.; Kutner, W.; Sannicolo, F.; Mussini, P. R. "Nowa sonda DNA zawierajaca pochodne tiofenu i sposob jej wytwarzania, warstwa przewodzacego polimeru wdrukowywanego molekularnie z zastosowaniem tych pochodnych i sposob jej wytwarzenia oraz zastosowanie tej sondy do selektywnego wykrywania i oznaczania oligonukleotydu TATAAA", Polish Pat. Appl. No. 409328, 29 Aug. 2014.

[145] Iskierko, Z.; Sosnowska, M.; Sharma, P. S.; D'Souza, F.; Benincori, T.; Noworyta, K. "Pochodne tiofenu i sposob ich otrzymywania, warstwa rozpoznajacego polimeru przewodzacego wytworzonego metoda wdrukowywania molekularnego z zastosowaniem pochodnych tiofenu, sposob jej otrzymywania, jak rowniez jej zastosowanie do selektywnego wykrywania i oznaczania inozyny", Polish Pat. Appl. No. 408507, 11 Jun. 2014.

[146] Wojnarowicz, A.; Sharma, P. S.; Sosnowska, M.; D'Souza, F.; Kutner, W. "Nowy przewodzacy bisbitiofenowy polimer molekularnie wdrukowany za pomoca karnozyny i sposob jego przygotowania oraz zastosowanie do selektywnego wykrywania i oznacznia karnozyny", Polish Pat. Appl. No. 409325, 29 Aug. 2014.

[147] Sharma, P. S.; Dabrowski, M.; Noworyta, K.; Huynh, T.-P.; KC, C. B.; Sobczak, J. W.; Pieta, P.; D'Souza, F.; Kutner, W. *Anal. Chim. Acta* **2014,** .

[148] Marczak, R.; Hoang, V.; Noworyta, K.; Zandler, M.; Kutner, W.; D'Souza, F. *J. Mater. Chem.* **2002,** *12,* 2123-2129.

[149] Pietrzyk, A.; Suriyanarayanan, S.; Kutner, W.; Chitta, R.; D'Souza, F. *Anal. Chem.* **2009,** *81,* 2633-2643.

[150] Chitta, R., *Studies on self-assembled porphyrin-fullerene and porphyrin-carbon nanotube donor-acceptor conjugates*, PhD thesis, Wichita State University, Wichita, TX, USA, 2007.

[151] Kryatova, O.; Kaklinski, A.; Rybak-Ahimov, E. *Tetrahedron* **2003,** *59,* 231.

[152] Prato, M.; Maggini, M.; Giacometti, C.; Scorrano, G.; Sandonh, G.; Farnia, G. *Tetrahedron* **1996,** *52,* 5221-5234.

[153] Kay, B. K.; Thai, S.; Volgina, V. V. *Methods Mol. Biol.* **2009,** *498,* 185-196.

[154] Pieta, P.; Zukowska, G. Z.; Das, S. K.; D'Souza, F.; Petr, A.; Dunsch, L.; Kutner, W. *J. Phys. Chem. C* **2010,** *114,* 8150-8160.

[155] Pieta, P.; Obraztsov, I.; Sobczak, J. W.; Chernyayeva, O.; Das, S. K.; D'Souza, F.; Kutner, W. *J. Phys. Chem. C* **2013,** *117,* 1995-2007.

[156] Cragg, P. J.; Vahora, R. *Supramolecular chemistry: from molecules to nanomaterials;* pp. 733-752, ed. Gale, P. and Steed, J., John Wiley and Sons: New York, 2012.

[157] Baldini, L.; Sansone, F.; Casnati, A.; Ungaro, R. *Supramolecular chemistry: from molecules to nanomaterials;* 863-894, ed. Gale, P. and Steed, J., John Wiley and Sons: New York, 2012.

[158] Terada, Y.; Hashimoto, W.; Endo, T.; Seto, H.; Murakami, T.; Hisamoto, H.; Hoshino, Y.; Miura, Y. *J. Mater. Chem., B* **2014,** *2,* 3324-3332.

[159] Tanaka, M.; Yoshioka, K.; Hirata, Y.; Fujimaki, M.; Kuwahara, M.; Niwa, O. *Langmuir* **2013,** *29,* 13111-13120.

[160] Wang, X.; Zhang, X.; Gao, C.; Liao, X.; Hang, L.; Jiang, S.; Gao, F.; Huang, L.; Wang, Q. *Int. J. Electrochem. Sci.* **2013,** *8,* 7529-7541.

[161] Fontana, M.; Pinnen, F.; Lucente, G.; Pecci, L. *Cell. Mol. Life Sci.* **2002,** *59,* 546-551.

[162] Alhamdani, M.-S. S.; Al-Azzawie, H. F.; Abbas, F. K. H. *Perit. Dial. Int.* **2007,** *27,* 86-91.

[163] Price, D. L.; Rhett, P. M. andThorpe, S. R.; Baynes, J. W. *J. Biol. Chem.* **2001,** *276,* 48967-48972.

[164] Zieba, R. *Wiad. Lek.* **2007,** *60,* 73.

[165] Zschocke, J.; Nebel, A.; Wicks, K.; Peters, V.; El Mokhtari, N. E.; Krawczak, M.; van der Woude, F.; Janssen, B.; Schreiber, S. *Mech. Ageing Dev.* **2006,** *127,* 817-820.

[166] Willi, S. M.; Zhang, Y.; Hill, J. B.; Phelan, M. C.; Michaelis, R. C.; Holden, K. R. *Pediatr. Res.* **1997,** *41,* 210-213.

[167] Brox, L. W.; Birkett, W.; Belch, A. *Cancer Chemother. Pharmacol.* **1981,** *6,* 35-38.

[168] Moore, E. C.; LePage, G. A. *Cancer Res.* **1958,** *18,* 1075-1083.

[169] Vora, A.; Mitchell, C.; Lennard, L.; Eden, T.; Kinsey, S.; Lilleyman, J.; Richards, S. *Lancet* **2006,** *368,* 1339-1348.

[170] Watson, J. D.; Crick, F. H. C. *Nature* **1953,** *171,* 737-738.

[171] Webster, R. A., Ed.; *Neurotransmitters, drugs and brain function;* John Wiley and Sons: New York, 2011.

[172] Song, M. J.; Kim, S.; Min, N. K.; Jin, J.-H. *Biosens. Bioelectron.* **2014,** *52,* 411-416.

[173] Filik, H.; Avan, A. A.; Ayda, S. *Int. J. Electrochem. Sci.* **2014,** *9,* 2922-2933.

[174] Lee, D. J.; Robinson, W. E. *Antimicrob. Agents Chemother.* **2006,** *50,* 134-142.

[175] Hiller, Y.; Gershoni, J. M.; Bayer, E. A.; Wilchek, M. *Biochem. J.* **1987,** *248,* 167-171.

[176] Wojciechowski, M.; Sundseth, R.; Moreno, M.; Henkens, R. *Clin. Chem.* **1999,** *45,* 1690-1693.

[177] Huynh, T.-P.; KC, C. B.; Lisowski, W.; D'Souza, F.; Kutner, W. *Bioelectrochemistry* **2013,** *93,* 37-45.

[178] Levie, R. D. *Electrochim. Acta* **1965,** *10,* 113-130.

[179] Goldman, L.; Schafer, A. I. *Goldman's Cecil medicin;* Saunders Elsevier: Philadelphia, 2012.

[180] Cocchi, M.; Vascellari, M.; Gallina, A.; Angeletti, R.; Mutinelli, F. *J. Vet. Med. Sci.* **2010,** *72,* 103-107.

[181] Shen, J. S.; Wang, J. Q.; Wei, H. Y.; Bu, D. P.; Sun, P.; Zho, L. Y. *J. Dairy Sci.* **2010,** *93,* 2060-2066.

[182] Gao, C.-Q.; Wu, S.-G.; Yue, H.-Y.; Ji, F.; Zhang, H.-J.; Liu, Q.-S.; Fan, Z.-Y.; Liu, F.-Z.; Qi, G.-H. *J. Agric. Food Chem.* **2010,** *58,* 5199-5205.

[183] Stine, C. B.; Reimschuessel, R.; Gieseker, C. M.; Evans, E. R.; Mayer, T. D.; Hasbrouck, N. R.; Tall, E.; Boehmer, J.; da Costa, G. G.; Ward, J. L. *Regul. Toxicol. Pharmacol.* **2011,** *60,* 363-372.

[184] Pernites, R.; Ponnapati, R.; Felipe, M. J.; Advincula, R. *Biosens. Bioelectron.* **2011,** *26,* 2766-2771.

[185] Lautner, G.; Kaev, J.; Reut, J.; Öpik, A.; Rappich, J.; Syritsk, V.; Gyurcsányi, R. E. *Adv. Funct. Mater.* **2011,** *21,* 591-597.

[186] Crescenzo, G.; Boucher, C.; Duroucher, Y.; Jolicoeur, M. *Cell. Mol. Bioeng.* **2008,** *1,* 204-215.

[187] Garcia-Calzon, J. A.; Diaz-Garcia, M. E. *Sens. Actuators, B* **2007,** *123,* 1180-1194.

[188] Chapman, R. P.; Averell, P. R.; Harris, R. R. *Ind. Eng. Chem.* **1943,** *35,* 137-138.

Appendix

A. The NMR and MS spectra
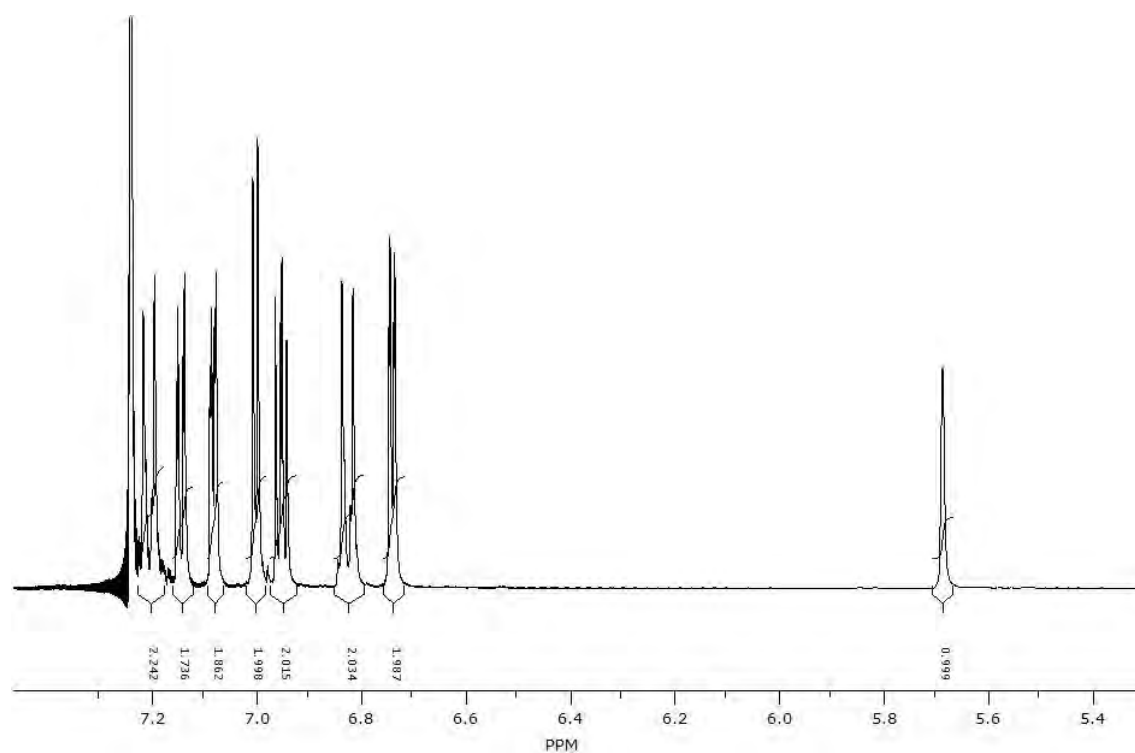
Figure A.1 The ^{1}H NMR spectrum of 4-bis-2,2'-bithiophen-5-yl)methylphenol **1** in deuterated chloroform.
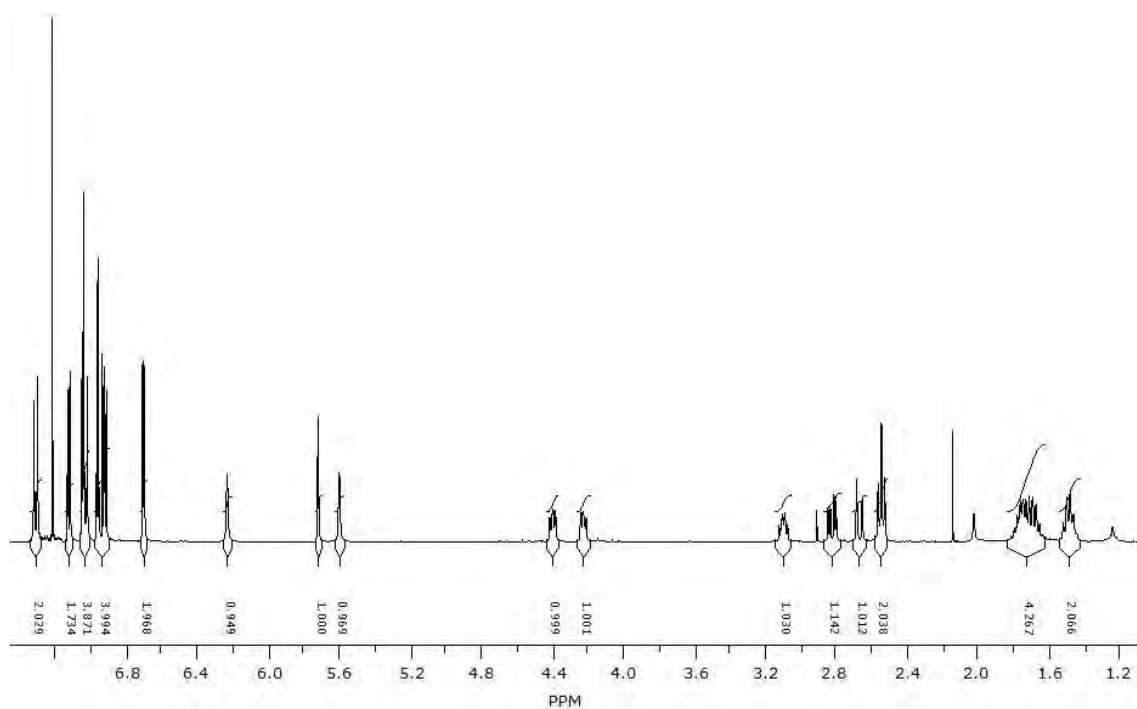
Figure A.2 The ^{1}H NMR spectrum of 4-bis(2,2'-bithien-5-yl)methylphenol biotin ester **2** in deuterated chloroform.
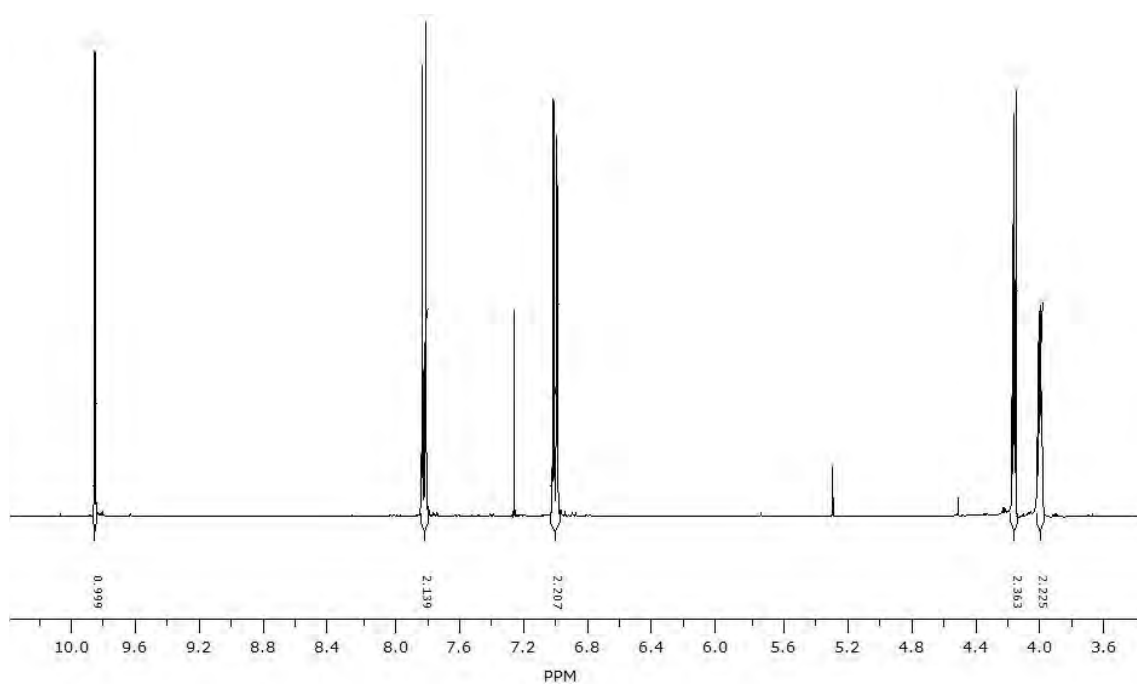
Figure A.3 The ^{1}H NMR spectrum of 4-(2-hydroxyethoxy)benzaldehyde **3a** in deuterated chloroform.
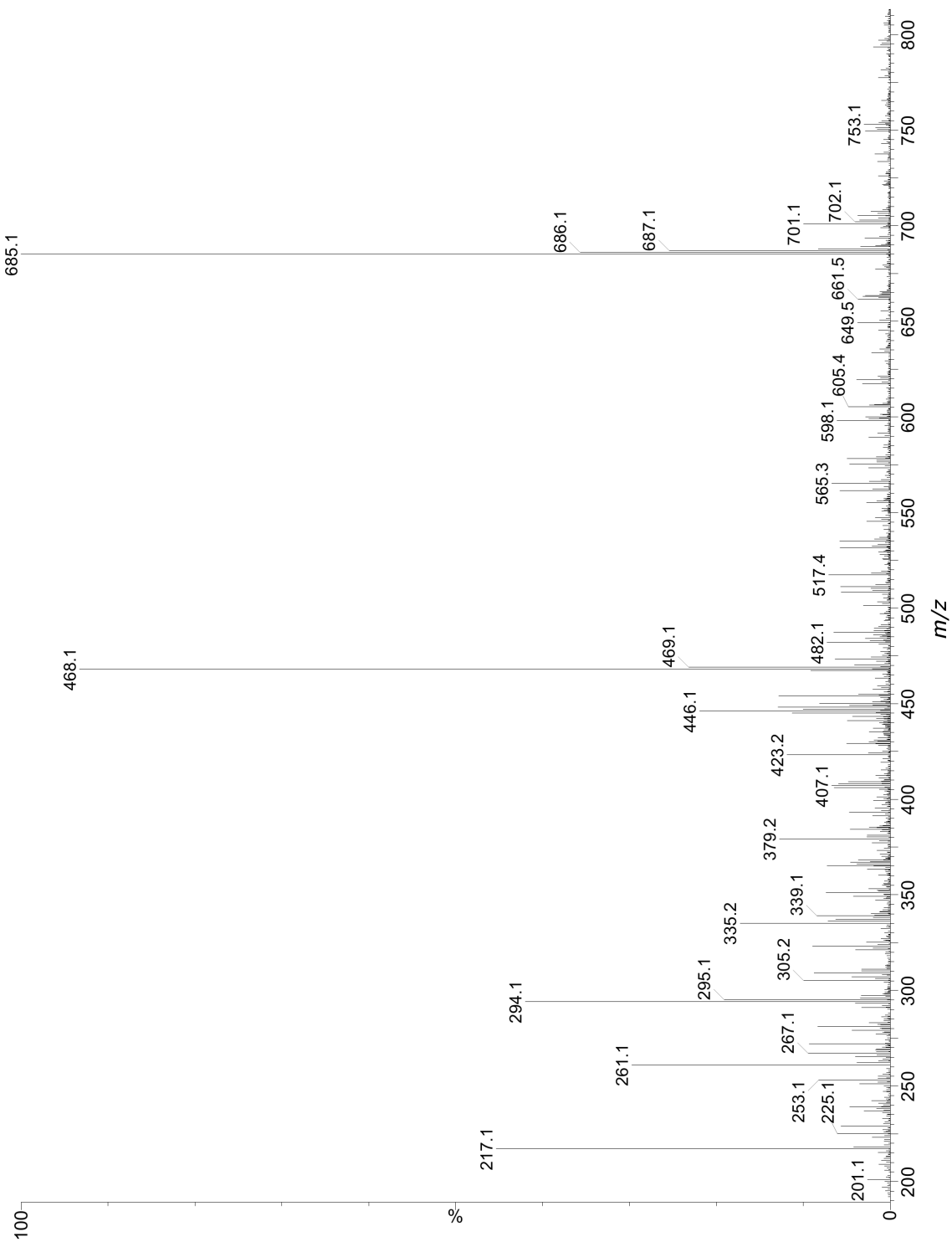
Figure A.4 The ESI(-)-MS spectrum of 4-bis(2,2'-bithien-5-yl)methylphenol biotin ester **2**.
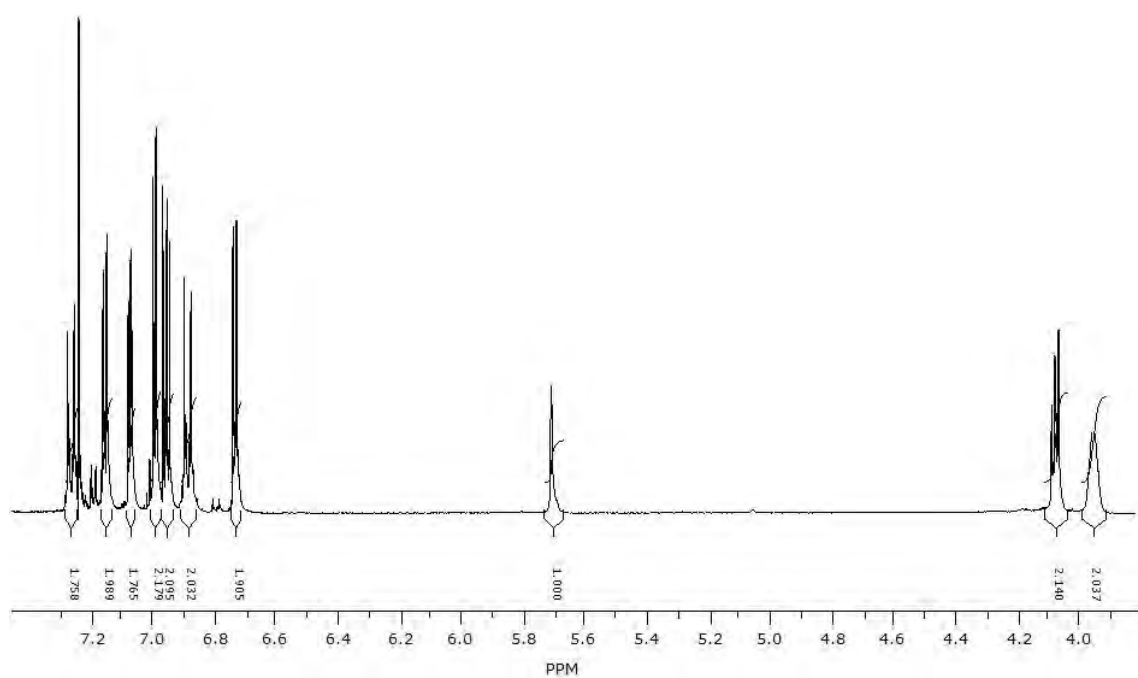
Figure A.5 The ^{1}H NMR spectrum of 4-bis(2,2'-bithien-5-yl)methylphenol glycol ether **3** in deuterated chloroform.
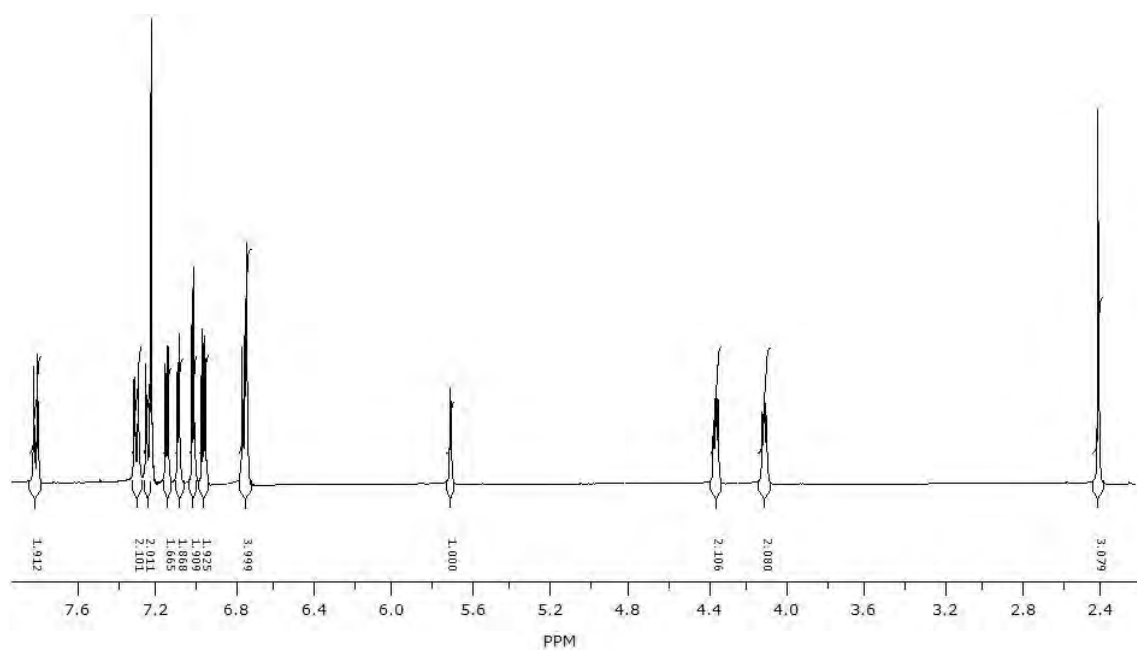
Figure A.6 The ^{1}H NMR spectrum of 4-bis(2,2'-bithienyl)-(4-[2-tosyl]ethoxy) methane **4a** in deuterated chloroform.
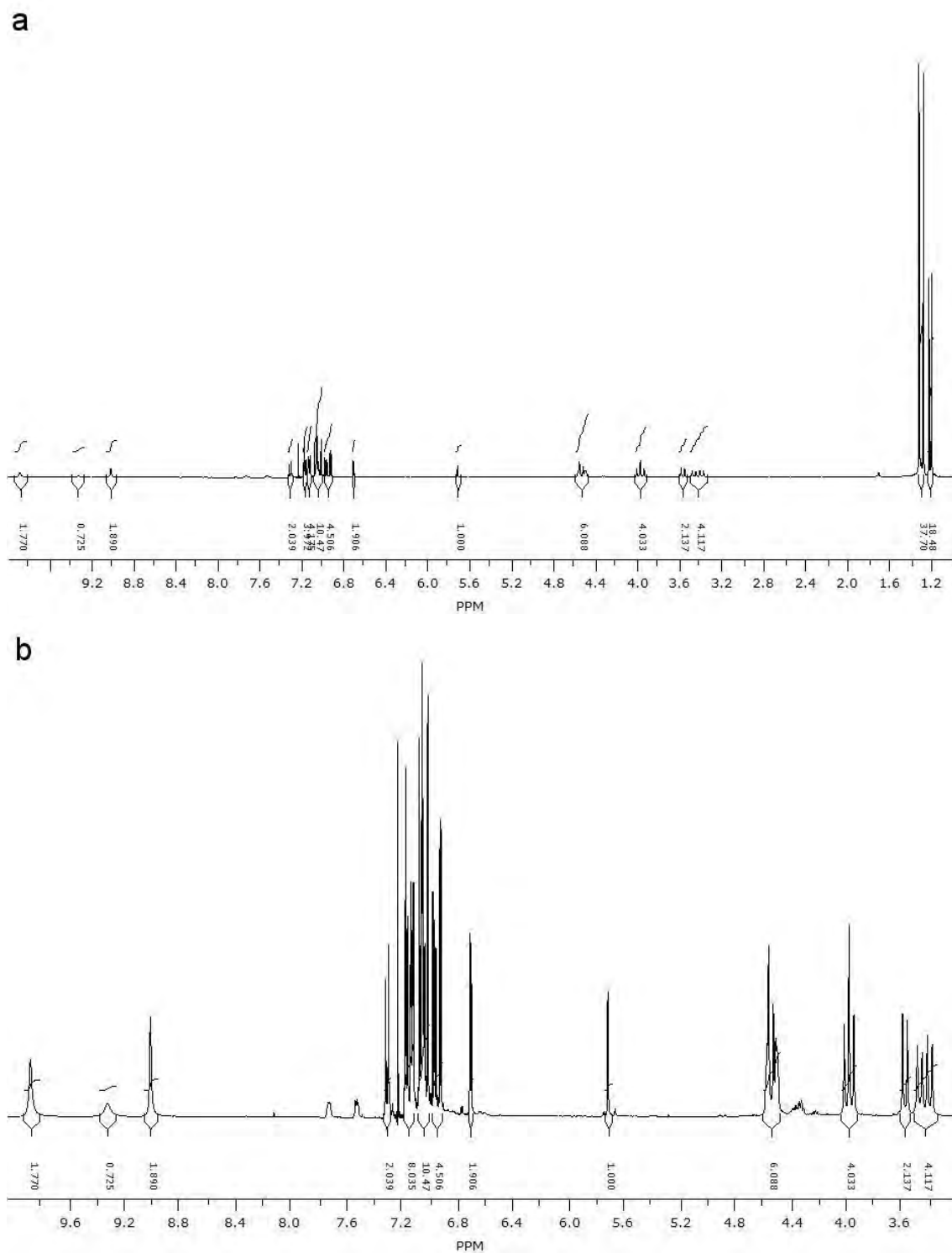
Figure A.7 The ^{1}H NMR spectrum of 4-bis(2,2'-bithien-5-yl)methylphenol 2-*O*-(4-tertbutylcalix[6]arene) ethoxyl ether **4** in deuterated chloroform in the range of (a) 1.0 to 10.0 and (b) 3.2 to 10.0 ppm.
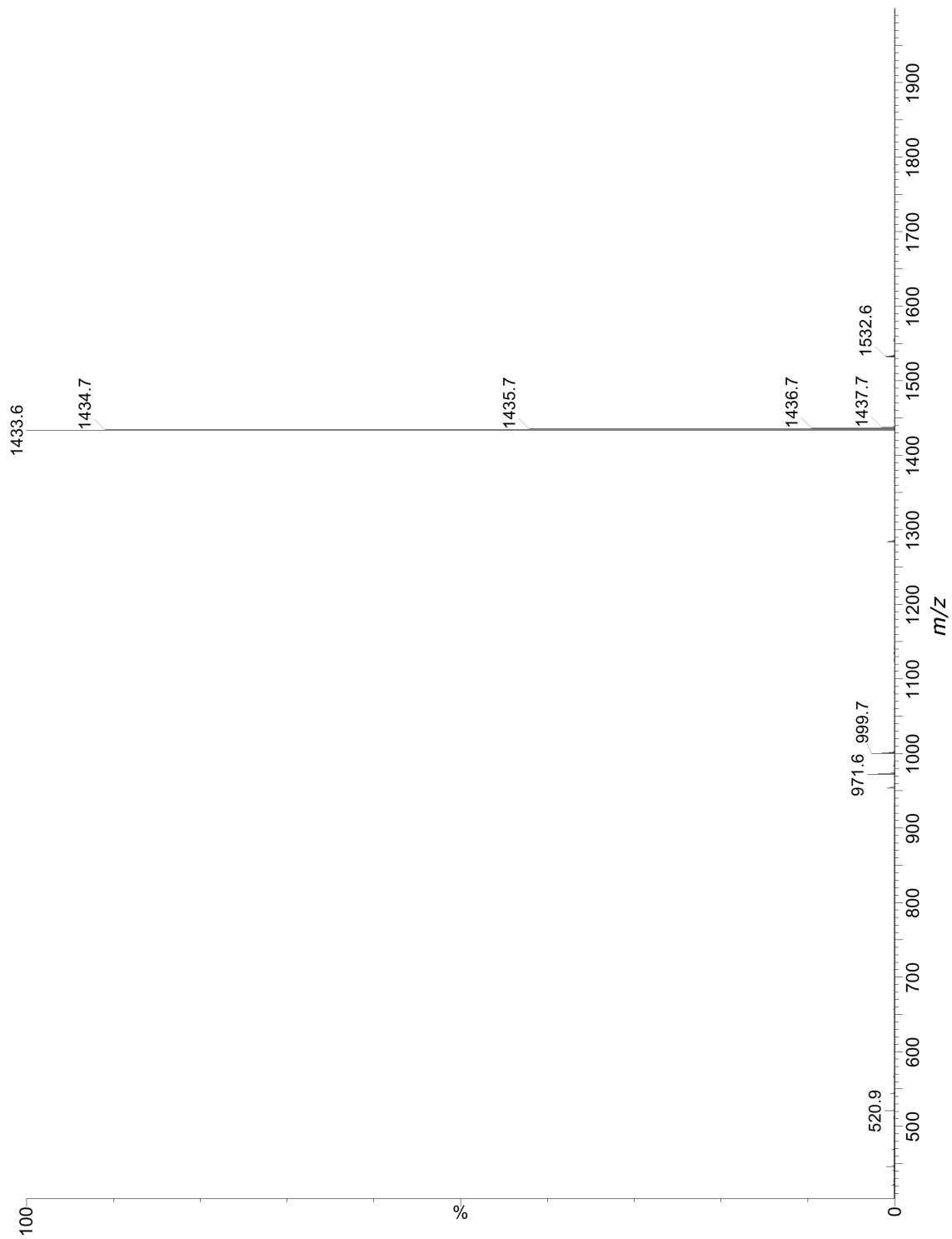
Figure A.8 The ESI(-)-MS spectrum of 4-bis(2,2'-bithien-5-yl)methylphenol 2-*O*-(4-tertbutylcalix[6]arene) ethoxyl ether **4.**
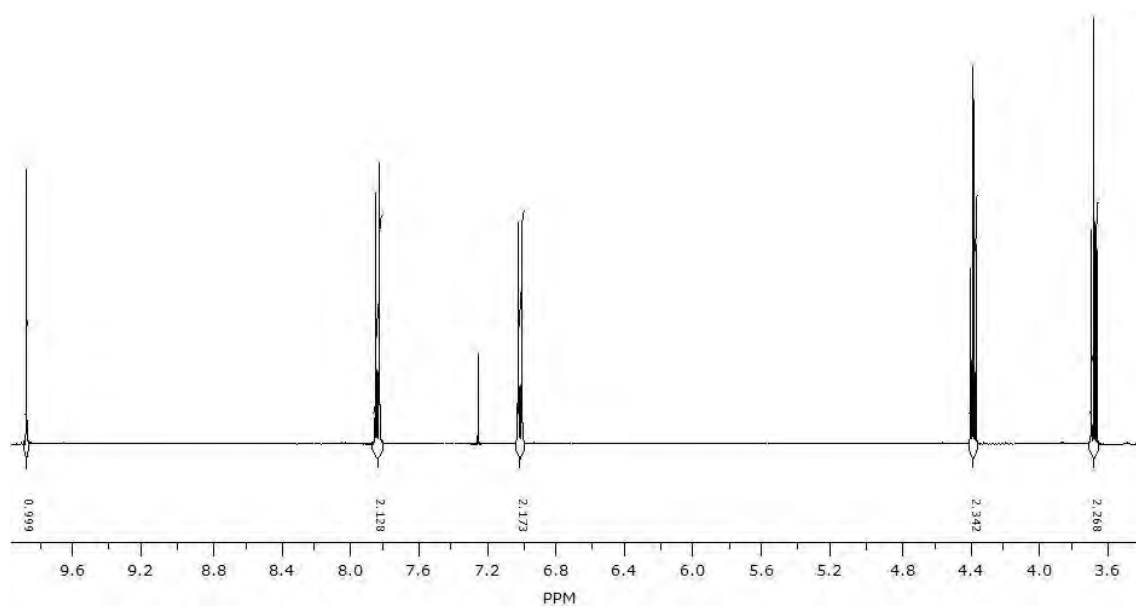
Figure A.9 The ¹H NMR spectrum of 4-(2-bromoethoxy)benzaldehyde **5a** in deuterated chloroform.
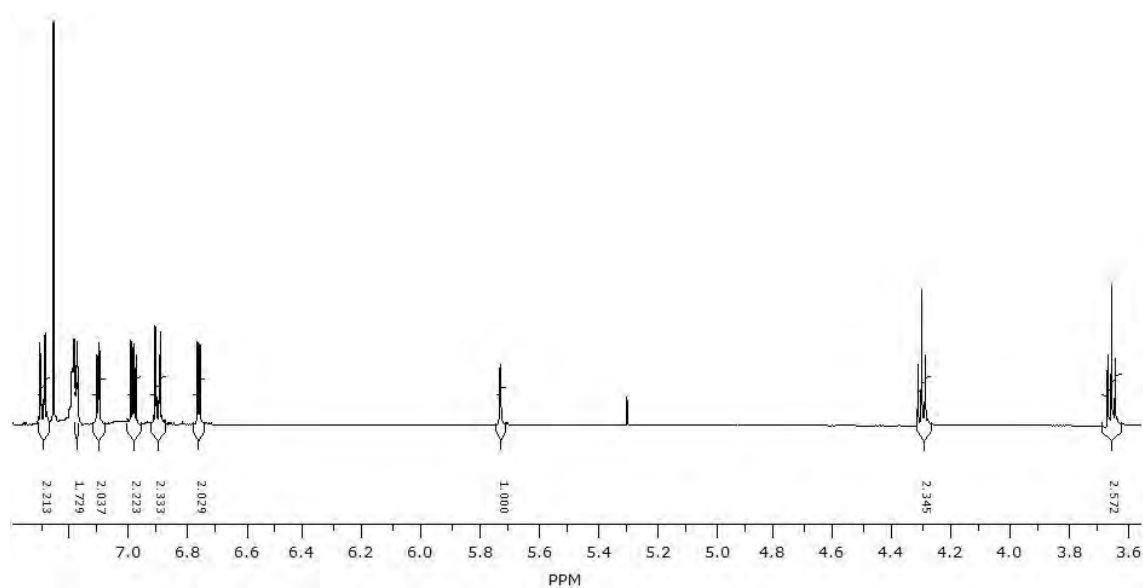
Figure A.10 The ¹H NMR spectrum of 4-bis(2,2'-bithien-5-yl)methylphenol 2-bromoethyl ether **5** in deuterated chloroform.
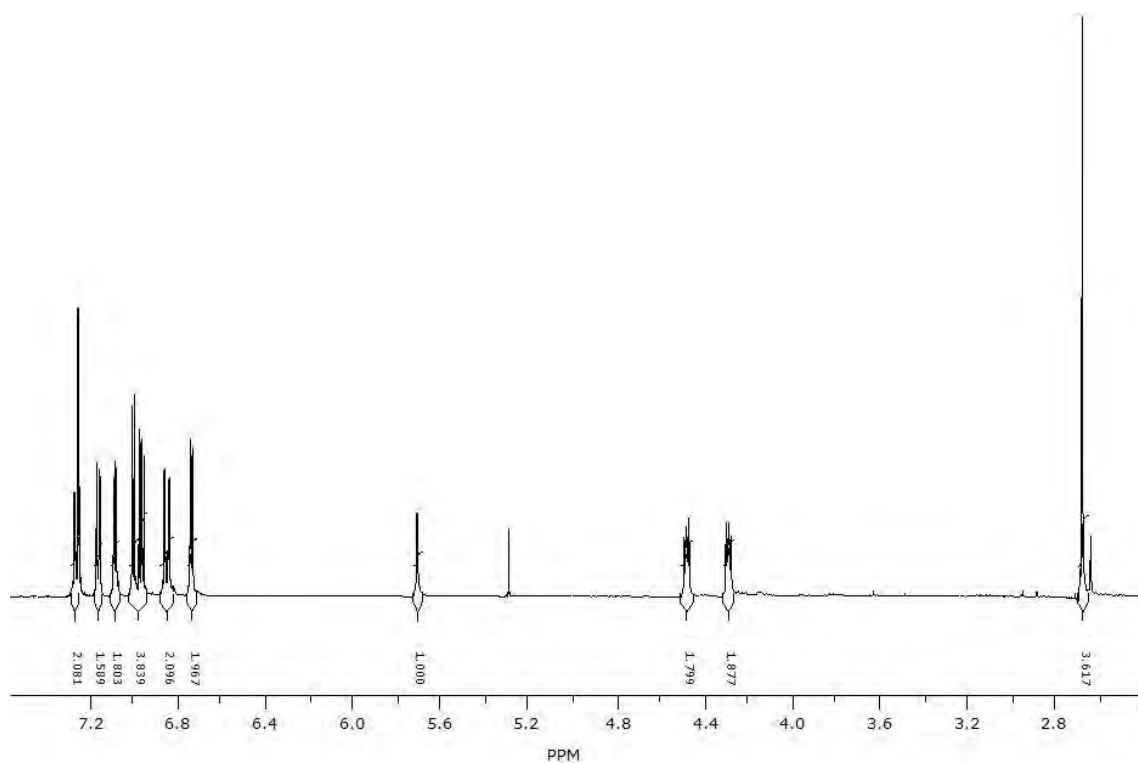
Figure A.11 The ^{1}H NMR spectrum of 4-bis(2,2'-bithien-5-yl)methylphenol 2-(1-N-succinimidoxy)ethyl ether **6** in deuterated chloroform.
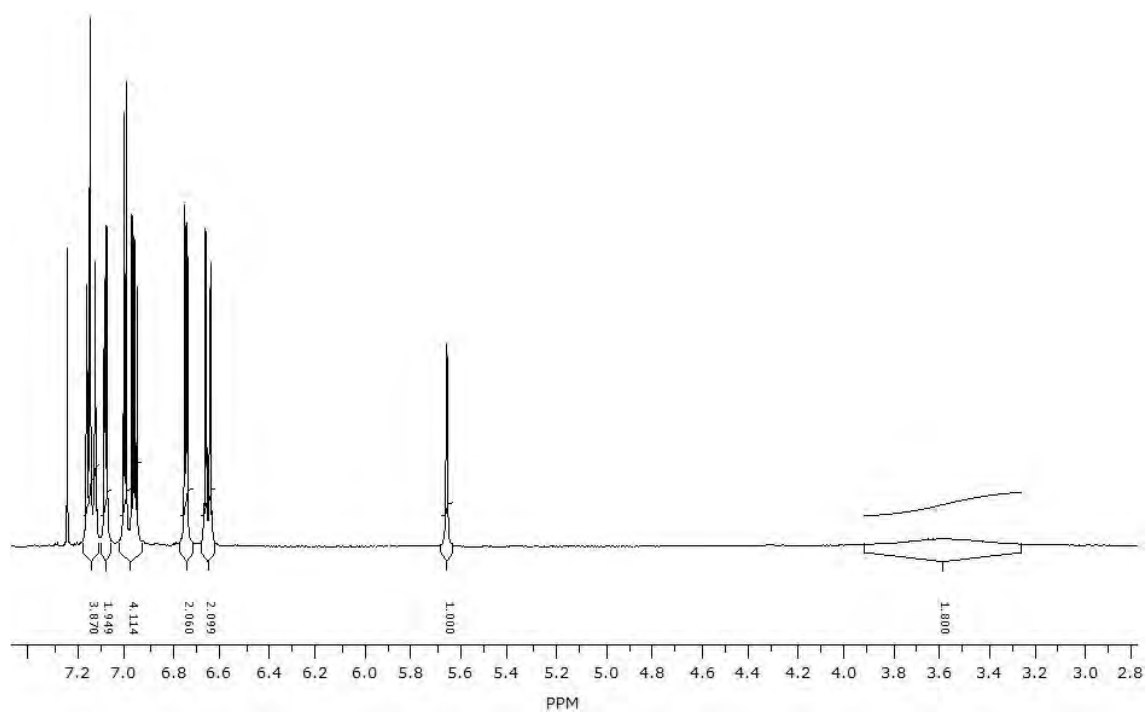
Figure A.12 The ^{1}H NMR spectrum of 4-bis(2,2'-bithien-5-yl)methylalanine **7** in deuterated chloroform.
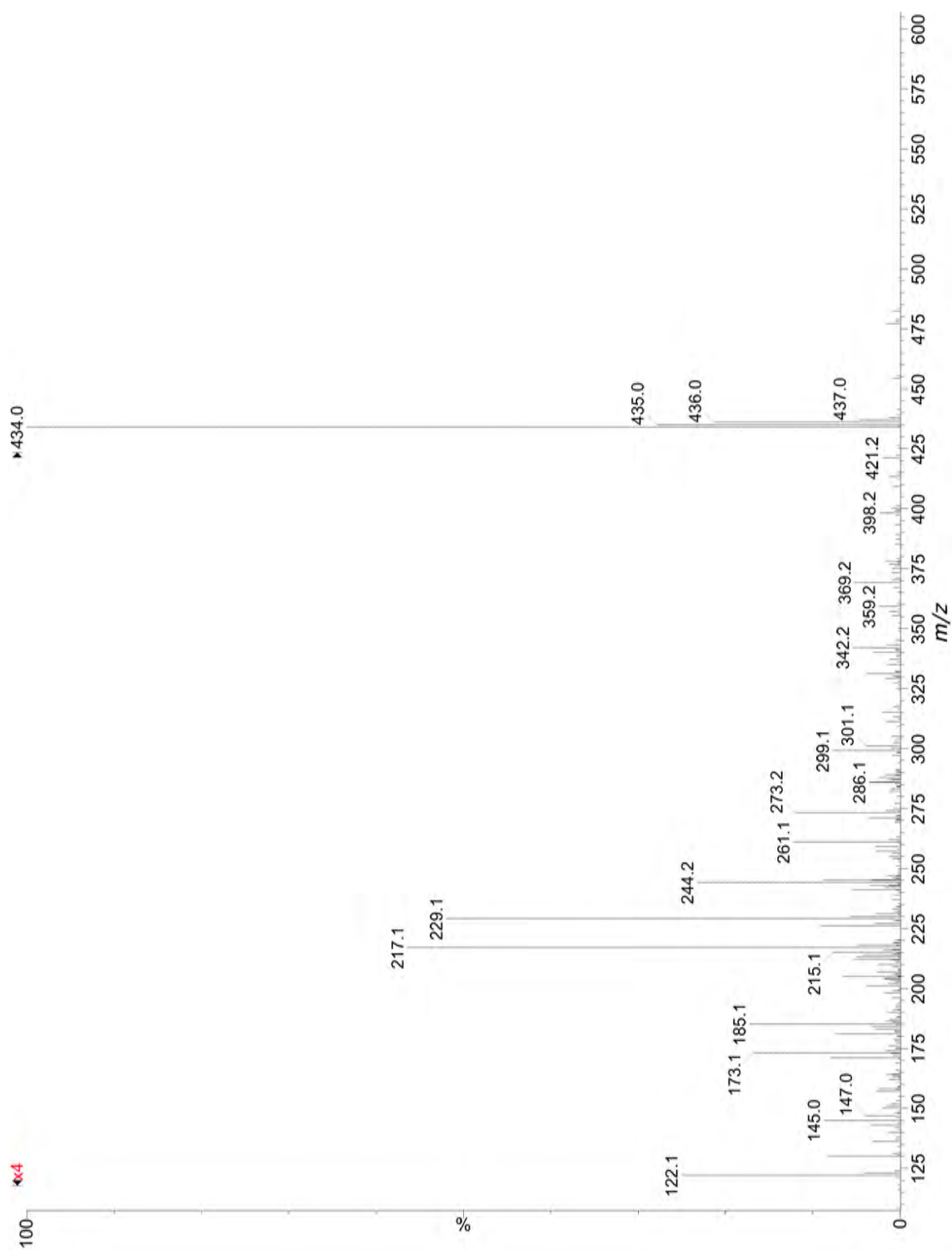
Figure A.13 The ESI-MS spectrum of 4-bis(2,2'-bithien-5-yl)methylalanine **7**.
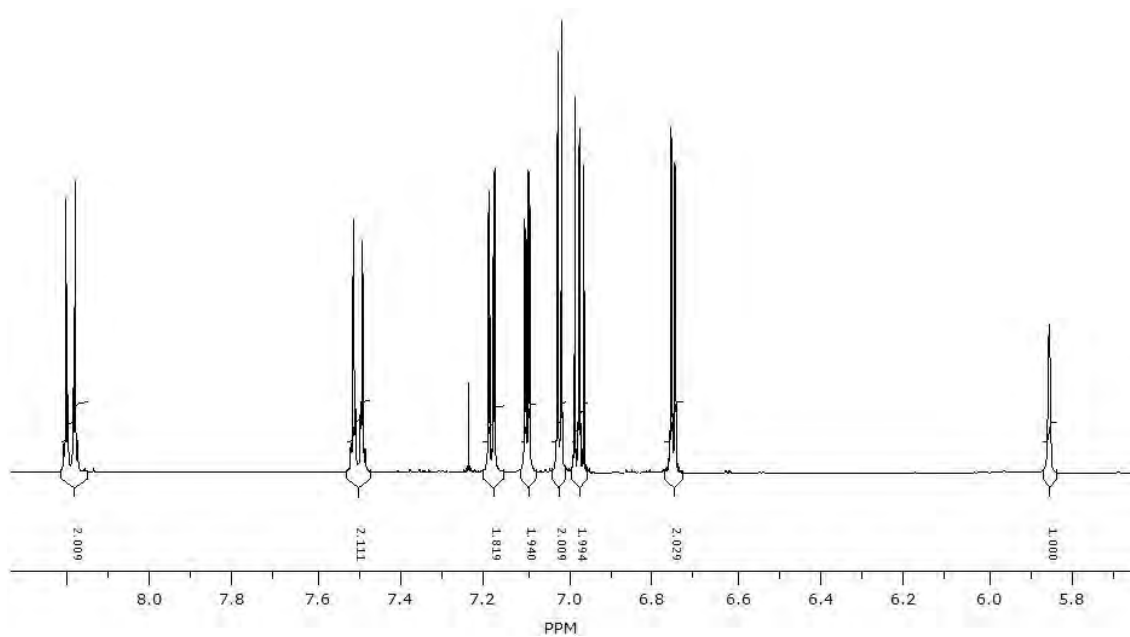
Figure A.14 The ^{1}H NMR spectrum of 4-bis(2,2'-bithien-5-yl)methyl-nitrobenzene **8** in deuterated chloroform.
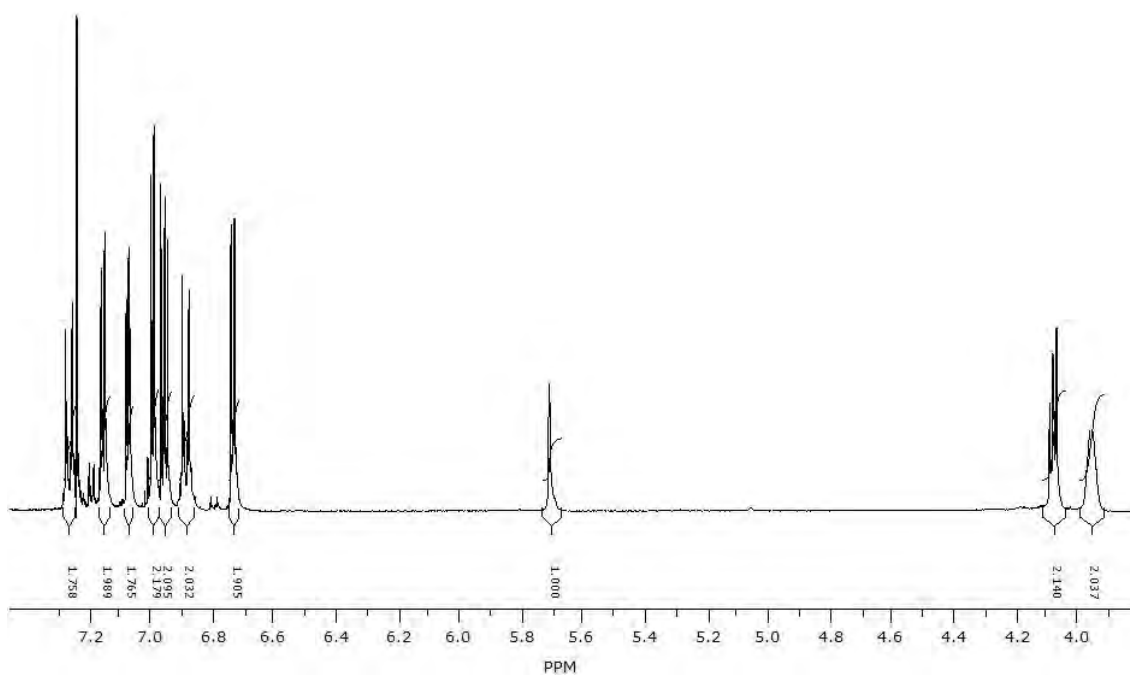
Figure A.15 The ^{1}H NMR spectrum of 4-bis(2,2'-bithien-5-yl)methylbenzoic acid glycol ester **9** in deuterated chloroform.
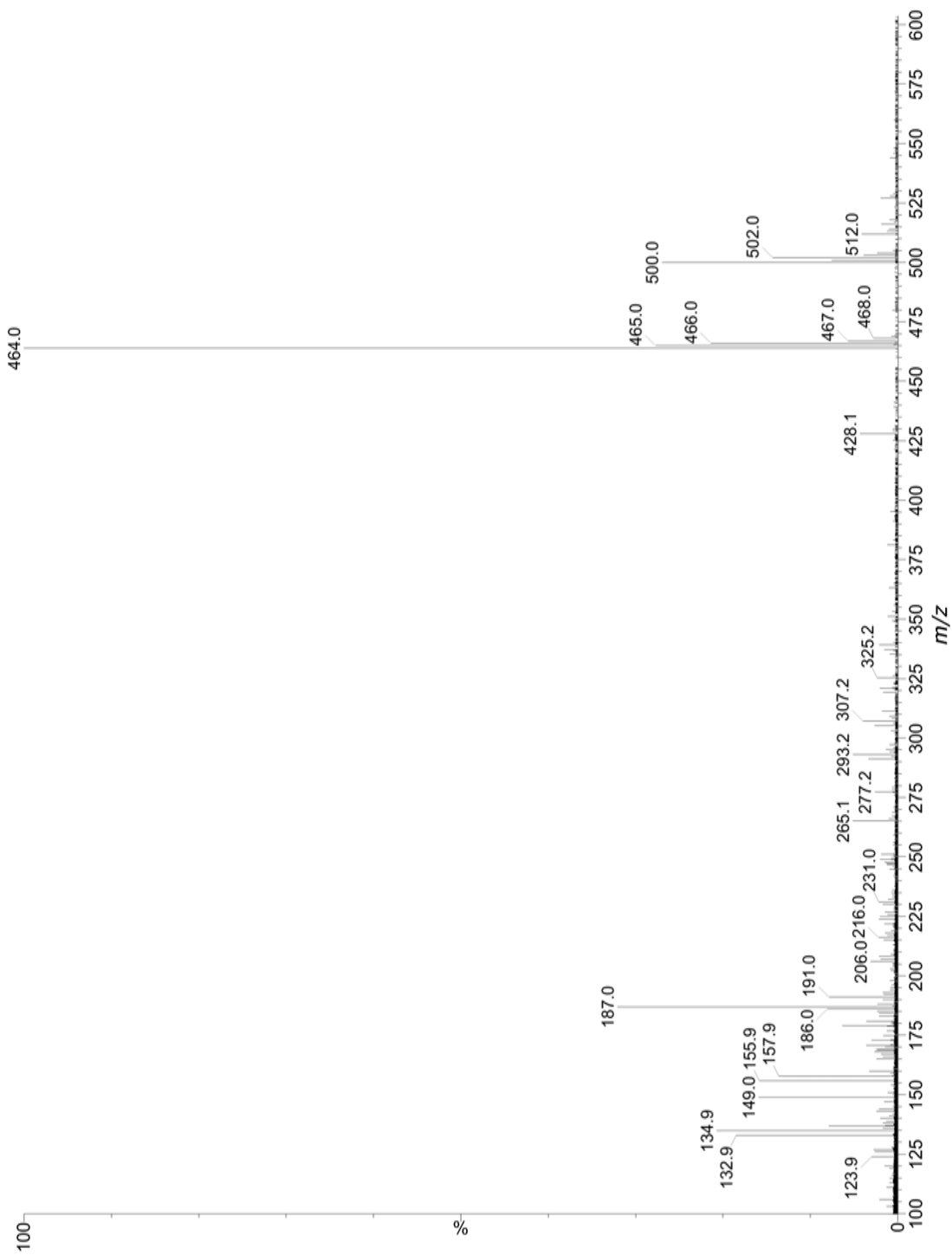
Figure A.16 The ESI(-)-MS spectrum of 4-bis(2,2'-bithien-5-yl)methyl-nitrobenzene **8**.
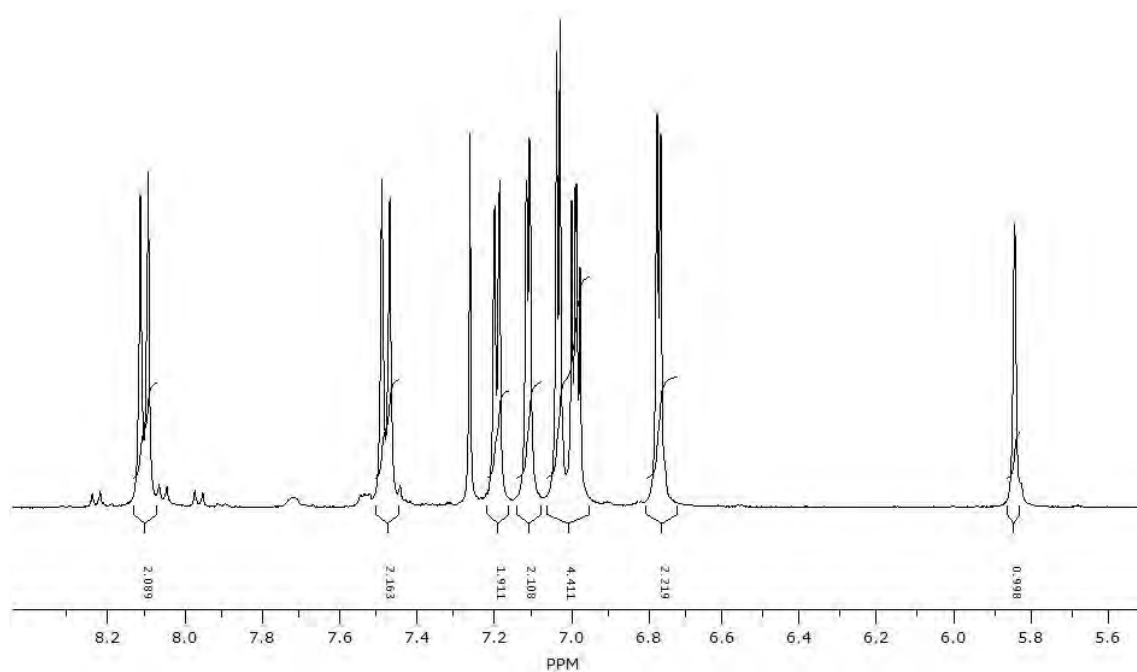
Figure A.17 The ^{1}H NMR spectrum of 4-bis(2,2'-bithien-5-yl)methylbenzoic acid **10** in deuterated chloroform.
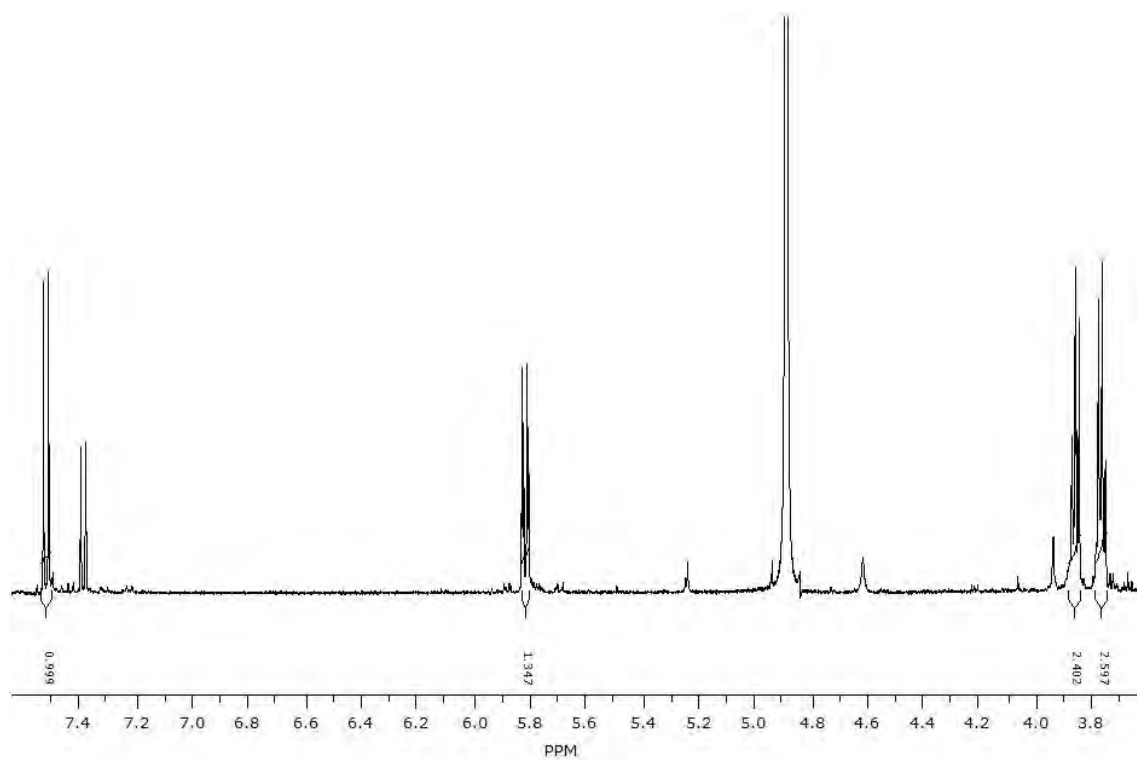
Figure A.18 The ^{1}H NMR spectrum of 1-(2'-hydroxyethyl)-cytosine **11a** in deuterated chloroform.
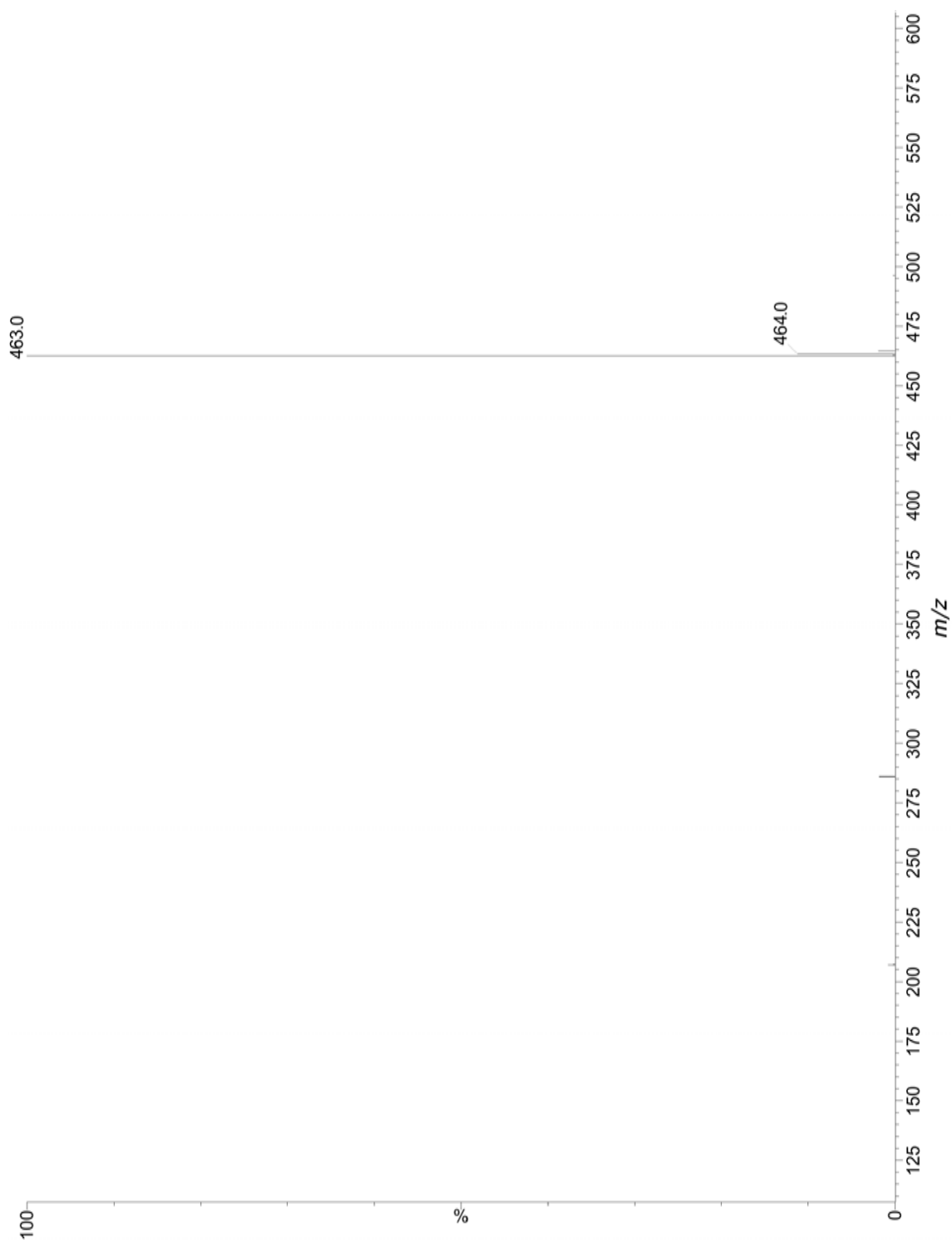
Figure A.19 The ESI(-)-MS spectrum of 4-bis(2,2'-bithien-5-yl)methylbenzoic acid **10**.
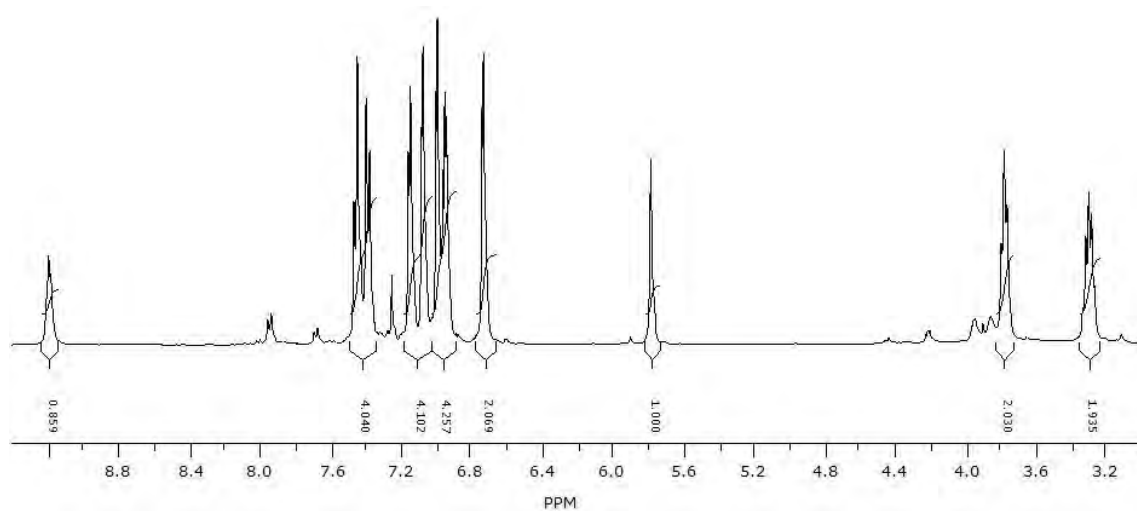
Figure A.20 The ^{1}H NMR spectrum of 2-(cytosin-1-yl)ethyl 4-bis(2,2'-bithien-5-yl)methylbenzolate **11** in deuterated chloroform.
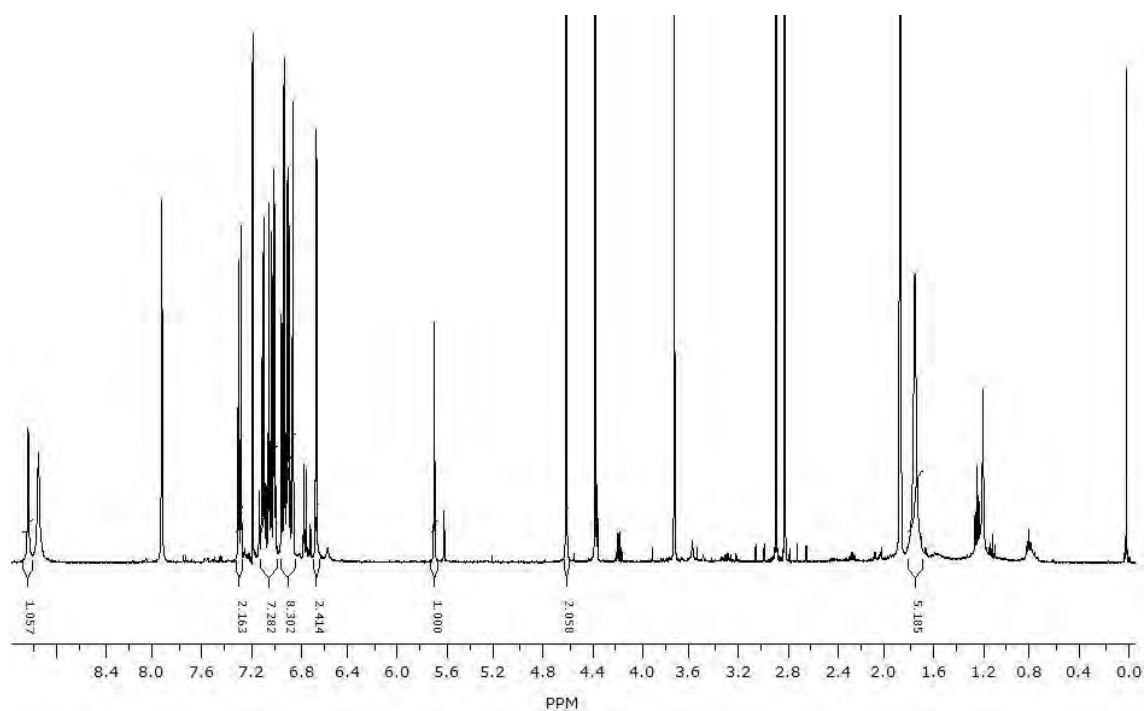
Figure A.21 The ^{1}H NMR spectrum of 4-bis(2,2'-bithienyl)-(4-hydroxyphenyl) methane thymine-1-acetate **12** in deuterated chloroform.
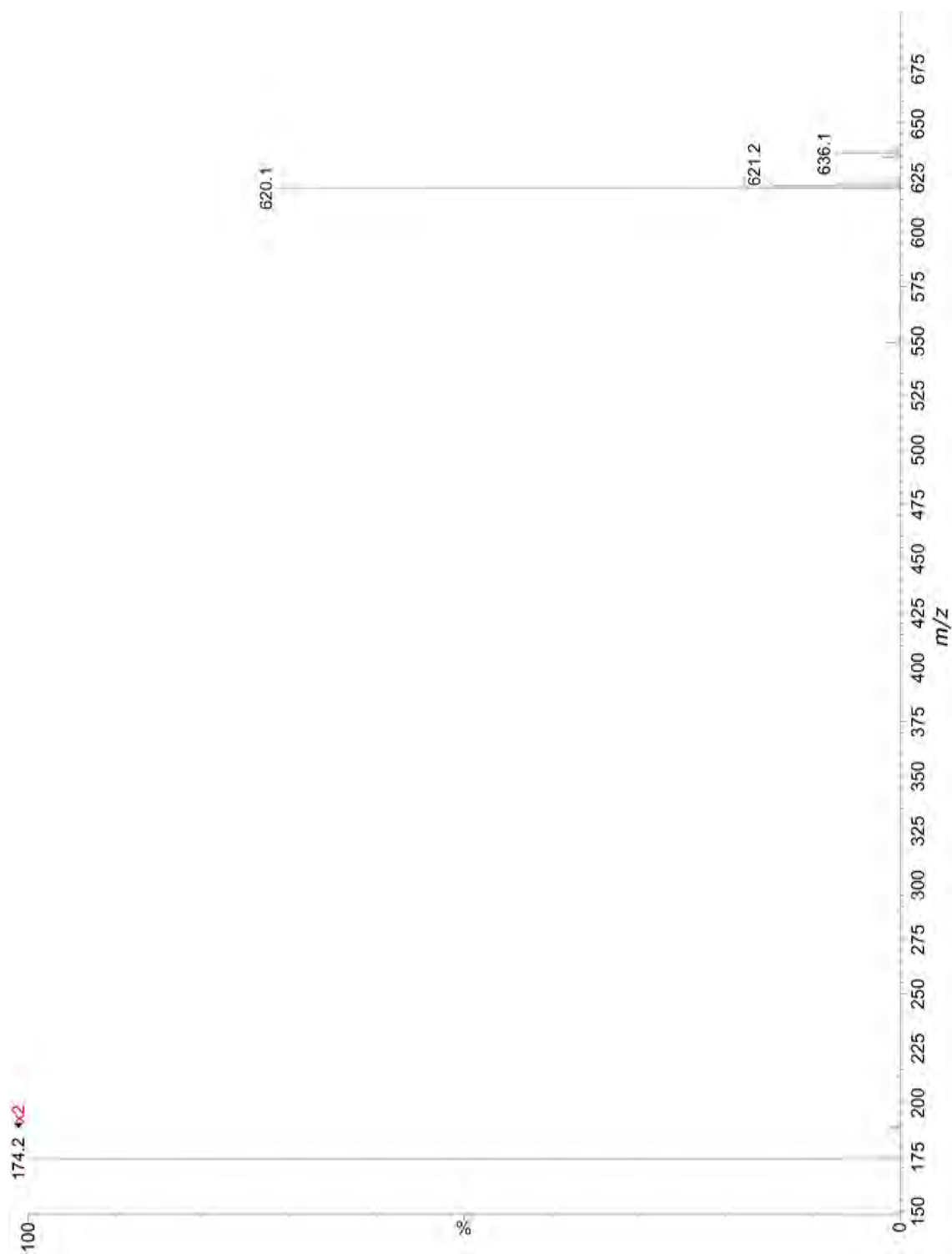
Figure A.22 The ESI-MS spectrum of 2-(cytosin-1-yl)ethyl-4-bis(2,2'-bithien-5-yl)methylbenzolate **11**.
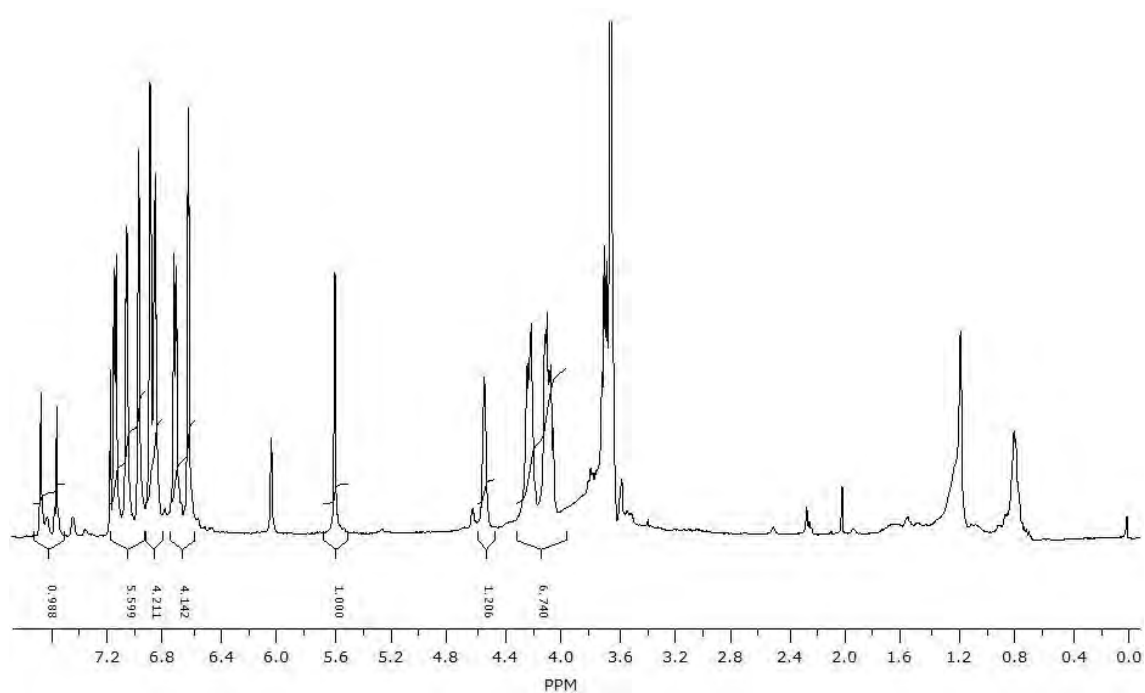
Figure A.23 The ^{1}H NMR spectrum of 4-bis(2,2'-bithien-5-yl)methylphenol-2-(guanin-9-yl)ethyl ether **13** in deuterated chloroform.
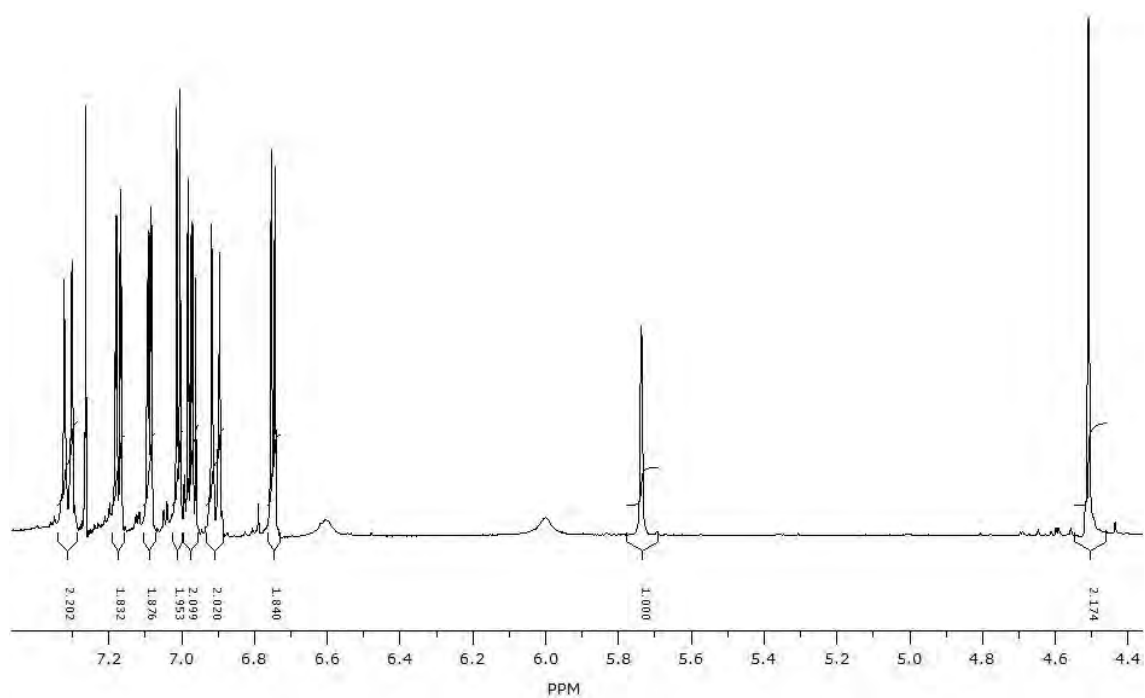
Figure A.24 The^{1}H NMR spectrum of 4-bis(2,2'-bithien-5-yl)methylphenol-2-hydroxyacetamide ether **14** in deuterated chloroform.
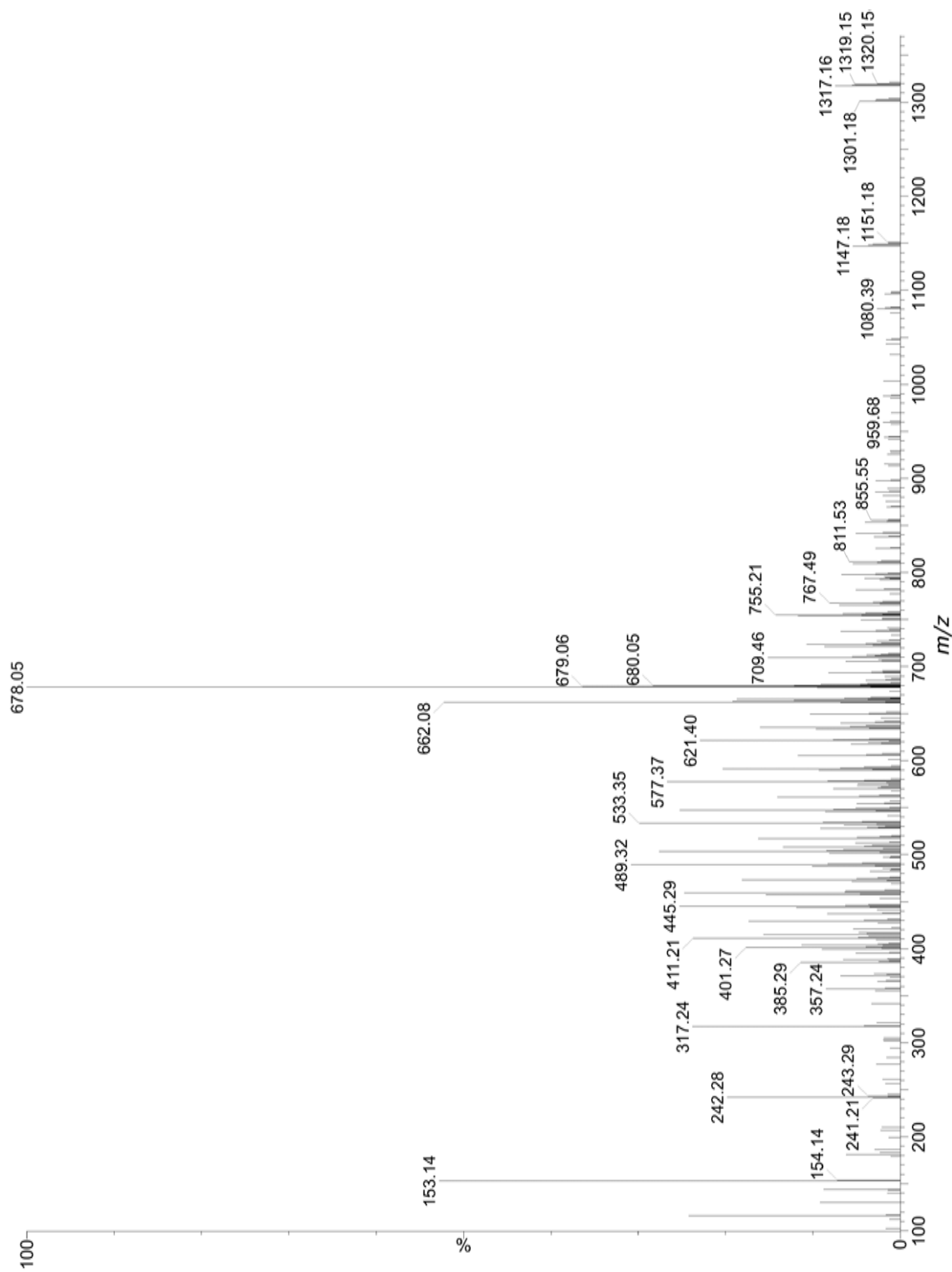
Figure A.25 The ESI-MS spectrum of 4-bis(2,2'-bithien-5-yl)methylphenol-2-(guanin-9-yl)ethyl ether **13**.
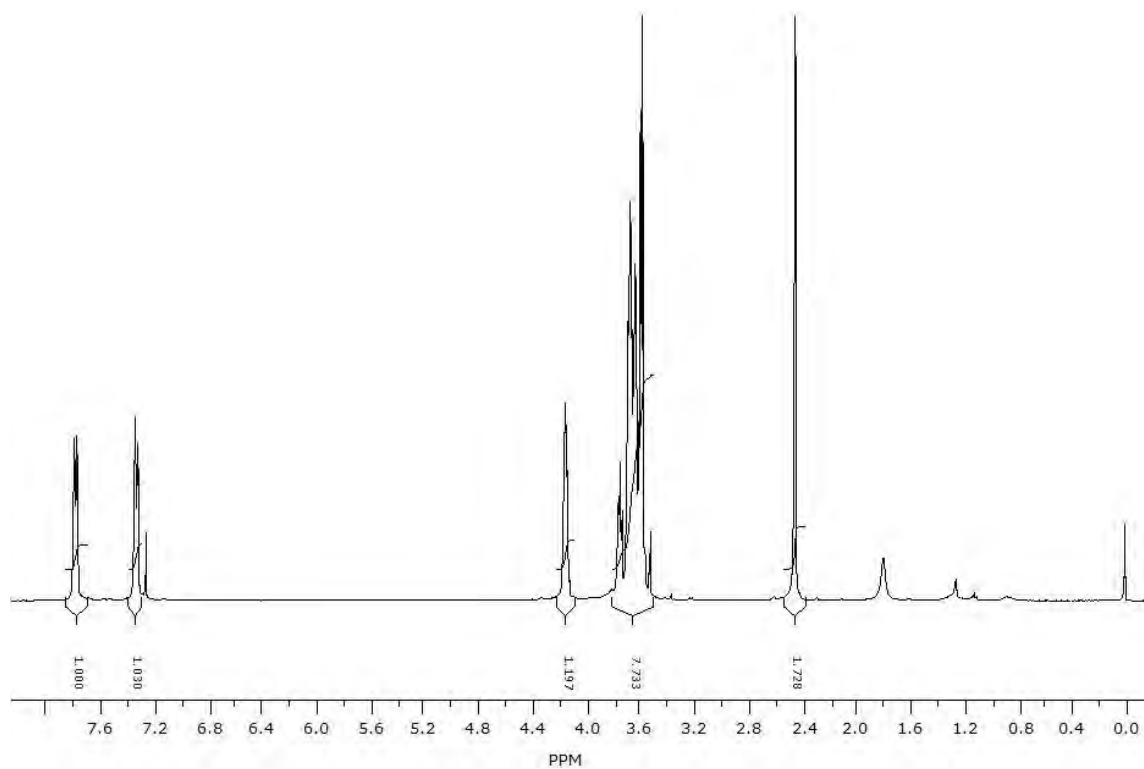
Figure A.26 The ^{1}H NMR spectrum of pentaethylene glycol p-toluenesulfonate **15a** in deuterated chloroform.
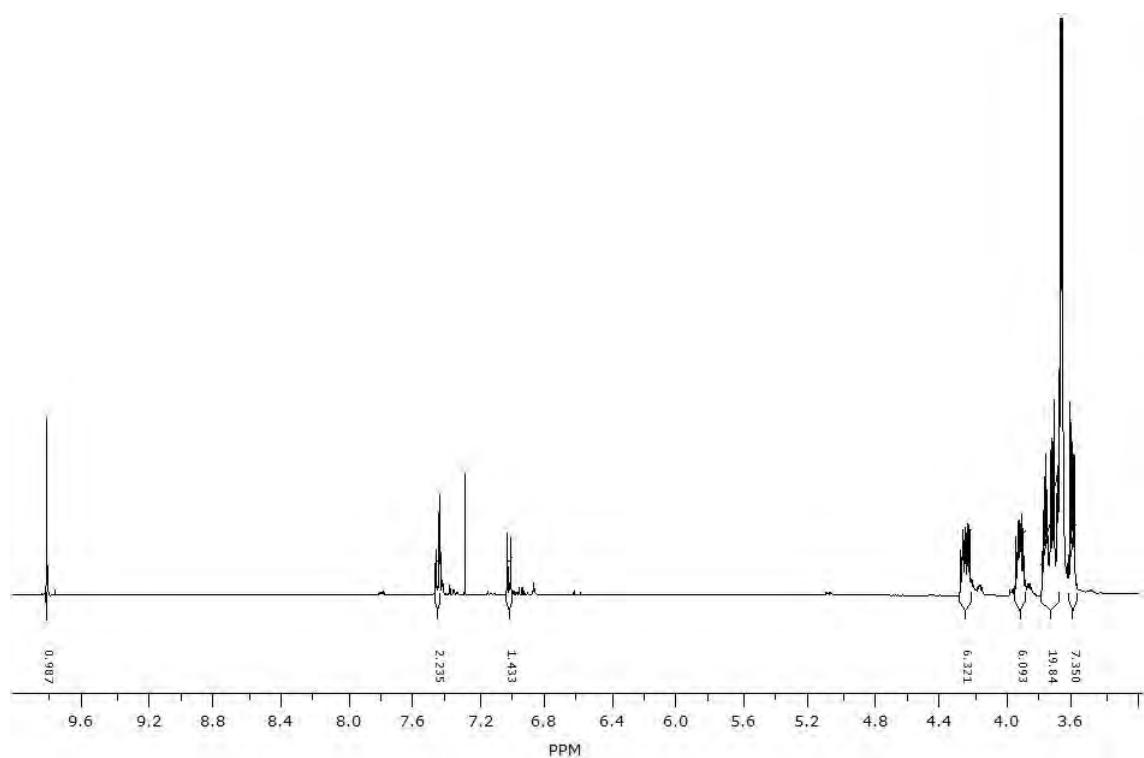
Figure A.27 The ^{1}H NMR spectrum of 3,4-bis(pentaethyleneglycol)benzaldehyde **15b** in deuterated chloroform.
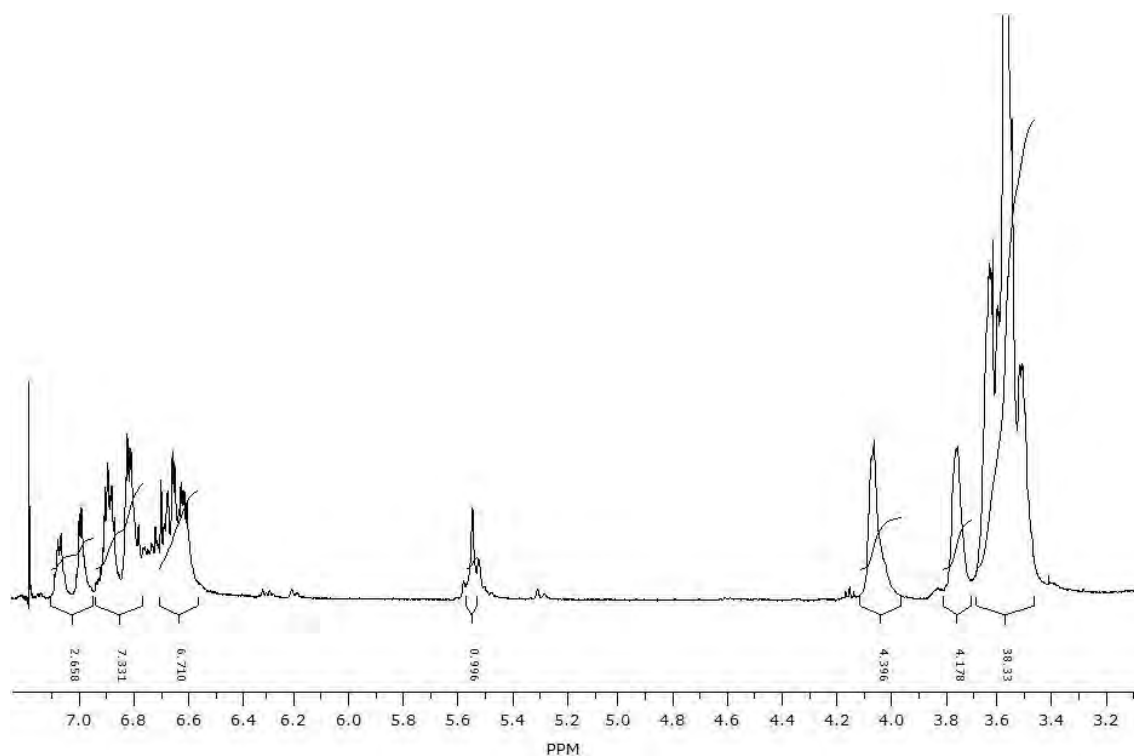
Figure A.28 The ^{1}H NMR spectrum of 4-bis(2,2'-bithien-5-yl)methyl-o-catechol pentaethyleneglycol diether **15** in deuterated chloroform.
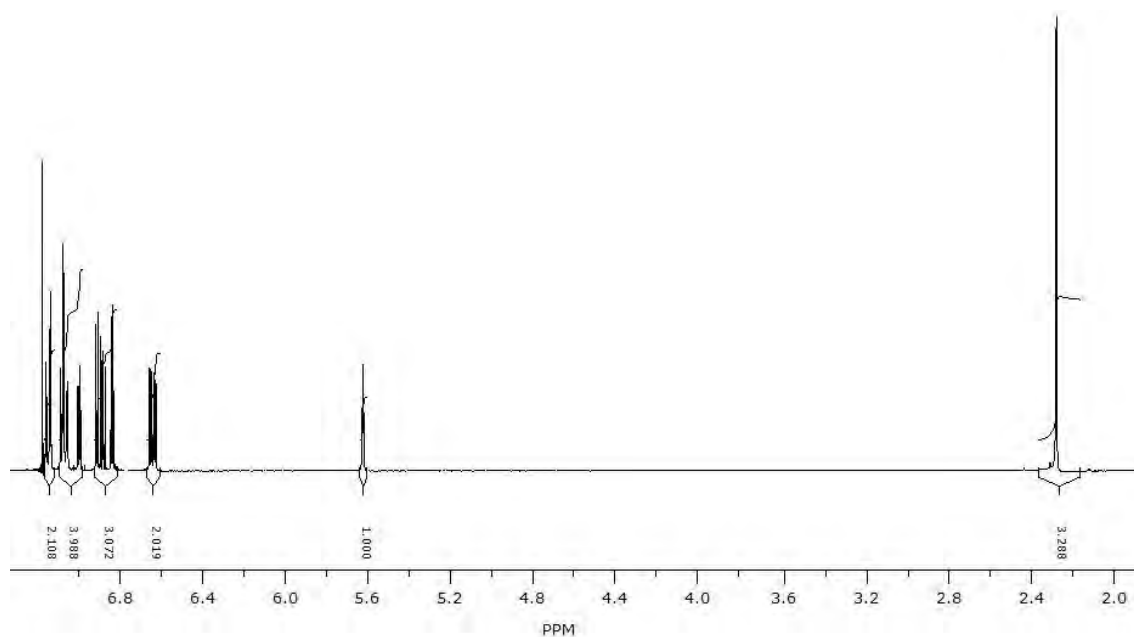
Figure A.29 The ^{1}H NMR spectrum of 4-bis(2,2'-bithien-5-yl)methylphenol 2-hydroxyacetamide ether **16** in deuterated chloroform.
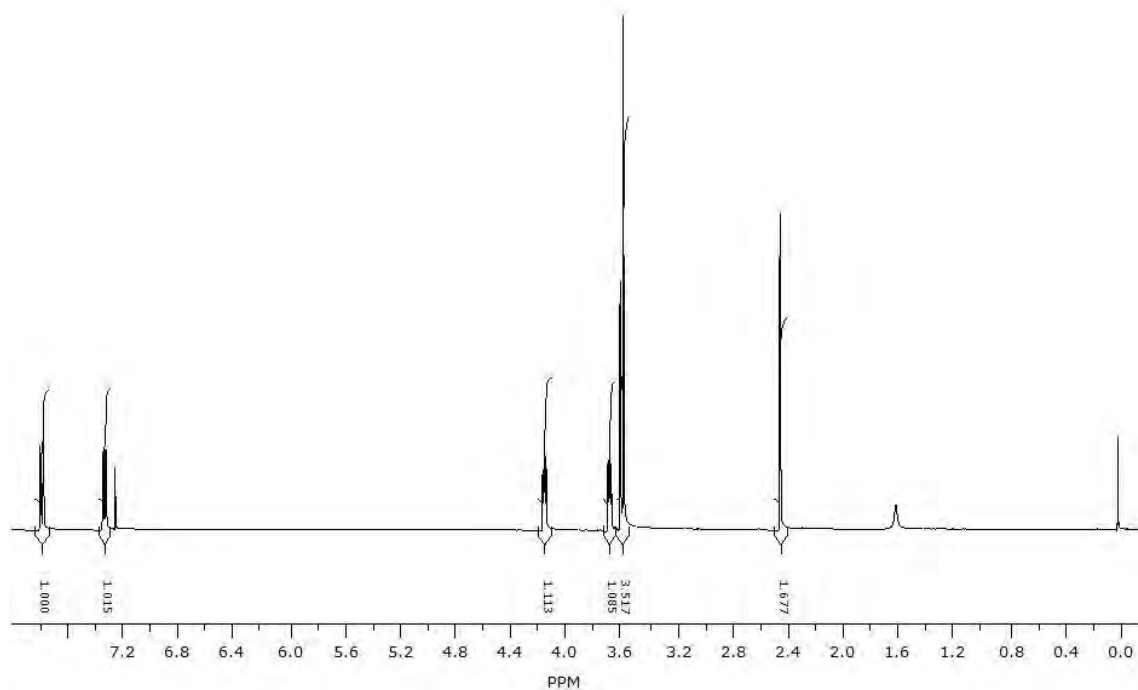
Figure A.30 The ^{1}H NMR spectrum of pentaethylene glycol di(p-toluenesulfonate) **17a** in deuterated chloroform.
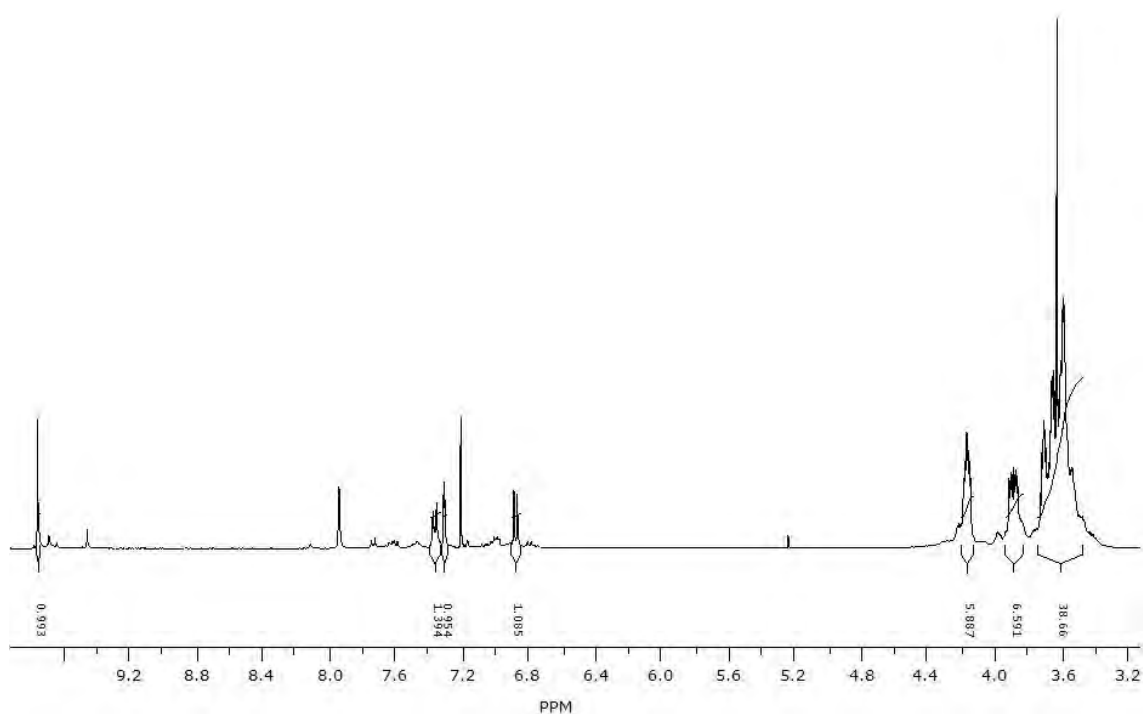
Figure A.31 The ^{1}H NMR spectrum of 4'-formylbenzo[18-crown-6] **17b** in deuterated chloroform.
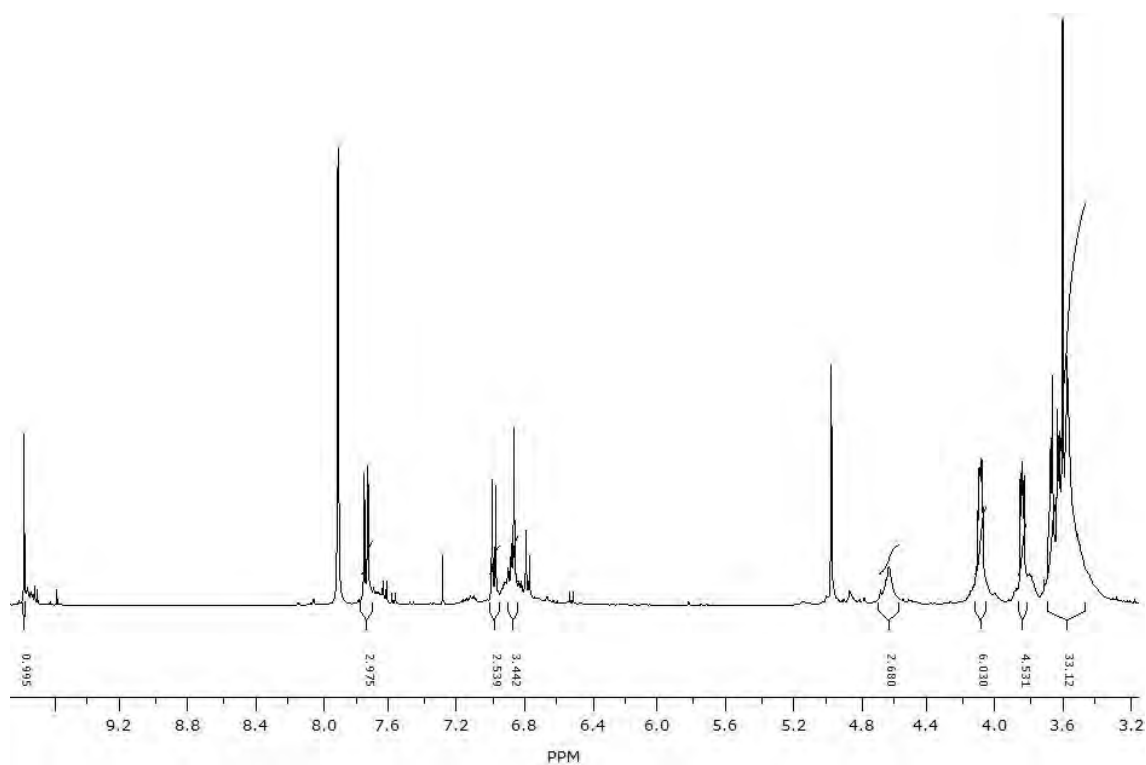
Figure A.32 The ^{1}H NMR spectrum of 3-([18-crown6]benzyl]oxy)benzaldehyde **17e** in deuterated chloroform.
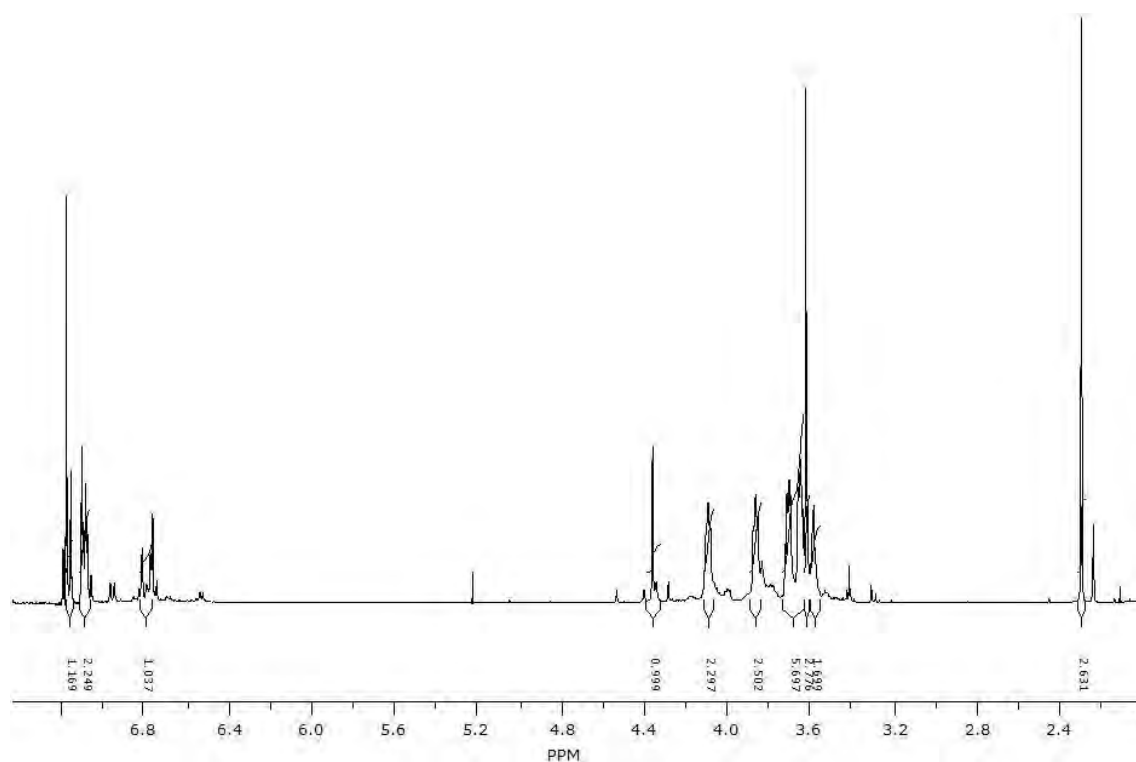
Figure A.33 The ^{1}H NMR spectrum of 4-(1-methylfulleropyrrolidin-2-yl)phenol 3,4-[18-crown-6]-benzyl ether **17** in deuterated chloroform.
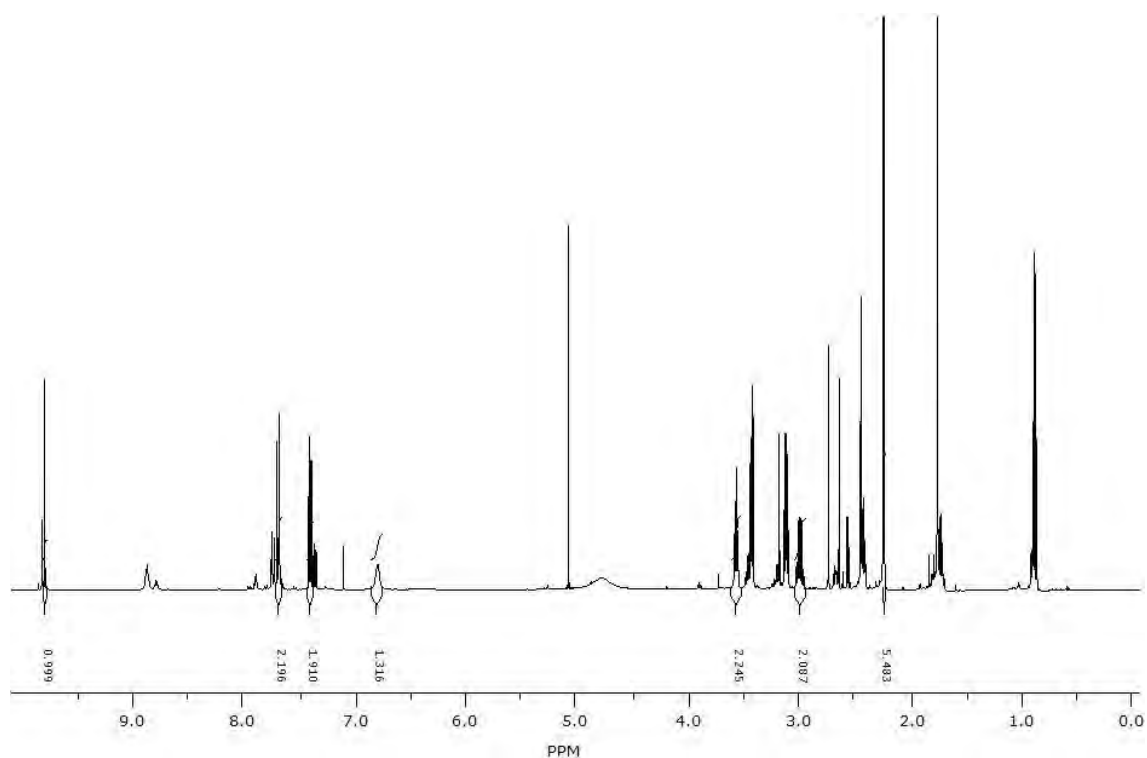
Figure A.34 The ¹H NMR spectrum of 2-(acetylamino)ethyl 3-formylbenzoate **18a** in deuterated chloroform.
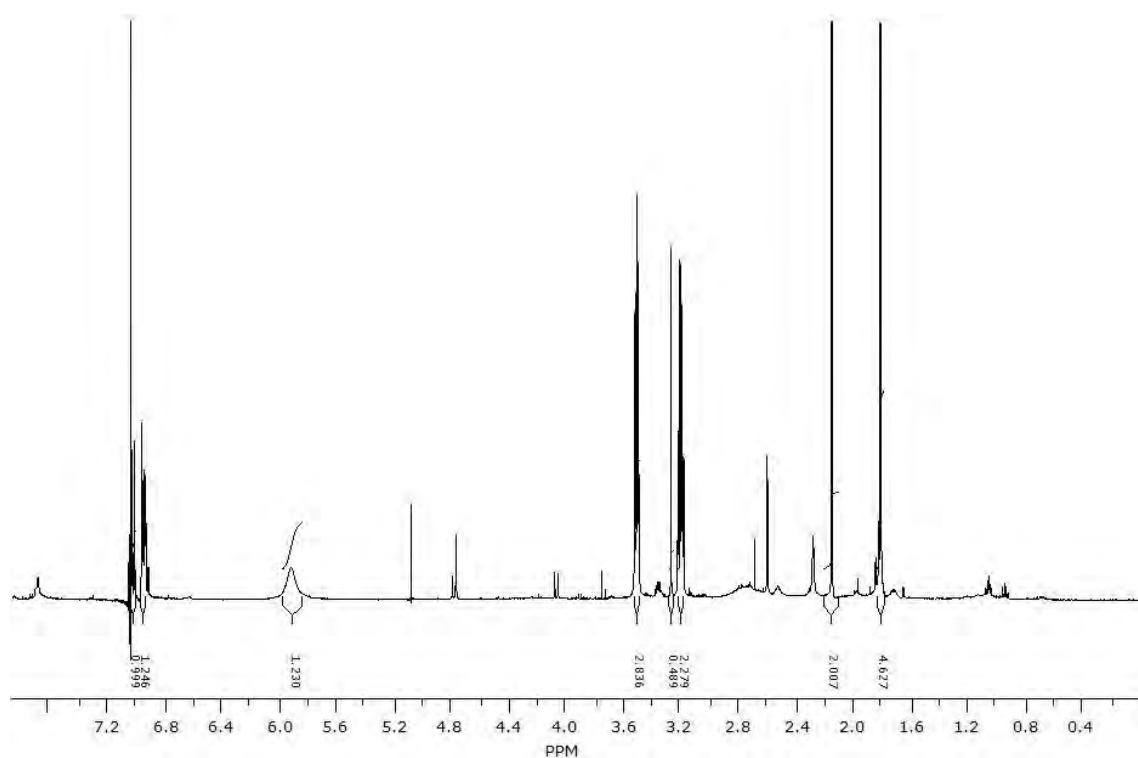
Figure A.35 The ¹H NMR spectrum of 2-acetamidethyl 4-(1-methylfulle-ropyrrolidin-2-yl)benzolate **18** in deuterated chloroform.

B. Crystallography data

Table B.1 Atomic coordinates ($\times 10^4$) and values of the equivalent isotropic displacement parameter, U(eq) ($\text{Å}^2 \times 10^3$) for 4-bis(2,2'-bithien-5-yl)methylalanine, **7**, defined as one third of the trace of the orthogonalized Uij tensor.

Atom	x	y	z	U(eq)
S(1)	8970(2)	249(1)	2350(1)	24(1)
S(3)	7517(2)	4309(1)	3616(1)	26(1
S(4)	5099(2)	7652(1)	4836(1)	36(1)
S(2)	12493(2)	-2827(1)	3164(1)	39(1)
C(2)	7239(6)	902(4)	2865(2)	22(1)
C(13)	5765(6)	5160(4)	4071(2)	23(1)
C(15)	8933(6)	6810(4)	4771(2)	15(1)
C(6)	11548(6)	-1754(4)	2660(2)	26(1)
C(10)	5328(6)	3022(4)	3233(2)	23(1)
C(12)	3600(6)	4442(5)	3927(2)	24(1)
C(1)	5678(6)	1919(5)	2705(2)	25(1)
C(3)	7370(7)	284(5)	3387(2)	28(1)
C(5)	9880(6)	-865(4)	2840(2)	25(1)
C(19)	8424(7)	3678(5)	2133(2)	31(1)
C(14)	6689(6)	6418(4)	4522(2)	22(1)
C(11)	3349(6)	3255(4)	3453(2)	25(1)
C(7)	12607(7)	-1820(5)	2096(2)	38(1)
C(4)	8865(7)	-728(5)	3371(2)	28(1)
C(8)	14204(8)	-2822(5)	2135(2)	36(1)
C(18)	6331(7)	2763(5)	2166(2)	28(1)
C(9)	14277(7)	-3400(5)	2663(2)	33(1)
C(17)	7225(8)	8691(5)	5285(2)	35(1)
C(16)	9095(7)	8151(5)	5210(2)	32(1)
C(22)	5314(10)	3482(10)	1218(3)	74(2)
N(1)	7936(11)	5243(8)	682(2)	87(2)
C(20)	8939(9)	4495(5)	1643(2)	43(1)
C(21)	7402(11)	4400(8)	1202(2)	61(2)
C(23)	4786(8)	2688(8)	1709(2)	52(2)

Table B.2 Bond lengths and angles between bonds for 4-bis(2,2'-bithien-5-yl)methylalanine, **7**.

Atoms	Bond lengths / Å
S(1)-C(5)	1.728(4)
S(1)-C(2)	1.728(4)
S(3)-C(10)	1.731(4)
S(3)-C(13)	1.735(4)
S(4)-C(17)	1.690(5)
S(4)-C(14)	1.725(4)
S(2)-C(9)	1.703(5)
S(2)-C(6)	1.732(4)
C(2)-C(3)	1.364(6)
C(2)-C(1)	1.518(5)
C(13)-C(12)	1.374(5)
C(13)-C(14)	1.446(6)
C(15)-C(14)	1.444(5)
C(15)-C(16)	1.453(6)
C(15)-H(15A)	0.95
C(6)-C(7)	1.442(7)
C(6)-C(5)	1.462(5)
C(10)-C(11)	1.374(5)
C(10)-C(1)	1.508(6)
C(12)-C(11)	1.404(6)
C(12)-H(12A)	0.95
C(1)-C(18)	1.521(6)
C(1)-H(1A)	1
C(3)-C(4)	1.417(5)
C(3)-H(3A)	0.95
C(5)-C(4)	1.367(6)
C(19)-C(18)	1.389(6)
C(19)-C(20)	1.397(6)
C(19)-H(19A)	0.95
C(11)-H(11A)	0.95
C(7)-C(8)	1.469(6)
C(7)-H(7A)	0.95
C(4)-H(4A)	0.95
C(8)-C(9)	1.353(7)
C(8)-H(8A)	0.95
C(18)-C(23)	1.378(6)
C(9)-H(9A)	0.95
C(17)-C(16)	1.346(6)
C(17)-H(17A)	0.95
C(16)-H(16A)	0.95
C(22)-C(21)	1.383(10)
C(22)-C(23)	1.391(8)
C(22)-H(22A)	0.95
N(1)-C(21)	1.472(7)
N(1)-H(1B)	0.88

148

Atoms	Bond lengths / Å
N(1)-H(1C)	0.88
C(20)-C(21)	1.347(8)
C(20)-H(20A)	0.95
C(23)-H(23A)	0.95

Atoms	Angles between bonds / degree
C(5)-S(1)-C(2)	92.12(19)
C(10)-S(3)-C(13)	92.60(19)
C(17)-S(4)-C(14)	92.9(2)
C(9)-S(2)-C(6)	91.1(2)
C(3)-C(2)-C(1)	127.2(4)
C(3)-C(2)-S(1)	111.1(3)
C(1)-C(2)-S(1)	121.5(3)
C(12)-C(13)-C(14)	130.4(4)
C(12)-C(13)-S(3)	109.8(3)
C(14)-C(13)-S(3)	119.7(3)
C(14)-C(15)-C(16)	107.4(3)
C(14)-C(15)-H(15A)	126.3
C(16)-C(15)-H(15A)	126.3
C(7)-C(6)-C(5)	127.1(4)
C(7)-C(6)-S(2)	113.7(3)
C(5)-C(6)-S(2)	119.2(3)
C(11)-C(10)-C(1)	127.6(4)
C(11)-C(10)-S(3)	110.3(3)
C(1)-C(10)-S(3)	121.9(3)
C(13)-C(12)-C(11)	113.9(3)
C(13)-C(12)-H(12A)	123
C(11)-C(12)-H(12A)	123
C(10)-C(1)-C(2)	111.7(3)
C(10)-C(1)-C(18)	111.0(3)
C(2)-C(1)-C(18)	114.2(3)
C(10)-C(1)-H(1A)	106.4
C(2)-C(1)-H(1A)	106.4
C(18)-C(1)-H(1A)	106.4
C(2)-C(3)-C(4)	112.8(4)
C(2)-C(3)-H(3A)	123.6
C(4)-C(3)-H(3A)	123.6
C(4)-C(5)-C(6)	129.6(4)
C(4)-C(5)-S(1)	110.6(3)
C(6)-C(5)-S(1)	119.8(3)
C(18)-C(19)-C(20)	120.3(4)
C(18)-C(19)-H(19A)	119.9
C(20)-C(19)-H(19A)	119.9
C(15)-C(14)-C(13)	126.9(3)
C(15)-C(14)-S(4)	111.7(3)
C(13)-C(14)-S(4)	121.4(3)
C(10)-C(11)-C(12)	113.3(4)
C(10)-C(11)-H(11A)	123.3

Atoms	Angles between bonds / degree
C(12)-C(11)-H(11A)	123.3
C(6)-C(7)-C(8)	106.8(4)
C(6)-C(7)-H(7A)	126.6
C(8)-C(7)-H(7A)	126.6
C(5)-C(4)-C(3)	113.4(4)
C(5)-C(4)-H(4A)	123.3
C(3)-C(4)-H(4A)	123.3
C(9)-C(8)-C(7)	114.6(4)
C(9)-C(8)-H(8A)	122.7
C(7)-C(8)-H(8A)	122.7
C(23)-C(18)-C(19)	118.6(4)
C(23)-C(18)-C(1)	119.6(4)
C(19)-C(18)-C(1)	121.7(4)
C(8)-C(9)-S(2)	113.8(3)
C(8)-C(9)-H(9A)	123.1
S(2)-C(9)-H(9A)	123.1
C(16)-C(17)-S(4)	112.2(4)
C(16)-C(17)-H(17A)	123.9
S(4)-C(17)-H(17A)	123.9
C(17)-C(16)-C(15)	115.8(4)
C(17)-C(16)-H(16A)	122.1
C(15)-C(16)-H(16A)	122.1
C(21)-C(22)-C(23)	119.0(5)
C(21)-C(22)-H(22A)	120.5
C(23)-C(22)-H(22A)	120.5
C(21)-N(1)-H(1B)	120
C(21)-N(1)-H(1C)	120
H(1B)-N(1)-H(1C)	120
C(21)-C(20)-C(19)	120.0(5)
C(21)-C(20)-H(20A)	120
C(19)-C(20)-H(20A)	120
C(20)-C(21)-C(22)	121.1(5)
C(20)-C(21)-N(1)	120.4(6)
C(22)-C(21)-N(1)	118.5(6)
C(18)-C(23)-C(22)	121.0(5)
C(18)-C(23)-H(23A)	119.5
C(22)-C(23)-H(23A)	119.5

Table B.3 Anisotropic displacement parameters ($\mathring{A}^2\times 10^3$) for 4-bis(2,2'-bithien-5-yl)methylalanine, **7**. Exponent of the anisotropic displacement factor takes the form: $-2\pi^2[\ h^2\ a^{*2}\ U^{11} + ... + 2\ h\ k\ a^*\ b^*\ U^{12}\ ]$

Atom	U^{11}	U^{22}	U^{33}	U^{23}	U^{13}	U^{12}
S(1)	18(1)	27(1)	32(1)	12(1)	3(1)	8(1)
S(3)	12(1)	30(1)	36(1)	4(1)	4(1)	6(1)
S(4)	29(1)	33(1)	51(1)	8(1)	5(1)	13(1)
S(2)	25(1)	38(1)	60(1)	22(1)	2(1)	11(1)
C(2)	18(2)	22(2)	29(2)	6(2)	4(2)	3(1)
C(13)	19(2)	24(2)	31(2)	14(2)	5(2)	10(2)
C(15)	12(2)	15(2)	16(2)	5(1)	2(1)	-4(1)
C(6)	16(2)	23(2)	40(2)	9(2)	-3(2)	5(2)
C(10)	16(2)	20(2)	35(2)	9(2)	1(2)	4(1)
C(12)	15(2)	28(2)	35(2)	13(2)	3(2)	8(2)
C(1)	14(2)	29(2)	34(2)	6(2)	2(2)	7(2)
C(3)	24(2)	26(2)	34(2)	9(2)	4(2)	5(2)
C(5)	17(2)	19(2)	41(2)	10(2)	0(2)	4(1)
C(19)	34(2)	27(2)	35(2)	9(2)	7(2)	8(2)
C(14)	15(2)	23(2)	31(2)	11(2)	7(2)	6(1)
C(11)	15(2)	24(2)	38(2)	13(2)	1(2)	4(2)
C(7)	19(2)	20(2)	75(3)	-7(2)	-6(2)	10(2)
C(4)	28(2)	23(2)	37(2)	12(2)	-3(2)	7(2)
C(8)	33(2)	26(2)	51(3)	1(2)	-1(2)	8(2)
C(18)	23(2)	37(2)	32(2)	12(2)	5(2)	17(2)
C(9)	25(2)	25(2)	53(3)	11(2)	1(2)	10(2)
C(17)	39(3)	22(2)	46(3)	8(2)	13(2)	7(2)
C(16)	24(2)	30(2)	40(3)	8(2)	3(2)	-1(2)
C(22)	49(3)	164(7)	38(3)	45(4)	16(3)	67(4)
N(1)	111(5)	125(5)	67(3)	69(4)	51(3)	88(4)
C(20)	54(3)	30(2)	49(3)	13(2)	22(2)	12(2)
C(21)	79(4)	90(5)	41(3)	36(3)	29(3)	64(4)
C(23)	23(2)	102(5)	37(3)	19(3)	4(2)	26(3)

Table B.4 Hydrogen coordinates ($\times 10^4$) and values of the isotropic displacement parameter, U(eq) ($\text{Å}^2 \times 10^3$), for 4-bis(2,2'-bithien-5-yl)methylalanine, **7**.

Atom	x	y	z	U(eq)
H(15A)	10091	6287	4668	18
H(12A)	2383	4724	4131	29
H(1A)	4207	1221	2597	30
H(3A)	6547	507	3725	33
H(19A)	9511	3748	2444	37
H(11A)	1949	2672	3300	30
H(7A)	12326	-1313	1764	46
H(4A)	9136	-1260	3697	34
H(8A)	15112	-3047	1816	44
H(9A)	15236	-4064	2746	40
H(17A)	7114	9556	5559	42
H(16A)	10437	8617	5429	38
H(22A)	4256	3394	898	89
H(1B)	9268	5813	658	104
H(1C)	6925	5177	395	104
H(20A)	10375	5117	1622	52
H(23A)	3337	2086	1730	62

Table B.5 Atomic coordinates ($\times$ 10^4) and values of the equivalent isotropic displacement parameter, $U(\text{eq})$ (Å^2 $\times$ 10^3) for 4-bis(2,2'-bithien-5-yl)methyl-nitrobenzene, **8**, defined as one third of the trace of the orthogonalized Uij tensor.

Atom	x	y	z	$U(\text{eq})$
S(1)	3615(1)	2612(1)	2255(1)	18(1)
O(1)	-1553(3)	4884(1)	3911(2)	35(1)
N(1)	-1510(3)	4533(1)	3045(2)	23(1)
C(1)	1841(3)	2066(1)	3736(2)	19(1)
S(2)	6722(1)	1868(1)	153(1)	32(1)
O(2)	-2156(2)	4675(1)	2038(2)	30(1)
C(2)	2837(3)	1940(1)	2864(2)	18(1)
S(3)	-320(1)	1161(1)	2534(1)	23(1)
C(3)	3369(3)	1341(1)	2546(2)	20(1)
S(4)	-3638(1)	-158(1)	3510(1)	35(1)
C(4)	4405(3)	1418(1)	1797(2)	21(1)
C(5)	4647(3)	2079(1)	1547(2)	18(1)
C(6)	5545(3)	2367(1)	763(2)	20(1)
C(7)	5558(3)	3044(1)	372(2)	20(1)
C(8)	6550(3)	3103(1)	-436(2)	20(1)
C(9)	7227(3)	2526(2)	-619(3)	36(1)
C(10)	797(3)	1486(1)	3788(2)	19(1)
C(11)	487(3)	1198(1)	4780(2)	22(1)
C(12)	-663(3)	715(1)	4538(2)	24(1)
C(13)	-1215(3)	631(1)	3361(2)	22(1)
C(14)	-2374(3)	186(1)	2766(3)	25(1)
C(15)	-2675(3)	-15(1)	1584(3)	26(1)
C(16)	-3909(4)	-461(2)	1336(3)	41(1)
C(17)	-4525(4)	-578(2)	2281(3)	40(1)
C(18)	985(3)	2727(1)	3533(2)	17(1)
C(19)	31(3)	2862(1)	2455(2)	16(1)
C(20)	-783(3)	3454(1)	2286(2)	18(1)
C(21)	-648(3)	3903(1)	3223(2)	20(1)
C(22)	268(3)	3783(1)	4308(2)	23(1)
C(23)	1080(3)	3192(1)	4449(2)	21(1)

Table B.6 Bond lengths and angles between bonds for 4-bis(2,2'-bithien-5-yl)methyl-nitrobenzene, **8**.

Atoms	Bond lengths / Å
S(1)-C(2)	1.730(2)
S(1)-C(5)	1.735(2)
O(1)-N(1)	1.226(3)
N(1)-O(2)	1.228(3)
N(1)-C(21)	1.473(3)
C(1)-C(10)	1.510(3)
C(1)-C(2)	1.516(3)
C(1)-C(18)	1.525(3)
C(1)-H(1A)	1
S(2)-C(9)	1.699(3)
S(2)-C(6)	1.723(3)
C(2)-C(3)	1.363(4)
S(3)-C(10)	1.726(3)
S(3)-C(13)	1.738(3)
C(3)-C(4)	1.424(3)
C(3)-H(3A)	0.95
S(4)-C(17)	1.706(4)
S(4)-C(14)	1.726(3)
C(4)-C(5)	1.370(4)
C(4)-H(4A)	0.95
C(5)-C(6)	1.463(3)
C(6)-C(7)	1.417(3)
C(7)-C(8)	1.440(3)
C(7)-H(7A)	0.95
C(8)-C(9)	1.340(4)
C(8)-H(8A)	0.95
C(9)-H(9A)	0.95
C(10)-C(11)	1.362(3)
C(11)-C(12)	1.417(4)
C(11)-H(11A)	0.95
C(12)-C(13)	1.362(4)
C(12)-H(12A)	0.95
C(13)-C(14)	1.450(4)
C(14)-C(15)	1.395(4)
C(15)-C(16)	1.427(4)
C(15)-H(15A)	0.95
C(16)-C(17)	1.348(5)
C(16)-H(16A)	0.95
C(17)-H(17A)	0.95
C(18)-C(23)	1.393(3)
C(18)-C(19)	1.399(3)
C(19)-C(20)	1.385(3)
C(19)-H(19A)	0.95
C(20)-C(21)	1.388(3)
C(20)-H(20A)	0.95

Atoms	Bond lengths / Å
C(21)-C(22)	1.385(4)
C(22)-C(23)	1.383(4)
C(22)-H(22A)	0.95
C(23)-H(23A)	0.95

Atoms	Angles between bonds / degree
C(2)-S(1)-C(5)	92.05(12)
O(1)-N(1)-O(2)	123.6(2)
O(1)-N(1)-C(21)	118.2(2)
O(2)-N(1)-C(21)	118.2(2)
C(10)-C(1)-C(2)	112.4(2)
C(10)-C(1)-C(18)	110.05(19)
C(2)-C(1)-C(18)	114.0(2)
C(10)-C(1)-H(1A)	106.6
C(2)-C(1)-H(1A)	106.6
C(18)-C(1)-H(1A)	106.6
C(9)-S(2)-C(6)	92.10(14)
C(3)-C(2)-C(1)	128.5(2)
C(3)-C(2)-S(1)	111.03(18)
C(1)-C(2)-S(1)	120.11(18)
C(10)-S(3)-C(13)	92.04(13)
C(2)-C(3)-C(4)	113.2(2)
C(2)-C(3)-H(3A)	123.4
C(4)-C(3)-H(3A)	123.4
C(17)-S(4)-C(14)	92.25(15)
C(5)-C(4)-C(3)	112.9(2)
C(5)-C(4)-H(4A)	123.6
C(3)-C(4)-H(4A)	123.6
C(4)-C(5)-C(6)	129.8(2)
C(4)-C(5)-S(1)	110.81(18)
C(6)-C(5)-S(1)	119.26(19)
C(7)-C(6)-C(5)	127.5(2)
C(7)-C(6)-S(2)	111.54(18)
C(5)-C(6)-S(2)	120.90(19)
C(6)-C(7)-C(8)	109.3(2)
C(6)-C(7)-H(7A)	125.3
C(8)-C(7)-H(7A)	125.3
C(9)-C(8)-C(7)	114.3(2)
C(9)-C(8)-H(8A)	122.8
C(7)-C(8)-H(8A)	122.8
C(8)-C(9)-S(2)	112.7(2)
C(8)-C(9)-H(9A)	123.7
S(2)-C(9)-H(9A)	123.7
C(11)-C(10)-C(1)	126.8(2)
C(11)-C(10)-S(3)	110.9(2)
C(1)-C(10)-S(3)	122.05(18)
C(10)-C(11)-C(12)	113.3(2)
C(10)-C(11)-H(11A)	123.4

Atoms	Angles between bonds / degree
C(12)-C(11)-H(11A)	123.4
C(13)-C(12)-C(11)	113.2(2)
C(13)-C(12)-H(12A)	123.4
C(11)-C(12)-H(12A)	123.4
C(12)-C(13)-C(14)	129.8(2)
C(12)-C(13)-S(3)	110.5(2)
C(14)-C(13)-S(3)	119.7(2)
C(15)-C(14)-C(13)	128.4(2)
C(15)-C(14)-S(4)	110.6(2)
C(13)-C(14)-S(4)	121.0(2)
C(14)-C(15)-C(16)	111.6(3)
C(14)-C(15)-H(15A)	124.2
C(16)-C(15)-H(15A)	124.2
C(17)-C(16)-C(15)	113.3(3)
C(17)-C(16)-H(16A)	123.3
C(15)-C(16)-H(16A)	123.3
C(16)-C(17)-S(4)	112.2(2)
C(16)-C(17)-H(17A)	123.9
S(4)-C(17)-H(17A)	123.9
C(23)-C(18)-C(19)	118.7(2)
C(23)-C(18)-C(1)	120.1(2)
C(19)-C(18)-C(1)	121.1(2)
C(20)-C(19)-C(18)	121.0(2)
C(20)-C(19)-H(19A)	119.5
C(18)-C(19)-H(19A)	119.5
C(19)-C(20)-C(21)	118.2(2)
C(19)-C(20)-H(20A)	120.9
C(21)-C(20)-H(20A)	120.9
C(22)-C(21)-C(20)	122.5(2)
C(22)-C(21)-N(1)	119.2(2)
C(20)-C(21)-N(1)	118.3(2)
C(23)-C(22)-C(21)	118.2(2)
C(23)-C(22)-H(22A)	120.9
C(21)-C(22)-H(22A)	120.9
C(22)-C(23)-C(18)	121.4(2)
C(22)-C(23)-H(23A)	119.3
C(18)-C(23)-H(23A)	119.3

Table B.7 Anisotropic displacement parameters ($\mathring{A}^2 \times 10^3$) for 4-bis(2,2'-bithien-5-yl)methyl-nitrobenzene, **8**. Exponent of the anisotropic displacement factor takes the form: $-2\pi^2[\ h^2\ a^{*2}\ U^{11} + ... + 2\ h\ k\ a^*\ b^*\ U^{12}\ ]$

Atom	U^{11}	U^{22}	U^{33}	U^{23}	U^{13}	U^{12}
S(1)	16(1)	22(1)	17(1)	0(1)	6(1)	0(1)
O(1)	48(1)	30(1)	27(1)	-8(1)	9(1)	11(1)
N(1)	27(1)	23(1)	22(1)	-1(1)	8(1)	1(1)
C(1)	17(1)	26(1)	13(1)	0(1)	3(1)	1(1)
S(2)	24(1)	45(1)	29(1)	2(1)	10(1)	6(1)
O(2)	39(1)	30(1)	22(1)	2(1)	5(1)	11(1)
C(2)	15(1)	24(1)	14(1)	1(1)	3(1)	-1(1)
S(3)	23(1)	27(1)	18(1)	4(1)	3(1)	-5(1)
C(3)	19(1)	24(1)	19(1)	1(1)	4(1)	0(1)
S(4)	29(1)	37(1)	40(1)	7(1)	12(1)	-3(1)
C(4)	19(1)	25(1)	18(1)	-2(1)	4(1)	2(1)
C(5)	13(1)	28(1)	14(1)	-2(1)	3(1)	2(1)
C(6)	12(1)	32(1)	16(1)	-2(1)	2(1)	0(1)
C(7)	13(1)	34(1)	14(1)	2(1)	1(1)	-10(1)
C(8)	13(1)	34(1)	14(1)	2(1)	1(1)	-10(1)
C(9)	18(1)	70(2)	22(1)	-4(1)	8(1)	-11(1)
C(10)	18(1)	24(1)	17(1)	2(1)	5(1)	4(1)
C(11)	26(1)	24(1)	18(1)	5(1)	8(1)	8(1)
C(12)	27(1)	22(1)	27(1)	7(1)	14(1)	7(1)
C(13)	20(1)	19(1)	30(1)	6(1)	11(1)	5(1)
C(14)	23(1)	20(1)	33(1)	6(1)	9(1)	4(1)
C(15)	25(1)	23(1)	32(1)	-8(1)	10(1)	-3(1)
C(16)	39(2)	37(2)	46(2)	-7(1)	4(2)	-5(1)
C(17)	28(2)	31(2)	60(2)	6(2)	6(1)	-3(1)
C(18)	14(1)	23(1)	16(1)	0(1)	6(1)	-2(1)
C(19)	17(1)	20(1)	11(1)	-3(1)	2(1)	1(1)
C(20)	17(1)	23(1)	15(1)	0(1)	4(1)	-1(1)
C(21)	19(1)	21(1)	20(1)	-1(1)	7(1)	-1(1)
C(22)	25(1)	26(1)	18(1)	-6(1)	5(1)	-4(1)
C(23)	20(1)	29(1)	15(1)	-2(1)	2(1)	-4(1)

Table B.8 Hydrogen coordinates ($\times$ 10^4) and values of the isotropic displacement parameter, $U(\text{eq})$ ($\text{Å}^2 \times 10^3$), for 4-bis(2,2'-bithien-5-yl)methyl-nitrobenzene, **8**.

Atom	x	y	z	$U(\text{eq})$
H(1A)	2498	2098	4535	22
H(3A)	3077	915	2800	24
H(4A)	4879	1049	1501	25
H(7A)	4999	3403	607	25
H(8A)	6711	3516	-808	25
H(9A)	7915	2490	-1125	43
H(11A)	993	1309	5556	27
H(12A)	-1015	474	5136	29
H(15A)	-2127	128	1016	31
H(16A)	-4262	-656	581	49
H(17A)	-5357	-861	2263	48
H(19A)	-59	2544	1829	19
H(20A)	-1417	3548	1549	22
H(22A)	336	4097	4938	28
H(23A)	1717	3102	5187	26

Table B.9 Atomic coordinates ($\times 10^4$) and values of the equivalent isotropic displacement parameter, U(eq) ($\mathring{A}^2 \times 10^3$) for 4-bis(2,2'-bithien-5-yl)methylbenzoic acid glycol ester, **9**, defined as one third of the trace of the orthogonalized Uij tensor.

Atom	x	y	z	U(eq)
S(1)	5339(1)	9027(1)	7120(1)	18(1)
S(2)	1956(1)	12491(1)	7899(1)	36(1)
S(3)	7084(1)	5392(1)	8505(1)	21(1)
S(4)	9869(1)	2344(1)	9760(1)	31(1)
O(1)	6738(5)	3776(3)	5302(1)	56(1)
C(1)	8752(3)	7494(2)	7542(1)	17(1)
C(2)	7155(4)	8544(2)	7702(1)	17(1)
O(2)	7692(8)	1300(4)	4594(2)	38(1)
C(3)	7076(4)	9350(3)	8261(1)	24(1)
C(4)	5538(4)	10351(3)	8227(1)	25(1)
C(5)	4450(4)	10309(2)	7634(1)	20(1)
C(6)	2751(4)	11138(2)	7413(1)	22(1)
C(7)	1560(4)	10989(2)	6804(1)	25(1)
C(8)	-21(5)	12008(3)	6798(2)	35(1)
C(9)	41(5)	12859(3)	7339(2)	37(1)
C(10)	9205(3)	6557(2)	8115(1)	17(1)
C(11)	11245(4)	6383(3)	8355(1)	22(1)
C(12)	11111(4)	5303(2)	8854(1)	20(1)
C(13)	8967(4)	4654(2)	8991(1)	17(1)
C(14)	8167(4)	3506(2)	9460(1)	19(1)
C(15)	5955(3)	3177(2)	9730(1)	15(1)
C(16)	5892(4)	1942(3)	10176(1)	28(1)
C(17)	7837(5)	1420(3)	10237(1)	30(1)
C(18)	8081(4)	6526(3)	6940(1)	20(1)
C(19)	6016(4)	5568(2)	6878(1)	22(1)
C(20)	5497(5)	4627(3)	6345(1)	30(1)
C(21)	7073(6)	4646(3)	5860(1)	36(1)
C(22)	9126(5)	5582(4)	5907(1)	40(1)
C(23)	9622(4)	6508(3)	6445(1)	30(1)
C(24)	5305(10)	2633(5)	5233(2)	24(1)
C(25)	5647(8)	1873(5)	4604(2)	22(1)
O(2A)	2228(7)	910(4)	4511(2)	38(1)
C(25A)	4271(7)	1942(5)	4608(2)	22(1)
C(24A)	4325(9)	2773(5)	5258(2)	24(1)

Table B.10 Bond lengths and angles between bonds for 4-bis(2,2'-bithien-5-yl)methylbenzoic acid glycol ester, **9**.

Atoms	Bond lengths / Å
S(1)-C(2)	1.726(2)
S(1)-C(5)	1.730(2)
S(2)-C(9)	1.700(3)
S(2)-C(6)	1.720(2)
S(3)-C(10)	1.727(2)
S(3)-C(13)	1.734(2)
S(4)-C(17)	1.692(3)
S(4)-C(14)	1.717(2)
O(1)-C(24)	1.242(5)
O(1)-C(21)	1.381(3)
O(1)-C(24A)	1.586(5)
C(1)-C(10)	1.510(3)
C(1)-C(2)	1.515(3)
C(1)-C(18)	1.524(3)
C(1)-H(1A)	1
C(2)-C(3)	1.365(3)
O(2)-C(25)	1.429(6)
O(2)-H(2A)	0.84
C(3)-C(4)	1.417(3)
C(3)-H(3A)	0.95
C(4)-C(5)	1.373(3)
C(4)-H(4A)	0.95
C(5)-C(6)	1.452(3)
C(6)-C(7)	1.429(4)
C(7)-C(8)	1.449(3)
C(7)-H(7A)	0.95
C(8)-C(9)	1.348(4)
C(8)-H(8A)	0.95
C(9)-H(9A)	0.95
C(10)-C(11)	1.362(3)
C(11)-C(12)	1.418(3)
C(11)-H(11A)	0.95
C(12)-C(13)	1.365(3)
C(12)-H(12A)	0.95
C(13)-C(14)	1.450(3)
C(14)-C(15)	1.442(3)
C(15)-C(16)	1.453(3)
C(15)-H(15A)	0.95
C(16)-C(17)	1.352(4)
C(16)-H(16A)	0.95
C(17)-H(17A)	0.95
C(18)-C(23)	1.390(3)
C(18)-C(19)	1.400(3)
C(19)-C(20)	1.386(3)
C(19)-H(19A)	0.95

Atoms	Bond lengths / Å
C(20)-C(21)	1.386(4)
C(20)-H(20A)	0.95
C(21)-C(22)	1.384(5)
C(22)-C(23)	1.384(4)
C(22)-H(22A)	0.95
C(23)-H(23A)	0.95
C(24)-C(25)	1.495(6)
C(24)-H(24A)	0.99
C(24)-H(24B)	0.99
C(25)-H(25A)	0.99
C(25)-H(25B)	0.99
O(2A)-C(25A)	1.431(5)
O(2A)-H(2AA)	0.84
C(25A)-C(24A)	1.527(5)
C(25A)-H(25C)	0.99
C(25A)-H(25E)	0.99
C(24A)-H(24C)	0.99
C(24A)-H(24D)	0.99

Atoms	Angles between bonds / degree
C(2)-S(1)-C(5)	92.53(11)
C(9)-S(2)-C(6)	92.42(13)
C(10)-S(3)-C(13)	92.33(10)
C(17)-S(4)-C(14)	93.07(12)
C(24)-O(1)-C(21)	125.3(3)
C(24)-O(1)-C(24A)	21.8(3)
C(21)-O(1)-C(24A)	113.3(3)
C(10)-C(1)-C(2)	112.71(17)
C(10)-C(1)-C(18)	110.80(18)
C(2)-C(1)-C(18)	114.21(18)
C(10)-C(1)-H(1A)	106.1
C(2)-C(1)-H(1A)	106.1
C(18)-C(1)-H(1A)	106.1
C(3)-C(2)-C(1)	127.8(2)
C(3)-C(2)-S(1)	110.60(17)
C(1)-C(2)-S(1)	121.17(15)
C(25)-O(2)-H(2A)	109.5
C(2)-C(3)-C(4)	113.5(2)
C(2)-C(3)-H(3A)	123.3
C(4)-C(3)-H(3A)	123.3
C(5)-C(4)-C(3)	113.0(2)
C(5)-C(4)-H(4A)	123.5
C(3)-C(4)-H(4A)	123.5
C(4)-C(5)-C(6)	129.7(2)
C(4)-C(5)-S(1)	110.42(17)
C(6)-C(5)-S(1)	119.92(17)
C(7)-C(6)-C(5)	127.6(2)
C(7)-C(6)-S(2)	111.72(17)

Atoms	Angles between bonds / degree
C(5)-C(6)-S(2)	120.63(18)
C(6)-C(7)-C(8)	108.8(2)
C(6)-C(7)-H(7A)	125.6
C(8)-C(7)-H(7A)	125.6
C(9)-C(8)-C(7)	114.4(3)
C(9)-C(8)-H(8A)	122.8
C(7)-C(8)-H(8A)	122.8
C(8)-C(9)-S(2)	112.6(2)
C(8)-C(9)-H(9A)	123.7
S(2)-C(9)-H(9A)	123.7
C(11)-C(10)-C(1)	126.9(2)
C(11)-C(10)-S(3)	110.77(17)
C(1)-C(10)-S(3)	122.05(16)
C(10)-C(11)-C(12)	113.2(2)
C(10)-C(11)-H(11A)	123.4
C(12)-C(11)-H(11A)	123.4
C(13)-C(12)-C(11)	113.4(2)
C(13)-C(12)-H(12A)	123.3
C(11)-C(12)-H(12A)	123.3
C(12)-C(13)-C(14)	129.4(2)
C(12)-C(13)-S(3)	110.34(17)
C(14)-C(13)-S(3)	120.28(16)
C(15)-C(14)-C(13)	126.76(19)
C(15)-C(14)-S(4)	111.64(16)
C(13)-C(14)-S(4)	121.61(17)
C(14)-C(15)-C(16)	108.1(2)
C(14)-C(15)-H(15A)	125.9
C(16)-C(15)-H(15A)	125.9
C(17)-C(16)-C(15)	114.9(2)
C(17)-C(16)-H(16A)	122.6
C(15)-C(16)-H(16A)	122.6
C(16)-C(17)-S(4)	112.29(19)
C(16)-C(17)-H(17A)	123.9
S(4)-C(17)-H(17A)	123.9
C(23)-C(18)-C(19)	117.8(2)
C(23)-C(18)-C(1)	119.3(2)
C(19)-C(18)-C(1)	122.78(19)
C(20)-C(19)-C(18)	121.8(2)
C(20)-C(19)-H(19A)	119.1
C(18)-C(19)-H(19A)	119.1
C(21)-C(20)-C(19)	118.7(3)
C(21)-C(20)-H(20A)	120.7
C(19)-C(20)-H(20A)	120.7
O(1)-C(21)-C(22)	115.3(3)
O(1)-C(21)-C(20)	124.0(3)
C(22)-C(21)-C(20)	120.7(2)
C(21)-C(22)-C(23)	119.8(3)
C(21)-C(22)-H(22A)	120.1

162

Atoms	Angles between bonds / degree
C(23)-C(22)-H(22A)	120.1
C(22)-C(23)-C(18)	121.1(3)
C(22)-C(23)-H(23A)	119.4
C(18)-C(23)-H(23A)	119.4
O(1)-C(24)-C(25)	110.1(4)
O(1)-C(24)-H(24A)	109.6
C(25)-C(24)-H(24A)	109.6
O(1)-C(24)-H(24B)	109.6
C(25)-C(24)-H(24B)	109.6
H(24A)-C(24)-H(24B)	108.1
O(2)-C(25)-C(24)	113.0(4)
O(2)-C(25)-H(25A)	109
C(24)-C(25)-H(25A)	109
O(2)-C(25)-H(25B)	109
C(24)-C(25)-H(25B)	109
H(25A)-C(25)-H(25B)	107.8
C(25A)-O(2A)-H(2AA)	109.5
O(2A)-C(25A)-C(24A)	112.2(4)
O(2A)-C(25A)-H(25C)	109.2
C(24A)-C(25A)-H(25C)	109.2
O(2A)-C(25A)-H(25E)	109.2
C(24A)-C(25A)-H(25E)	109.2
H(25C)-C(25A)-H(25E)	107.9
C(25A)-C(24A)-O(1)	105.1(3)
C(25A)-C(24A)-H(24C)	110.7
O(1)-C(24A)-H(24C)	110.7
C(25A)-C(24A)-H(24D)	110.7
O(1)-C(24A)-H(24D)	110.7
H(24C)-C(24A)-H(24D)	108.8

Table B.11 Anisotropic displacement parameters ($\text{Å}^2 \times 10^3$) for 4-bis(2,2'-bithien-5-yl)methylbenzoic acid glycol ester, **9**. Exponent of the anisotropic displacement factor takes the form: $-2\pi^2[\ h^2\ a^{*2}\ U^{11} + ... + 2\ h\ k\ a^*\ b^*\ U^{12}\ ]$

Atom	U^{11}	U^{22}	U^{33}	U^{23}	U^{13}	U^{12}
S(1)	19(1)	18(1)	18(1)	-3(1)	0(1)	6(1)
S(2)	32(1)	27(1)	49(1)	-10(1)	6(1)	10(1)
S(3)	14(1)	26(1)	22(1)	6(1)	0(1)	3(1)
S(4)	31(1)	27(1)	36(1)	5(1)	1(1)	10(1)
O(1)	99(2)	50(1)	26(1)	-21(1)	-11(1)	37(1)
C(1)	16(1)	19(1)	17(1)	1(1)	2(1)	3(1)
C(2)	17(1)	16(1)	18(1)	1(1)	1(1)	2(1)
O(2)	60(2)	24(1)	30(1)	2(1)	6(1)	4(1)
C(3)	31(1)	23(1)	20(1)	-4(1)	-2(1)	7(1)
C(4)	32(1)	21(1)	23(1)	-6(1)	3(1)	6(1)
C(5)	21(1)	14(1)	24(1)	-2(1)	6(1)	3(1)
C(6)	23(1)	13(1)	29(1)	0(1)	7(1)	4(1)
C(7)	22(1)	14(1)	42(1)	7(1)	-1(1)	10(1)
C(8)	30(1)	28(1)	49(2)	10(1)	0(1)	10(1)
C(9)	28(1)	22(1)	62(2)	2(1)	10(1)	11(1)
C(10)	16(1)	18(1)	17(1)	-1(1)	2(1)	2(1)
C(11)	24(1)	21(1)	20(1)	-3(1)	1(1)	2(1)
C(12)	16(1)	22(1)	21(1)	-2(1)	-2(1)	5(1)
C(13)	18(1)	17(1)	18(1)	-3(1)	-2(1)	6(1)
C(14)	21(1)	17(1)	19(1)	-1(1)	-3(1)	4(1)
C(15)	19(1)	12(1)	11(1)	2(1)	0(1)	-4(1)
C(16)	30(1)	25(1)	26(1)	3(1)	0(1)	-4(1)
C(17)	40(1)	19(1)	31(1)	2(1)	-7(1)	3(1)
C(18)	24(1)	22(1)	16(1)	0(1)	0(1)	11(1)
C(19)	26(1)	20(1)	20(1)	1(1)	0(1)	10(1)
C(20)	45(2)	21(1)	27(1)	-4(1)	-9(1)	11(1)
C(21)	60(2)	33(1)	21(1)	-11(1)	-8(1)	26(1)
C(22)	48(2)	59(2)	21(1)	-8(1)	4(1)	30(2)
C(23)	27(1)	46(2)	22(1)	-2(1)	3(1)	15(1)
C(24)	31(1)	23(1)	20(1)	-4(1)	-2(1)	7(1)
C(25)	24(1)	21(1)	20(1)	-3(1)	1(1)	2(1)
O(2A)	60(2)	24(1)	30(1)	2(1)	6(1)	4(1)
C(25A)	24(1)	21(1)	20(1)	-3(1)	1(1)	2(1)
C(24A)	31(1)	23(1)	20(1)	-4(1)	-2(1)	7(1)

Table B.12 Hydrogen coordinates ($\times 10^4$) and values of the isotropic displacement parameter, U(eq) ($\text{Å}^2 \times 10^3$), for 4-bis(2,2'-bithien-5-yl)methylbenzoic acid glycol ester, **9**.

Atom	x	y	z	U(eq)
H(1A)	10214	8137	7439	21
H(2A)	7649	629	4874	58
H(3A)	7966	9250	8637	29
H(4A)	5287	10985	8577	30
H(7A)	1770	10329	6460	30
H(8A)	-1019	12071	6443	42
H(9A)	-884	13586	7401	44
H(11A)	12620	6929	8204	27
H(12A)	12387	5056	9071	23
H(15A)	4748	3681	9633	18
H(16A)	4584	1532	10408	34
H(17A)	8039	625	10515	36
H(19A)	4941	5562	7211	26
H(20A)	4089	3983	6312	36
H(22A)	10192	5591	5571	48
H(23A)	11040	7141	6477	36
H(24A)	3791	2897	5235	29
H(24B)	5418	1951	5600	29
H(25A)	4378	1046	4528	27
H(25B)	5646	2589	4243	27
H(2AA)	2175	208	4776	58
H(25C)	4450	2670	4249	27
H(25E)	5547	1399	4595	27
H(24C)	4096	2065	5625	29
H(24D)	3144	3396	5268	29

Table B.13 Atomic coordinates ($\times$ 10^4) and values of the equivalent isotropic displacement parameter, U(eq) (Å^2 $\times$ 10^3) for 4-bis(2,2'-bithien-5-yl)methylbenzoic acid, **10**, defined as one third of the trace of the orthogonalized Uij tensor.

Atom	x	y	z	U(eq)
S(1)	5063(3)	8434(1)	2060(1)	23(1)
O(1)	8217(9)	9368(3)	3730(1)	30(1)
C(1)	7411(12)	9679(3)	2150(2)	20(2)
S(2)	6641(4)	6522(1)	1585(1)	51(1)
O(2)	11820(9)	9656(3)	3601(1)	32(1)
C(2)	7260(12)	9010(3)	1984(2)	20(2)
S(3)	5033(4)	10869(1)	2308(1)	24(1)
C(3)	8865(12)	8719(4)	1781(2)	24(2)
S(4)	-645(4)	12025(1)	1885(1)	42(1)
C(4)	8338(13)	8052(4)	1690(2)	26(2)
C(5)	6358(12)	7816(4)	1821(2)	23(2)
C(6)	5208(12)	7135(3)	1798(2)	27(2)
C(7)	3050(10)	6931(3)	1939(1)	12(1)
C(8)	2857(10)	6225(3)	1841(1)	12(1)
C(9)	4582(14)	5972(4)	1658(2)	32(2)
C(10)	5365(12)	10125(3)	2087(2)	23(2)
C(11)	3745(11)	10090(3)	1852(2)	21(2)
C(12)	2241(12)	10647(4)	1837(2)	24(2)
C(13)	2716(12)	11119(4)	2071(2)	24(2)
C(14)	1480(12)	11759(3)	2138(2)	22(2)
C(15)	1922(13)	12225(3)	2397(2)	26(2)
C(16)	256(16)	12754(4)	2374(2)	38(2)
C(17)	-1192(14)	12716(4)	2116(2)	36(2)
C(18)	8001(12)	9617(3)	2512(2)	18(2)
C(19)	6440(12)	9365(3)	2733(2)	23(2)
C(20)	6996(12)	9314(3)	3061(2)	21(2)
C(21)	9159(11)	9516(4)	3167(2)	21(2)
C(22)	10740(12)	9774(3)	2944(2)	24(2)
C(23)	10164(13)	9812(3)	2620(2)	24(2)
C(24)	9693(13)	9503(3)	3527(2)	24(2)
S(1A)	148(3)	8724(1)	753(1)	24(1)
C(1A)	2424(12)	9996(3)	814(2)	21(2)
S(2A)	-2058(4)	7191(1)	687(1)	34(1)
C(2A)	2282(12)	9256(3)	895(2)	22(2)
S(3A)	80(4)	11235(1)	827(1)	28(1)
O(3)	2571(9)	10356(3)	-769(1)	31(1)
C(3A)	3876(13)	8892(4)	1070(2)	27(2)
O(4)	6186(9)	10647(3)	-634(1)	41(2)
C(4A)	3406(12)	8200(4)	1088(2)	25(2)
C(5A)	1436(12)	8016(3)	921(2)	22(2)
C(6A)	505(12)	7346(4)	884(2)	24(2)
C(7A)	1530(12)	6741(3)	991(2)	22(2)
C(8A)	125(16)	6171(4)	898(2)	36(2)

Atom	x	y	z	$U(\text{eq})$
C(9A)	-1829(14)	6348(4)	735(2)	32(2)
C(10A)	405(12)	10395(3)	945(2)	20(2)
C(11A)	-1195(12)	10232(3)	1166(2)	21(2)
C(12A)	-2681(12)	10767(4)	1250(2)	23(2)
C(13A)	-2198(13)	11348(4)	1093(2)	25(2)
S(4A)	-5520(19)	12120(4)	1343(3)	52(2)
C(14A)	-3490(100)	12040(30)	1106(15)	25(5)
C(15A)	-2840(40)	12655(10)	869(5)	20(3)
C(16A)	-4540(30)	13164(11)	1032(5)	30(4)
C(17A)	-6030(80)	12850(20)	1331(8)	64(7)
C(15B)	-5830(60)	12015(14)	1381(8)	20(3)
C(14B)	-3310(110)	11960(30)	1130(16)	25(5)
S(4B)	-2342(13)	12730(4)	975(2)	52(2)
C(17B)	-4680(60)	13136(14)	1166(6)	64(7)
C(16B)	-6040(60)	12845(19)	1252(6)	30(4)
C(18A)	2842(12)	10130(3)	449(2)	20(2)
C(19A)	4910(14)	10382(3)	349(2)	27(2)
C(20A)	5340(13)	10501(4)	20(2)	30(2)
C(21A)	3654(12)	10353(4)	-207(2)	24(2)
C(22A)	1544(12)	10105(4)	-108(2)	27(2)
C(23A)	1146(12)	9986(4)	219(2)	25(2)
C(24A)	4079(14)	10458(4)	-563(2)	27(2)
C(2S)	-154(16)	6591(4)	-134(2)	38(2)
N(1S)	3732(14)	6524(4)	163(2)	50(2)
C(1S)	2028(15)	6549(4)	35(2)	34(2)

Table B.14 Bond lengths and angles between bonds for 4-bis(2,2'-bithien-5-yl)methylbenzoic acid, **10**.

Atoms	Bond lengths / Å
S(1)-C(5)	1.740(7)
S(1)-C(2)	1.744(7)
O(1)-C(24)	1.226(8)
C(1)-C(2)	1.493(9)
C(1)-C(10)	1.507(9)
C(1)-C(18)	1.524(9)
C(1)-H(1A)	1
S(2)-C(9)	1.649(8)
S(2)-C(6)	1.713(7)
O(2)-C(24)	1.311(9)
O(2)-H(2A)	0.84
C(2)-C(3)	1.379(10)
S(3)-C(13)	1.734(7)
S(3)-C(10)	1.740(7)
C(3)-C(4)	1.406(10)
C(3)-H(3A)	0.95
S(4)-C(17)	1.695(8)
S(4)-C(14)	1.697(7)
C(4)-C(5)	1.356(10)
C(4)-H(4A)	0.95
C(5)-C(6)	1.510(9)
C(6)-C(7)	1.441(7)
C(7)-C(8)	1.459(6)
C(7)-H(7A)	0.95
C(8)-C(9)	1.351(10)
C(8)-H(8A)	0.95
C(9)-H(9A)	0.95
C(10)-C(11)	1.351(9)
C(11)-C(12)	1.411(10)
C(11)-H(11A)	0.95
C(12)-C(13)	1.369(9)
C(12)-H(12A)	0.95
C(13)-C(14)	1.484(10)
C(14)-C(15)	1.432(9)
C(15)-C(16)	1.432(10)
C(15)-H(15A)	0.95
C(16)-C(17)	1.354(11)
C(16)-H(16A)	0.95
C(17)-H(17A)	0.95
C(18)-C(19)	1.378(9)
C(18)-C(23)	1.391(10)
C(19)-C(20)	1.388(9)
C(19)-H(19A)	0.95
C(20)-C(21)	1.392(10)
C(20)-H(20A)	0.95

Atoms	Bond lengths / Å
C(21)-C(22)	1.397(10)
C(21)-C(24)	1.507(9)
C(22)-C(23)	1.370(9)
C(22)-H(22A)	0.95
C(23)-H(23A)	0.95
S(1A)-C(2A)	1.731(7)
S(1A)-C(5A)	1.734(7)
C(1A)-C(2A)	1.505(9)
C(1A)-C(10A)	1.516(9)
C(1A)-C(18A)	1.538(9)
C(1A)-H(1AA)	1
S(2A)-C(9A)	1.689(8)
S(2A)-C(6A)	1.724(8)
C(2A)-C(3A)	1.377(10)
S(3A)-C(13A)	1.730(8)
S(3A)-C(10A)	1.741(7)
O(3)-C(24A)	1.236(9)
C(3A)-C(4A)	1.401(10)
C(3A)-H(3AA)	0.95
O(4)-C(24A)	1.317(9)
O(4)-H(4B)	0.84
C(4A)-C(5A)	1.386(10)
C(4A)-H(4AA)	0.95
C(5A)-C(6A)	1.442(10)
C(6A)-C(7A)	1.410(9)
C(7A)-C(8A)	1.446(10)
C(7A)-H(7AA)	0.95
C(8A)-C(9A)	1.367(11)
C(8A)-H(8AA)	0.95
C(9A)-H(9AA)	0.95
C(10A)-C(11A)	1.341(9)
C(11A)-C(12A)	1.411(10)
C(11A)-H(11B)	0.95
C(12A)-C(13A)	1.349(9)
C(12A)-H(12B)	0.95
C(13A)-C(14B)	1.38(6)
C(13A)-C(14A)	1.56(6)
S(4A)-C(17A)	1.47(4)
S(4A)-C(14A)	1.54(6)
C(14A)-C(15A)	1.61(6)
C(15A)-C(16A)	1.56(3)
C(15A)-H(15B)	0.95
C(16A)-C(17A)	1.63(4)
C(16A)-H(16B)	0.95
C(17A)-H(17B)	0.95
C(15B)-C(16B)	1.73(4)
C(15B)-C(14B)	1.80(7)
C(15B)-H(15C)	0.95

169

Atoms	Bond lengths / Å
C(14B)-S(4B)	1.75(6)
S(4B)-C(17B)	1.76(3)
C(17B)-C(16B)	1.04(5)
C(17B)-H(17C)	0.95
C(16B)-H(16C)	0.95
C(18A)-C(19A)	1.366(10)
C(18A)-C(23A)	1.395(9)
C(19A)-C(20A)	1.391(9)
C(19A)-H(19B)	0.95
C(20A)-C(21A)	1.385(10)
C(20A)-H(20B)	0.95
C(21A)-C(22A)	1.386(10)
C(21A)-C(24A)	1.491(10)
C(22A)-C(23A)	1.381(9)
C(22A)-H(22B)	0.95
C(23A)-H(23B)	0.95
C(2S)-C(1S)	1.450(12)
C(2S)-H(2SC)	0.98
C(2S)-H(2SA)	0.98
C(2S)-H(2SB)	0.98
N(1S)-C(1S)	1.125(10)

Atoms	Angles between bonds / degree
C(5)-S(1)-C(2)	92.3(3)
C(2)-C(1)-C(10)	113.2(6)
C(2)-C(1)-C(18)	112.8(6)
C(10)-C(1)-C(18)	113.1(6)
C(2)-C(1)-H(1A)	105.6
C(10)-C(1)-H(1A)	105.6
C(18)-C(1)-H(1A)	105.6
C(9)-S(2)-C(6)	91.1(4)
C(24)-O(2)-H(2A)	109.5
C(3)-C(2)-C(1)	127.4(6)
C(3)-C(2)-S(1)	109.4(5)
C(1)-C(2)-S(1)	122.8(5)
C(13)-S(3)-C(10)	92.2(3)
C(2)-C(3)-C(4)	113.9(7)
C(2)-C(3)-H(3A)	123.1
C(4)-C(3)-H(3A)	123.1
C(17)-S(4)-C(14)	92.7(4)
C(5)-C(4)-C(3)	113.9(7)
C(5)-C(4)-H(4A)	123.1
C(3)-C(4)-H(4A)	123.1
C(4)-C(5)-C(6)	131.3(6)
C(4)-C(5)-S(1)	110.5(6)
C(6)-C(5)-S(1)	118.1(5)
C(7)-C(6)-C(5)	127.7(6)
C(7)-C(6)-S(2)	115.6(5)

Atoms	Angles between bonds / degree
C(5)-C(6)-S(2)	116.7(5)
C(6)-C(7)-C(8)	103.0(5)
C(6)-C(7)-H(7A)	128.5
C(8)-C(7)-H(7A)	128.5
C(9)-C(8)-C(7)	116.8(6)
C(9)-C(8)-H(8A)	121.6
C(7)-C(8)-H(8A)	121.6
C(8)-C(9)-S(2)	113.5(5)
C(8)-C(9)-H(9A)	123.3
S(2)-C(9)-H(9A)	123.3
C(11)-C(10)-C(1)	130.2(6)
C(11)-C(10)-S(3)	109.7(5)
C(1)-C(10)-S(3)	119.7(5)
C(10)-C(11)-C(12)	115.1(6)
C(10)-C(11)-H(11A)	122.4
C(12)-C(11)-H(11A)	122.4
C(13)-C(12)-C(11)	112.2(6)
C(13)-C(12)-H(12A)	123.9
C(11)-C(12)-H(12A)	123.9
C(12)-C(13)-C(14)	127.9(7)
C(12)-C(13)-S(3)	110.8(5)
C(14)-C(13)-S(3)	121.3(5)
C(15)-C(14)-C(13)	126.9(6)
C(15)-C(14)-S(4)	112.6(5)
C(13)-C(14)-S(4)	120.5(5)
C(16)-C(15)-C(14)	107.6(6)
C(16)-C(15)-H(15A)	126.2
C(14)-C(15)-H(15A)	126.2
C(17)-C(16)-C(15)	115.6(6)
C(17)-C(16)-H(16A)	122.2
C(15)-C(16)-H(16A)	122.2
C(16)-C(17)-S(4)	111.3(6)
C(16)-C(17)-H(17A)	124.3
S(4)-C(17)-H(17A)	124.3
C(19)-C(18)-C(23)	119.3(6)
C(19)-C(18)-C(1)	121.3(6)
C(23)-C(18)-C(1)	119.5(6)
C(18)-C(19)-C(20)	120.7(7)
C(18)-C(19)-H(19A)	119.7
C(20)-C(19)-H(19A)	119.7
C(19)-C(20)-C(21)	119.5(6)
C(19)-C(20)-H(20A)	120.2
C(21)-C(20)-H(20A)	120.2
C(20)-C(21)-C(22)	119.8(6)
C(20)-C(21)-C(24)	119.2(6)
C(22)-C(21)-C(24)	120.8(6)
C(23)-C(22)-C(21)	119.6(6)
C(23)-C(22)-H(22A)	120.2

Atoms	Angles between bonds / degree
C(21)-C(22)-H(22A)	120.2
C(22)-C(23)-C(18)	121.0(7)
C(22)-C(23)-H(23A)	119.5
C(18)-C(23)-H(23A)	119.5
O(1)-C(24)-O(2)	123.9(6)
O(1)-C(24)-C(21)	121.4(6)
O(2)-C(24)-C(21)	114.6(6)
C(2A)-S(1A)-C(5A)	92.8(3)
C(2A)-C(1A)-C(10A)	112.8(6)
C(2A)-C(1A)-C(18A)	113.1(5)
C(10A)-C(1A)-C(18A)	112.1(6)
C(2A)-C(1A)-H(1AA)	106
C(10A)-C(1A)-H(1AA)	106
C(18A)-C(1A)-H(1AA)	106
C(9A)-S(2A)-C(6A)	93.1(4)
C(3A)-C(2A)-C(1A)	126.0(6)
C(3A)-C(2A)-S(1A)	109.9(5)
C(1A)-C(2A)-S(1A)	123.9(5)
C(13A)-S(3A)-C(10A)	91.9(3)
C(2A)-C(3A)-C(4A)	114.1(7)
C(2A)-C(3A)-H(3AA)	122.9
C(4A)-C(3A)-H(3AA)	122.9
C(24A)-O(4)-H(4B)	109.5
C(5A)-C(4A)-C(3A)	113.1(7)
C(5A)-C(4A)-H(4AA)	123.4
C(3A)-C(4A)-H(4AA)	123.4
C(4A)-C(5A)-C(6A)	127.3(6)
C(4A)-C(5A)-S(1A)	110.0(5)
C(6A)-C(5A)-S(1A)	122.7(5)
C(7A)-C(6A)-C(5A)	126.2(6)
C(7A)-C(6A)-S(2A)	111.2(5)
C(5A)-C(6A)-S(2A)	122.6(5)
C(6A)-C(7A)-C(8A)	110.0(6)
C(6A)-C(7A)-H(7AA)	125
C(8A)-C(7A)-H(7AA)	125
C(9A)-C(8A)-C(7A)	113.7(7)
C(9A)-C(8A)-H(8AA)	123.2
C(7A)-C(8A)-H(8AA)	123.2
C(8A)-C(9A)-S(2A)	112.1(6)
C(8A)-C(9A)-H(9AA)	124
S(2A)-C(9A)-H(9AA)	124
C(11A)-C(10A)-C(1A)	130.8(6)
C(11A)-C(10A)-S(3A)	110.0(5)
C(1A)-C(10A)-S(3A)	119.0(5)
C(10A)-C(11A)-C(12A)	114.2(6)
C(10A)-C(11A)-H(11B)	122.9
C(12A)-C(11A)-H(11B)	122.9
C(13A)-C(12A)-C(11A)	113.3(7)

172

Atoms	Angles between bonds / degree
C(13A)-C(12A)-H(12B)	123.3
C(11A)-C(12A)-H(12B)	123.3
C(12A)-C(13A)-C(14B)	127(3)
C(12A)-C(13A)-C(14A)	129(2)
C(14B)-C(13A)-C(14A)	4(5)
C(12A)-C(13A)-S(3A)	110.5(6)
C(14B)-C(13A)-S(3A)	123(3)
C(14A)-C(13A)-S(3A)	120(2)
C(17A)-S(4A)-C(14A)	104(3)
S(4A)-C(14A)-C(13A)	119(4)
S(4A)-C(14A)-C(15A)	118(4)
C(13A)-C(14A)-C(15A)	122(4)
C(16A)-C(15A)-C(14A)	95(3)
C(16A)-C(15A)-H(15B)	132.5
C(14A)-C(15A)-H(15B)	132.5
C(15A)-C(16A)-C(17A)	114(3)
C(15A)-C(16A)-H(16B)	122.8
C(17A)-C(16A)-H(16B)	122.8
S(4A)-C(17A)-C(16A)	107(3)
S(4A)-C(17A)-H(17B)	126.5
C(16A)-C(17A)-H(17B)	126.5
C(16B)-C(15B)-C(14B)	87(2)
C(16B)-C(15B)-H(15C)	136.7
C(14B)-C(15B)-H(15C)	136.7
C(13A)-C(14B)-S(4B)	125(4)
C(13A)-C(14B)-C(15B)	120(4)
S(4B)-C(14B)-C(15B)	115(3)
C(14B)-S(4B)-C(17B)	89(2)
C(16B)-C(17B)-S(4B)	119(3)
C(16B)-C(17B)-H(17C)	120.4
S(4B)-C(17B)-H(17C)	120.4
C(17B)-C(16B)-C(15B)	125(4)
C(17B)-C(16B)-H(16C)	117.5
C(15B)-C(16B)-H(16C)	117.5
C(19A)-C(18A)-C(23A)	119.8(6)
C(19A)-C(18A)-C(1A)	119.6(6)
C(23A)-C(18A)-C(1A)	120.6(6)
C(18A)-C(19A)-C(20A)	120.7(7)
C(18A)-C(19A)-H(19B)	119.6
C(20A)-C(19A)-H(19B)	119.6
C(21A)-C(20A)-C(19A)	119.2(7)
C(21A)-C(20A)-H(20B)	120.4
C(19A)-C(20A)-H(20B)	120.4
C(20A)-C(21A)-C(22A)	120.4(6)
C(20A)-C(21A)-C(24A)	120.7(7)
C(22A)-C(21A)-C(24A)	118.9(7)
C(23A)-C(22A)-C(21A)	119.6(7)
C(23A)-C(22A)-H(22B)	120.2

Atoms	Angles between bonds / degree
C(21A)-C(22A)-H(22B)	120.2
C(22A)-C(23A)-C(18A)	120.1(7)
C(22A)-C(23A)-H(23B)	119.9
C(18A)-C(23A)-H(23B)	119.9
O(3)-C(24A)-O(4)	123.8(7)
O(3)-C(24A)-C(21A)	121.8(7)
O(4)-C(24A)-C(21A)	114.3(7)
C(1S)-C(2S)-H(2SC)	109.5
C(1S)-C(2S)-H(2SA)	109.5
H(2SC)-C(2S)-H(2SA)	109.5
C(1S)-C(2S)-H(2SB)	109.5
H(2SC)-C(2S)-H(2SB)	109.5
H(2SA)-C(2S)-H(2SB)	109.5
N(1S)-C(1S)-C(2S)	179.1(10)

Table B.15 Anisotropic displacement parameters ($\text{Å}^2 \times 10^3$) for 4-bis(2,2'-bithien-5-yl)methylbenzoic acid, **10**. Exponent of the anisotropic displacement factor takes the form: $-2\pi^2[\ h^2\ a^{*2}\ U^{11} + ... + 2\ h\ k\ a^*\ b^*\ U^{12}\ ]$

Atom	U^{11}	U^{22}	U^{33}	U^{23}	U^{13}	U^{12}
S(1)	20(1)	26(1)	22(1)	-2(1)	2(1)	1(1)
O(1)	35(3)	39(3)	17(3)	0(2)	-4(2)	-17(3)
C(1)	14(4)	31(4)	15(3)	4(3)	-1(3)	-4(3)
S(2)	51(2)	52(1)	49(1)	-2(1)	-4(1)	6(1)
O(2)	25(3)	53(3)	19(3)	0(2)	-7(2)	-9(3)
C(2)	24(4)	23(4)	15(3)	6(3)	-2(3)	2(3)
S(3)	24(1)	28(1)	20(1)	-2(1)	-5(1)	-1(1)
C(3)	20(4)	32(4)	19(4)	5(3)	0(3)	-1(3)
S(4)	43(1)	44(1)	38(1)	-6(1)	-10(1)	8(1)
C(4)	28(4)	32(4)	18(4)	1(3)	0(3)	7(4)
C(5)	22(4)	30(4)	17(4)	-5(3)	3(3)	8(3)
C(6)	38(5)	23(4)	21(3)	-1(3)	-6(4)	2(4)
C(7)	14(2)	8(2)	14(2)	5(2)	-5(2)	-4(2)
C(8)	14(2)	8(2)	14(2)	5(2)	-5(2)	-4(2)
C(9)	42(5)	20(4)	33(4)	-1(3)	-12(4)	10(4)
C(10)	27(4)	26(4)	14(3)	1(3)	3(3)	-7(3)
C(11)	21(4)	19(4)	23(4)	-3(3)	-7(3)	0(3)
C(12)	20(4)	39(4)	14(3)	-1(3)	-3(3)	-14(3)
C(13)	21(4)	34(4)	17(4)	2(3)	-2(3)	0(3)
C(14)	21(4)	22(4)	21(4)	5(3)	-1(3)	-2(3)
C(15)	34(4)	26(4)	17(4)	-12(3)	-14(3)	21(4)
C(16)	45(5)	34(4)	36(4)	-18(3)	-5(4)	-3(4)
C(17)	37(5)	33(4)	38(5)	2(4)	4(4)	1(4)
C(18)	20(4)	23(4)	12(3)	1(3)	-2(3)	2(3)
C(19)	24(4)	25(4)	19(4)	-4(3)	-2(3)	-3(3)
C(20)	26(4)	23(4)	14(3)	-3(3)	5(3)	2(3)
C(21)	14(3)	29(4)	20(4)	2(3)	-2(3)	3(3)
C(22)	19(4)	33(4)	20(4)	-10(3)	-9(3)	3(3)
C(23)	19(4)	31(4)	24(4)	-1(3)	2(3)	-6(4)
C(24)	28(4)	24(4)	20(3)	-4(3)	-8(4)	-2(3)
S(1A)	22(1)	27(1)	24(1)	1(1)	-6(1)	0(1)
C(1A)	19(4)	26(4)	19(3)	-2(3)	6(3)	-2(3)
S(2A)	34(1)	33(1)	35(1)	-1(1)	-6(1)	2(1)
C(2A)	20(4)	23(4)	21(4)	-1(3)	5(3)	0(3)
S(3A)	29(1)	25(1)	30(1)	3(1)	9(1)	-2(1)
O(3)	35(3)	42(3)	16(3)	-4(2)	4(2)	6(3)
C(3A)	30(4)	34(4)	18(4)	-7(3)	-6(3)	-3(3)
O(4)	35(3)	69(4)	19(3)	1(3)	6(2)	-16(3)
C(4A)	23(4)	34(4)	17(4)	2(3)	-1(3)	7(3)
C(5A)	27(4)	27(4)	11(3)	2(3)	-1(3)	7(3)
C(6A)	22(4)	32(4)	17(3)	-2(3)	11(3)	8(3)
C(7A)	19(4)	24(4)	22(4)	-1(3)	1(3)	-5(3)
C(8A)	43(5)	28(4)	36(4)	3(3)	5(4)	10(5)

Atom	U^{11}	U^{22}	U^{33}	U^{23}	U^{13}	U^{12}
C(9A)	37(5)	33(4)	25(4)	2(3)	4(4)	-1(4)
C(10A)	21(4)	25(4)	15(3)	1(3)	-4(3)	-4(3)
C(11A)	25(4)	18(4)	20(4)	-3(3)	-1(3)	-2(3)
C(12A)	24(4)	33(4)	12(3)	1(3)	-1(3)	-11(3)
C(13A)	27(4)	25(4)	24(4)	-3(3)	-2(3)	1(3)
S(4A)	50(3)	41(3)	64(4)	0(2)	1(2)	4(2)
C(14A)	24(7)	27(8)	25(6)	2(6)	2(5)	1(6)
C(15A)	28(8)	24(8)	7(6)	7(5)	6(5)	11(6)
C(16A)	23(6)	31(6)	34(7)	13(6)	16(5)	-2(5)
C(17A)	106(19)	39(11)	46(15)	4(10)	24(12)	11(10)
C(15B)	28(8)	24(8)	7(6)	7(5)	6(5)	11(6)
C(14B)	24(7)	27(8)	25(6)	2(6)	2(5)	1(6)
S(4B)	50(3)	41(3)	64(4)	0(2)	1(2)	4(2)
C(17B)	106(19)	39(11)	46(15)	4(10)	24(12)	11(10)
C(16B)	23(6)	31(6)	34(7)	13(6)	16(5)	-2(5)
C(18A)	24(4)	24(4)	12(3)	-5(3)	-1(3)	4(3)
C(19A)	25(4)	32(4)	23(4)	-1(3)	0(4)	0(4)
C(20A)	14(4)	46(4)	29(4)	-6(3)	6(3)	0(4)
C(21A)	20(4)	32(4)	20(4)	1(3)	3(3)	1(3)
C(22A)	22(4)	42(5)	16(4)	6(3)	-2(3)	5(3)
C(23A)	26(4)	32(4)	18(4)	1(3)	0(3)	-7(3)
C(24A)	32(4)	26(4)	24(4)	1(3)	6(3)	-6(3)
C(2S)	42(5)	51(5)	22(4)	-4(3)	-1(4)	-9(5)
N(1S)	43(5)	71(5)	37(4)	-10(4)	-1(4)	5(4)
C(1S)	39(5)	40(5)	22(4)	-3(4)	5(4)	-13(4)

Table B.16 Hydrogen coordinates ($\times 10^4$) and values of the isotropic displacement parameter, U(eq) ($\text{Å}^2 \times 10^3$), for 4-bis(2,2'-bithien-5-yl)methylbenzoic acid, **10**.

Atom	x	y	z	U(eq)
H(1A)	8746	9915	2048	24
H(2A)	11985	9649	3804	48
H(3A)	10206	8947	1709	29
H(4A)	9282	7791	1549	31
H(7A)	2007	7193	2064	14
H(8A)	1579	5957	1903	14
H(9A)	4607	5521	1580	38
H(11A)	3628	9717	1707	25
H(12A)	1036	10689	1682	29
H(15A)	3106	12190	2556	31
H(16A)	172	13109	2530	46
H(17A)	-2364	13036	2071	43
H(19A)	4967	9226	2660	27
H(20A)	5909	9142	3213	25
H(22A)	12206	9922	3015	29
H(23A)	11259	9974	2467	29
H(1AA)	3809	10171	930	25
H(3AA)	5180	9093	1170	33
H(4B)	6363	10643	-838	61
H(4AA)	4343	7888	1204	30
H(7AA)	2937	6712	1107	26
H(8AA)	522	5717	946	43
H(9AA)	-2928	6032	657	38
H(11B)	-1315	9794	1259	25
H(12B)	-3902	10722	1402	28
H(15B)	-1802	12696	692	24
H(16B)	-4684	13620	963	36
H(17B)	-7045	13086	1471	76
H(15C)	-6668	11723	1522	24
H(17C)	-4690	13612	1191	76
H(16C)	-7511	13052	1260	36
H(19B)	6066	10476	506	32
H(20B)	6773	10681	-48	36
H(22B)	378	10016	-265	32
H(23B)	-286	9807	288	31
H(2SC)	-710	7058	-129	57
H(2SA)	-1271	6296	-27	57
H(2SB)	45	6447	-361	57